Modelling of fluidised dense-phase pneumatic conveying of powders

Soumya Suddha Mallick
University of Wollongong

Modelling of Fluidised Dense-Phase Pneumatic Conveying of Powders

A thesis submitted in fulfilment of the requirements for the
award of the degree

Doctorate of Philosophy

from

UNIVERSITY OF WOLLONGONG

by

Soumya Suddha Mallick, BE, MTech

Centre for Bulk Solids and Particulate Technologies, Faculty of Engineering

2009

This thesis is dedicated to my parents Shukla and Dipta Sundar Mallick, wife Priyanka and brother Soumyarya for their love, support and patience

THESIS CERTIFICATION

I, Soumya Suddha Mallick, declare that this thesis, submitted in fulfilment of the requirements for the award of Doctor of Philosophy, in the Centre for Bulk Solids and Particulate Technologies, Faculty of Engineering, University of Wollongong, is wholly my own work unless otherwise referenced or acknowledged. The document has not been submitted for qualifications at any other academic institution.

Soumya Suddha Mallick

March 2009

ACKNOWLEDGEMENTS

It has been a great honour for me to be a student of Associate Professor Peter Wypych. I started my PhD knowing he would be my "supervisor" and he has always been outstanding in that role, but what is even better and perhaps more valuable to me – I have found a friend, mentor and father in him. I will try to emulate him in my life.

I am indebted to Jose Humberto Dominguez Davila for his presence, support and patient listening during my good and difficult times. I especially thank him for taking care of me when I was terribly sick during the winter of 2008.

I thank Mary Sparks, Meeta Chatterjee Padmanabhan and Padma Iyer for their support and mentoring during my first week in Australia. I was struggling to adapt to a new country. Additional thanks to Mary for arranging my accommodation in Kooloobong.

I was fortunate to have Alexander Rolfe as my first housemate at the Kooloobong accommodation. Alex helped me adjust to Wollongong during my initial days. I thank him for his generous support, positive attitude and continuous encouragement.

Thanks to David Hastie for assisting me in searching for the experimental data (of various previous projects), which I used extensively in my thesis. David was always willing to help and available for discussions.

I acknowledge the support of the technical staff of the Bulk Materials Handling Laboratory for the experimental work.

The financial support provided by the University of Wollongong to carry out my studies is greatly appreciated.

ABSTRACT

Dense-phase pneumatic conveying of powders is becoming increasingly popular in various industries such as power, pharmaceutical, cement, alumina, chemical, limestone, refinery, and so on. Some of the reasons include: minimum gas flows and power consumption; improved product quality; increased workplace safety. However, due to the highly concentrated and turbulent mode of the solids-gas flow, only limited progress has been be achieved so far in understanding the fundamental transport mechanisms and accurately predicting pipeline pressure drop, which is a key system design parameter. This thesis aims to overcome the present limitations and provide the industry with a new validated modelling procedure for the accurate prediction and scale-up of pressure drop and optimal operating conditions for fluidised dense-phase pneumatic conveying systems.

Various popular/existing models (and model formats) for solids friction (for straight horizontal pipes) have been evaluated for scale-up accuracy and stability. It has been found that the models (and their use of parameter groupings) are generally not capable of accurately predicting pressure drop under scale-up conditions of pipeline diameter and/or length. Two new approaches and another method based on the parameters used by other researcher have been employed in this study as improved design techniques. One approach, derived by modifying an existing reliable dilute-phase model to make it suitable for dense-phase, has resulted in a substantial relative improvement in the overall accuracy of predictions under scale-up conditions for two types of fly ash, ESP dust, pulverised coal and fly ash/cement mixture. Another

method has been derived using the concept of "two-layer" slurry flow modelling (i.e. suspension flow occurring on top of a non-suspension moving layer), and this has also resulted in similar improvements. The third method, using parameters that were mentioned by another researcher as providing better representation of the flow phenomenon, has also resulted in similar reliable predictions.

Three different popular/existing bend models have been evaluated to select an optimal (bend loss) model for dense-phase powder conveying. It has been found that the estimation of bend pressure drop can have a considerable impact towards correctly predicting the total pressure loss in a pneumatic conveying system.

An existing method of representing "minimum transport criteria" (based on superficial air velocity and solids loading ratio) has been found inadequate for predicting the unstable boundary, especially under diameter scale-up conditions. Based on the experimental data of various powders conveyed over a wide range of pipe lengths and diameters, it is found that with increase in pipe diameter, the requirement of minimum conveying air velocity increases. To capture the pipe diameter effect, a Froude number based approach has been introduced to reliably represent the minimum transport boundary.

The thesis also investigates the suitability of using a direct differential pressure (DP) measurement technique across a straight length of pipe for fine powder conveying in dense-phase. Standard Deviations (SD) of the DP, as well as the static pressure

signals are presented. The trend shows the SD values are increasing with increase in pipe length from pipe inlet to exit (i.e. a dependence on tapping location).

TABLE OF CONTENTS

LIST OF FIGURES

LIST OF TABLES

LIST OF SYMBOLS AND ABBREVIATIONS

A	Cross sectional area of the pipe [m^2]
A_1	Portion of cross sectional area of pipe occupied by the non-suspension layer in dense-phase regime [m^2]
A_2	Portion of cross sectional area of pipe occupied by the suspension layer in dense-phase regime [m^2]
Ar	Archimedes number
B	Bend loss factor
b_e	Equivalent length for bends [m]
C	Particle velocity in suspension [m/s]
D	Internal diameter of pipe [m]
d_s	Particle diameter [m]
d_{50}	Median particle diameter [μm]
$D_{h\ (non-sus)}$	Hydraulic diameter for the non-suspension layer in dense-phase regime [m]
$D_{h\ (sus)}$	Hydraulic diameter for the suspension layer in dense-phase regime [m]
$Fr = V/(gD)^{0.5}$	Froude number of flow
Fr_i	Froude number at pipe inlet

$Fr_m = V_m/(gD)^{0.5}$ — Mean Froude number related to the section of pipe

$Fr_p = V/(gd_s)^{0.5}$ — Particle Froude number based on superficial air velocity and particle diameter

$Fr_s = \omega_{fo}/(d_s g)^{0.5}$ — Froude number of particle related to particle diameter

$Fr_s = \omega_{fo}/(Dg)^{0.5}$ — Froude number of particle related to pipe diameter

Fr_{bo} — Froude number of flow at bend outlet

$Fr^* = C/(gD)^{0.5}$ — Froude number related to particle velocity

f_r — Sliding friction factor between of solids and pipe wall

Fri — Friction number

g — Acceleration due to gravity $[m/s^2]$

K — Pressure drop coefficient (equation 2.35)

K — Constant of power function (equation 7.1)

K_b — Bend loss coefficient (equation 2.20)

$K_1 = w_f/w_{f0}$ — Ratio of particle settling velocities in a cloud to single particle in an undisturbed fluid

L — Length of pipe or test section [m]

L_h — Length of a horizontal portion of pipe [m]

L_v — Height of a vertical section of pipe [m]

M_f	Mass of air in a control volume [kg]
M_s	Mass of solids in a control volume [kg]
m_f	Mass flow rate of air [kg/s]
m_s	Mass flow rate of solids [kg/s]
$m^* = m_s / m_f$	Solids loading ratio = m_s / m_f
$m_{s\,(non\text{-}sus)}$	Mass flow rate of solids being conveyed in non-suspension layer in dense-phase regime[kg/s]
$m_{s\,(sus)}$	Mass flow rate of solids being conveyed in suspension layer in dense-phase regime [kg/s]
N	Number of bends
ΔP	Pressure drop through a straight horizontal pipe or pipe section [Pa]
ΔP_{accel}	Pressure drop due to initial acceleration [Pa]
ΔP_b	Pressure drop through a bend [Pa]
$\Delta P_f, \Delta P_0$	Pressure drop due to air only in a pipe [Pa]
ΔP_T	Total pipeline pressure drop [Pa]
ΔP_v	Pressure drop due to verticals [Pa]
$(\Delta p_{bend})_{solids}$	Pressure drop through a bend due to solids only [Pa]
R_B	Centerline radius of bend [m]

r	Radius of pipe [m]
Re	Reynolds number of gas $= \rho V D / \mu$
$Re_{non\text{-}sus}$	Reynolds number for the non-suspension layer in dense-phase regime
Re_p	Reynolds number of particle $= \rho_s V d_s / \mu$
S_1	Wetted perimeter on the pipe wall due to non-suspension layer in dense-phase regime [m]
S_2	Wetted perimeter on the pipe wall due to suspension layer in dense-phase regime [m]
St	Stokes number
V	Superficial air/gas velocity [m/s]
V_{bo}	Air velocity at bend outlet [m/s]
V_i , V_{entry}	Superficial air/gas velocity at the inlet or entry of a pipe section [m/s]
$V_{i,\ min}$	Minimum conveying air velocity requirement at pipe inlet
V_1	Actual air velocity in the suspension layer in dense-phase regime [m/s]
$V_{non\text{-}sus}$	Conveying velocity for the non-suspension layer in

dense-phase regime [m]

V_f	Volume of air in a control volume [m^3]
V_s	Volume of solids in a control volume [m^3]
ε	Void fraction of the strand
ε_p	Volumetric concentration of particles
ρ	Density of air [kg/m^3]
ρ_m	Mean air density for a pipeline section [kg/m^3]
ρ_s	Particle density [kg/m^3]
ρ_{bl}	Loose-poured bulk density [kg/m^3]
ρ_{bo}, ρ_o	Density of air bend outlet [kg/m^3]
ρ_{sus}	Suspension density in equation (2.35) [kg/m^3]
$\rho_{non\ sus}$	Apparent density of the non-suspension layer in dense-phase regime [kg/m^3]
λ_{bs}	Solids friction factor through bends
λ_f	Air/gas only friction factor
λ_{fb}	Air only friction factor in bend
λ_s	Solids friction factor through straight pipe
$\lambda_s{}^*$	Impact and friction factor

λ_T	Combined solids-air friction factor
λ_{sus}	Friction factor for the suspension layer in dense-phase regime
$\lambda_{non\text{-}sus}$	Friction factor for the non-suspension layer in dense-phase regime
Ψ_{bs}	Bend resistance number
α	C/V ratio at minimum transport condition
$\beta = \omega_f/V$	Velocity ratio related to particle fall velocity in a cloud
$\beta_0 = \omega_{fo}/V$	Velocity ratio related to particle fall velocity in undisturbed fluid
ω_f	Particle settling velocity in a cloud [m/s]
ω_{fo}	Single particle settling (or terminal) velocity in undisturbed fluid [m/s]
φ	Shape factor of particles
τ_1	Shear stress on the pipe wall due to non-suspension layer in dense-phase regime [Pa]
τ_2	shear stress on the pipe wall due to suspension layer in dense-phase regime [Pa]
μ	Dynamic viscosity for single fluid (e.g. air) [Pas]

$\mu_{non\text{-}sus}$ Apparent viscosity for the non-suspension layer in dense-phase regime [Pas]

Superscripts

a,b,c,d   Exponents of the power function (equations 7.1 and 7.23)

Subscripts

e   Equivalent (equation 8.9)

f   Fluid (air)

h   Horizontal (equation 8.9)

i   inlet condition

m   Mean value for the section/interval of pipe, based on average air density

min   Minimum

s   Solids

v   Vertical (equation 8.9)

1   Experimental data pertaining to test rig (equations 8.1 to 8.8)

| 2 | Scaled-up data pertaining to an actual or proposed plant (equations 8.1 to 8.8) |
| 1, 2, 3 | Subscripts of m_s in Figure 9.1 |

Abbreviations

I.D.	Internal diameter of pipe
PCC	Pneumatic conveying characteristics
PMC	Pressure minimum curve
SD	Standard deviation

CHAPTER 1: Introduction

1.   Introduction

Pneumatic conveying of fine powders, especially under (fluidised) dense-phase conditions, is becoming increasingly popular in various industries such as power, cement, chemical, pharmaceutical, alumina, limestone, refinery, due to the reasons of high efficiency, reduced gas flows and power consumption, improved product quality and increased workplace safety. For reliably designing optimal industrial plants, the accurate prediction of the total pipeline pressure loss for the dense-phase pneumatic conveying of powders through a given pipeline system is of significant importance. While more fundamental modelling methods based on powder mechanics have been developed for certain products and modes of flows, such as low-velocity slug-flow of granular products (Mi and Wypych, 1994, 1995; Pan and Wypych, 1997), due to the highly concentrated and turbulent nature of the solids-gas mixture during dense-phase conveying of powders, fundamentally understanding the flow mechanism and modelling the solids friction to accurately predict the pressure drop as an important system design parameter has remained a far more complex problem to be resolved at a similar level of detail. Due to this reason, empirical power function based models for solids friction have been employed over the years by various researchers (Stegmaier, 1978; Pan, 1992; Pan and Wypych, 1998; Jones and Williams, 2003; Williams and Jones, 2004) to avoid the need to develop fundamental relationships between friction factor and the relevant particle and bulk properties. These models have used different parameter groupings and have shown good results when applied to the researchers' own data, but have not been tested against important criteria, such as scale-up accuracy and stability. Hence, there is a requirement to evaluate the

2

models (and their use of parameter groupings) under significant scale-up conditions of diameter and/or length and if the models are found unreliable, further research would need to be conducted at a more fundamental level, properly addressing the particle/wall/air interactions, for a better understanding of the flow mechanisms (especially, for dense-phase).

The main aim of the thesis is to provide the industry with a standardised (validated) test-design procedure for the accurate prediction of pressure drop for fluidised dense-phase pneumatic conveying of powders. Particular research objectives include:

a) Conducting test program for different products using a wide range of pipe diameters and lengths and to develop extensive databases, for the derivation of new models and validation of the same for scale-up accuracy and stability; developing a direct differential pressure measurement arrangement for measuring pressure drop across a horizontal straight section of pipe (Chapters 3 and 4).

b) Studying pneumatic conveying characteristics (PCC), especially for the straight horizontal sections (installed at different locations for a test pipe and also, on pipes of different diameters and lengths) for an improved understanding on the change in flow mechanisms along the pipeline, and also the effect of changing pipe diameter and/or length on pressure drop characteristics (Chapter 5).

c) Investigating the scale-up accuracy and stability of existing/popular models and their use of parameter groupings, using the so-called "component" approach (Chapters 6 and 7).

d) Evaluating the validity of the so-called "system" approach under scale-up conditions of diameter and length, especially for dense-phase (Chapter 8).

e) Investigating and developing a validated procedure to predict the minimum transport condition (or unstable boundary) for dense-phase conveying of powders (Chapter 9).

f) Developing a validated test-design/modelling procedure for solids friction for the accurate scale-up prediction of pressure drop for fluidised dense-phase pneumatic conveying systems (Chapter 10).

g) Evaluating the different existing/popular bend models for their suitability and accuracy for the dense-phase conveying of powders (Chapter 11).

The outcome of this study will benefit the industry through:

i) Reducing air flow and compressor power requirements (providing less green-house gas emissions).

ii) Minimising the design margin on the predicted values of pressure drop.

iii) Optimumising pipe size calculation.

iv) Improving the ability to troubleshoot pneumatic conveying systems.

v) Industry accepting the fluidised dense-phase pneumatic conveying technology as an efficient and environment-friendly mode of conveying.

NOTES:

1.   This thesis essentially investigates and seeks to improve the modelling of solids friction for horizontal straight pipes. Hence, unless otherwise stated, terms such as "solids friction" and "solids friction factor" would relate to horizontal straight pipe lengths.

2.   In this thesis, terms such as "powders" and "fine powders" refer to powders that have good air retention properties (i.e. fluidise well upon aeration). Some examples include: cement, fly ash, pulverised coal, skim milk powder, carbon fines, certain grades of alumina and ESP dust.

CHAPTER 2: Literature Review

The purpose of this Chapter is to present a review of the various studies conducted over the years (by different researchers) on the subject of modelling pressure drop for dense-phase pneumatic conveying of fine powders. During the initial part of the thesis, the majority of the studies was focused on solids friction through straight pipes (especially, horizontal). Afterwards, it was realised that the issue of pressure drop in bends was also important (for predicting total pipeline pressure loss) and due attention was provided in this area.

In line with the broad scope of the thesis, a conscious effort is being made to present here only those studies that deal with fine powder transport in dense-phase, but in some cases references to dilute-phase and coarse particle conveying are also provided for their apparent potential towards modelling the dense-phase conveying of fine powders. Reports on previous studies are presented in chronological order as far as possible to illustrate the evaluation of the various modeling methods over time (covering about a span of 50 years). This chapter has been written intentionally without any subheadings (such as straight pipe pressure drop, bend loss etc), as many of the previous studies being referred to here had explored multiple aspects of pressure loss under one reference (such as "straight pipe" loss, pressure drop in bends and loss due to the verticals). This makes it difficult to precisely categorise them under a particular subheading. It is to be noted that the literature review extends into various other areas related to multiphase systems, such as fluidisation/fluidised-beds, turbulence modulation due to "two-way" coupling, slurry flow etc. These are not being included and reviewed here, but are referred to in (other) appropriate chapters of this thesis.

One of the earlier researchers to propose an expression for pressure drop for solids-gas flow in a straight horizontal pipe was Barth (1958). He considered that total losses due to the solids-gas mixture can be represented as the sum of individual losses due to the solids and gas only, as given by equation (2.1).

$$\Delta P = (\lambda_f + m^* \lambda_s)\ L/D\ \rho\ V^2/2 \tag{2.1}$$

This expression was considered by Weber (1981) as applicable for "especially dilute conveying" (in fact, representation of equation 2.1 suggests distinctly separate existence of solids and gas-phase, which seems to indicate dilute-phase flow). However, this equation has been used subsequently by various researchers (Stegmaier, 1978; Rizk, 1982; Pan, 1992; Pan and Wypych, 1998; Wypych, 1989; Jones and Williams, 2003; Williams and Jones, 2004) to predict the pressure loss for dense-phase flow of fine powders, such as fly ash. Undoubtedly, Barth's representation has remained the most popular (and fundamental) equation for accounting solids friction in pneumatic conveying systems (dilute- and fluidised dense-phase).

Schuchart (1968) was one of the first researchers to study the gas-solid flow through pipe bends (Marcus et al., 1990). His work was based on a number of different bends using glass and plastic as the test materials. However, the particles were of a rather larger size, 1.5 to 3 mm in diameter for volumetric concentrations up to only 5%. The

solids contribution of the pressure drop due to solids-gas flow through bends was expressed as:

$$(\Delta p_{\text{bend}} / \Delta p_z)_{\text{solids}} = 210 (2R_B / D)^{-1.15} \tag{2.2}$$

where, $(\Delta p_z)_{\text{solids}}$ is the pressure drop due to solids for an equivalent straight length of the bend, to be obtained from using solids friction model (for straight pipes). Finally, the total loss through the bend is to be calculated by adding the pressure drop due gas-only friction term with $(\Delta p_{\text{bend}})_{\text{solids}}$. Ito's (1959) expression can be used to calculate the gas-only pressure drop for bends (Marcus et al., 1990; Wypych and Pan, 1991). It is to be noted that the equation (2.2) includes the $(\Delta p_z)_{\text{solids}}$ term, the reliability of Schuchart's (1968) bend model would depend on the accuracy of modelling solids friction through straight pipes.

Mason and Boothroyd (1971) studied the axial pressure gradient in vertical pipe flow by pneumatically conveying alumina of different mesh sizes (fine to coarse) through vertical test sections under dilute-phase condition (m* < 10). They mentioned that fine particles behave differently than coarser materials and would follow the random motion of the gas more closely because of their smaller sizes. Due to their "close spacing", fine particles were mentioned to have a greater potential to interfere with gas turbulence. A combined friction factor for the suspension was expressed as:

$$\lambda_T = \Delta P \, D/(0.5 \, \rho \, V^2 \, L) \tag{2.3}$$

9

Values of λ_T/λ_f were plotted against m* for different mesh sizes and it was concluded that there was a non-linear variation of λ_T/λ_f with an increase in the value of m*.

Pressure drop due to the suspension flow of fine particles around vertical to horizontal 90 degree bends were studied by Mason and Smith (1973) by pneumatically conveying alumina of different mesh sizes (fine to coarse) through bends of different geometries. Tests were carried out in dilute-phase mode (m* < 10). The pressure drop through bends was expressed by introducing a bend resistance number (Ψ_{bs}) for the suspension, which was defined as:

$$\Psi_{bs} = \Delta P_b\, D/(0.5\, \lambda_f\, V^2\, L) \tag{2.4}$$

It was found that at very low values of m* (m* < 2), the increment of Ψ_{bs} with an increase in m* was non-linear. For m* > 2, the trend became linear.

The work of Stegmaier (1978) was a major advancement towards the use of power function type formats to represent solids friction factor. His work was subsequently considered by Weber (1981) and Weber (1982). Stegmaier investigated a number of fine and coarse particles, including fly ash, alumina, quartz powder, sand, catalyst for horizontal transport (with particle size and particle density ranging from 15 to 112 μm and 1500 to 4100 kg/m^3, respectively) and established a correlation for solids friction factor, which can be expressed as:

$$\lambda_s = 2.1\, m^{*-0.3}\, Fr^{-2}\, Fr_s^{0.5}\, (D/d_s)^{0.1} \tag{2.5}$$

From the range of values of Fr shown in the plot of λ_s m*$^{0.3}$ Fr Fr$_s$$^{-0.25}$ (D/d$_s$)$^{-0.1}$ versus Fr (Stegmaier, 1978), it seems that Stegmaier had conveyed the products from dilute-to dense-phase. However, there appear to be some uncertainties in the definition of Fr$_s$. Stegmaier (1978) and Weber (1982) used Fr$_s$ = ω_{fo}/(d$_s$g)$^{0.5}$, whereas Weber (1981) used Fr$_s$=ω_{fo}/(Dg)$^{0.5}$.

Rizk (1982) attempted to identify the factors that contributed to the overall solids friction factor (λ_s). He mentioned λ_s can be separated into two terms:

$$\lambda_s = \lambda_s\text{* } C/V + 2\beta/ \{(C/V) Fr^2\} \tag{2.6}$$

where, λ_s* is related to the impact and friction of the solid particles (particle to particle/wall). The term [2β/ {(C/V) Fr^2}] takes into account the influence of weight (i.e. energy loss due to keeping the particles in suspension). It is interesting to note that β refers to the particle fall velocity in a cloud. This indicates Rizk (1982) considered the individual particles in suspension to be influenced by its surrounding particles. This form of representation was provided also in Marcus et al. (1990).

Mills et al. (1982) appears to be first researchers to propose a design tool for scaling-up test rig conveying characteristics to larger/longer industrial systems. Their scale-up laws were subsequently modified by Wypych and Arnold (1987) to improve scale-up accuracy. Details of their work are provided in Chapter 8.

Wirth and Molerus (1983) developed an expression for pressure drop for strand conveying by introducing a dimensionless friction number term:

$$\text{Fri} = V / [(\rho_s/ \rho) (1 - \rho_s/ \rho) (1 - \varepsilon) D g f_r]^{0.5} \tag{2.7}$$

It has been observed experimentally that there exists a dense non-suspension layer at the bottom of pipe for the dense-phase conveying of fine powders, on top of which a dilute-phase suspension flow occurs, resembling a strand. Therefore, this work (Wirth and Molerus, 1983) is considered of interest to this thesis. Wirth and Molerus (1983) did not validate their model under scale-up conditions.

Marcus et al. (1984) compared the pressure drop occurring in long and short radius bends and a blind tee bends. Fine powder (cement) was used as the test material. They found that the long radius bend produced a larger pressure drop than the short radius bend. This was reported as "contrary to popular belief".

In order to investigate the suitability of material conveying in dense-phase, Wypych and Arnold (1984) tested seven products, out of which three materials (cement, pulverized coal and power station fly ash) are believed to be potential candidates for fluidised dense-phase. Using different test rings (combinations of four pipe lengths and three pipe diameters), Wypych and Arnold (1984) experimentally determined the blockage boundary for the above materials. The authors, however, had experienced considerable difficulties in obtaining a well-defined locus of blockage conditions.

Similar work was presented by Wypych and Arnold (1985), where they described a standardized test procedure for designing pneumatic conveying systems.

The pressure loss due to the initial acceleration (at product feed zone) and flow through bends were studied by Marcus et al. (1985). For acceleration pressure loss (ΔP_{accel}), the model provided in equation (2.8) was proposed. In this expression, ρ and V are the density and velocity of the gas at the solid intake zone respectively as per Marcus et al. (1990). The formula presented for bend pressure loss is given in equation (2.9).

$$\Delta P_{accel} = m^* \, \rho V \, C \tag{2.8}$$

$$\Delta P_b = B \, \rho \, V^2/2 \tag{2.9}$$

The value of B can be determined from the following table:

Table 2.1: Values of bend pressure loss factor, Marcus et al. (1985)

'Please see print copy for image'

The above table indicates that the sharper the bend, the higher the calculated pressure drop.

Bohnet (1985) investigated solids friction for strand type conveying using the data of several products including fly ash, fire-extinguisher powder, catalyst and silica sand. For strand type conveying, he modified equation (2.6) to:

$$\lambda_s = \lambda_s^* \, (m_1^*/m^*) \, w_{p1} / V + 2\beta \, (m_2^* / m^*) / \{(w_{p2}^2 / V) \, Fr\} \qquad (2.10)$$

where, m_1^* and m_2^* are the solids loading ratio above and within the strand and w_{p1} and w_{p2} are the solid velocities above and within the strand, respectively. This appears to be somewhat contradictory to the physical flow phenomenon, as one would have expected m_2^* to be associated with the λ_s^* term (inter-particle impact/friction are expected to be more prominent within the strand, assuming there is some degree of turbulence within the strand to cause the impact) and m_1^* to be associated with the $2\beta / \{(w_{p2}^2 / V) \, Fr\}$ (describing energy loss to keep the particles in suspension). However, as this model contains terms such as w_{p1}, w_{p2}, which are difficult to measure/estimate (especially for fine powders), further studies to answer the above doubts were not pursued. In fact, the author of this paper (Bohnet, 1985) commented that for practical purposes, it is usually easier to measure the value of λ_s directly than to calculate it from the knowledge of λ_s^*, β, m_1^*, m_2^*, w_{p1} and w_{p2}.

Mills and Mason (1985) examined the influence of bend geometry on pressure drop in pneumatic conveying pipelines in a test program in which long radius bends, short radius bends, elbows and blind tees were investigated. Tests were performed using pulverised fuel ash in a 50 mm bore horizontal pipeline having a double loop

14

configuration under both dense and dilute flow condition. The ratio of bend diameter to pipe bore are 24:1, 6:1 and 2:1 for long radius, short radius and elbows respectively. From the plots, it was stated that with blind tee, the pressure drop in the pipeline was about 40% greater than that for the line using long radius bends, in both dense and dilute-phase flows. Also, it was suggested that the elbows were slightly better than long radius bends from the aspect of minimising pressure loss. Furthermore, from the comparison of the short radius and long radius bends, it was suggested that the short radius bends are generally the best in terms of minimum pressure drop. However, with very high solid flow rate condition, the long radius bends are slightly better. The blind tees were referred to as the worst choice from the view of pressure loss.

Chambers and Marcus (1986) presented a set of models to predict the total pipeline pressure drop using a so-called "component" approach, i.e. by individually calculating straight pipe drop, bend loss, vertical lift loss and loss due to the initial acceleration, using the following relationships:

Acceleration loss : $\Delta P_{accel} = \rho V^2 (1 + 2m^* \, C/V)/2$ (2.11)

Vertical loss : $\Delta P_v = m^* \, \rho \, g \, L_v \, V/C$ (2.12)

Straight pipe loss : $\Delta P = (\lambda_f + m^* \lambda_s) \, L/D \, \rho \, V^2/2$ (2.13)

Bend loss : $\Delta P_b = N \, B \, (1 + m^*) \, \rho \, V^2/2$ (2.14)

Total loss : $\Delta P_T = \Delta P_{accel} + \Delta P_v + \Delta P + \Delta P_b$ (2.15)

$\lambda_s = 2.1 \, m^{*-0.3} \, Fr^{-1} \, Fr_s^{0.25} \, (D/d_s)^{0.1}$ for $d_s < 0.5$ mm (2.16)

Chambers and Marcus (1986) did not provide any derivation or reference for the bend model. It was stated that the model generally predicted the pipe pressure loss "to better than a factor of 2" for wide range of m* from 2 to 530. However, the model performance was observed to get decreased with increasing value of pipe length and for pipe length greater than 500 m. It was claimed that using $Fr_s = \omega_{fo} /\sqrt{gD}$ instead of $Fr_s = \omega_{fo}/\sqrt{g}\, d_s$ may introduce some improvement. In any case, an uncertainty factor of 2 (even within 500 m length) can not be acceptable as a reliable design procedure.

Westman et al. (1987) conducted studies on bend pressure loss by conveying four different coarse materials (dilute-phase flow) through 90 degree bends of various geometries. The authors proposed that total bend loss can be expressed as a sum of air and solids only pressure drop through the bend. The solids contribution of the bend loss was expressed as:

$$\Delta P_{bs} = 0.5\, \lambda_{bs}\, \rho\, V^2 \tag{2.17}$$

where, λ_{bs} was empirically found as: $\lambda_{bs} = 5.4\, m*^{1.293}\, Fr^{0.84}\, (R/r)^{0.39}$ $\qquad$ (2.18)

It appears that the authors obtained experimental bend loss values by installing a number of pressure transducers (in succession) before and after the bend and by using a method of "pressure drop gradient". However, Pan (1992) had shown that this approach can be quite inaccurate, where a change (or inaccuracy) of only ± 1.8 % in static pressure measurement can result in ± 62.8 % variation in estimated bend pressure drop.

Michaelides (1987) derived an expression for pressure drop for horizontal straight pipes, as given in equation (2.19):

$$\Delta P = \Delta P_0 \left[1 + k \ m^* \ (Dg)^{0.5}/(V \ \lambda_f)\right] \qquad\qquad (2.19)$$

Combining test data of several products (such as coal, sand, wheat etc), the value of "k" was found as 0.72. It is believed that the model is applicable to dilute-phase flow. Michaelides (1987) did not validate the accuracy of his model under scale-up conditions.

The issue of pressure drop through bends was further taken up by Bradley and Mills (1988). They argued that a more accurate estimation of the overall pressure loss can be achieved by estimating the pressure drop through the bends and straight sections separately, rather than the previous approaches of dealing with total pipeline losses (Mills, 1982). Also, it was pointed out that the concept of correlating the equivalent length with pipeline inlet air velocity for predicting the bend pressure loss suffers fundamentally from a limitation that due to the falling pressure along the pipeline, the air expands continuously, resulting in an increase in conveying air velocity. Hence, the equivalent length does not remain constant. Wheat flour was conveyed in a 2 inch nominal bore (53 mm internal diameter) pipeline, having $R_B/D = 5.3$. The bend affected zone was about 8 m for high velocity (suspension flow) and about 2 to 4 m for low velocity (non-suspended flow). A plot of the pressure drop caused by the bend against the bend exit velocity for different suspension velocities indicated that

pressure drop caused by the bend increases with an increase in exit air velocity from the bend and suspension density.

Studies, similar to the above, were further conducted by Bradley (1989) using pipeline loops of 2, 3 and 4 inch nominal bore. In the test program, bends of seven different designs with different radii were used. One of the materials tested was white wheat flour. A wide range of conveying conditions was employed (V = 4 to 45 m/s; m* = 0 to 130). The following model was used to define the bend pressure loss:

$$\Delta P_b = \frac{1}{2} K_b \, \rho_{sus} \, V^2 \tag{2.20}$$

where, ρ_{sus} is the suspension density (kg of product flowing per cubic meter of conveying air). A plot of "K_b" versus suspension density showed that with an increase in suspension density from about 50 to 150 kg/m^3, the "K_b" values continued to drop and then became constant. The trend was applicable for white wheat flour only. Bradley (1990) conducted further studies on the bend pressure drop with test programs similar to that presented by Bradley (1989) using wheat flour and with seven different types of bends. It was concluded that all radius bends produce similar loss, irrespective of the radius of curvature of the bends. This seems to contradict the findings of Mills and Mason (1985).

Wypych (1989) wrote a thesis that covered various aspects of the design of pneumatic conveying systems. Fine powders such as pulverised coal, fly ash and fly ash/cement mixture were conveyed using different test rigs. His work included establishing the

18

conveying characteristics of the fine powders, exploring scope of improvement of the previously used scale-up techniques and developing a test-design procedure to determine an accurate solid friction factor correlation.

Wypych and Arnold (1989a) and Wypych et al. (1989b) explored the optimisation of long distance, large throughput pneumatic conveying systems. Using fine pulverised coal as a test material and a test design procedure proposed by the authors, the following correlation for λ_s (equation 2.21) was obtained. The authors had also investigated stepping pipeline criteria.

$$\lambda_s = 1.8076 \ (m^*)^{-0.5} \ (Fr_m)^{-0.1.423} \ (\rho_m)^{-0.2846} \tag{2.21}$$

Wypych et al. (1990, 1990a) conducted further investigations into long distance conveying of fine pulverised coal (d_{50} = of 21μm; ρ_s = 1495 kg/m^3). Experimental PCC (for pipeline of length up to 947.5 m) showed important design criteria, such as the unstable duning boundary. A model for solids friction was presented as:

$$\lambda_s = (m^*)^{-0.4555} \ (Fr_m)^{-1.3419} \ (\rho_m)^{-0.2931} (D)^{-0.1088} \tag{2.22}$$

Wypych et al. (1990, 1990a) also presented a dilute-phase model (equation 2.23), which was based on equation (2.6), originally presented by Rizk (1982). Wypych et al. (1990, 1990a), however, replaced the term $\beta = w_f/V$ by $\beta_0 = w_{fo}/V$.

$$\lambda_s = \lambda_s^* \ C/V + 2\beta_0/\{(C/V) \ Fr^2\} \tag{2.23}$$

where, $C/V = 1/[1 + w_{fo}(\lambda_s*/(2gD))^{0.5}]$ (2.24)

Wypych and Pan (1991) conducted tests to investigate the validity of existing models to calculate pressure drop in smooth turbulent flow in straight pipes and pressure loss through bends for air-only flows. It was concluded that the existing models can be applied, i.e. the models of Blasius (1913) and Ito (1959), provided mean conditions (based on average air density) for straight sections of pipe and conditions at the outlet of bend were used in the analysis, respectively.

Weber (1991) investigated several formats of solid friction factor for fine granular solids. As opposed to Weber (1981), where pressure drop due to air-only and that due to solids-only were considered separately, he suggested that the pressure drop of the solids air mixture was integral in nature (i.e. the pressure drop due to air-only and that due to the solids-only were difficult to separate individually) and developed a new format of representing pressure drop:

$\Delta P = \lambda_T \rho\, V^2 L/2D$ (2.25)

Weber (1991) did not validate his model under scale-up of length and diameter.

Pan and Wypych (1992) conducted extensive studies to find out the expressions for the solids friction factor through straight pipe (λ_s) and bends (λ_{bs}). They expressed the pressure drop due to solids-air flow through straight section and bends as below:

$$\Delta P = \Delta P_f + \Delta P_s \tag{2.26}$$

$$\Delta P_b = \Delta P_{bf} + \Delta P_{bs} \tag{2.27}$$

The authors represented their data using simple power law curve fit models for solids friction factor through straight pipe sections and bends (λ_s and λ_{bs}, respectively) as follows:

$$\lambda_s = x1 \, (m^*)^{x2}(Fr_m)^{x3}(\rho_m)^{x4} \tag{2.28}$$

$$\lambda_{bs} = y1 \, (m^*)^{y2}(Fr_{bo})^{y3}(\rho_{bo})^{y4} \tag{2.29}$$

where, x1, y1 are the constants and x2, x3, x4, y2, y3, y4 are the exponents of power function. Power station fly ash was conveyed through different test rigs, having lengths of 102, 135, 137 m and diameters of 52.5 and 80.5 mm. From the test data obtained, the values of constants and exponents of power function were determined by using the technique of "minimising the sum of square errors".

Pan (1992) wrote a thesis, which was aimed towards improving the scale-up procedures for the design of pneumatic conveying systems. Based on mathematical and dimensional analysis, semi-empirical correlations were derived predicting the solids friction through bends and straight pipes. Fly ash was used as the test material for majority of the experiments with d_{50}, ρ_s and ρ_{bl} as 15.5 μm, 2197 and 634 kg/m^3, respectively. Some of the major findings of his thesis were presented in Wypych and Pan (1991) and Pan and Wypych (1992). To properly investigate the issue of bend pressure drop, Pan used a test bend between two long horizontal straight pipes

sections (i.e. the test bend was sufficiently distant away from the influence of any other bends). Bends with different R_B/D ratio were used. By "minimising the sum of squared errors", Pan (1992) derived the following bend model for long radius bends:

$$\Delta P_{bs} = 0.5 \; m^* \; \lambda_{bs} \; \rho_{bo} \; V_{bo}{}^2 \qquad (2.30)$$

where, $\lambda_{bs} = 0.0052 \; (m^*)^{0.49} \; (Fr_{bo})^{1.1182} \; (\rho_{bo})^{-0.1286} \qquad (2.31)$

Similar use of dimensionless groupings can be found in Wypych (1993) and Arnold et al. (1994). However, it is to be noted that Pan (1992) did not derive other bend models by installing his test bend at (other) different locations along the pipe. It would have been interesting to evaluate whether the "constant" and exponents of equation (2.31) would have differed depending on the location of the test bend in pipeline. Also, Pan (1992) obtained his model for horizontal to horizontal bends. It is possible that the model is not valid for horizontal to vertical or vertical to horizontal bends.

Keys and Chambers (1993, 1995) carried out the power function modeling approach for solids friction with different fly ash samples as the test material using different test rig configurations. Expressing pressure drop of the entire pipe as $\Delta P_T = (\lambda_f + m^*\lambda_s) \; L \; \rho \; V^2/2D$ (i.e, including the effects bends), the solid friction factor (λ_s) was derived as:

$$\lambda_s = 0.75 \; (m^*)^{-0.3}(Fr)^{-0.58} \qquad (2.30)$$

22

By eliminating the bend effects (calculated as per Chambers and Marcus, 1986) from the total pipeline pressure loss, the correlation for λ_s was derived as:

$$\lambda_s = 1.24 \ (m^*)^{-0.3}(Fr)^{-0.73} \hspace{4cm} (2.31)$$

Using the above correlation, the predicted values of the pipeline friction drop were calculated within 10% of the measured pipeline pressure loss. Incorporating the effect of d_s/D, the above correlation was modified to:

$$\lambda_s = 0.553 \ (m^*)^{-0.3}(Fr)^{-0.73} \ (d_s/D)^{0.1} \hspace{3cm} (2.32)$$

Keys and Chambers (1993, 1995) did not validate their models for length and/or diameter scale-up conditions.

Pan et al. (1994) studied the conveying characteristics for powders by conveying different samples of coal and fly ash (ρ_s 1390 to 2197 kg/m^3; ρ_{bl} 541 to 634 kg/m^3; d_{50} 16 to 41 μm) in various test rig combinations (D = 25.4 to 105 mm; L = 48 to 553 m). They concluded that fine powders can be transported smoothly and reliably from dilute- to dense-phase. A correlation for the pressure minimum curve (PMC) was also provided. However, it is to be noted that the above PMC were based on total pipeline PCC. The shape of total pipeline PCC (and hence position of PMC) is significantly influenced by the numbers, types and location of bends and verticals in the pipeline. In other words, PMC based on the total pipeline PCC is very much layout dependent

23

of the particular test rig. Hence, the usefulness of deriving such a correlation for PMC is not very clear. Similar skepticism was also raised by Mason et al. (1998).

Further research was conducted by Pan and Wypych (1998) on scale-up test design procedures by conveying four different samples of fly ash (ρ_s 2197 to 2540 kg/m^3; ρ_{bl} 634 to 955 kg/m^3; d_{50} 4 to 58 µm) in various test rig combinations (D = 52.5 to 105 mm; L = 70 to 564 m). It was found that different fly ash samples produce different conveying characteristics. Also, the corresponding models for solids friction for horizontal straight pipes and bends (in the form of equations 2.28 and 2.29, respectively) were also found to be different. Combining the data of all four fly ash samples, the following correlations were derived (exponents are quoted up to 2 significant figures):

$$\Delta\lambda_s = 3.2343 \ (m^*)^{-0.47} \ (Fr_m)^{-1.56} \ (\rho_m)^{-0.43} \tag{2.33}$$

$$\Delta\lambda_{bs} = 0.0097 \ (m^*)^{0.57} \ (Fr_{bo})^{0.97} \ (\rho_{bo})^{-0.62} \tag{2.34}$$

It is to be noted that previously Bradley (1989) mentioned the equivalent length of bends depend strongly on conveying conditions (air velocity and solids loading) and is affected by product and bend type. As a result of this, the true equivalent length of a bend will depend heavily on the location of the bend in pipeline and also on "many other factors" and that is why the bend and straight lengths will have to be measured and scaled separately. Equations (2.33) and (2.34) appear to suggest the same that different expressions for solids friction exist for straight pipes and bends.

In recent years, Datta and Ratnayaka (2003) investigated the characteristics of solids friction for horizontal and vertical conveying for both dilute- and dense-phase systems. Instead of considering air and solids friction drop separately (as given by Weber, 1981), they considered the solids-air mixture as an integrated entity having its own flow characteristics. Pressure drop for a straight pipe section (horizontal or vertical) was expressed as:

$$\Delta P = K \, L \, \rho_{sus} \, V_{entry}^2 / 2D \qquad\qquad (2.35)$$

In the calculation of ρ_{sus}, gas volume was calculated at the entry of a pipe section. Barite (ρ_s: 4200 kg/m^3; "mean particle size": 12 μm) and cement (ρ_s: 3100 kg/m^3; "mean particle size": 15.5μm) were conveyed through three test rigs: L = 75 m, L$_v$ = 8.25 m, D = 80 mm; L = 66 m, D = 100; L = 68 m, D = 125 m. Using pressure drop values recorded by the several pressure transmitters installed along the horizontal and vertical sections, "K" values were obtained for all the tests. The distances between two consecutive transmitters were always kept limited to within 3 m. This can be a point of concern. Because of the considerable fluctuation in the pressure signal of a solids-gas system, it may be quite difficult to obtain an accurate estimate of pressure differential between two pressure transmitters, particularly if they are separated by such small distance. A detail analysis of this aspect is provided in Chapter 4 of this thesis. Datta and Ratnayaka (2003) obtained plots of the calculated values of "K" versus V_{entry}^2 for both the products and different pipelines. Plots for barite (for both horizontal and vertical sections) for D = 80 and 100 mm are shown in Figure 2.1 and 2.2, respectively.

'Please see print copy for image'

Figure 2.1: Variation of "K" for barite for horizontal and vertical sections, D = 80 mm (Datta and Ratnayaka, 2003)

'Please see print copy for image'

Figure 2.2: Variation of "K" for barite for horizontal and vertical sections, D = 100 mm (Datta and Ratnayaka, 2003)

Afterwards, data from all three pipes (D = 80, 100 and 125 mm, for barite) were combined and plotted in similar format, as shown in Figure 2.3.

'Please see print copy for image'

Figure 2.3: Variation of "K" for barite for horizontal section, D = 80, 100 and 125 mm (Datta and Ratnayaka, 2003)

From the above plots, it was commented that all the data followed the same trend and "K" was stated to be independent of pipe size. This made the authors comment that the "K" method would be a "valuable tool for scaling up to any pipe size". It is to be noted that as per Figure 2.3, the "K" factor becomes highly sensitive to the change in (air velocity)^2 values at the low values of (air velocity)^2, with sharp increase in K, even with a small decreases in (air velocity)^2. The above work, though claimed to have obtained a "simple technique" for scale-up, has certain areas of uncertainty that must be addressed. In Figures 2.1 to 2.3, almost all of the "K" values seem to be within the upper range of 0.00055 (only one data point was found having K = 0.001 and there could be some scepticism whether this was a valid data point as it is surprisingly far away from the other data). In spite of this, the plots had their maximum ordinate at 0.0014. Such representation makes it considerable difficult to

properly examine the scatter of data (the data sets look closely spaced) and this can be misleading. It may be possible that "K" values for all three pipes followed the "same trend", but that does not guarantee that the data will have same values, i.e. the resulting relationship between "K" and V_{entry}^2 could actually be quite different depending on pipe size, in contrary to the conclusion of (Datta and Ratnayaka, 2003). Furthermore, specifically addressing the generalised curve shown in Figure 2.3, it would have been interesting if the authors had used the relationship (shown by the curve passing through the data points) to predict pressure losses under significant scale-up conditions of length and/or diameter. Results of such evaluation were not presented. Therefore, there exist sufficient uncertainties in this modelling approach ("K" method) to believe that accuracy of this method is inconclusive unless scale-up evaluation is pursued. Similar approach was further extended Datta and Ratnayaka (2005) and Ratnayake et al. (2007) using other product data (such as cements, alumina etc) and for studying bend losses.

Jones and Williams (2003) investigated the solids friction factor for fluidised dense-phase transport. Conveying various powders, such as pulverised fuel ash, iron powder, copper ore and flour (ρ_s: 1470 to 5710 kg/m^3; "mean diameter": 42 to 90 μm) in a test rig (L = 50 m, D = 53 mm, 9 bends), the following model for solids friction factor was derived used "back calculation" method:

$$\lambda_s = 83/\{(m^*)^{0.9} \, Fr_i^2\} \tag{2.36}$$

The magnitude of the "constant" term of the above power function model appears large compared to the other previous models (Wypych, 1989, 1990; Pan and Wypych, 1998; Keys and Chambers, 1993, 1995). Calculated values of total pipe pressure drops, using the above expression for λ_s, when compared with the measured values, resulted in an average error of only 2% and an associated standard deviation of 12%. It is to be noted that the model (equation 2.36) was obtained using "back calculation" method from the same total pipeline pressure drop data. Hence, it is expected that the model will agree with the experimental data quite well. It was concluded that fluidised dense-phase type flow is relatively insensitive to the material properties (provided the materials have sufficient air retention capability to be conveyed in fluidized dense phase flow), since it was possible to assign a single model to represent the pressure drops of the various products having different physical properties. The authors remarked this as "counter to existing expectations". A possible reason of the above could be: as there were too many (9) bends in such a short pipe (50 m length), so the predicted bend losses (using Chambers and Marcus, 1986 model) were a major loss for the pipe, leaving only a small magnitude of "straight pipe" losses obtained by "back-calculation" method. Thus, "straight pipe" losses being numerically within a narrow range, there were not much variations in the derived models for λ_s. Scale-up accuracy of the derived λ_s model was not tested.

Williams and Jones (2004) conducted further studies to model solids friction for cement meal, having d_s: 22 μm, ρ_{bl}: 1300 kg/m^3 and fluidised bulk density: 930 kg/m^3. The cement meal was conveyed in a 50 mm nominal bore pipeline, 176 m in

length, with 14 short radius bends. The pressure drop of the system was expressed by the following equation:

$$\Delta P = (m^* \lambda_e) \, \rho_m \, V_m{}^2 \, L/2D \qquad\qquad (2.37)$$

It is interesting to note that Williams and Jones (2004) had opted for a combined single friction factor (λ_e) representing losses due to both air and solids. Using a back calculation method, the following model was obtained:

$$\lambda_e = 104 \, m^{*-0.9} \, Fr^{-2.2} \qquad\qquad (2.38)$$

Again, it can be observed that the magnitude of "constant" term of the above power function model appears large. Similar modelling using "back calculation" method was further pursued by Williams and Jones (2006).

From the above studies, it is evident that considerable discrepancies exist between the various models for solids friction derived by the various researchers over the years. Also, the models were not tested under scale-up conditions of length and/or diameters for their scale-up accuracy and stability. Hence, it is evident that further research is to be conducted to understand solids-gas flow and to predict pressure loss accurately under a wide range of scale-up conditions. However, it is to be appreciated that the development of friction factor relationships for the turbulent flow of even single fluids took researchers almost one hundred years (Darcy, 1857 to Moody and Princeton, 1944) and was purely based on empirical methods using dimensionless

parameter groupings such as Reynolds number (Nikuradse, 1932; Colebrook, 1939; Moody and Princeton, 1944; Swamee and Jain, 1976). Therefore, it may still take some time and effort before "dense" turbulent solids-gas flows can be modelled accurately.

CHAPTER 3: Test Facility and Procedures

3.1   Introduction

The pressure drop characteristics of pneumatic conveying systems depend to a great
extent on the product properties, such as particle size, size distribution, particle and
bulk densities, shape and surface roughness (Pan, 1992). A change in any (or in
combinations) of the above can cause significant variations in solids friction, even for
the same pipe (Wypych, 1989). Due to such strong (and complex) product property
dependence, especially for fluidised dense-phase conveying, no procedure has been
established so far for modelling and prediction of solids friction based on bench-scale
testing of product properties. As a result, pilot-plant testing is often necessary,
although such work requires significant capital investment and large space
requirement (to build-up the test rigs), also the time spent and operating cost for the
conveying trials are quite significant. The conveying characteristics obtained from the
testing of products in short and/or small test rigs, can be directly used to predict
pressure drops in larger and/or longer pipelines using suitable scale-up techniques
("system" approach, as described by Mills, 2004). Alternatively, models for solids
friction can be derived using the test data, which can be used to predict pressure drop
for scale-up systems using "component" approach (such as Chambers and Marcus,
1986; Wypych, 1989; Bradley, 1989; Pan, 1992; Jones and Williams 2003; Williams
and Jones 2004). Also, the conveying characteristics obtained from such pilot-plant
testing can be used to evaluate a material's suitability to be conveyed pneumatically
either in dense- or even dilute-phase, to predict minimum transport boundaries and
any unforeseen operational problems may be identified (Wypych, 1989). For this
thesis, test data (and conveying characteristics) from various pipes of different

diameter and length were considered to be important for derivation of models for solids friction and their scale-up evaluations.

3.2   Experimental program

The initial plan was to carry out extensive test program with different powders in various pipelines of different diameters and lengths (mainly for the purpose of modelling and scale-up evaluation), and also to explore the effectiveness of direct differential pressure (DP) measuring arrangement for fine powders (mainly in dense-phase) by installing the same in straight pipe lengths. However, due to various unforeseen circumstances, such as compressor breakdown, wearing out of pipeline bend and finally reconstruction of laboratory building, the progress of the experimental work was severely hindered. Only the testing of DP measuring arrangement could be pursued in one pipeline using "white powder" (this product was obtained for the purpose of a contract research project). It was decided that extensive test data of previous experimental programs (Wypych, 1989; Pan, 1992; Wypych et al., 2005) carried out in the Bulk Material Handling Laboratory (University of Wollongong) with various powders conveyed in different pipelines would be used in this thesis. Test data of work carried out by other researchers were also used and these are referenced.

3.2.1   Properties of test products

Test data from the following powders were used in this study for the purpose of modelling and scale-up:

a) Fly ash (Wypych et al., 2005)

b) ESP dust (Wypych et al., 2005)

c) "White powder"

d) Fly ash (Pan, 1992)

e) Pulverised brown coal (Pan, 1992)

f) Fly ash and cement mixture (Wypych, 1989)

Table 3.1 lists the physical properties of these powders:

Table 3.1: Some Physical Properties of the Powders

Product	ρ_s (kg/m3)	ρ_{bl} (kg/m3)	d_{50}* (μm)
Fly ash (Wypych et al., 2005)	2300	700	30
ESP dust (Wypych et al., 2005)	3637	610	76.6
"White powder"	1600	620	55
Fly ash (Pan, 1992)	2197	634	16
Pulverised brown coal (Pan, 1992)	1488	437	26
Fly ash (89% weight) and cement (11% weight) mixture (Wypych, 1989)	2130 3100	700 950	19 20

* d_{50} : median particle size

Unless otherwise mentioned, "fly ash" and "ESP dust" data refers to the experimental data provided in Wypych et al. (2005) for these powders.

Particle size distribution was determined using a laser diffraction analyser (Malvern, Mastersizer 2000) and particle density was measured using a pycnometer.

The work on minimum conveying criteria (Chapter 9) has used the conveying data of several other products, obtained from the work carried out by previous other

researchers. Some physical properties for these products are provided in Table 9.3 and 9.4.

3.2.2 Pneumatic conveying test facility

Wypych et al. (2005) conveyed power station fly ash and ESP dust (from dilute- to fluidised dense-phase) through different diameters and lengths of pipes (69 mm I.D. × 168 m, 105 mm I.D. × 168 m and 69 mm I.D. × 554 m long). A schematic of the test set up for the 69 mm I.D. × 168 m long pipline (for fly ash) is shown in Figure 3.1.
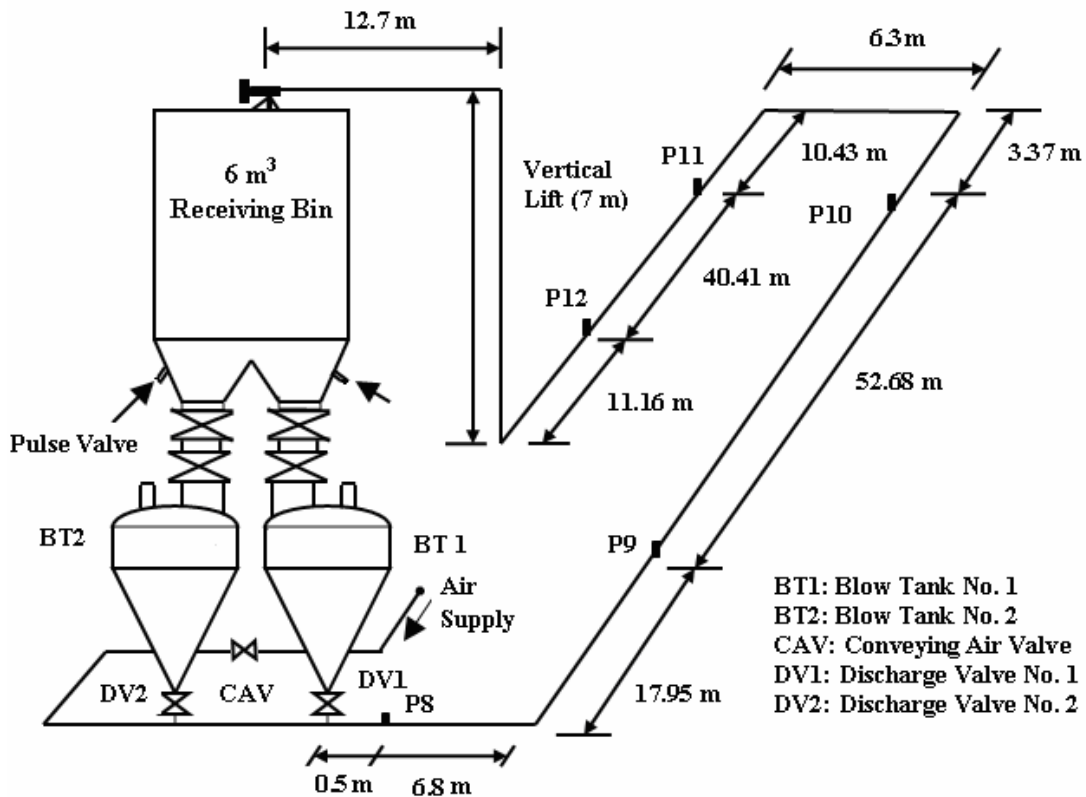
Figure 3.1: Layout of the 69 mm I.D. × 168 m Long Test Rig (for Fly Ash)

The test facility comprised:

- Tandem 0.9 m^3 bottom-discharge blow tank feeding system;

- 69 mm I.D. × 168 m long mild steel pipeline, including 7 m vertical lift, five 1 m radius 90° bends and 150 mm N.B. tee-bend connecting the end of the pipeline to the feed bin;

- 6 m^3 receiving bin with insertable pulse-jet dust filter;

- All necessary instrumentation (e.g. static pressure transmitters – details provided later in this chapter), load cells on feed bin and receiving bin, annubar with DP meter). Exploded view of the static pressure measuring tapping points can be found in Appendix A1 - Figure A1.1. For the measurement of air flow rates, there were annubars of five different sizes (appropriate for different ranges of air flow) on the compressed air line. Air flow rate was measured by the upstream of differential pressure for the annubar. A flow control/needle valve was used to control the air flow rate. Mass of solids leaving the blow tank and entering in the receiver bin was measured by the shear beam type load cells. Typical channels which are recorded with respect to cycle time, include: blow tank air pressure, static pressure and (DP signal in the pipeline for "white powder" only – see later in

the chapter), upstream pipeline and differential pressure (annubar) for air flow rate measurement, the mass of material leaving the blow tank and entering into the receiver bin. Actual values of these can not be directly measured. The generated electrical signal are transferred to a data acquisition unit, which converts the electrical signal to physical quantities, such as static pressures, mass flow rates of solids and air etc. Similar instrumentation arrangement was provided for "white powder".

- Data acquisition unit for data recording and analysis (provided in details in later section of this chapter).

A schematic of the test set up for the 105 mm I.D. × 168 m and 69 mm I.D. × 554 m long pipes (for fly ash) are shown in Figures 3.2 and 3.3, respectively. It is to be noted that all the pipes are confirming to the relevant Australian/International code for mild steel pipes. The seam in the pipes would have been none-existent as these pipes had been installed for around 20 years and the seam would have been worn away through continual use. Spigotted flanges also were employed to ensure smooth internal surfaces at each pipe-pipe and pipe-bend connection.

BT : Blow tank
V : Vertical
P : Pressure
tapping point

6.3 m

11.7 m

12.9 m

P 11

P 10

44.5 m

40.1 m

P 12

5.8 m

P 9

12.7 m

6.95 m (V)

21 m

Silo

P 6 | BT 2 | BT 1 | P 7

P 5

P 8

1.3 m   0.5 m   6.8 m

Figure 3.2: Schematic of the 105 mm I.D. × 168 m Long Test Rig (for Fly Ash)
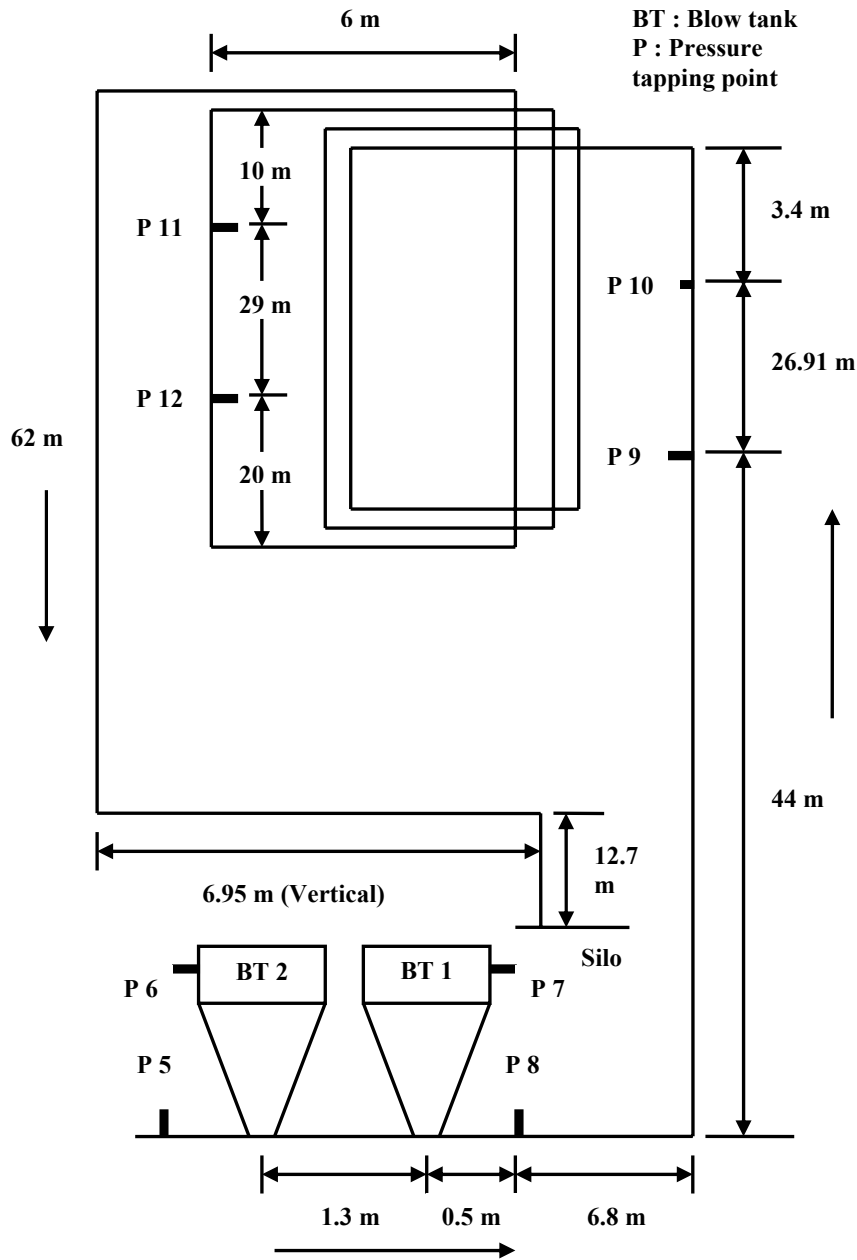
Figure 3.3: Schematic of the 69 mm I.D. × 554 m Long Test Rig (for Fly Ash)

For fly ash and ESP dust, static pressure measurement points, such as P8, P9, P10, P11 and P12, were employed along all the pipes. The P8 tapping location was used for total pipeline pressure drop. P9-P10 and P11-P12 tapping points were installed to

provide "straight pipe" pressure loss data for the modelling of solids friction. A picture of the test loop is shown in Figure 3.4.

'Please see print copy for image'
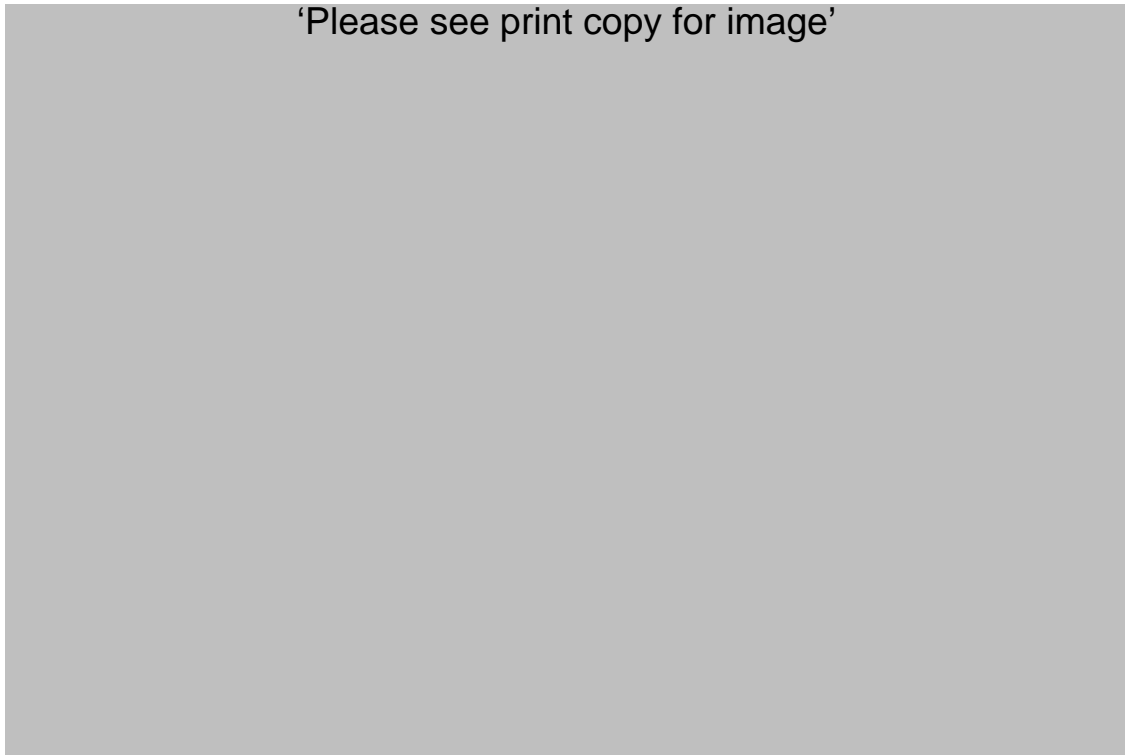
Figure 3.4: Pneumatic Conveying Test Pipe Loops – Up to 1.2 km Long (University of Wollongong)

Fine "white powder" was conveyed through another test rig, as shown in Figure 3.5. The test facility comprised:

- 0.5 m^3 bottom-discharge blow tank feeding system;

- 69 mm I.D. × 148 m long mild steel pipeline, including 4 m vertical lift, six 1 m radius 90° bends;

- Static pressure measurements via two sets of tapping locations on the straight pipe lengths: P9-P10 (52.68 m apart) and P11$^+$-P12 (19.9 m apart). The tapping locations were similar to that of the fly ash test rig (described previously), except the new tapping P11$^+$ was introduced almost mid-way between P11 and P12. Differential pressure (DP) measuring arrangement was built and installed between P11$^+$ and P12, in addition to the static pressure tapping points at P11$^+$ and P12 (details of the DP arrangement is provided in later section of this chapter). During building of the DP arrangement, it was found that accommodating both the static and DP connections within the same taping point is rather difficult. Hence, it was considered that the DP pressure tapping points will be located approximately 5 cm away from the static pressure tapping points (however, the DP tapping points are still denoted by P11$^+$ and P12 in this thesis). Again, the P8 tapping location was used to record total pipeline pressure drop. The static pressure transducers were of the specification: manufacture: Endress and Hauser, model: Cerabar PMC133, pressure range: 0-6 and 0-2 bar, maximum pressure: 40 bar (absolute), signal: 4-20 mA.

- "Sight glass" just after the P12 location (approximate length of 1 m) for flow visualisation. The sight glass is made of toughened glass and is connected into the pipeline with struab coupling and braced with rods to protect the glass and keep it straight. Other necessary instrumentation, data acquisition unit etc were similar to the arrangement shown in Figure 3.1.

"White powder" was not conveyed through the larger and longer pipes.
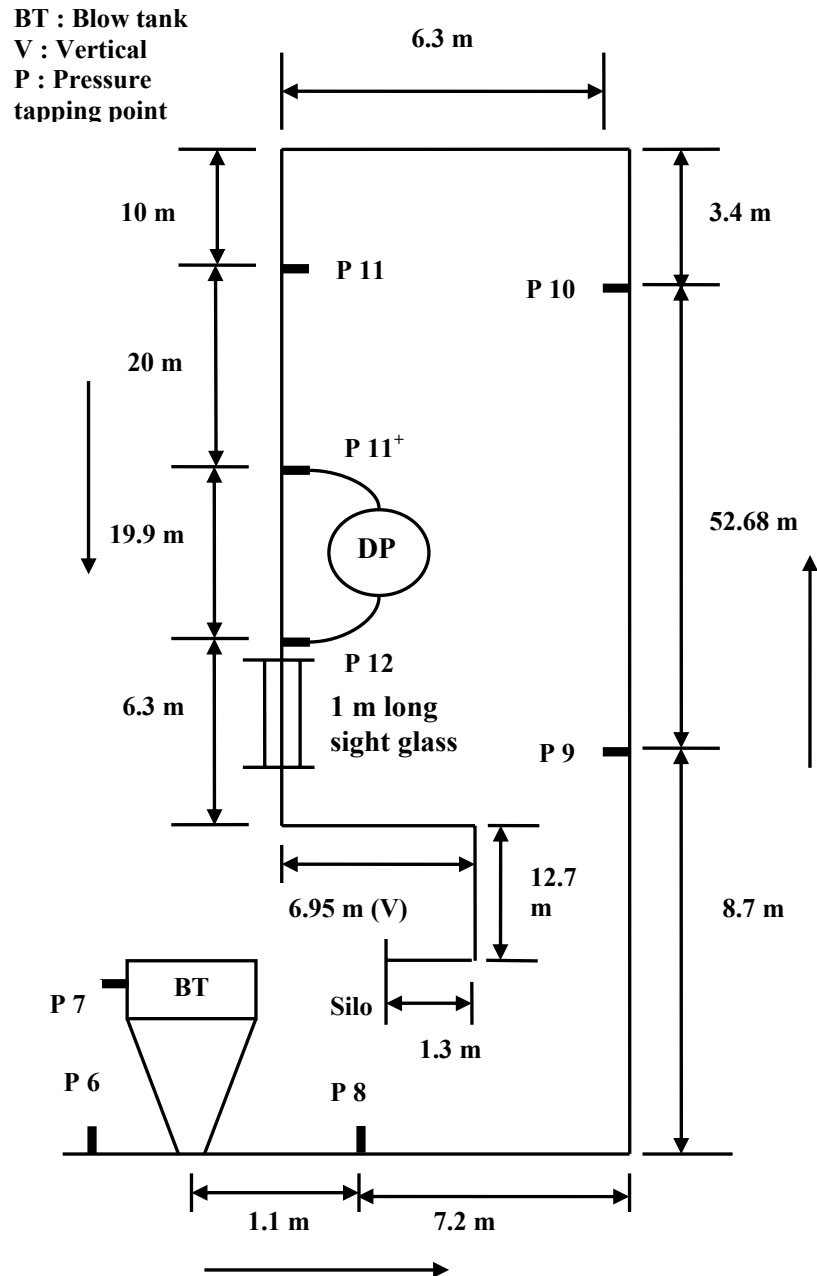
Figure 3.5: Schematic of the 69 mm I.D. × 148 m Long Test Rig, with DP Arrangement (for "White Powder")

3.2.3 Differential pressure (DP) measurement and product conveying

Designing a direct differential pressure (DP) measuring arrangement and evaluating the accuracy of same for the dense-phase pneumatic conveying of fine powders was initially considered to be an important part of the experimental program. The idea behind the DP work was to measure and study the difference between fluctuating signals coming from two different tapping locations (i.e. to measure difference between two increasing/decreasing pressure signals or simply measuring differences between "same" troughs and crests). It was considered that this would work if the two pressure tappings are close enough so that the offset between the two signals are reduced. In the present test program, the distance between the tappings was in initially kept as 19.9 m. It was decided that if the DP measuring technique performs well in the initial investigation, then similar other set of DP tapping arrangements would be installed in the pipeline at different locations and with varying tapping to tapping distances. However, because of the various hindrances to the test program (mentioned previously), the DP system could only be tested for one set of tapping points for "white powder" (Figure 3.5). Description of the DP measuring arrangement and results of preliminary investigation are provided in the subsequent portion this chapter and in Chapter 4, respectively.

A DP pressure tapping point consisted of:

- An 1 inch BSP socket welded to the pipe;

- "O" ring was inserted into the socket (so that the filter can be securely placed over it without displacement, especially under the actual test conditions);

- PCM- 10 was used as the filter material. PCM-10 (Dynapore) is a product of Martin Kurz and Co. Inc., USA, and the available information from the manufacturer mentions this as "diffusion-bonded multi-layer laminates". The manufacturer also mentioned that this can be used for fluidising media (e.g. fly ash, cement). Hence, PCM-10 was tried in this study. The material was cut into proper shape (circular) and size. The smoother surface was positioned facing the product end. Otherwise, the product would clog the rough side very quickly during the actual solids-gas flow situation. Also the smoother side was considered to be easier to clean (by air-purging) than the rough side;

- Plug having 1 inch BSP thread;

- A nipple connecting the tapping point to the DP meter and air purging system (through an ON/OFF ball valve);

- Air purging system to clean-up the filter of the differential pressure tappings. A manual system was set-up. It was discovered that a compressed air supply pipeline passes all along the pneumatic conveying pipelines. This was originally envisaged (years ago) to cater for any additional/special needs which could come in future (such as this). A hose was connected between this

compressed air line and the nipple of the DP tapping. From time to time (after every 2 experiments during the test program), air was purged by quick manual opening of the ON/OFF ball valve.

Exploded view of a DP tapping point is provided in Figure 3.6. A picture of the DP and static tapping points at the P12 location is shown in Figure 3.7. One complete DP arrangement consisted of two individual DP tapping points connected to a DP meter (digital) and separated by 19.9 m distance on the horizontal straight pipe length (Figure 3.5).
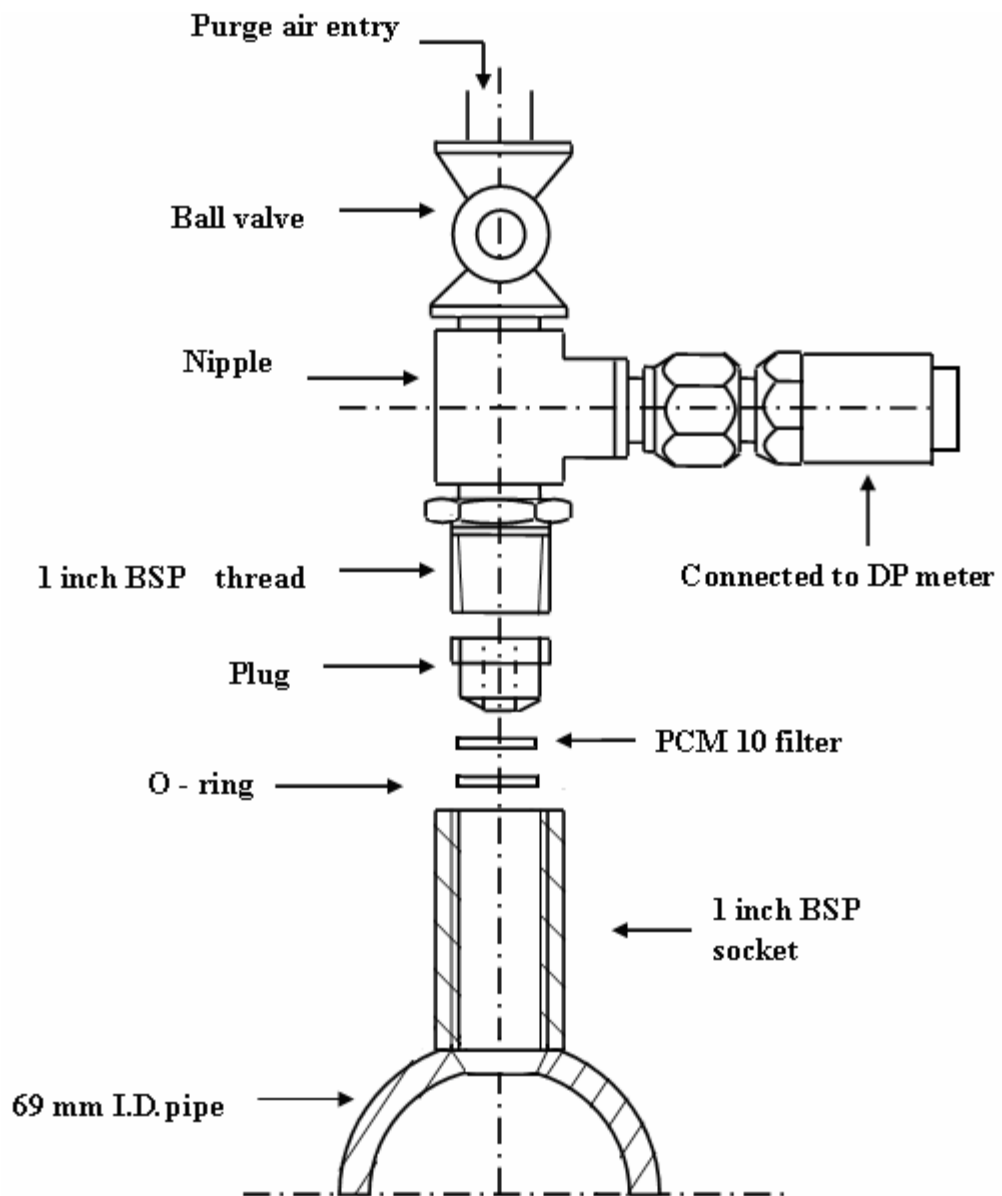
Figure 3.6: Exploded View of a Typical DP Pressure Tapping

Figure 3.7: DP and static pressure tapping points at the P12 location of the 69 mm I.D. × 148 m Long Pipe

Calibrations of load cells (blow tank, receiver bin) and static pressure transducers

Calibrations of the above were performed using the standardised calibration procedure of the Bulk Material Handling Laboratory, as described in Pan (1992). However, the procedure for calibration of static pressure transducer is described here. All the pressure transducers in the test program are calibrated by maintaining a constant pressure in the pipeline and simultaneously recording the voltages of the transducers. The calibration procedure is established as below:

a) Connect all transducers by cable to transducer signal conditioning unit/zero box.

b) With all material in the receiving hopper (hopper valve and fill valve closed), close the ball valve at the end of the pipeline, vent valve and open the discharge valve.

c) Close a flow control valve located upstream of the product feel point and close it until a designated pressure (e.g. 200 kPag) is reached in the pipeline.

d) Check whether there is a leak on each tapping by soapy water. If so, open the vent valve, rectify any leakage point and go back to (c). If not, then go to (e).

e) Open the vent valve until there is atmospheric pressure in the pipeline. Then close the vent valve.

f) Adjust the pressure regulator (e.g. 50 kPag), then open the valves to the blow tank top and ring air.

g) Measure the static pressure in the pipeline by using a pressure meter and record the voltages of all the pressure transducers simultaneously after the pressure in the pipeline is very stable.

h) Close the valves to the blow tank top and ring air. Repeat steps (e) to (g) for different static pressures.

Typical experimental results and calibration factor for a pressure transducer are in Table 3.2 and Figure 3.8, respectively.

Table 3.2: Pressure and voltage for a pressure transducer

Pressure (kPag)	0	53.1	101.5	148.2	201.7
Voltage (mv)	0	3.927	7.182	10.687	14.447
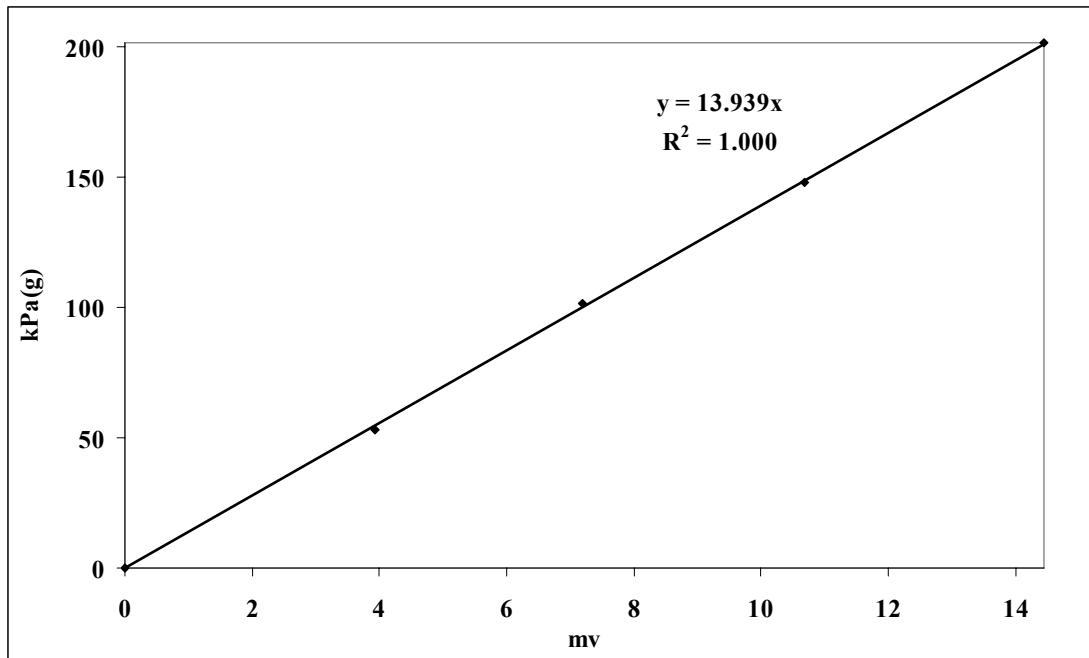
Figure 3.8: Calibration factor for a pressure transducer

From Figure 3.8, the calibration factor for the pressure transducer is 13.393 kPa/mv.

Calibration of DP meters

Due to the absence of any previously available data of "white powder" conveyed in 69 mm I.D. pipe, it was difficult to assume the expected pressure drop for the $P11^{+}$-P12 straight pipe. As a result, it was considered prudent to calibrate two DP meters

with different ranges of pressure drop - equivalent to 80 and 150 inch (i.e. 2.03 and 3.81 m in SI unit) height of water column. The DP meters were Rosemount DP meter, digital readout with 4 – 20 MA signal generated. DP meters were calibrated as per ISO 10474 3.1B or EN 10204 3.1 by the manufacturer. The procedure of DP meter calibration for the test program was: a compressed air line was connected to a pressure regulator. A T-piece was added in the other side of the pressure regulator. The T-piece was connected to the DP meter and a pressure transmitter (calibrated previously). The other side of the DP meter was left to atmosphere (zero gauge pressure). Both the DP and pressure transmitter were attached to the same data-logging system. The pressure differential was varied using the pressure regulator to various percentages of the full range of operation of the DP meter, such as 10, 20, 30 to 100% (approximately). The DP meter was calibrated for its full range so that the DP meter is capable of providing accurate pressure differential in its entire range, as the range of expected pressure differential during actual conveying of products could not be predicted beforehand. The datataker program received and recorded the signal (differential pressure) as electrical signal (millivolt, "mv"), then the "mv" values were multiplied with the "set" calibration factor to generate plots of pressure differential (kPa) versus time (s), as shown in Figure 3.9. The calibration factor was derived by forcing the recorded differential pressures (plots of DP with time, Figure 3.9) to match with the actual values of the differential pressures (observed from the digital DP meter panel). Two trials of calibration for each of the 80 inch and 150 inch were carried out. For each DP meter, the two set of calculated calibration factors were averaged to get a mean calibration factor for that DP meter. The calculation sheet for the above is provided in Appendix A1.1.
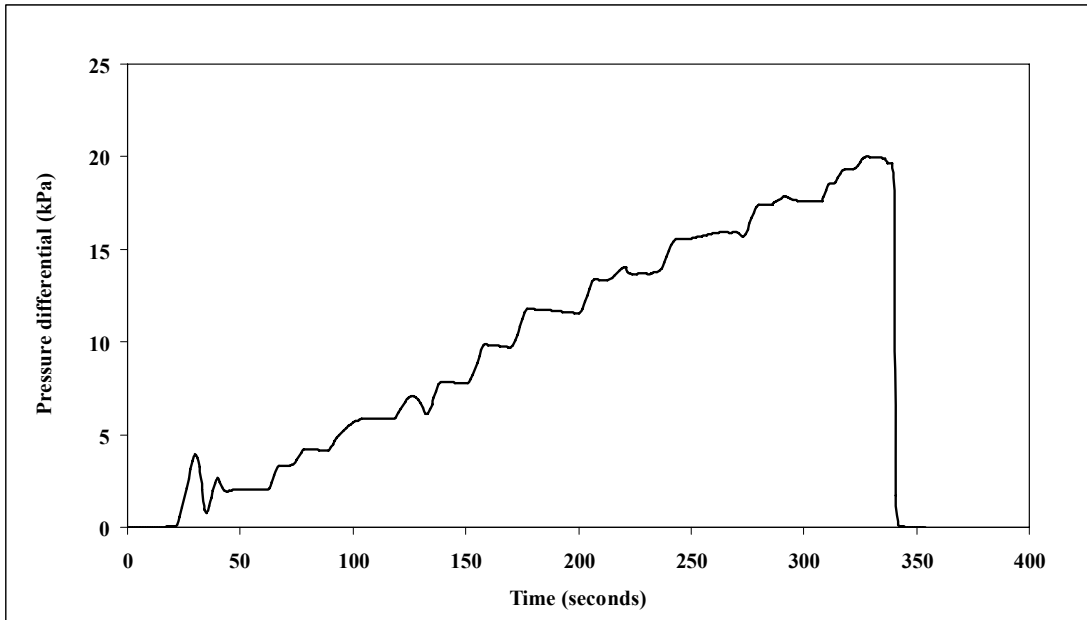
Figure 3.9: Plots of 80 Inch DP Meter Calibration

Preliminary Air- Only Tests with 80 Inch Differential Pressure (DP) Meter

Preliminary air-only tests were conducted by connecting the 80 inch DP meter with the DP tapping points (P11[+] and P12) on the 69 mm I.D. × 148 m long pipeline. Mass flow rate of air was varied from 0.04 to 0.2 kg/s. It was considered that the accuracy of DP measuring arrangement could best be evaluated using air-only tests, as having powders flowing with the air stream would only increase the fluctuation of the pressure signal, making it difficult to properly evaluate the accuracy of the DP arrangement. The results of the air-only tests are provided in Appendix A1.2. The results show that the differences in the values of differential pressures obtained from direct DP measuring arrangement and estimated from static pressure tapping point

measurements are drastically large for low air flow rates (DP meter readings under-predict the differential pressure values estimated from the static pressure tapping point measurements by a factor of 2). However, for the higher air flow range, values of differential pressures obtained from the direct and indirect DP measuring methods matched relatively better.

As it was found that the values of differential pressures obtained from the above two methods (direct approach using a DP meter and indirect approach of estimation from static pressure measurements) were significantly different and it was not clear which of the two methods was actually the more accurate, it was decided to install a water manometer between the two tapping points (P11$^+$ and P12), which would act like a third reference (i.e. to have an independent "cross check", for the air-only tests). For the above, another set of tapping points were created (in the same circumferential location of P11$^+$ and P12). It was considered prudent to have an entirely independent system for cross checking. Hooking up with either of the direct DP or static tapping (e.g. with a "T" piece) could have influenced the investigation, e.g. there were 4 number of filters (2 for static and 2 for direct DP) and the discrepancy in result could have been possible by anyone of them not working properly (e.g. the reason may be somehow one of these filter is chocked by conveying of residual product in line) and if the manometer was hooked with this defective tapping, the manometer readings (which was selected as reference for cross checking) would be erroneous and the purpose of the exercise would have failed. Hence, independent tappings were pursued. The manometer readings were recorded manually. The range of the manometer was ± 500 mm of water column. Thus the total pressure differential that

could be obtained with that manometer was equivalent to 1000 mm of water column, i.e. approximately 10 kPa. Therefore, it was a condition of testing that the air-only tests be performed within a certain range of air flow rates, so that the pressure differential would not go beyond 10 kPa. Air-only tests were carried out between air flow rates of 0.06 kg/s to 0.24 kg/s (approx). The corresponding air velocity values were typically in the range 8 to 40 m/s within $P11^+$ and P12. The results are provided in Appendix A1.3. Surprisingly, it was found that the values of the differential pressures obtained from the DP meter, static tapping points and the water manometer readings were in very good agreements with each other (for a wide range of air flow rates). Due to the contrasting degrees of accuracies obtained by the two different trials (i.e. poor agreement in the first trial with only DP meter, but without the manometer, and very good agreement in the second trial with both DP meter and manometer), the air-only tests with 80 inch DP meter and manometer installed were repeated again. Again, very good agreement was obtained amongst all three methods. Encouraged by this, air-only tests were carried out by installing the 150 inch DP meter. Again, the results provided good agreements. It was concluded that direct DP measuring arrangement provides good accuracy (for the air-only tests). It, however, remained unclear why the initial air-only tests (i.e. with 80 inch DP installed, but without manometer) provided drastic disagreements. Being reasonably satisfied with the accuracy of the direct DP measuring arrangement, it was decided to commence product testing.

Product conveying

The initial plan was to test DP meter with calcium carbonate that was present in the receiver bin. Conveying was commenced by setting the blow tank back pressure and blow tank air supply at 300 kPa, and 0.02 kg/s, respectively. The total conveying air flow rate was set at 0.125 kg/s. The solids (calcium carbonate) flow rate was 12 t/h. The value of differential pressure between ($P11^+$ and $P12$) estimated from the difference of the steady state static pressure was found to be 24 kPa. This exceeded the pressure differential range of the 80 inch DP meter (which is 20 kPa). As a result, the 80 inch DP meter was replaced by the 150 inch DP meter and the above test was repeated. Good steady state conditions were achieved during testing. However, at this stage, the test program had to be stopped as the test rig was to be utilised for a contract research project. Afterwards, using similar test procedures, the DP meter was evaluated for the conveying of "white powder". Detail report of such evaluation is provided in the following chapter (Chapter 4).

3.2.4   Data acquisition system

In order to record the electrical output signals from the load cells, pressure transducers (static tapping points and direct DP meter), a portable PC compatible data acquisition system (Datataker 800 or DT800 of Data Electronics) was used. DT800 is a high speed unit featuring 16 bit resolution. This has 42 analogue inputs, giving 42 separate single ended channels or 24 differential channels. The sampling speed varies with input type, mode and number of channels. Data logging was done at 1 scan per

second. The data logger has inbuilt filtering. Detail specification of DT800 is provided in Annexure A1.4. Major components of the system are shown in Figure 3.10.
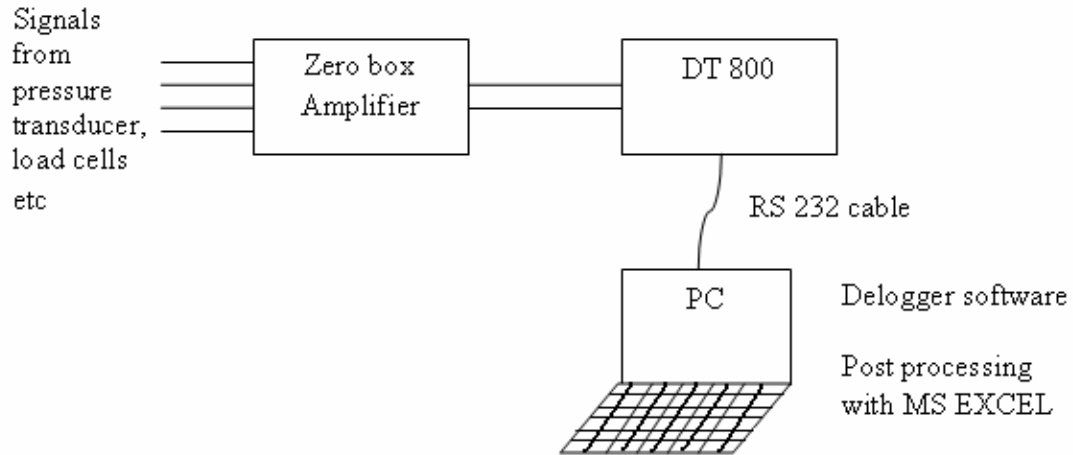
Figure 3.10: Schematic Layout of Data Acquisition System

3.2.5 Compressed air supply

Compressed air at maximum available pressure of approximately 800 kPag can be supplied from any combination of the following three rotary screw compressors:

(a)   Atlas Copco electric-powered Model GA-308, 3.1 m^3/min free air delivery.

(b)   Ingersoll Rand diesel-powered Model P375-WP, 10.6 m^3/min free air delivery.

(c)   Ingersoll Rand diesel-powdered Model P850-WGM, 24.1 m^3/min free air delivery.

The test work started with using the larger diesel compressor (c) for the initial experiments of "white powder". After this, the same broke down and the rest of the conveying trials of "white powder" was achieved using smaller diesel compressor (b), which also subsequently broke down after a few months. Some limited dense-phase tests could have been performed using compressor (a), but the purpose of the research was to investigate the full range of flow modes and possible flow mechanism changes along the pipeline. Also, the aim was to generate sufficient data for modelling purposes. Measuring some data points close to minimum transport would have been inadequate, as it was needed to ensure steady-state flow. Hence, tests using compressor (a) was not pursued.

Further description regarding the general arrangement of the compressed air system is provided in Pan (1992).

CHAPTER 4: Study of Pressure Signals

4.1 Introduction

Due to the presence of solids in the gas stream and the highly turbulent nature of flow, the pressure signals obtained from the various static pressure tapping points are fluctuating in nature, even under steady-state conditions. This chapter presents results of study on these fluctuating pressure signals. The response of a differential pressure (DP) meter (Chapter 3) is also examined to evaluate its effectiveness in monitoring the dense-phase pneumatic conveying of powders.

4.2 Analysis of pressure signals

Figure 4.1 shows the plots of pressure signals obtained from the various static pressure tapping points (such as P9, P10, P11 and P12) installed on the 69 mm I.D. × 168 m long pipeline (Figure 3.1) for fly ash (Wypych et al., 2005). The flow condition for this particular experiment was: m_f = 0.051 kg/s; m_s = 4.28 kg/s; estimated mean superficial air velocity for P9-P10 and P11-P12 were 5.76 m/s and 7.39 m/s, respectively, which suggests non-suspension (dense-phase) flow condition at both tapping point locations.

Figure 4.1: Plots of Static Pressure Signals from P9, P10, P11 and P12 (Tapping Points); Fly Ash (Wypych et al., 2005); m_f = 0.051 kg/s; m_s = 4.28 kg/s

For a steady state interval of t = 160 to 220 seconds, the fluctuations in the pressure signals are provided below. The pressure values at the troughs and crests are read from the MS EXCEL plot of Figure 4.1

For P9: 118-109 kPa

For P10: 80-70 kPa

For P11: 70-58 kPa

For P12: 44-32 kPa

The ratio in percentage of amount of fluctuation (e.g. 108-109 = 9 kPa for P9) to the mean value (e.g. 114 kPa for P9) are 7.9, 12.8, 18.9 and 30.8% for P9, P10, P11 and

P12, respectively. This ratio values and also the absolute values of fluctuation (kPa) have increased along the length of pipeline (i.e. from feed to the discharge end). To obtain a steady state constant value of the pressure drop from the fluctuating signal, the common approach is to use an "averaging" method, where the post processing software based on MS EXCEL (Figure 3.9) calculates the arithmetic average of the fluctuating waveform within a specified time interval (steady-state condition). However, the accuracy of this "averaging" method may be considerably influenced if there exists a spike (although this is not shown in Figure 4.1). Therefore, time spans are to be are to be carefully selected so there is no spike in the signal within the span. To crosscheck the correctness of the EXCEL estimated averages, straight lines were manually drawn through the waveform up to visual satisfaction so that the line bisects the signal waveform fairly well (this is for satisfaction that the statistical averaging is not providing any noticeably biased mean, i.e. the statistical average seemingly matches with what should be the physical mean).

Figure 4.2 shows the plots for the same powder and pipeline, but under higher air velocity conditions (i.e. towards dilute-phase flow). The flow condition for this particular experiment was: m_f = 0.108 kg/s; m_s = 2.21 kg/s; estimated mean superficial air velocity for P9-P10 and P11-P12 were 13.2 m/s and 15.81 m/s, respectively. The velocity at pipe inlet (feed point) was estimated as 11.9 m/s. The ratio in percentage of amount of fluctuation to the mean value are 10.6, 8.45, 19.2 and 26.67% for P9, P10, P11 and P12, respectively.

‘Please see print copy for image’

Figure 4.2: Plots of Static Pressure Signals from P9, P10, P11 and P12 (Tapping Points); Fly Ash (Wypych et al., 2005); m_f = 0.108 kg/s; m_s = 2.21 kg/s

Further study of fluctuating signal for static and DP signals was carried out using the test data of "white powder" conveying for 33 experiments. Figure 4.3 to 4.10 shows typical plots of static and DP signals for 4 experiments. Standard deviation (SD) of static (P8 to P12) and DP signals were calculated for all the experiments and are provided in Table 4.1
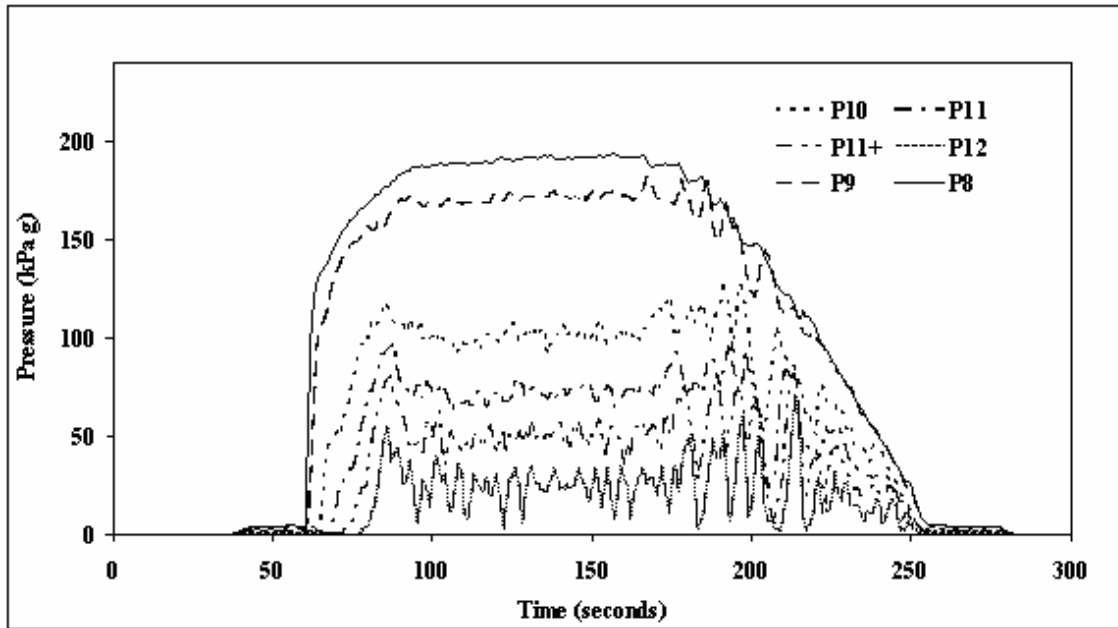
Figure 4.3: Plots of Static Pressure Signals from P8, P9, P10, P11 and P12 (Tapping Points); "white powder"; $m_f = 0.05$ kg/s; $m_s = 2.34$ kg/s; $V_i = 3.9$ m/s
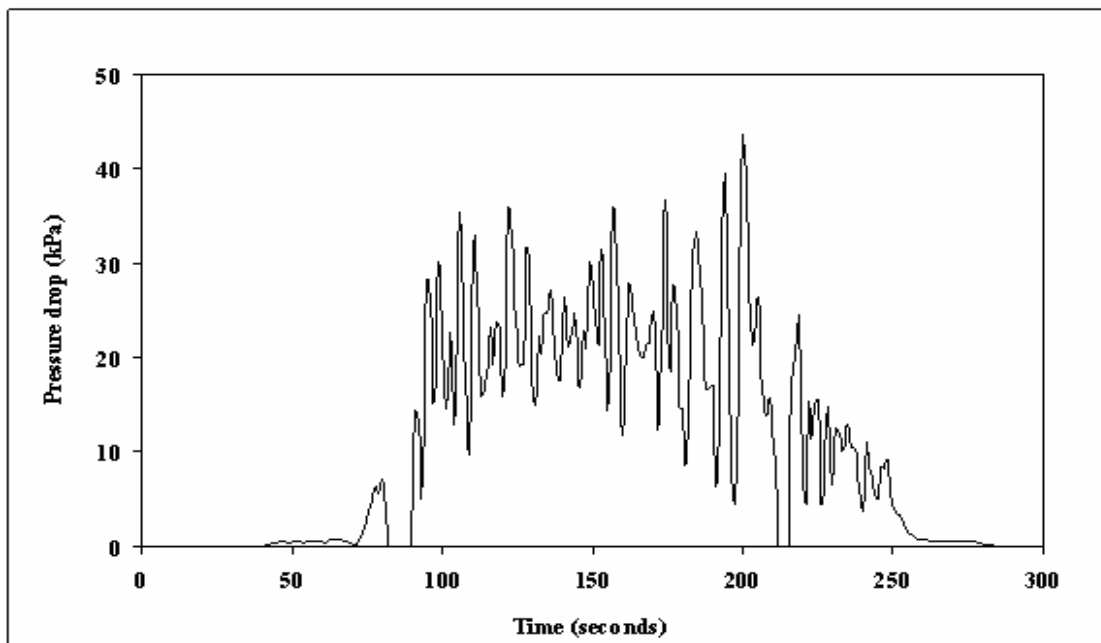
Figure 4.4: Plots of Differential Pressure Signals; "white powder"; $m_f = 0.05$ kg/s; $m_s = 2.34$ kg/s'; $V_i = 3.9$ m/s

64
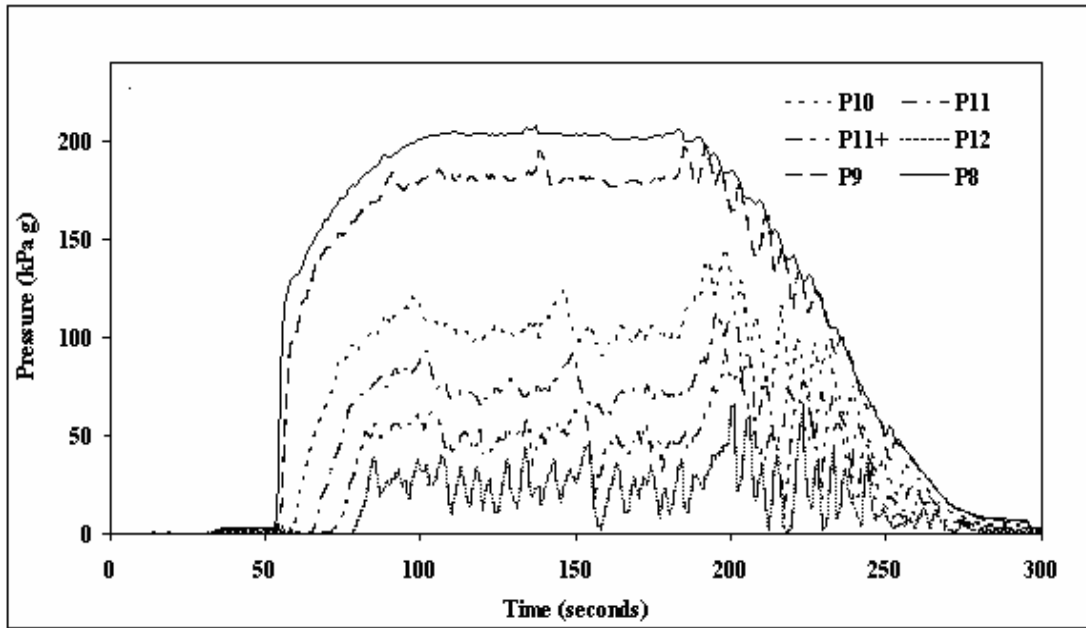
Figure 4.5: Plots of Static Pressure Signals from P8, P9, P10, P11 and P12 (Tapping Points); "white powder"; $m_f = 0.04$ kg/s; $m_s = 1.97$ kg/s; $V_i = 3$ m/s
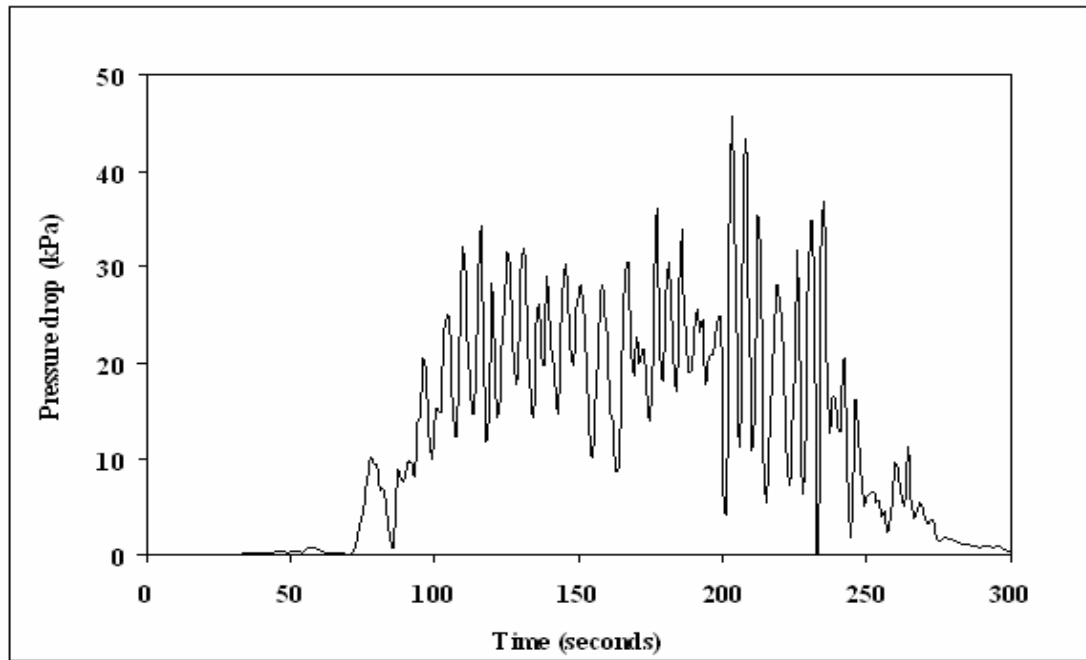
Figure 4.6: Plots of Differential Pressure Signals; "white powder"; $m_f = 0.04$ kg/s; $m_s = 1.97$ kg/s; $V_i = 3$ m/s

65
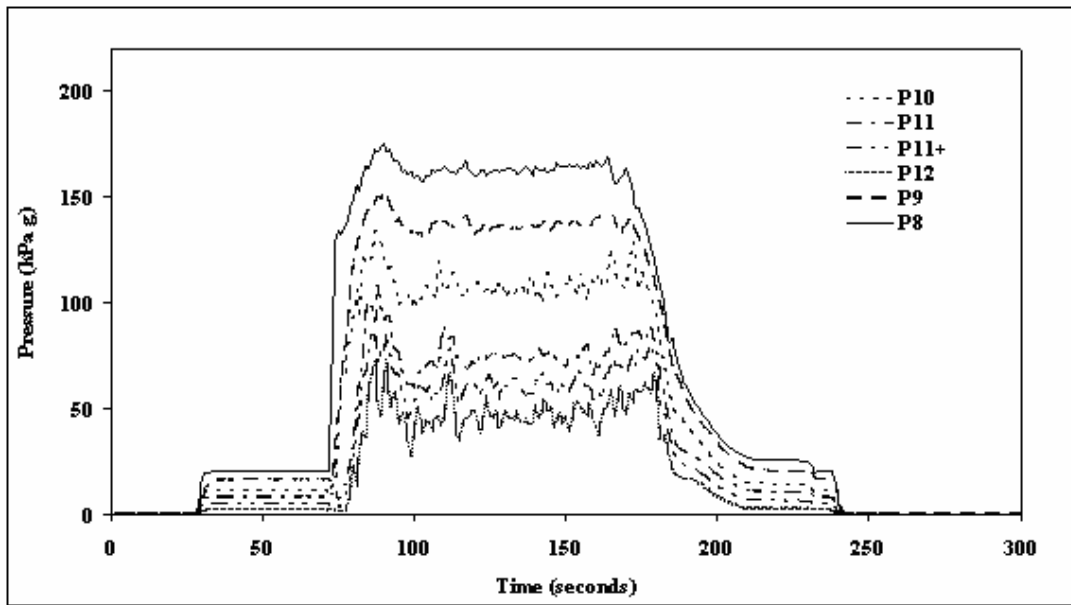
Figure 4.7: Plots of Static Pressure Signals from P8, P9, P10, P11 and P12 (Tapping

Points); "white powder"; m_f = 0.15 kg/s; m_s = 2.61 kg/s; V_i = 13.3 m/s
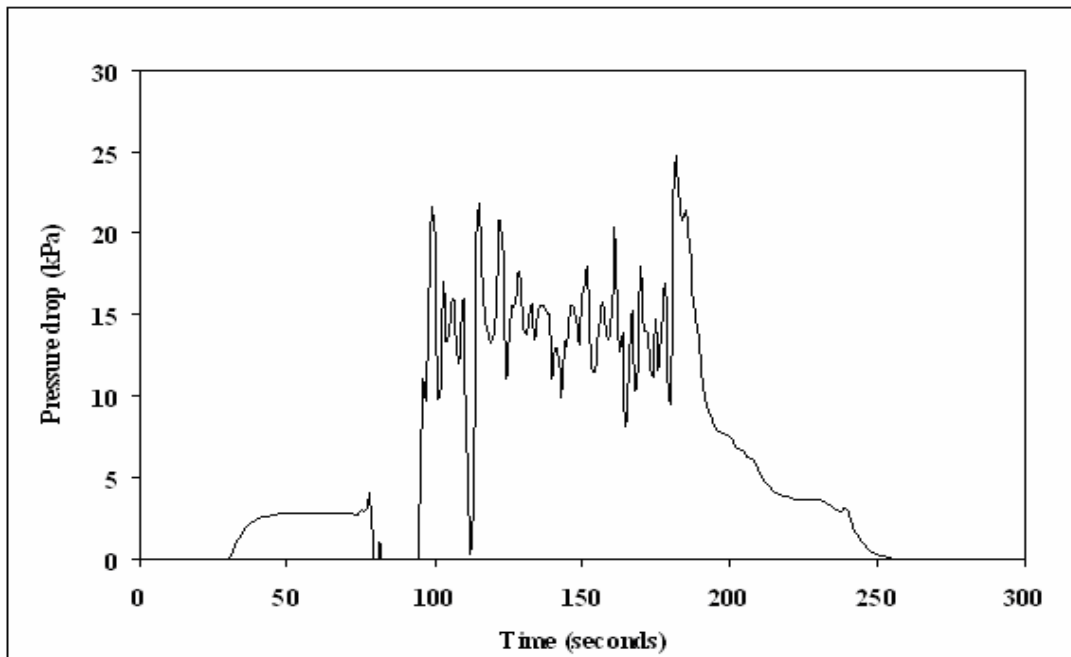
Figure 4.8: Plots of Differential Pressure Signals; "white powder"; m_f = 0.15 kg/s; m_s

= 2.61 kg/s; V_i = 13.3 m/s
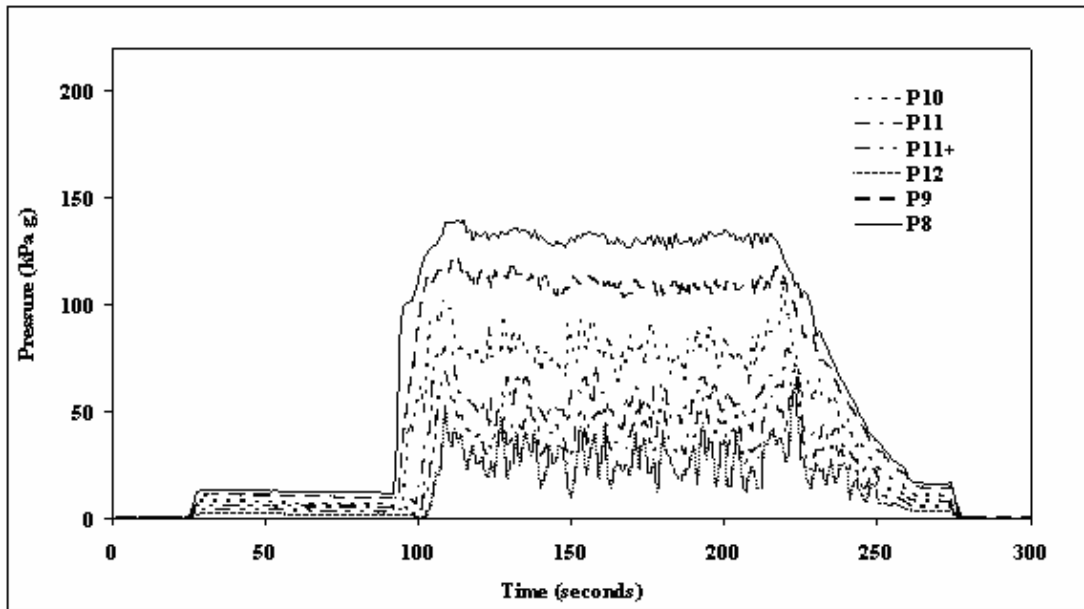
Figure 4.9: Plots of Static Pressure Signals from P8, P9, P10, P11 and P12 (Tapping Points); "white powder"; $m_f = 0.19$ kg/s; $m_s = 2.93$ kg/s; $V_i = 15.1$ m/s
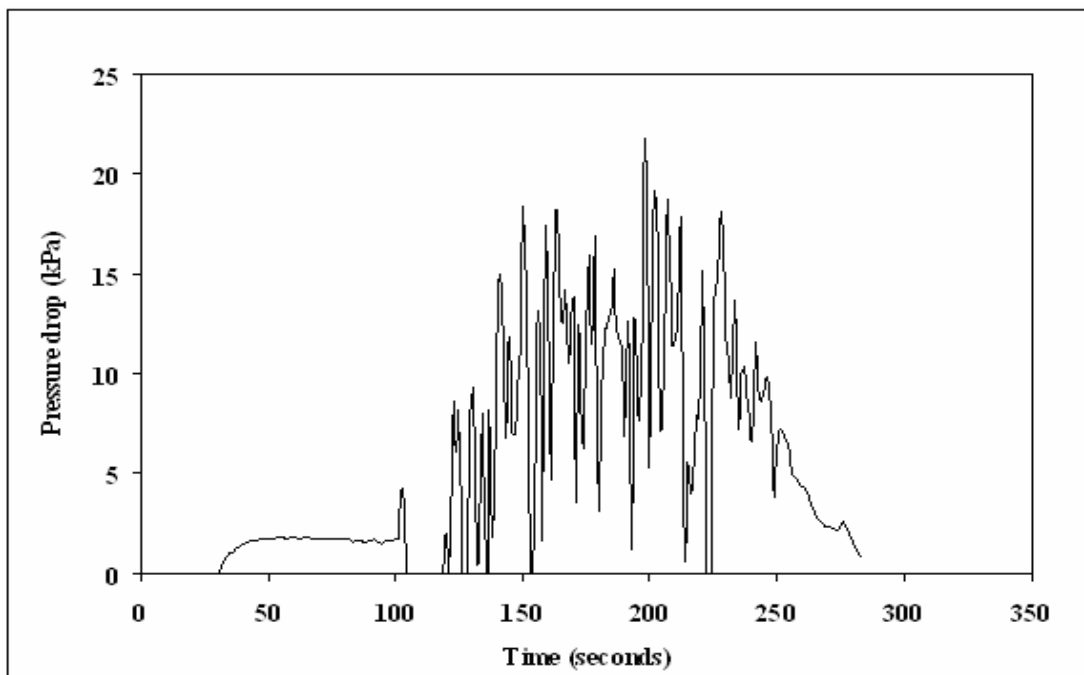
Figure 4.10: Plots of Differential Pressure Signals; "white powder"; $m_f = 0.19$ kg/s; $m_s = 2.93$ kg/s; $V_i = 15.1$ m/s

Table 4.1: Standard Deviation (SD) of Static and DP Pressure Signals

Test name	Air flow (kg/s)	Solids flow (kg/s)	P8	P9	P10	P11	P11+	P12	DP meter	SD of P8	SD of P9	SD of P10	SD of P11	SD of P11+	SD of P12	SD DP meter
	kg/s	kg/s	kPa (g)	kPa (g)	kPa (g)	kPa (g)	kPa (g)	kPa (g)	kPa	kPa	kPa	kPa	kPa	kPa	kPa	kPa
			Steady state values													
exp23	0.040	1.97	202.00	180.00	108.75	78.50	50.00	23.75	22.50	0.64	1.40	8.81	9.11	11.23	11.24	6.55
exp25	0.040	2.06	200.00	180.00	111.00	77.50	56.25	21.25	22.50	1.49	1.48	4.95	4.28	4.73	6.01	4.28
exp24	0.040	2.14	203.00	180.00	107.50	77.00	50.00	23.00	20.80	0.76	1.50	3.78	3.13	4.69	7.38	5.16
exp21	0.044	2.38	223.80	200.00	120.00	80.50	58.90	23.10	24.24	0.86	1.50	5.52	4.81	6.11	6.55	4.58
exp20	0.044	2.24	216.66	200.00	122.00	91.25	62.50	33.75	24.60	0.98	1.54	7.49	8.45	10.52	10.66	6.16
exp4	0.049	1.90	177.92	160.20	94.78	68.93	45.58	22.02	20.82	1.37	1.65	4.54	4.08	4.97	8.03	4.55
exp26	0.050	2.34	192.86	171.42	102.50	72.50	52.50	23.75	22.20	1.27	3.24	3.03	2.91	5.89	7.77	4.92
exp17	0.056	2.69	206.66	188.02	112.93	83.77	54.61	27.86		1.06	1.75	2.61	4.16	6.67	8.90	
exp3	0.064	2.10	168.98	153.95	95.37	69.49	48.00	25.81	19.92	1.02	1.85	6.22	5.03	6.42	7.65	4.26
exp11	0.070	1.81	135.22	120.17	74.59	55.22	37.16	18.86	14.64	1.08	2.03	7.50	4.98	6.93	8.99	5.58
exp16	0.077	2.68	197.55	181.84	113.00	83.76	57.14	31.66		1.03	1.50	4.02	4.45	6.45	9.95	
exp2	0.085	2.40	172.94	158.12	98.65	71.14	49.71	27.24	18.56	1.23	2.04	8.05	5.91	7.58	12.39	7.57
exp15	0.088	1.59	132.65	121.36	77.75	56.23	37.66	22.16		1.05	2.17	7.35	6.29	8.74	9.78	
exp65	0.094	3.03	195.50	162.98	113.54	79.42	58.41	34.82	14.53	1.44	1.42	3.81	3.81	5.86	7.03	3.67
exp55	0.103	2.17	183.22	151.49	101.27	70.86	49.46	30.73	17.42	2.09	1.59	7.79	6.28	9.26	11.07	6.39
exp60	0.107	1.75	130.10	108.16	78.12	53.84	39.79	26.04	11.37	2.27	2.82	6.99	7.67	7.55	7.57	4.44
exp19	0.108	2.99	189.27	178.75	117.61	86.94	63.18	39.38		1.89	2.69	6.38	4.84	6.61	9.63	
exp6	0.112	2.33	161.51	151.38	100.67	70.76	52.14	34.01	15.14	1.14	2.65	7.90	5.61	9.57	11.42	5.42
exp64	0.112	3.30	195.13	162.68	117.74	84.09	63.65	40.04	17.52	1.70	1.60	5.41	4.02	6.82	8.70	4.59
exp59	0.127	1.85	129.79	108.90	80.09	54.60	41.99	29.17	11.39	1.95	2.46	5.06	5.21	5.78	6.81	3.49
exp63	0.144	3.02	190.99	158.45	120.74	85.31	66.68	46.41	14.41	1.68	1.44	7.14	4.22	7.90	12.78	6.89
exp14	0.146	1.27	163.11	146.44	84.71	62.24	37.28	18.67		0.06	0.82	3.54	3.94	5.83	8.05	
exp8	0.153	2.37	151.15	142.18	105.19	72.02	59.57	42.86	13.61	1.21	2.51	4.17	3.63	4.62	5.98	3.25
exp54	0.154	2.61	163.29	136.41	106.93	73.95	61.26	46.38	14.24	1.34	1.33	3.81	2.15	3.77	4.09	1.95
exp5	0.164	1.69	191.52	170.42	95.30	68.09	43.21	21.98	19.53	0.62	1.53	6.44	6.82	7.26	8.74	5.81
exp62	0.167	3.06	190.07	162.31	125.05	86.74	72.12	51.68	14.75	2.57	3.26	6.35	9.05	9.72	9.63	6.71
exp58	0.176	2.08	134.78	110.90	88.04	59.64	50.79	38.61	11.40	1.22	1.22	2.79	2.74	3.64	4.58	2.36
exp57	0.176	1.93	134.47	110.96	88.03	59.68	50.67	38.85	11.20	1.26	1.07	2.19	1.65	2.21	4.49	2.63
exp9	0.177	2.28	169.462	139.601	106.523	72.580	64.366	46.232	13.478	2.060	2.760	4.500	4.010	4.750	4.120	3.020
exp61	0.194	2.93	191.11	161.34	131.41	89.43	81.02	60.71	18.03	1.38	1.57	2.92	2.66	3.66	4.07	2.86
exp53	0.200	2.52	170.76	143.04	117.07	79.79	70.73	55.84	14.99	1.89	1.49	4.52	2.14	4.44	6.20	3.17
exp52	0.201	2.27	173.25	147.94	115.52	77.44	67.55	53.64	14.37	1.62	1.97	6.40	3.10	5.37	7.66	4.10
exp56	0.201	1.80	136.73	113.01	93.79	64.83	54.79	43.80	10.53	1.63	1.06	2.67	2.07	2.31	3.31	1.94

DP meter did not record pressure signals for experiments:4, 15, 17, 19

68

The plots of SD values of static pressure signals of P8 to P12 are shown in Figures 4.11 to 4.15. A, B, C, D, E, F corresponds to tapping locations P8, P9, P10, P11, P11[+] and P12, respectively. P8 is at the beginning of pipeline; approximate distance between A and B: 16 m, B and C: 53 m, C and D: 11 m, D and E: 23 m, E and F: 20 m. There was 1 no. 90 degree bend between A and B and 2 no. 90 bends between C and D.
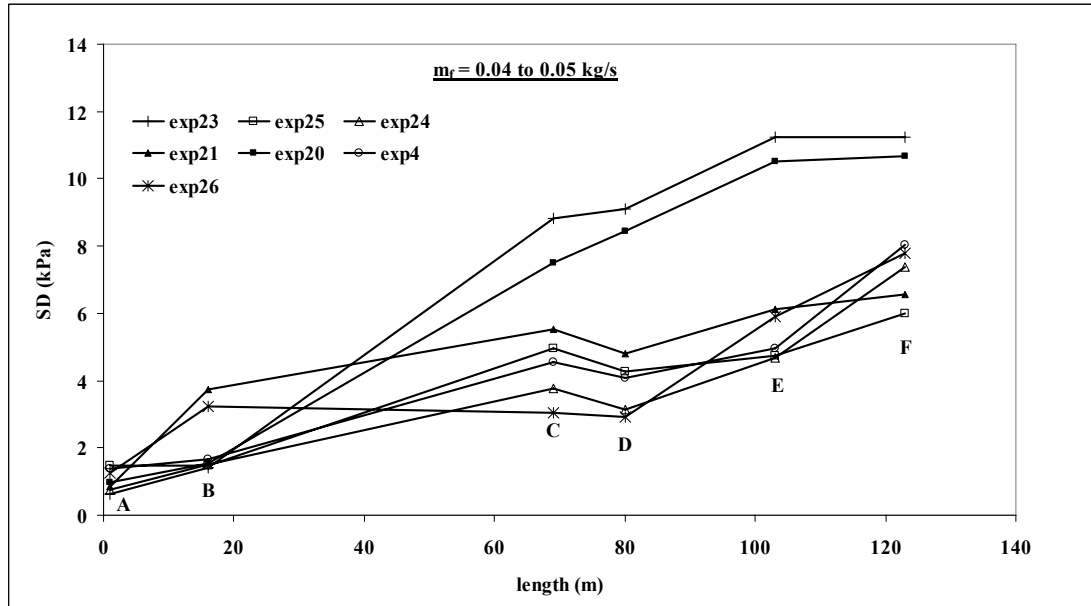
Figure 4.11: SD of static signals versus distance of tapping locations; "white powder"; m_f = 0.04 to 0.05 kg/s

69
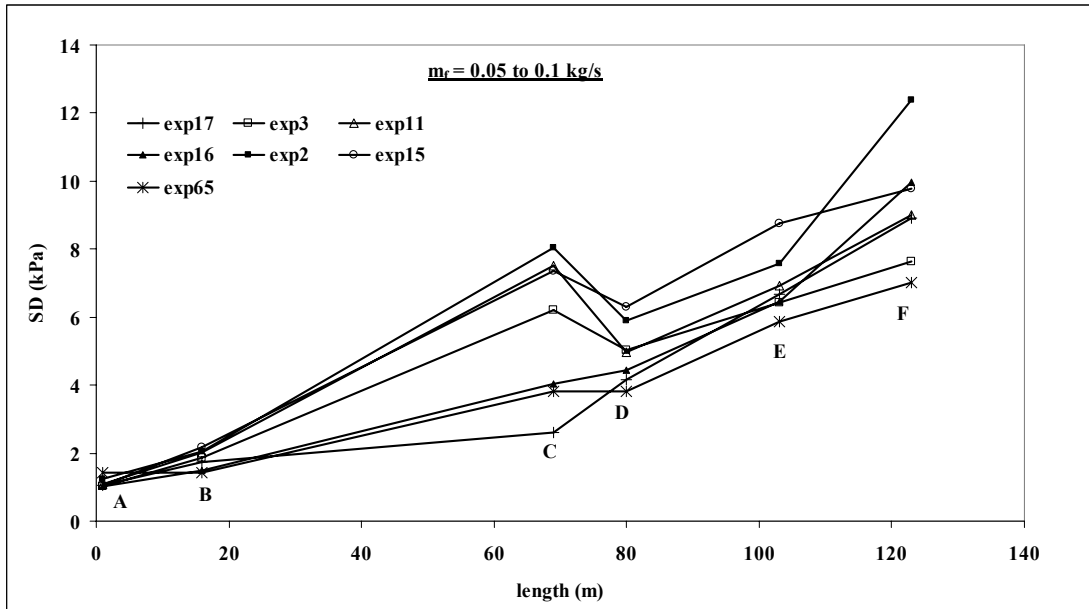
Figure 4.12: SD of static signals versus distance of tapping locations; "white powder"; $m_f = 0.05$ to 0.1 kg/s
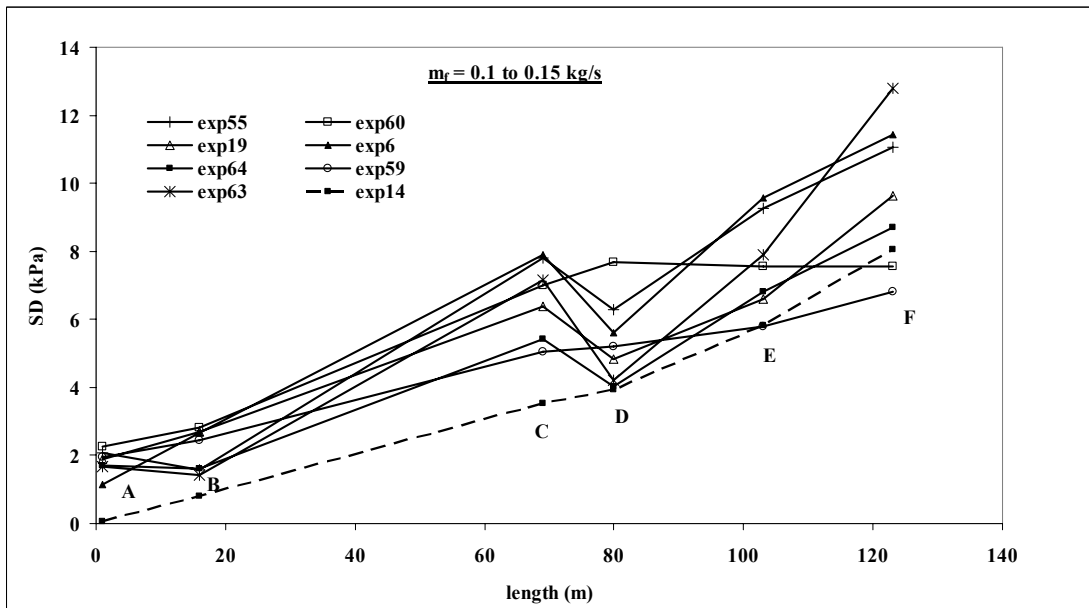
Figure 4.13: SD of static signals versus distance of tapping locations; "white powder"; $m_f = 0.1$ to 0.15 kg/s
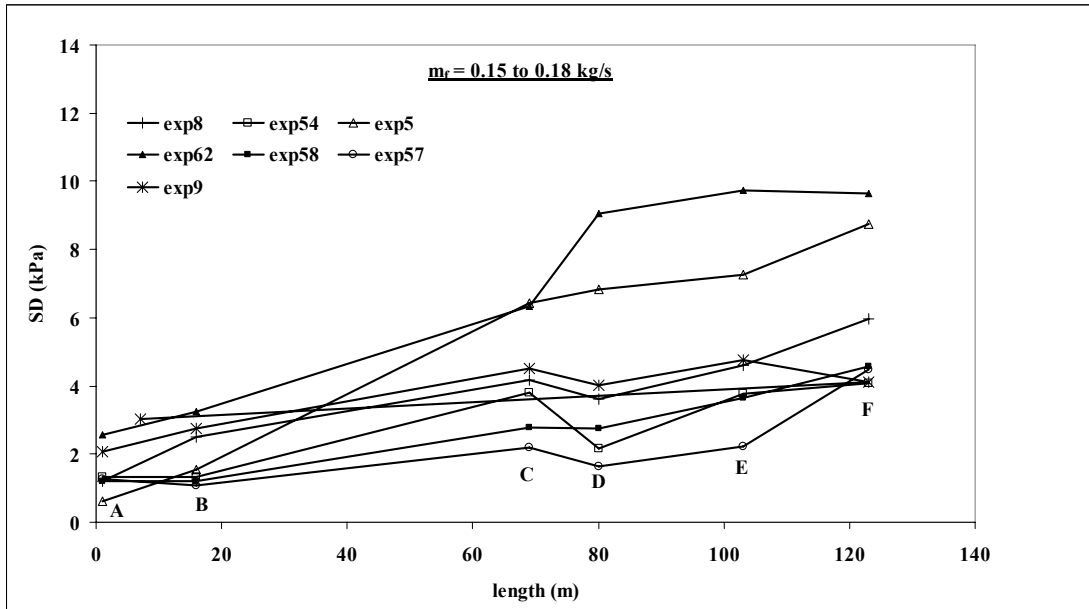
Figure 4.14: SD of static signals versus distance of tapping locations; "white powder"; m_f = 0.15 to 0.18 kg/s
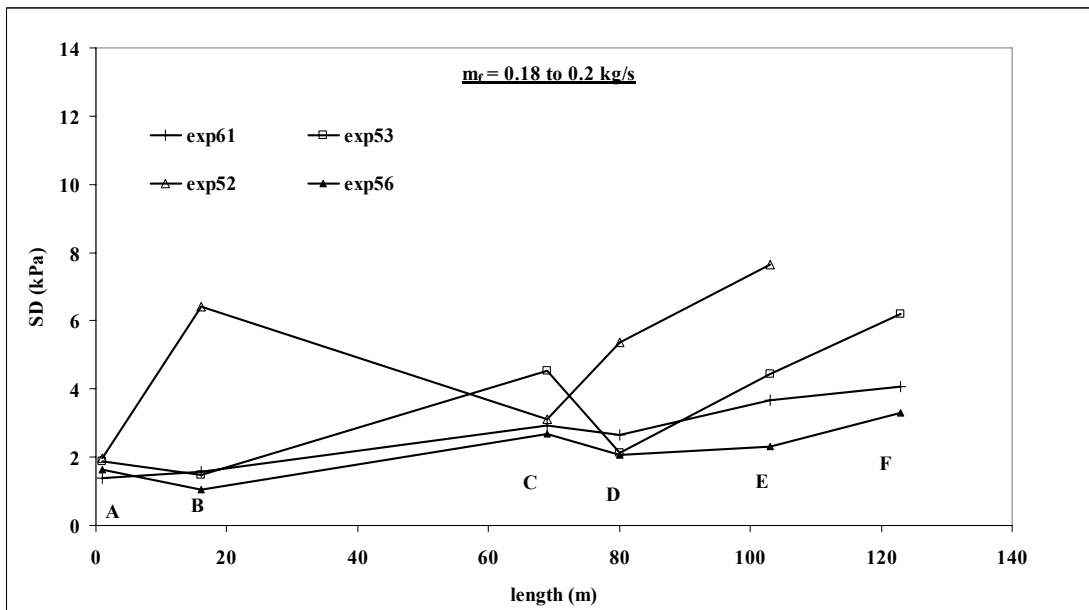
Figure 4.15: SD of static signals versus distance of tapping locations; "white powder"; m_f = 0.18 to 0.2 kg/s

Figure 4.11 to 4.15 show there is a overall trend of SD values, the SD values increase from P8 to P9 to P10, but then decrease at P11 (Note: there were 2 bends between P10 and P11), again the SD values increase from P11 to P11[+] to P12. However, there are some exceptions e.g. for experiments 14, 17, 20, 23, and 62, the dip in SD values at P11 are not present, and for experiments 57 and 63 there is a decrease of SD values at P9 compared to P8 (Note: there was 1 bend between P8 and P9). The total pipeline pressure drop data contain relatively less fluctuations (reduced SD values) and provides an advantage that the tapping point could be placed in the "clean" conveying air line (just prior to the product feed zone). This would be beneficial as the filter of the tapping point would remain "clean". However, for the purpose of research and industrial design (for a thorough study of the flow mechanisms), the use of "straight pipe" data is considered more appropriate. This is because the total pipe data would contain straight pipe and bend losses together and these have different correlations for solids friction. Hence they need to modelled and scaled up separately (Bradley, 1989; Pan and Wypych, 1998).

SD/√N values of m_f, m_s and various pressure measurement values are provided in Table A5.2 (Appendix A5) as a measurement of uncertainty (Dieck R. H., 4th ed.) (where N: number of data points = finish time in second – start time in second + 1). Coefficient of variation values for different static and DP pressure signals are provided in Appendix A5 (Table A5.3 and Figures A5.1 to A5.5).

This page has been intentionally left blank

4.3   Conclusions

SD of pressure signals for static tapping points P8 to P12 and for direct DP were calculated. Plots of SD versus pipe length (location of static tapping points) have shown generally there is an increase of SD from P8 to P12, with a dip at P11 (after 2 bends). The results may be useful for future investigations. Readers may also refer to Martinussen et al. (1995), who studied fluctuating pressure signals in much details.

CHAPTER 5: Pneumatic Conveying Characteristics

5.1 Introduction

Pneumatic conveying characteristics (PCC) constitute an essential requirement for the reliable design of pneumatic transportation systems (Wypych and Arnold, 1985). Steady state pipeline conveying characteristics can provide valuable information, such as the expected mode of flow condition (dilute/dense) for a particular combination of m_s and m_f, minimum conveying air velocity (either for dense- or dilute-phase) and the optimal operating conditions for a given product (e.g. based on the location of the pressure minimum curve). Further details on the importance of PCC to design or evaluate a proposed plant or for troubleshooting existing pneumatic conveying systems are provided in Wypych and Arnold (1985) and Wypych (1989). Using the steady state conveying data obtained from the different static pressure tapping points installed along the test pipe (e.g. see Figure 3.1) for various powders, such as fly ash, ESP dust and "white powder", PCC for the total pipeline and "straight pipe" sections were obtained. These are presented in this chapter. The total pipeline PCC have appeared repeatedly in various other subsequent chapters of this thesis (e.g. for the scale-up evaluation of models, in Chapters 6, 7, 8 and 10, where the predicted and experimental PCC have been compared). Also, various procedures for modelling solids friction employed in this thesis have used "straight pipe" pressure drop data. The "straight pipe" PCC (constructed using the "straight pipe" data) were believed to be useful as they could potentially present important information for a better understanding of the local flow phenomenon through the relevant pipe section. The format of presentations of PCC throughout this chapter

(and thesis) are plots of pressure drop (y-axis) versus mass flow rate of conveying air (x-axis) for different solids flow rates.

5.2   Pneumatic conveying characteristics (PCC)

5.2.1   Fly ash

The total pipeline PCC obtained for fly ash and 69 mm ID × 168 m long pipeline (schematic of test rig is shown in Figure 3.1) are presented in Figure 5.1 (Wypych et al., 2005). The total pipeline pressure drop (ΔP_T) includes all the losses across the entire pipeline, such as the losses occurring in the straight horizontal lengths, bends, verticals and due to initial acceleration (at the entry/feed point of the pipe). The ΔP_T values were obtained from the P8 transducer located at the beginning of the pipe (Figure 3.1). From the experimental data points, the final PCC are obtained using an interpolation relationship technique (Wypych et al., 2005). In this technique, the experimental data points are first plotted having the axis as shown in Figure 5.2. The experimental data points may not be on constant solids flow lines because even if the solids discharge rate of the blow tank is set to a constant value, the actual discharge values may vary to some extent for every test. Interpolation relationship is used with m_f and ΔP_T values of data points which are close to each other and up/down to get intermediate points for a selected m_s value. Figure 5.2 shows typical examples of some experimental data points. The numbers, such as 19.7, 15.6 etc are the

experimental m_s values in t/h. The intermediate points generated using the interpolation relation using points A and B, B and C, E and F, F and G, B and D, F and D are shown in Figure 5.3. As an example, experimental data points E (m_f = 0.0497 kg/s, m_s = 19.9 t/h and ΔP_T = 148.5 kPa) and F ((m_f = 0.051 kg/s, m_s = 16 t/h and ΔP_T = 128 kPa) when interpolated to m_s = 19 t/h, produced a point having m_f = 0.05 kg/s and ΔP_T = 143.9 kPa. This was done for other data points. Reasonably large numbers of intermediate points were generated for 19, 14 and 9 t/h of solids flow rates, so that the trend lines could be drawn through them with sufficient confidence.
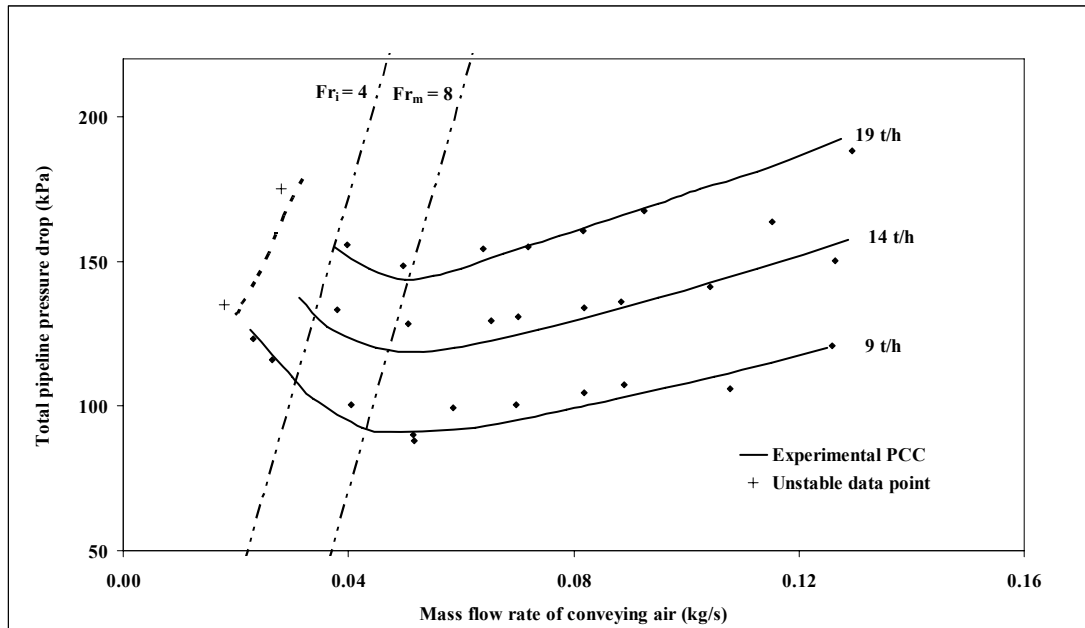
Figure 5.1: PCC for Total Pipeline Pressure Loss for Fly Ash and 69 mm I.D. × 168 m Pipe
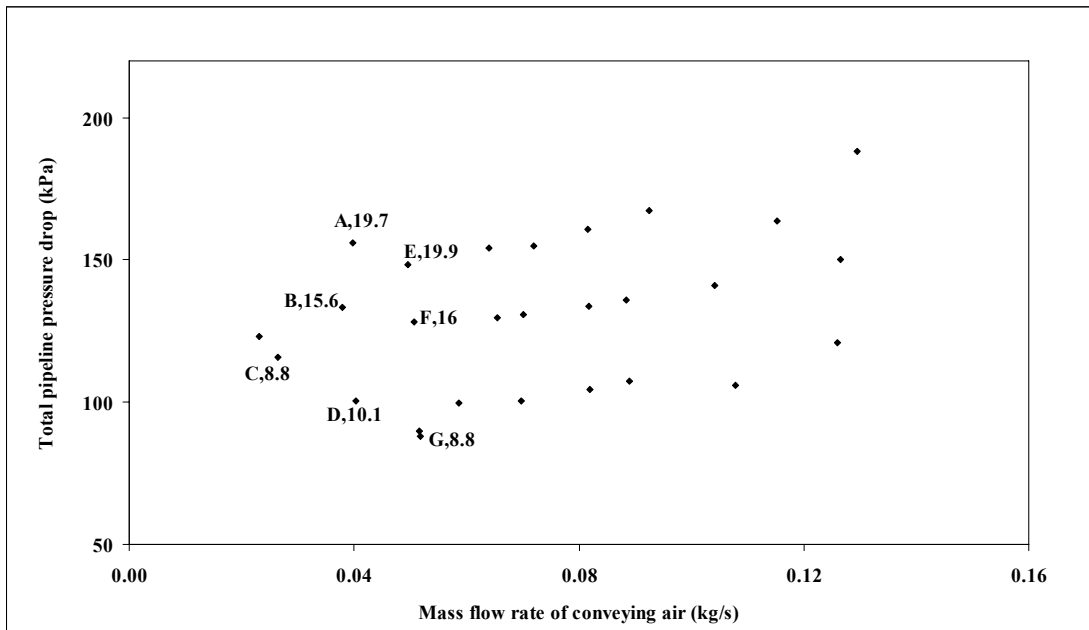
Figure 5.2: Experimental Data Points for Total Pipeline Pressure Loss for Fly Ash and 69 mm I.D. × 168 m Pipe
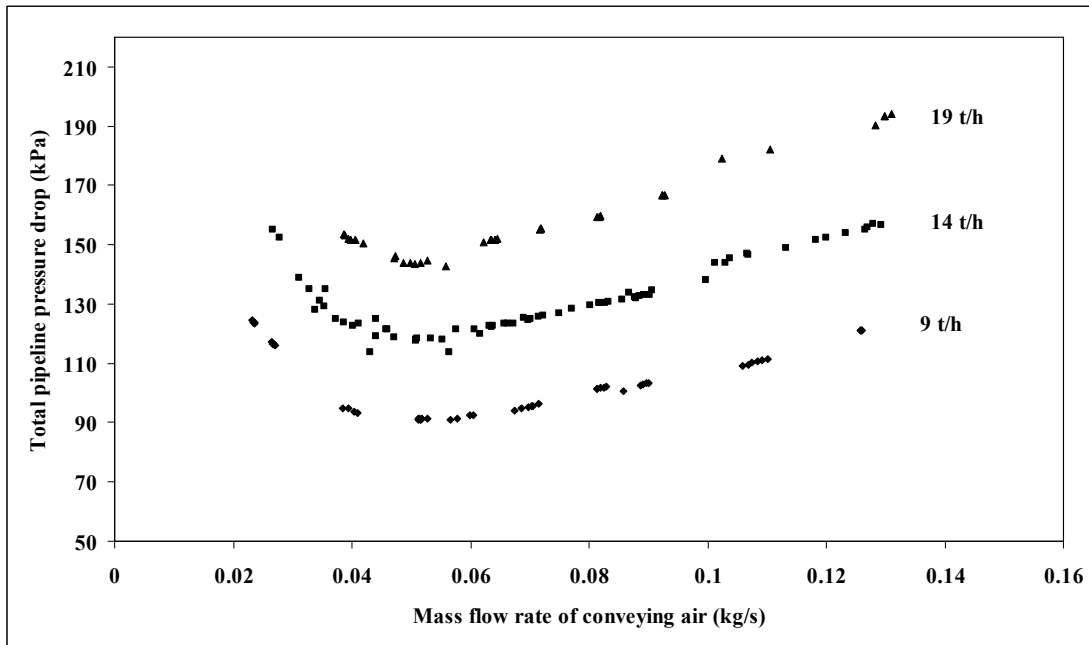
Figure 5.3: Intermediate Points for Total Pipeline Pressure Loss for Fly Ash and 69 mm I.D. × 168 m Pipe

79

It was found that the intermediate points were following clear trends (i.e. with low scattering of data), see Figure 5.3. For an example of estimating the scatter: the average of absolute deviation of the intermediate points for 19 t/h in Figure 5.3 (deviation from the 19 t/h line of Figure 5.1) is 2.75 kPa. Experimental data points and Froude number line at the entry of pipe (i.e. $Fr_i = 4$ line, approximately representing the minimum conveying conditions) have been superimposed on the PCC. The $Fr_i = 4$ line corresponds to $V = 3.3$ m/s at pipe inlet.

Based on the PCC in Figure 5.1, the flow transition from suspension to non-suspension mode for fly ash (suitable for fluidised dense-phase conveying), is relatively gradual, i.e. without any sudden changes in the flow mechanism causing instability, unlike the low-velocity slug-flow of granular products (Wypych and Yi, 2003). A reduction in gas flow rate beyond the good "steady state" dense-phase region caused the formation of unsteady dunes, characterised by enhanced pressure fluctuations. A further decrease of gas flow created build-up of product along the line in the form of deposits. This resulted in an inability of the system to attain a consistent steady-state conveying condition (i.e. the pressure signal would continue to gradually increase with time). This limit has been represented by the "unstable boundary" shown in the figure. A further reduction in gas flow rate would cause flow blockage, indicated by a rapid increase in pressure. It should be noted that due to the practical limit of minimum possible step change of air flow rates for the conveying tests, it was quite a difficult task to precisely locate the unstable boundary. Similar difficulty was also experienced by Mills (2004a). The PCC show reasonably sharp

"U"-shaped trends, with a fairly prominent location of the pressure minimum curve (PMC). The PMC is fairly well represented by a line $Fr_m = 9$, where Fr_m is based on the mean condition for entire pipeline. The PCC show a gradual rise in pressure drop with increasing in air flow rates towards the dilute-phase region. The total pipeline PCC do not explain the reason for this (i.e. whether this is due to a rise in pressure drop characteristic for the straight pipe only sections or due to the increased pressure drop in bends at higher air velocities) and the shape of PCC may be changed if the balance of straight pipe lengths and bends are altered in the pipeline. This has been elaborated in the later portions of this chapter.

Similar to the above, the total pipeline PCC for the 105 mm I.D. × 168 m and 69 mm I.D. × 554 m long pipes were generated using steady state data from the P8 pressure tapping point for the above pipes (Wypych et al., 2005) and are shown in Figures 5.4 and 5.5, respectively.
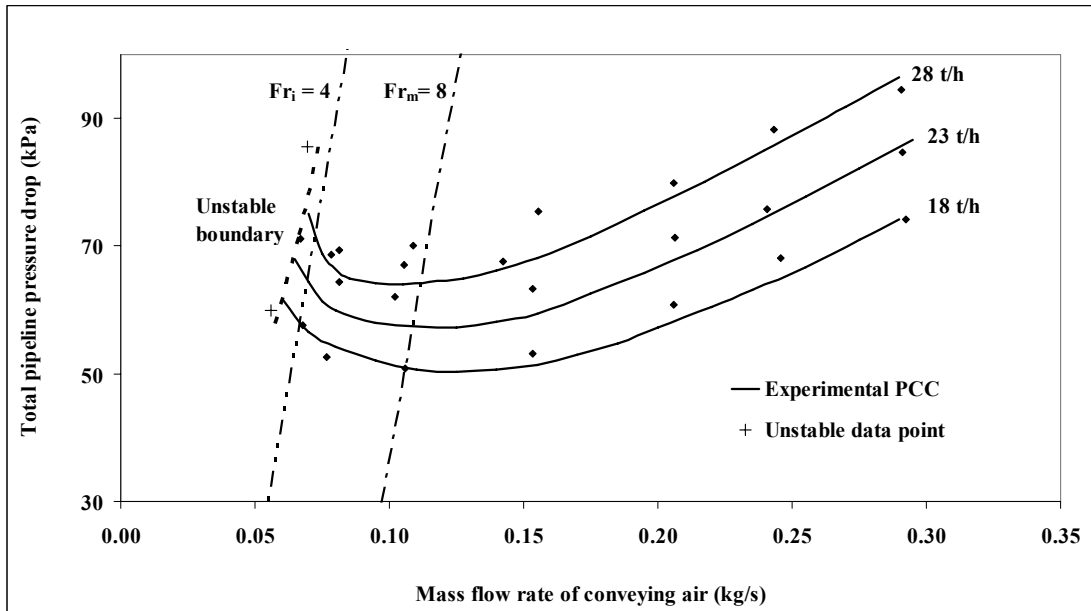
Figure 5.4: PCC for Total Pipeline Pressure Loss for Fly Ash and 105 mm I.D. × 168 m Pipe
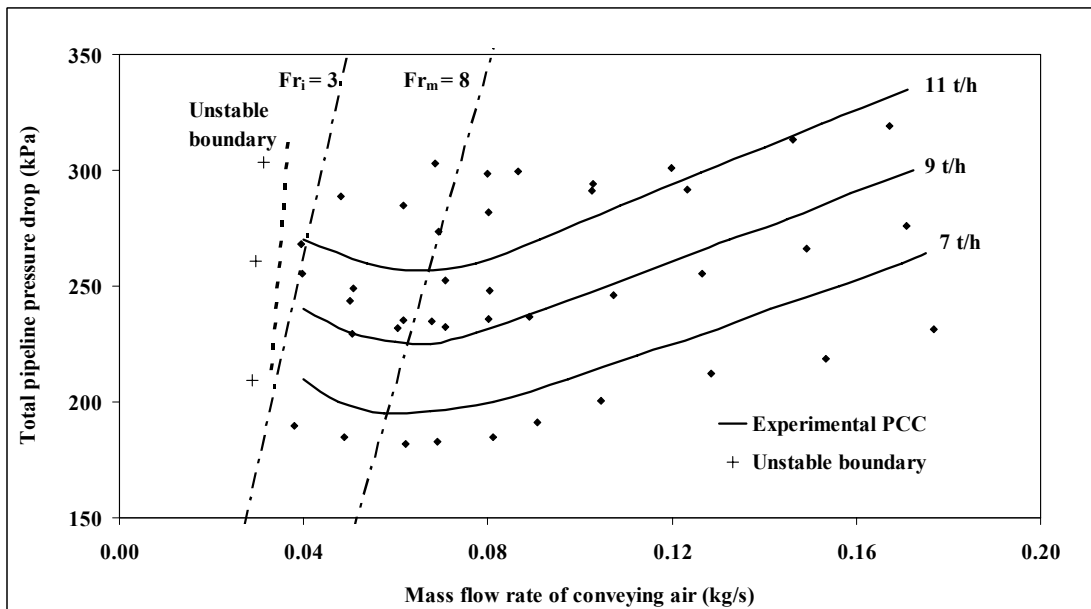
Figure 5.5: PCC for Total Pipeline Pressure Loss for Fly Ash and 69 mm I.D. × 554 m Pipe

Figures 5.2 and 5.3 again display "U"-shaped PCC. For the 105 mm I.D $\times$ 168 m. pipe, air velocity corresponding to $Fr_i = 4$ is 4.06 m/s. For the 69 mm $\times$ 554 m. pipe air velocity corresponding to $Fr_i = 3$ is 2.48 m/s. m/s. Comparing these with the minimum velocity requirement for the 69 mm I.D. $\times$ 168 m pipe (3.3 m/s), minimum velocity requirement at feed point has increased with increase in pipe diameter and decreased with pipe length for this set of data.

Using the "straight pipe" static pressure measurement data from the following pipes and tapping locations over a wide range of steady-state conveying conditions, the PCC for the straight pipe sections were obtained for different solids flow rates.

a) P9-P10 of 69 mm I.D. $\times$ 168 m long pipe

b) P11-P12 of 69 mm I.D. $\times$ 168 m long pipe

c) P9-P10 of 69 mm I.D. $\times$ 105 m long pipe

d) P9-P10 of 69 mm I.D. $\times$ 554 m long pipe

While constructing the PCC, it was appreciated that the construction of "straight pipe" PCC was a relatively more difficult task compared to the total pipeline PCC. This is due to the relatively great scatter of the data set after interpolation. This makes the contours of the constructed PCC somewhat subjective to the judgment of the person constructing the PCC. This is illustrated in the following. Figure 5.6 shows the intermediate points for the "straight pipe" section P9-P10 for the 69 mm I.D. $\times$ 168 m long pipe for different solids flow rates (19, 14 and 9 t/h). These intermediate points

were obtained using interpolation relationship method as explained for Figure 5.1. The final PCC (e.g. Figure 5.7) were obtained by drawing trend lines through these points.
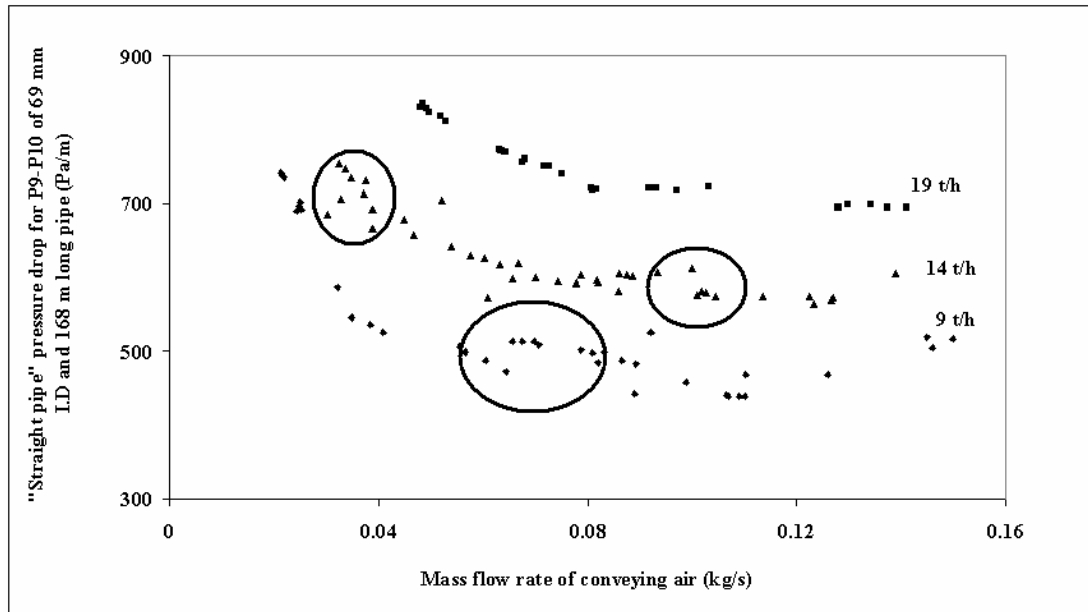
Figure 5.6: PCC Under Construction (Showing Intermediate Points) for P9-P10 "Straight Pipe" Pressure Loss for Fly Ash and 69 mm I.D. × 168 m Pipe

Comparing Figures 5.3 and 5.6, it can be seen that for total pipeline PCC for all the solids flow rate lines, the trends are relatively more consistent (i.e. less scatter of data). At certain portions of the 14 and 9 t/h lines of the "straight pipe" P9-P10 under construction PCC (Figure 5.6), the data points are somewhat scattered (as marked by the elliptical shapes), thus making it somewhat difficult to construct trend lines through these points.

The above effects were found to be more severe for the static pressure tapping points installed on the latter sections of pipes (e.g. at P11/P12 for the 69 mm I.D. × 168 m pipe, see Figure 3.1) and separated by relatively shorter pipe lengths (e.g. 29.24 m straight length between P11-P12 for the 69 mm I.D. × 554 m pipe as shown in Figure 3.3, compared to the 52.68 m distance between P9-P10 for the 69 mm I.D. × 168 m pipe, Figure 3.1). Some difficulty was faced for constructing the P11-P12 PCC for the 69 mm I.D. × 168 m pipe. It was believed that the P11 tapping point being sufficiently away from the preceding bend, the pressure signals were not influenced by bend effects. In fact, it was found that the data obtained from the P11-P12 tapping points of the 105 mm I.D. × 168 m and 69 mm I.D. × 554 m long pipes were too scattered (even after interpolation), thus making them unsuitable for use to construct "straight pipe" PCC. Figures 5.7 to 5.10 show the "straight pipe" PCC, which were able to be constructed with relatively more amount of accuracy and confidence (compared to the P11-P12 PCC).
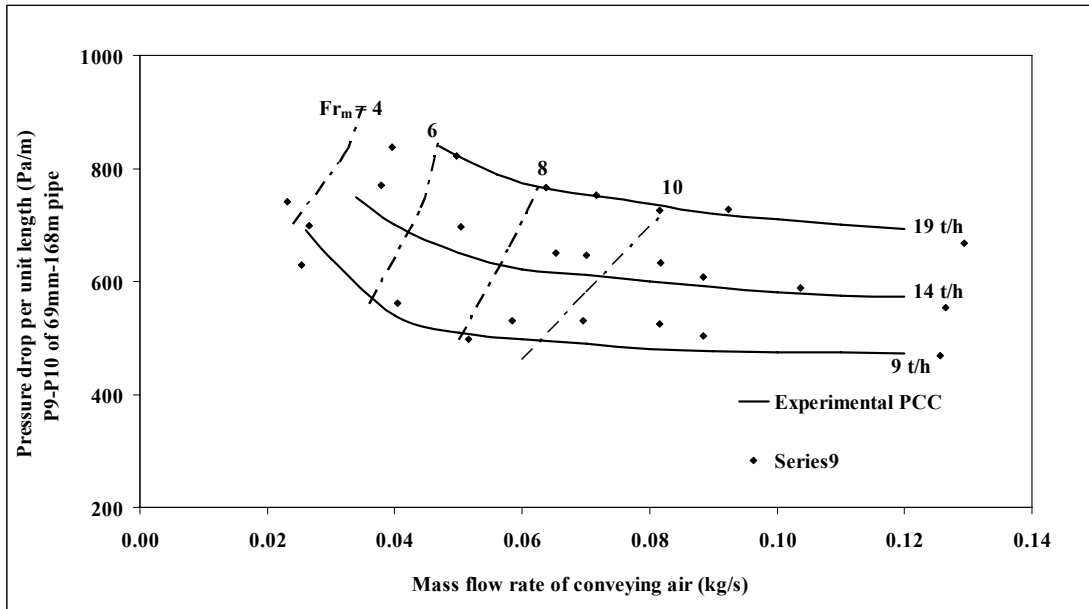
Figure 5.7: PCC for P9-P10 "Straight Pipe" Pressure Loss for Fly Ash and 69 mm
I.D. × 168 m Pipe
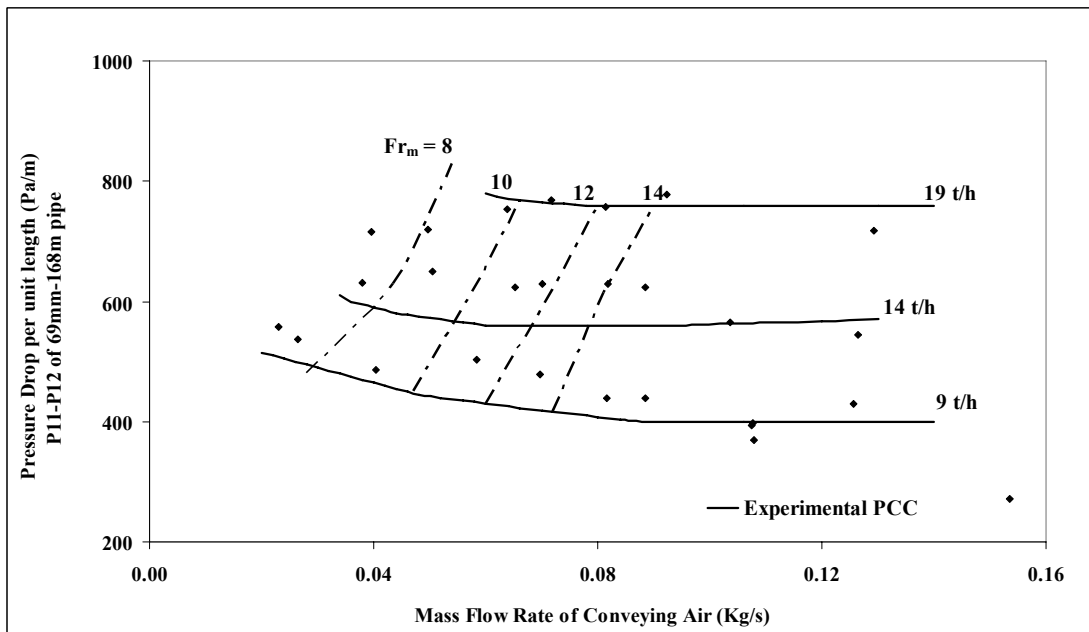
Figure 5.8: PCC for P11-P12 "Straight Pipe" Pressure Loss for Fly Ash and 69 mm
I.D. × 168 m Pipe
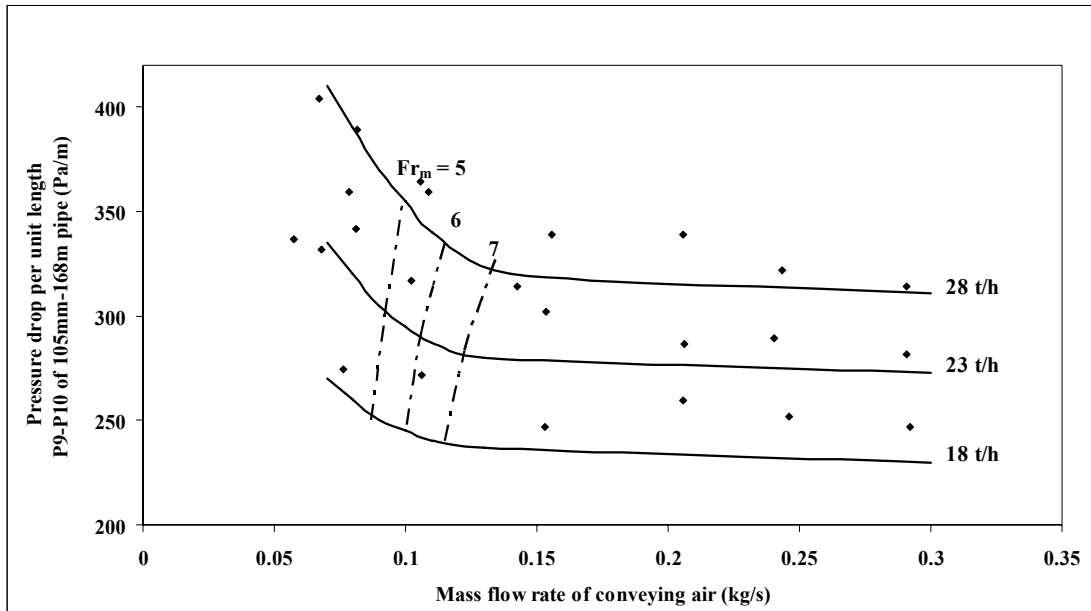
Figure 5.9: PCC for P9-P10 "Straight Pipe" Pressure Loss for Fly Ash and 105 mm

I.D. × 168 m Pipe
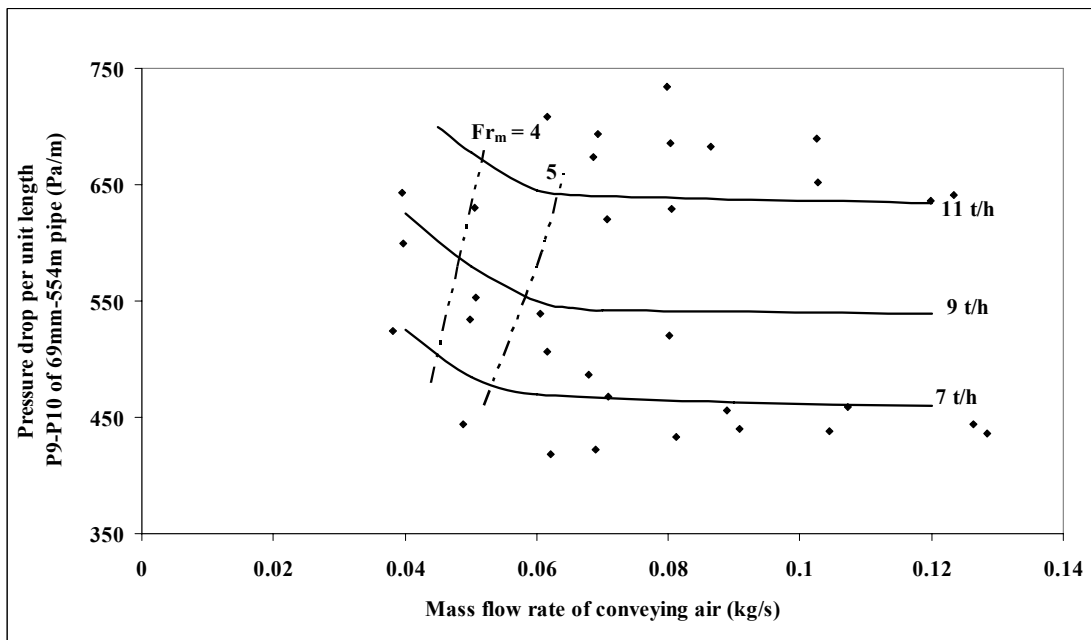
Figure 5.10: PCC for P9-P10 "Straight Pipe" Pressure Loss for Fly Ash and 69 mm

I.D. × 554 m Pipe

Comparing Figures 5.7 and 5.8, it becomes evident that the PCC for "straight pipe" sections (even for the same product, i.e. fly ash) differ depending upon the location of the tapping points, thus indicating a change in local flow mechanisms. For $m_f = 0.082$ kg/s, $m_s = 14.2$ t/h, mean velocity of within P9-P10 is calculated as 9 m/s, whereas for the same values of m_f and m_s (same experiment), mean velocity of within P11-P12 is calculated as 11.2 m/s. The PCC obtained from the initial section of the pipe loop (i.e. P9-P10) show a significant portion where pressure drop decreases with an increase in air flow rate. On the other hand, the PCC obtained from the latter section of the pipe loops (i.e. P11-P12) show a more significant flat section (i.e. pressure drop remains almost constant with increasing air flow rate). This indicates a possible change in flow characteristics along the pipeline. It should also be mentioned that the "straight pipe" PCC did not generate "U"-shaped curves with a sharp change in direction of slope. In fact the reason for "U"-shape which may happen in total pipeline PCC could be contributed significantly due to the rise in bend loss with increase in air velocity (Pan, 1992; Mills 2004). Due to the absence of a prominent change in slope of PCC, it is difficult to precisely locate the point of pressure minimum. It can be seen in Figures 5.7 and especially in Figures 5.9 and 5.10 that the rather sharp negative slope of the PCC (which exist in the low velocity zone) is reduced or gets nearly flat (though with still some negative slope, see Figures 5.9 and 5.10) after certain air flow rates. The constant Fr_m lines corresponding to this transition are $Fr_m = 8$ to 10 (mean air velocity: 6.6 to 8.2 m/s) for pipe, 7 (mean air

velocity: 7.1 m/s) and 6 (mean air velocity: 4.9 m/s) for the 69 mm I.D. × 168 m, 105 mm I.D. × 168 m and 69 mm I.D. × 554 m pipes, respectively.

To investigate the relative influence of straight pipe sections, bends and verticals on the location of the PMC on the total pipe PCC, PCC for the following different sections of the 69 mm I.D. × 168 m long pipe have been compared:

a)   Between pressure tappings P9 and P11 (pipe length: 72.78 m, having 2 × 90 degree bends) – see Figure 5.10;

b)   Between pressure tapping P11 and exit to the pipe (pipe length: 71.27 m, having 2 × 90 degree bends and a 7m vertical lift) – see Figure 5.11;

c)   Between pressure tapping P12 and exit to the pipe (pipe length: 30.86 m, having 2 × 90 degree bends and a 7m vertical lift) – see Figure 5.12.
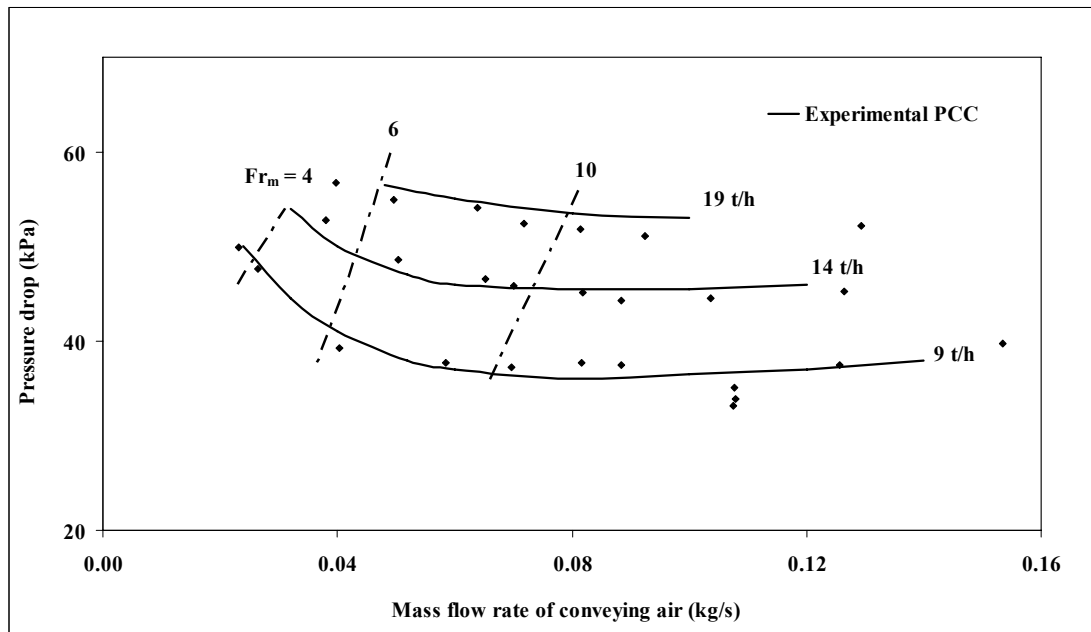
Figure 5.11: PCC between Pressure Tappings P9-P11 (Pipe Length: 72.78 m, Having

2 × 90 Degree Bends) for Fly Ash and 69 mm I.D. × 168 m Pipe
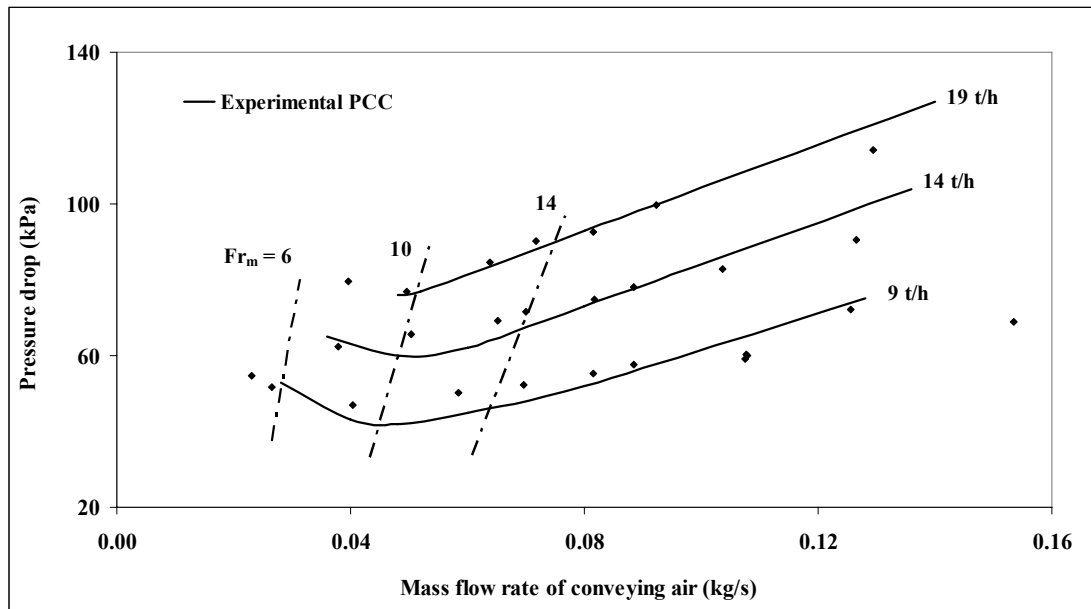
Figure 5.12: PCC between Pressure Tapping P11 and Pipe Exit (Pipe Length: 71.27 m, having 2 × 90 Degree Bends and a 7m Vertical Lift) for Fly Ash, 69 mm I.D. × 168 m Pipe
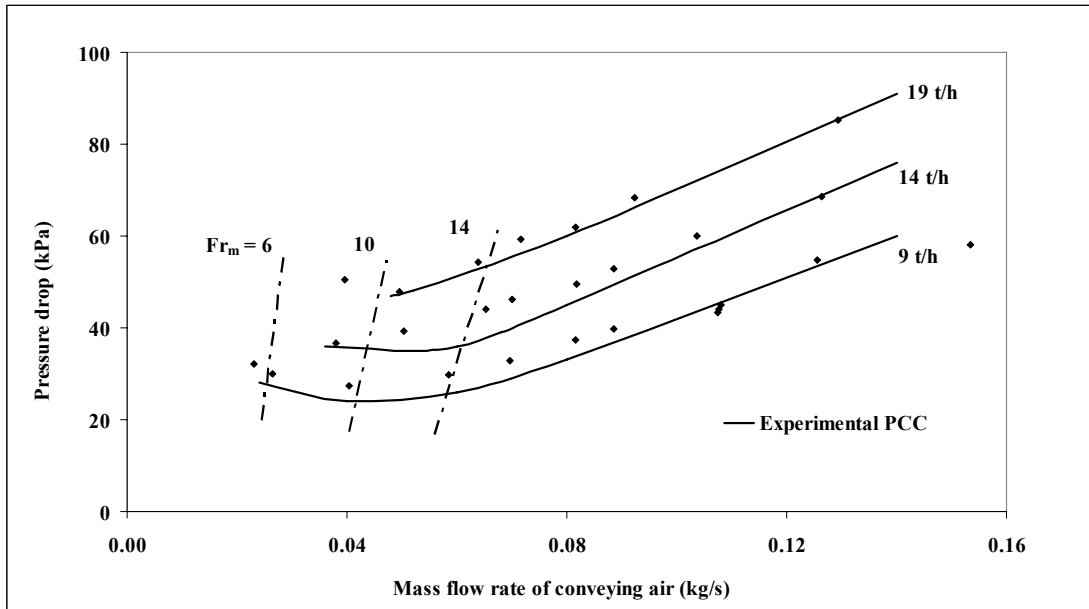
Figure 5.13: PCC between pressure tapping P12 and exit to the pipe (pipe length: 30.86 m, having 2 × 90 degree bends and a 7m vertical lift) for Fly Ash and 69 mm I.D. × 168 m Pipe

The results show that each pipe segment has its own PCC, the shape of which depends on the location of that pipe segment (i.e. location of pressure tappings) with respect to the total pipe length and also on the effect of any bends and verticals included in the segment. The pressure drop decreases or remains almost constant with an increase in the mass flow rate of air (within the tested range of air flow), as shown previously in Figures 5.7 to 5.10, respectively for sections with only "straight pipe" lengths, whereas, inclusion of bends and verticals have resulted in "U"-shaped PCC or sharply rising pressure drop characteristics in Figure 5.12 and 5.13. The PCC for the total pipe is a superimposition of the PCC of the individual pipe segments. As a result, the shape of the total pipeline PCC will depend on the relative contribution of the pressure drop characteristics of each of the individual pipe segments (such as

horizontal straight pipe, bends and verticals), e.g. addition of more bends in the system is expected to produce a sharply rising pressure drop characteristics towards the dilute-phase regime. This is to cause a shift of the PMC (for total pipe) towards the left.

5.2.2   ESP dust

Similar to the case of fly ash, total pipeline PCC for the 69 mm I.D. × 168 m, 105 mm I.D. × 168 m and 69 mm I.D. × 554 m long pipes were obtained (Wypych et al., 2005) using steady state data from P8 pressure tapping point data for for a wide range of air and solids flow rates. The total pipeline PCC are shown in Figures 5.14 to 5.16.
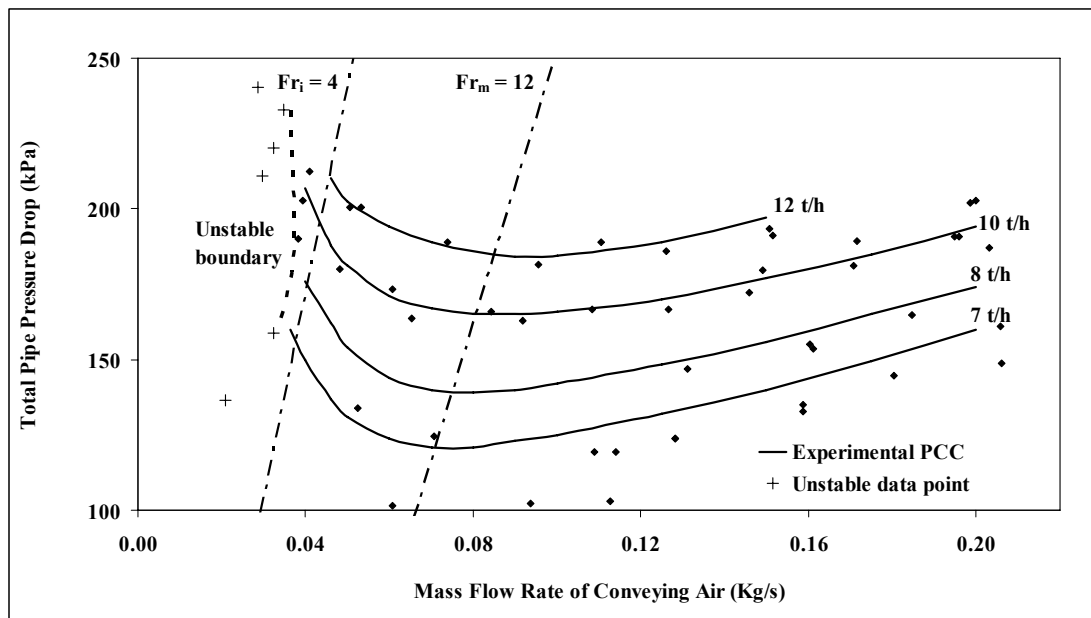
Figure 5.14: PCC for Total Pipeline Pressure Loss for ESP Dust and 69 mm I.D. × 168 m Pipe
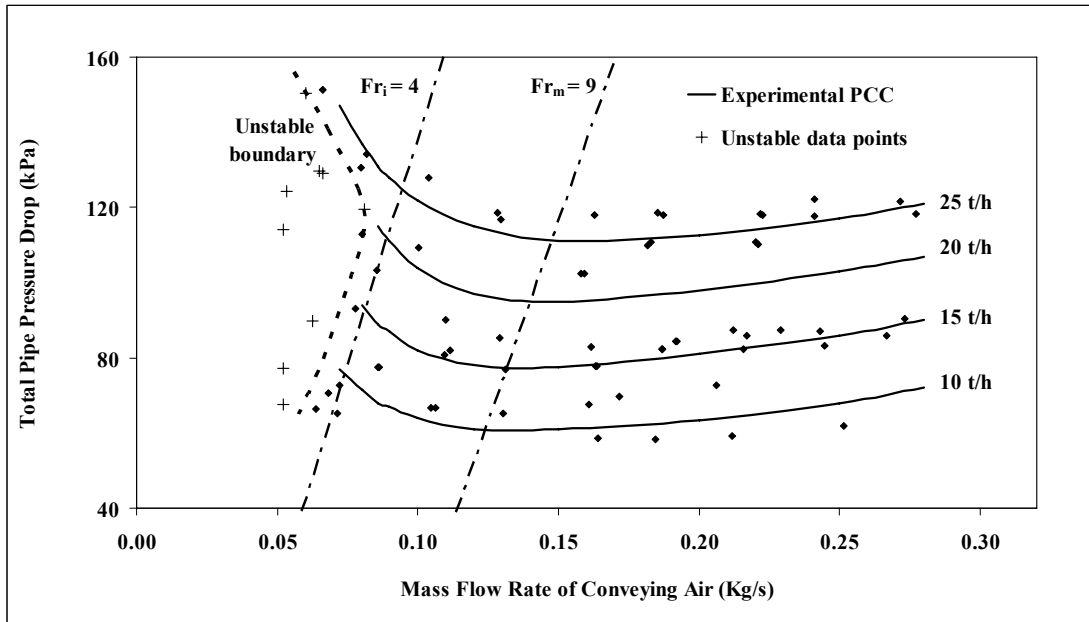
Figure 5.15: PCC for Total Pipeline Pressure Loss for ESP Dust and 105 mm I.D. × 168 m Pipe
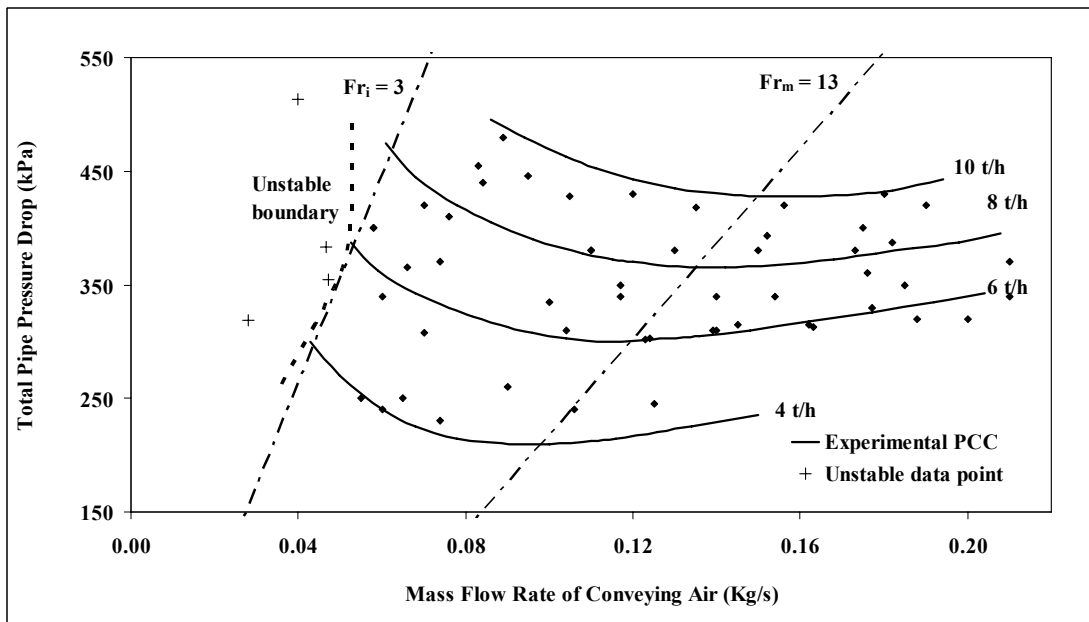
Figure 5.16: PCC for Total Pipeline Pressure Loss for ESP Dust and 69 mm I.D. × 554 m Pipe

The figures show that for all the three pipes, the pressure drop characteristics towards the high air flow region are surprisingly "flat" compared to fly ash PCC (Figure 5.1, 5.4, 5.5). This is perhaps due to comparatively larger dense-phase characteristics and/or lesser pressure drop occurring due to the bends for this powder. Also, comparing the pressure drop characteristics for fly ash and ESP dust for equivalent solids flow rates, conveying the ESP dust causes almost twice as much pressure drop as fly ash (especially in dense-phase). The PMC for the 69 mm I.D. × 168 m, 105 mm I.D. × 168 m and 69 mm I.D. × 554 m pipes correspond to the Fr_m = 12, 9 and 13 lines, respectively. Comparing Figures 5.14 and 5.15, it can be seen that the position of the unstable boundary has changed (in terms of minimum air flow rate requirement). Also, the solids mass flow rates achievable have reduced with decrease in pipe diameter. These are all the results of a change in pipeline diameter. Lower air flows were able to be achieved at high solids mass flow rates (e.g. refer to the 25 t/h curve shown in Figure 5.15) – it is possible that the higher throughput (and product turbulence) helps to "push through" the powder in the pipeline. It is also observed that fairly high solids loadings are possible for this powder and pipeline (e.g. m* = m_s/m_f = 70); for a wide range of m_s (e.g. 10 to 20 t/h), a suitable pick-up velocity appears to be $V_i \approx 4$ m/s and minimum conveying velocity $V_{i, min} \approx 3.5$ m/s (i.e. to avoid flow instabilities); for m_s = 25 t/h, the pick-up velocity can be reduced to $V_i \approx 3$ m/s.

The only "straight pipe" PCC, which could be reliably constructed, was that for the P9-P10 tapping point data of 69 mm I.D. × 554 m long pipe. This is shown in Figure 5.17. The P11-P12 data points for the same pipeline were found to be somewhat scattered to an extent of making them unsuitable to use (similar to the cases of P11-P12 data for fly ash for larger/longer pipes). A study of the DATA TAKER plots (graphical output of DATA TAKER) for the "straight pipe" pressure tapping points (such as P9, P10, P11 and P12) for the 69 mm I.D. × 168 m and 105 mm I.D. × 168 m pipes revealed that some of these tapping points were somewhat unresponsive to the local pipeline pressure (e.g. clearly displaying considerably lower pressure than expected). This could be caused due to the possible choking of the filters of these pressure tapping points by powders during test program (Wypych et al., 2005), especially because of the finer size of ESP dust powder (d_{50}: 7 µm). It seems that this portion of the test work was carried out (Wypych et al., 2005) without evaluating/analysing the DATA TAKER experimental plots periodically (e.g. after every 5 to 6 experiments, the practice followed while doing the test work with "white powder" – see Chapter 3), just to make sure that everything (e.g. instrumentation – pressure tapping points) was responding properly. As a result, a good part of the valuable information, which could have been obtained from such extensive test program, could not be used.
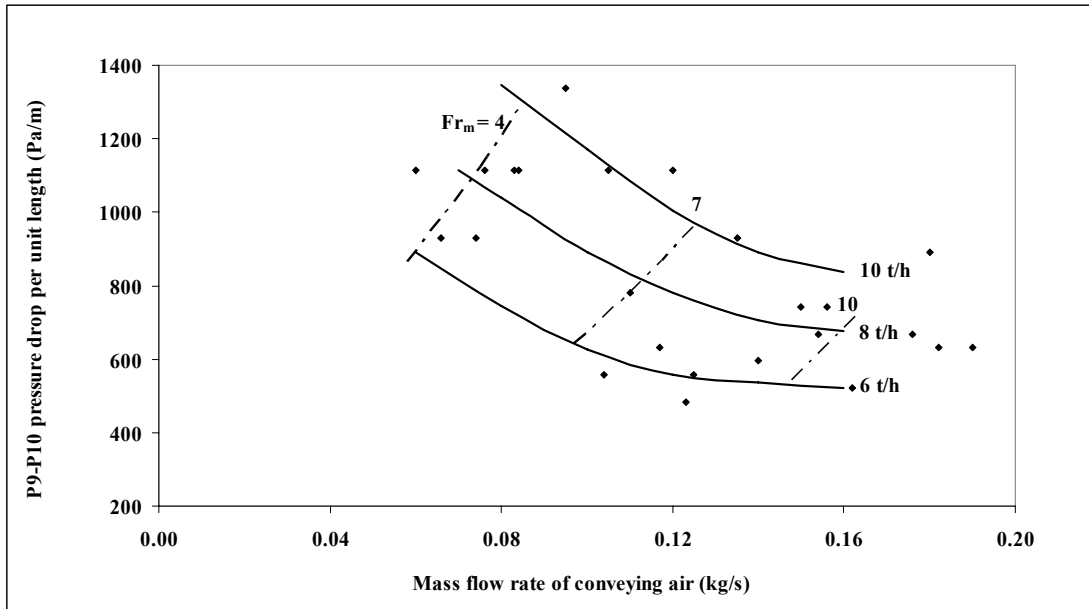
Figure 5.17: PCC for P9-P10 "Straight Pipe" Pressure Loss for ESP Dust and 69 mm I.D. × 554 m Pipe

Figure 5.17 shows a significant portion of PCC where the pressure drop decreases with an increase in air flow rate. This is followed by a narrow region where the pressure drop remains almost constant with increase in air flow rates ("flat" shaped PCC), possibly indicating a dense-to dilute-phase transition. It is difficult to accurately locate the location of the PMC. In this case, the pressure minimum points are considered where the PCC start to flatten out with increasing air flow rate, i.e. the PMC corresponds to $Fr_m = 10$ line. It is to be noted that this PMC line (for the "straight pipe") is to the left of that corresponding to the total pipeline PCC (i.e. $Fr_m = 13$, see Figure 5.15).

5.2.3 "White powder"

Using the steady state conveying data of "white powder" for a wide range of flow conditions (dilute- to fluidised dense-phase), obtained from the P8 pressure tapping point of the 69 mm I.D. × 148 m pipe (see Figure 3.5), total pipe PCC were constructed, shown in Figure 5.18.
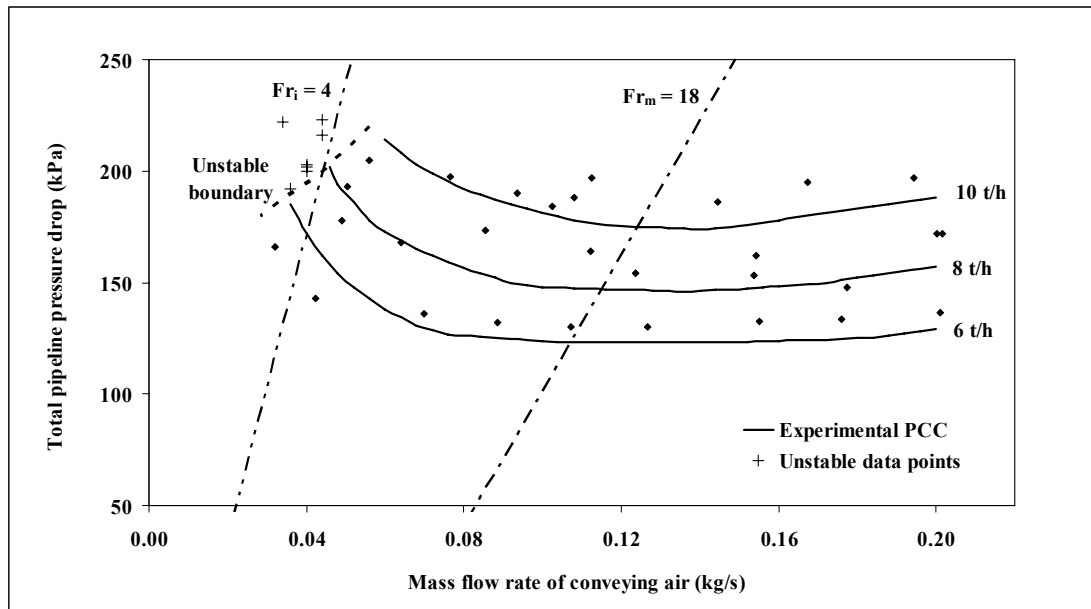
Figure 5.18: PCC for Total Pipeline Pressure Loss for "White Powder" and 69 mm I.D. × 148 m Pipe

Figure 5.18 displays slightly "U"-shaped trends (rather flat shaped), the changes in gradients of the PCC are not sharp (e.g. as compared to the fly ash PCC, Figure 5.1). The PMC seems to be satisfactorily represented by the $Fr_m = 18$ line, which is of considerably higher value than that of the corresponding PMC lines for fly ash and

ESP dust for similar lengths of pipe and having the same diameter (see Figures 5.1 and 5.13, respectively).

Using steady state "straight pipe" data obtained from the P9-P10 and P11[+]-P12 tapping points (Figure 3.5) for a wide range of flow conditions, the following "straight pipe" PCC were obtained, shown in Figures 5.19 and 5.20.
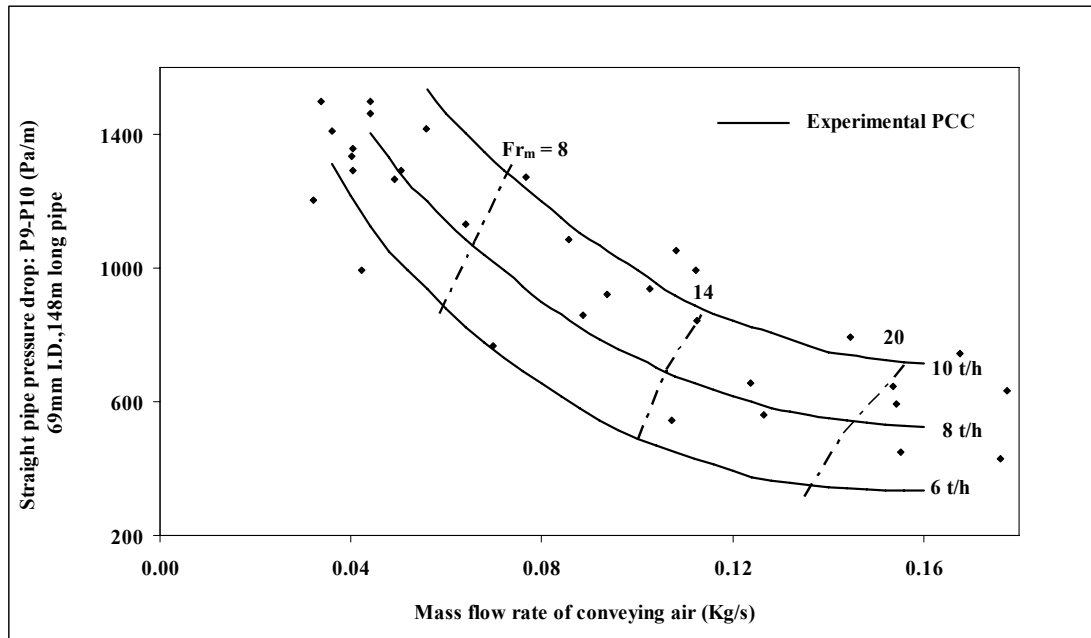
Figure 5.19: PCC for P9-P10 "Straight Pipe" Pressure Loss for "White Powder" and 69 mm I.D. × 148 m Pipe
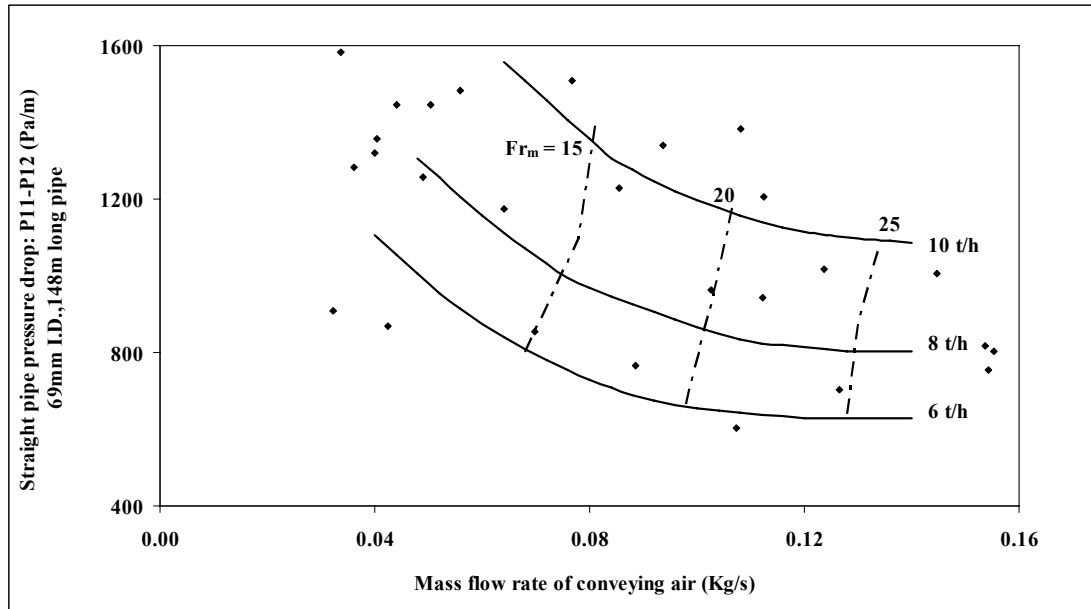
Figure 5.20: PCC for P11[+]-P12 "Straight Pipe" Pressure Loss for "White Powder" and 69 mm I.D. × 148 m Pipe

The above figures show that the PCC obtained from P9-P10 and P11[+]-P12 contain almost entirely region where the pressure drop decreases with an increase in air flow rate. PCC obtained from the latter section of the pipe loop (i.e. P11[+]-P12) show signs of "flat" portions (i.e. pressure drop remains almost constant with increasing air flow rate) in the high velocity end. Similar to the case of fly ash (Figures 5.7 and 5.8), this again indicates a change in flow characteristics along the flow direction (i.e. along the pipe length). It is to be highlighted that the PMC for total pipe (Figure 5.18) corresponds to $Fr_m = 18$ (though it is difficult to locate this accurately due to the flat nature of curves in this portion), whereas the straight pipe PCC (Figures 5.19 and 5.20) do not show a PMC.

100

5.3   Conclusions

Based on the results presented in this chapter, it can be concluded that the nature of the "U"-shape and the location of the PMC for the total pipeline PCC are significantly influenced by the pipe layout (e.g. location and number of bends) and not entirely by the dense- to dilute-phase transition of flow mechanism. This is in contrary to Pan et al. (1994), where PMC for total pipe PCC seem to have been used to distinguish between dense- and dilute-phase. "Straight pipes" generally show a decreasing pressure drop characteristics (as evident from the "straight pipe" PCC drawn in this chapter), whereas bends have increasing characteristics with increase in air flow rates (Pan, 1992; Mills, 2004) and these are to be modelled and scaled-up separately (Bradley, 1989; Pan and Wypych, 1998). It must also be mentioned that in a longer pipeline (or where the pressure drop across the pipe is sufficiently large), even if the flow condition near the feed point/initial section of pipe is dense-phase, due to the significant increment in velocity of flow (caused by the expansion of air along the pipe length), the flow mechanism could change from dense to dilute in the latter sections of the pipe, i.e. for a particular set of mass flow rate of air and product, it is possible to have two conditions of flow (dense- and dilute-phase) along the pipe. The value of the total pressure pipeline pressure drop will plot the data point either to the left or to the right of the PMC. Hence, if the PMC on the total pipe PCC was considered as the criterion to delineate the dense to dilute-phase transition, then the flow would have been termed as either "dense" or "dilute" -phase. This would be incorrect, because in reality the total system contains both phases (at different

portions of the pipe). However, confirming this aspect would require thorough investigation and may be considered as a potential area for future research.

CHAPTER 6: Scale-up Evaluation of Existing Models for Solids Friction

6.1   Introduction

From the review of the various literature (Chapter 2), it appears that the most popular form of representing pressure drop for a solids-gas mixture flowing through a straight horizontal section of pipe is by using equation (2.1), as given by Barth (1958). In this expression, the main challenge is to determine the solids friction factor accurately. Whereas more fundamental methods have been developed based on powder mechanics for certain products and modes of flows, such as low-velocity slug-flow of granular products, the modelling of dense-phase conveying of powders has been a far more difficult problem to solve at a similar level of detail. Due to this reason, empirical power function based models have been employed over the years by various researchers (Stegmaier, 1978; Pan, 1992; Pan and Wypych, 1998; Wypych, 1989; Jones and Williams, 2003; Williams and Jones, 2004) to avoid the need to develop fundamental relationships between friction factor and the relevant particle and bulk properties. These models have used different parameter groupings and have shown good results when applied to the researchers' own data, but have not been tested properly against important criteria, such as scale up accuracy and stability. As a result, at the beginning of project, there was not a clear idea about the "true" status of the existing design techniques (in terms of scale-up capability). This would also justify the requirement of further work, i.e. if the existing models are found unreliable for scale-up design, then only the requirement would be to pursue advanced studies towards improving the modelling procedure. Therefore, one preliminary objective of the project was to examine the accuracy and stability of the existing applicable and/or popular solids friction factor models by applying them under different scale-up

conditions of conveying pipeline diameter/length and comparing the predicted with the experimental pneumatic conveying characteristics (PCC). Initial investigations were carried out using the existing data of fly ash conveying in pipes of different diameter and length. Afterwards, similar evaluation work was extended using the test data of "white powder", ESP dust and a different sample of fly ash (Pan, 1992). Results of the above investigations are presented in the following sections of this chapter. During the above mentioned time frames, simultaneous efforts were also pursued to examine the accuracy of the existing modelling formats (and their use of parameter groupings). Results of such efforts are provided in the following chapter (Chapter 7).

6.2   Existing models for solids friction factor

Some of the other existing applicable/popular models for solids friction factor are mentioned below. The models also appear in the literature review chapter (Chapter 2). However, it was considered prudent to include a brief description here (mainly to justify the reasons for selection of the models for the present evaluation work).

Stegmaier (1978) developed a power function based model for data obtained on fine powders (d_s: 15 to 112 μm and ρ_s: 1500 to 4100 kg/m^3) and a range of pipe sizes. The original model is presented in equation (6.1). It is believed that the data used by Stegmaier (1978) was obtained directly from straight pipes. Weber (1981) presented a modified form of Stegmaier model (1978), as given in equation (6.2), by modifying

the particle Froude number (from being based on particle diameter to pipe diameter). Since the Stegmaier (1978) and (Weber, 1981) model was derived for a range of powders covering the size range of the powders used in this study (i.e. fly ash, ESP dust, "white powder" and fly ash, Pan, 1992), these models were considered relevant for the present investigation.

$$\lambda_s = 2.1 \ m^{*-0.3} \ Fr_m^{-2} \ Fr_{sd}^{0.5} \ (D/d_s)^{0.1} \tag{6.1}$$

$$\lambda_s = 2.1 \ m^{*-0.3} \ Fr_m^{-2} \ Fr_{sD}^{0.5} \ (D/d_s)^{0.1} \tag{6.2}$$

Pan and Wypych (1998) derived a model based on the experimental data from four different fly ash samples with median particle size ranging from 3.5 to 58 μm, particle density and loose poured bulk density ranging from 2180 to 2540 kg/m^3 and 634 to 955 kg/m^3, respectively. This model is given in equation (6.3). Although this model is a semi-empirical one, it was derived for fly ash of different size range, which covers the median size of the given fly ash samples (30 and 16 μm). Hence, this model was considered relevant for evaluation in this study (for fly ash cases).

$$\lambda_s = 3.2343 \ (m^*)^{-0.4673} \ (Fr_m)^{-1.5560} \ (\rho_m)^{-0.4312} \tag{6.3}$$

Jones and Williams (2003) obtained a solids friction factor model using "back calculation" method by conveying various powders, such as pulverised fuel ash, iron powder, copper ore and flour (ρ_s: 1470 to 5710 kg/m^3; "mean diameter": 42 to 90 μm) through a test rig (L = 50 m, D = 53 mm, 9 bends). The model is given by equation

106

(6.4). Although the size of powders conveyed by Jones and Williams (2003) are larger than the given ESP dust and fly ash samples, the model was still considered worthwhile for evaluation as Jones and Williams (2003) had conveyed their powders in fluidised-dense phase, which is of the same nature of flow achieved for the powders being considered for this study.

$$\lambda_s = 83/\{(m^*)^{0.9} Fr_i^2\} \tag{6.4}$$

6.3 Evaluation of models

6.3.1 Stegmaier (1978)
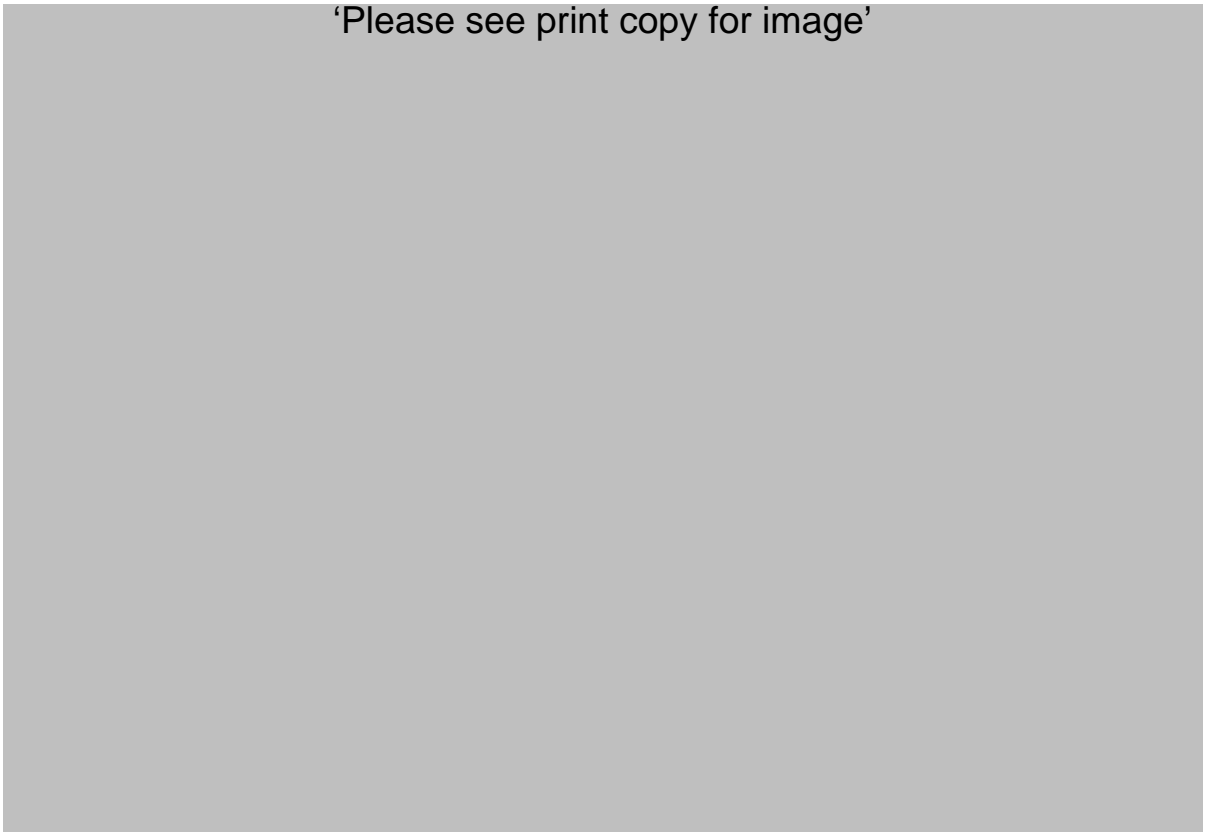
The model was evaluated for scale-up accuracy and stability by applying it to predict the total pipeline drop, initially for the 69 mm I.D. × 168 m pipe, for various solids flow rates for fly ash and comparing the predicted pneumatic conveying characteristics against the experimental plots. For calculation of total pipeline PCC, "Macro" based iterative programs were generated (for different pipes), which progressively calculate the pressure losses starting from the pipe exit to the inlet. Maximum length of straight section (in the program input) was limited to 40 m, by optimising the accuracy and complexity of programming. An example of a typical program using a model derived in Chapter 10 of this thesis (for the 69 mm I.D. × 168 m long pipe) is provided in Appendix A4.3.

The results of evaluation of Stegmaier (1978) model for the 69 mm I.D. × 168 m long pipe are shown in Figure 6.1. Losses due to the bends were calculated using Pan and Wypych (1998) bend model, as the same was derived exclusively using fly ash data, hence was thought to be more accurate when applied to fly ash conveying. Further discussions on the selection of appropriate bend models are provided in Chapter 11. Losses due to the vertical and initial acceleration were estimated as per Marcus et al. (1990). All the predicted conveying characteristics have been restricted to a minimum initial Froude number of approximately 4, as below this range flow instabilities/blockages were found to occur during the experimental program.

General note for all the evaluation work carried out in Chapter 6, 7 and 10: The total pipeline pressure drop is a sum of "straight pipe" losses and bend pressure drops (neglecting the vertical and initial acceleration loss). These two have been separately scaled up here, by using various "straight pipe" models and either Chambers and Marcus (1986) or Pan and Wypych (1998) bend models. Table 6.1 shows "estimated" bend loss values for 69 mm I.D. × 168 m, 105 mm I.D. × 168m and 69 mm I.D. × 554 m pipes for different rages of solids and air flow (dense- to dilute-phase) using Pan and Wypych (1998) and Chambers and Marcus (1986) models with fly ash. Similar results were obtained with ESP dust.

Table 6.1: Estimated bend loss for fly ash for different pipes with Pan and Wypych (1998) and Chambers and Marcus (1986) models

'Please see print copy for image'

Note: The estimated bend loss for the 69 mm I.D. × 554 m apparently looks lot less than what it should be (considering there were 17 bends in line), but the product was conveyed with relatively reduced m* in comparison to the other two pipes and the bend models have positive exponents of m* in their expressions.

The increase in estimated bend loss towards dilute-phase is in congruence with the experimental bend loss characteristics of Pan (1992) and Mills (2004). These estimated bend loss values in the dense-phase regime (which is the main scope of this thesis) are only up to approximately 10% to the corresponding total pipeline pressure losses (total pipeline PCC are provided later in the chapter). Hence, estimated bend

losses, on their own, do not influence the quality of prediction for total pipeline pressure loss in dense-phase. Example: if for the 69 mm I.D. × 168 m pipe, the predicted pressure drop for a dense-phase point (using a "straight pipe" model and Pan and Wypych (1998) bend model) is 200 kPa, whereas the actual/experimental pressure drop value for that point was 150 kPa, this would mean if the estimated bend loss of 20 kPa is subtracted from 200 kPa and approximately 15 kPa for vertical and acceleration loss (tentative values of vertical and acceleration losses are obtained using Marcus et al. 1990) , the estimated "straight pipe" loss (165 kPa) would still be more than the total pipe loss; in fact the actual experimental "straight pipe" loss will be below 150 kPa, as bend, vertical, acceleration losses are to similarly subtracted from 150 kPa. Hence, for this example, it can be inferred that there are some inaccuracy with the "straight pipe" model.

In the evaluation work of Chapter 6 and 7, Pan and Wypych (1998) bend model is used for fly ash cases and Chambers and Marcus (1986) model for the other products (such as ESP dust). Pan and Wypych (1998) model was developed for fly ash. Hence the same was expected to be relatively more accurate for the same product. Chambers and Marcus (1986) model was for other products, as other researchers (such as Jones and Williams, 2003) have also used this model. So, there could be some merit in it. In any case, it should be noted that the issue of bend loss estimation in dense-phase did not influence the evaluation "straight pipe" models (as provided in Table 6.1 and the subsequent discussion).

General note regarding assessing the accuracy of prediction: Appendix A.5 lists ratio of the amount of over/under-prediction (using different models and pipelines) to the respective experimental PCC of all the evaluation work carried out this thesis. The ratio are provided in percentages. Percentages are provided only for dense-phase region, as the contribution of straight pipe losses (the aim is to find the accuracy of prediction of this) in the predicted total pipeline pressure drop values are relatively more in dense-phase than in dilute. The overall percentages are obtained by averaging individual percentages for each solids flow rates.

‘Please see print copy for image’

Figure 6.1: Experimental Versus Predicted PCC for Fly Ash and 69 mm I.D. × 168 m Pipe using Stegmaier (1978) Model

Stegmaier (1978) model generated dramatically inaccurate results for both dilute- and dense-phase. As a result, it was decided not to pursue this model any further in this investigation for this sample of fly ash. Afterwards, the model was used to predict for ESP dust for various solids flow rates for pipelines of different diameters and lengths (viz. 69 mm I.D. × 168 m, 105 mm I.D. × 168 m and 69 mm I.D. × 554 m long). Figures 6.2 to 6.4 compare the predicted and experimental PCC. The Chambers and Marcus (1986) model was used to predict the losses due to the bends, as the model is considered to be a general purpose model and was used by other researchers for various powders (Jones and Williams, 2003).

‘Please see print copy for image’

Figure 6.2: Experimental Versus Predicted PCC for ESP Dust and 69 mm I.D. × 168 m Pipe using Stegmaier (1978) Model

‘Please see print copy for image’

Figure 6.3: Experimental Versus Predicted PCC for ESP Dust and 105 mm I.D. × 168 m Pipe using Stegmaier (1978) Model

'Please see print copy for image'

Figure 6.4: Experimental Versus Predicted PCC for ESP Dust and 69 mm I.D. × 554 m Pipe using Stegmaier (1978) Model

The results show that for the 69 mm I.D. ×168 m long pipe, the predicted PCC under-predicts the experimental PCC, with the amount of inaccuracy increasing towards the dilute-phase region. However, the shape of the predicted PCC appears to indicate a "U"-shaped trend. The predicted PCC for diameter scale-up (105 mm I.D. × 168 m long pipe) provide over-prediction in dense-phase and under-prediction in dilute-phase. However, the degree of inaccuracy is not too alarming (especially comparing with the dilute-phase predictions of Figure 6.3, which provided significant under-prediction that will have threat of designing an undersized system). Quite surprisingly, in the dense-phase region for the longer pipe (69 mm I.D. × 554 m long), the model predicts quite well. However, the model starts to result in some

under-prediction towards the dilute-phase region. The overall accuracy of prediction is much better as compared to that obtained for the other fly ash sample (Figure 6.1).

Subsequently, the Stegmaier (1978) model was further evaluated by applying it to predict the total pipeline pressure losses for fly ash (Pan, 1992) (69 mm I.D. × 168 m and 69 mm I.D. × 554 m long pipes) and "white powder" (69 mm I.D. × 148 m long pipe). The results are shown in figures A2.1 to A2.3 (Appendix A2). For this sample of fly ash (Pan, 1992), Chambers and Marcus (1986) model was used to predict the bend losses instead of the Pan and Wypych (1998) model, as by the time this part of the work was undertaken (at later stages of this thesis), it was realised that there can not be any conclusive statement as yet on the superiority of one bend model over the other (Chapter 11). Chambers and Marcus (1986) model was also used for the case of "white powder". The results show that for fly ash (Pan, 1992), 69 mm I.D. × 168 m long pipe and "white powder", 69 mm I.D. × 148 m long pipe, the model results in significant over-prediction for the dense-phase region (especially for the higher solids flow rates). For the dilute-phase, the model results in some under-predictions. For longer pipe (69 mm I.D. × 554 m long), the model results in gross over-predictions (especially in dense-phase).

6.3.2   Weber (1981)

The model was evaluated for scale-up accuracy and stability by applying it to predict the total pipeline drop initially for fly ash for various solids flow rates and different

diameters and lengths of pipes (viz. 69 mm I.D. × 168 m, 105 mm I.D. × 168 m, 69 mm I.D. × 554 m long) and comparing the predicted pneumatic conveying characteristics against the experimental plots. The results are shown in Figures 6.5 to 6.7. Note that the Pan and Wypych (1998) bend model was used again to predict the pressure loss due to the bends.

'Please see print copy for image'
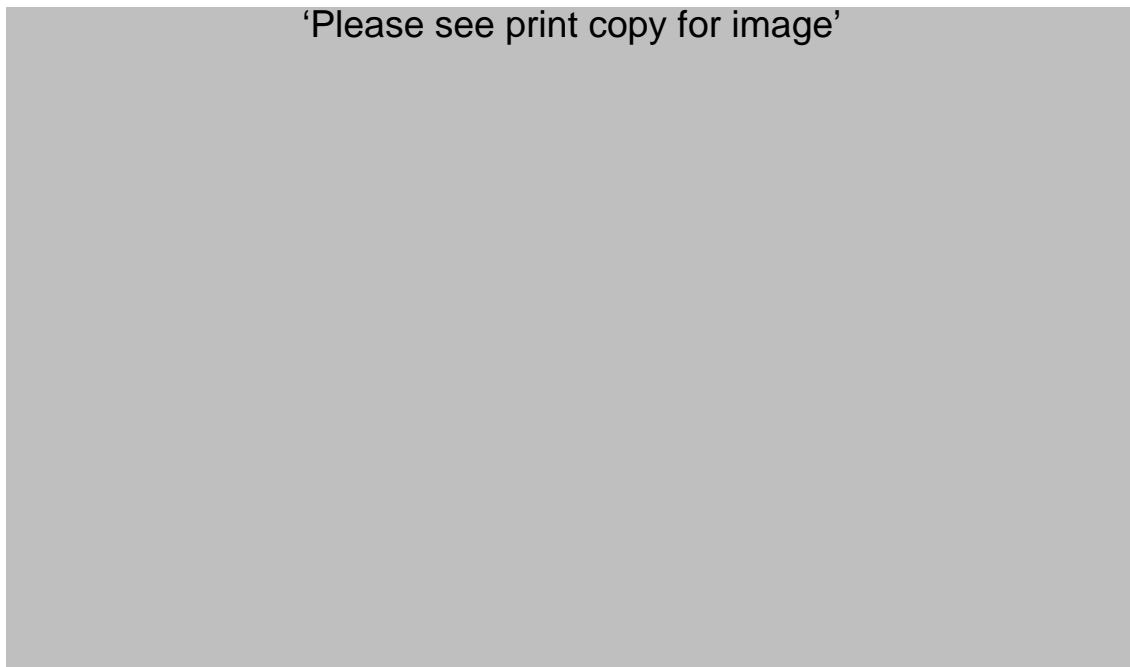
Figure 6.5: Experimental Versus Predicted PCC for Fly Ash and 69 mm I.D. × 168 m Pipe using Weber (1981) Model

'Please see print copy for image'

Figure 6.6: Experimental Versus Predicted PCC for Fly Ash and 105 mm I.D. ×168 m Pipe using Weber (1981) Model

'Please see print copy for image'

Figure 6.7: Experimental Versus Predicted PCC for Fly Ash and 69 mm I.D. × 554 m Pipe using Weber (1981) Model

The results in Figure 6.5 show that for the 69 mm I.D. × 168 m long pipe, the predicted PCC under-predict the experimental PCC quite considerably. However, the model results in "U"-shaped PCC (with a trend similar to the experimental plots). For the 105 mm I.D. × 168 m long pipe (see Figure 6.6), it can be seen that the predicted PCC still somewhat under-predict the experimental PCC. The predicted PCC are also displaying a "U"-shaped trend (again similar to the experimental data). For the 69 mm I.D. × 554 m long pipe (see Figure 6.7), the predicted PCC significantly under-predict the experimental PCC. However, again it can be seen that the predicted PCC exhibit "U"-shaped trends similar to the experimental PCC.

The model was further evaluated for scale-up accuracy and stability by applying it to predict the total pipeline drop initially for ESP dust, fly ash (Pan, 1992) and "white powder" for various solids flow rates and different diameters and lengths of pipes. The Chambers and Marcus (1986) model was used again to predict the pressure loss due to the bends. Predicted PCC were compared with the experimental plots. The model provided in gross under-prediction (for all the pipes). Typical results are shown in Figures 6.8, A2.4 and A2.5.

'Please see print copy for image'

Figure 6.8: Experimental Versus Predicted PCC for ESP Dust and 69 mm I.D. × 168 m Pipe using Weber (1981) Model

6.3.3   Pan and Wypych (1998)

The model was evaluated by using it to predict the total pipeline drop for fly ash for various solids flow rates and different diameters and lengths of pipes (viz. 69 mm I.D. × 168 m, 105 mm I.D. × 168 m long, 69 mm I.D. × 554 m long). Comparisons between predicted and experimental PCC are shown in Figures 6.9 to 6.11. Pressure drops due to the bends were estimated using the Pan and Wypych (1998) bend model.

'Please see print copy for image'

Figure 6.9: Experimental Versus Predicted PCC for Fly Ash and 69 mm I.D. × 168 m Pipe using Pan and Wypych (1998) Model

'Please see print copy for image'

Figure 6.10: Experimental Versus Predicted PCC for Fly Ash and 105 mm I.D. × 168 m Pipe using Pan and Wypych (1998) Model

'Please see print copy for image'

Figure 6.11: Experimental Versus Predicted PCC for Fly Ash and 69 mm I.D. × 554 m Pipe using Pan and Wypych (1998) Model

Figure 6.9 shows that for the 69 mm I.D. × 168 m long pipe, the model predicts quite well (from dense- to dilute-phase). Even within the dense-phase region, the predicted pressure drop values continue to decrease with decrease in air flow rate, i.e. trends of predictions are similar to a dilute-phase model. For the 105 mm I.D. × 168 m and 69 mm I.D. × 554 m long pipes, the predicted PCC over-predicts the experimental data, but the amount of over-prediction is not too significant. Again, the predicted pressure drop values continue to decrease with decrease in air flow rate, even within dense-phase region.

The model was further evaluated by applying it to predict the total pipeline drop for fly ash (Pan, 1992) for various solids flow rates for different lengths of pipes. Pan and Wypych (1998) model was used to predict the pressure loss due to the bends. Predicted and experimental PCC are compared in Figure 6.12 and 6.13.
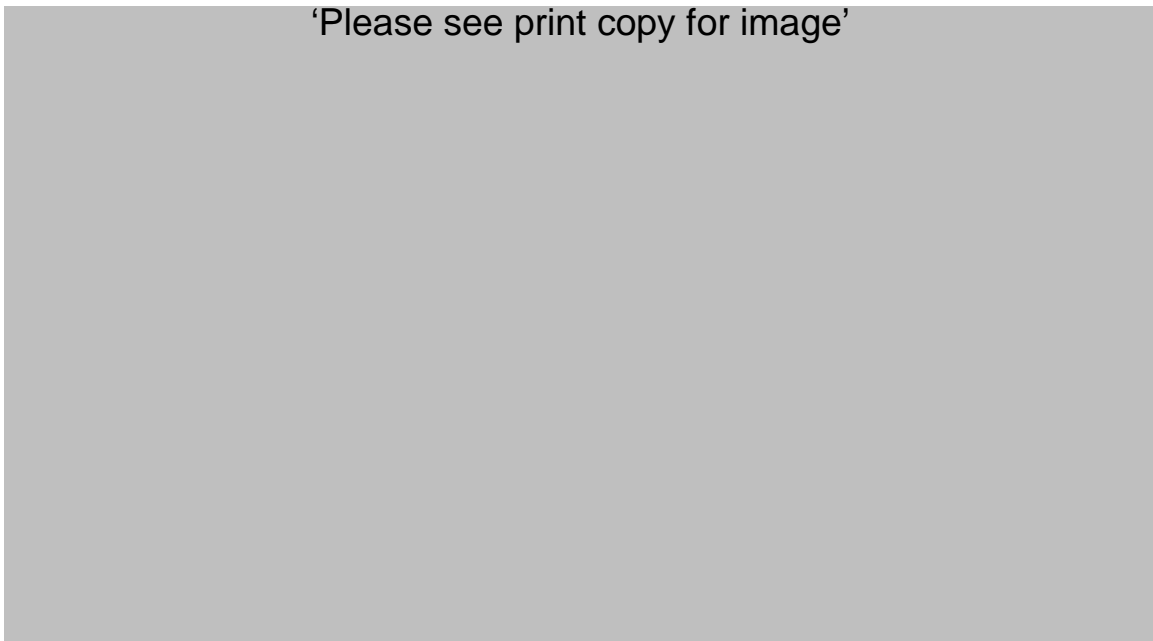
Figure 6.12: Experimental Versus Predicted PCC for Fly Ash (Pan, 1992) and 69 mm I.D. × 168 m Pipe using Pan and Wypych (1998) bend Model

'Please see print copy for image'

Figure 6.13: Experimental Versus Predicted PCC for Fly Ash (Pan, 1992) and 69 mm I.D. × 554 m Pipe using Pan and Wypych (1998) bend Model

Figure 6.12 shows that for the 69 mm I.D. × 168 m pipe, the model predicts reasonably well. However, the predicted PCC again do not show "U"-shaped trend. As a result, the predicted PCC somewhat under-predict the experimental PCC. Surprisingly, for the longer pipe (see Figure 6.13), the predictions are excellent, though again the predicted PCC display dilute-phase trend, but in any case, the experimental PCC also did not show any considerable increment in pressure drop values with decrease in air flow rates in low Froude number range. One reason for the promising response of the Pan and Wypych (1998) model could be that the model was derived using experimental data of a wide range of diameters and lengths of pipes (D: 52.5 to 105 mm, L: 70 to 945 m), i.e. by covering a broad range of flow conditions. Therefore, it is quite likely that the model would have superior scale-up capability as compared to the other existing models. However, it must be noted that

for designing industrial systems, availability of such wide range of data (i.e. data obtained from such significantly larger/longer pipes) can not be ensured in most cases and scaling-up predictions are to be carried out using the conveying data obtained from a smaller/shorter test pipeline.

Pan and Wypych (1998) model was not evaluated for ESP dust and "white powder" as the model was derived using only fly ash data, hence the same was inappropriate for applying to the other powders.

6.3.4   Jones and Williams (2003)

The model was applied to predict the total pipeline drop for fly ash for various solids flow rates for the 69 mm I.D. × 168 m long pipe. Comparisons between predicted and experimental PCC are shown in Figure 6.14. Pressure drops due to the bends were estimated using the Pan and Wypych (1998) bend model.

‘Please see print copy for image’

Figure 6.14: Experimental Versus Predicted PCC for Fly Ash and 69 mm I.D. × 168 m Pipe using Jones and Williams (2003) Model

Figure 6.14 shows that the model results in dramatic over-predictions. As a result, further prediction was not pursued for larger and longer pipes for this powder.

The model was further evaluated by predicting the total pipeline drop for ESP dust and fly ash (Pan, 1992) for various solids flow rates. Comparison between predicted and experimental PCC for 69 mm I.D. × 168 m and 105 mm I.D. × 168 m Pipes are shown in Figure 6.15, A2.6 and Figure A.6.7 for ESP dust and fly ash (Pan, 1992), respectively. The Chambers and Marcus (1986) model was used to estimate the losses due to the bends.

'Please see print copy for image'

Figure 6.15: Experimental Versus Predicted PCC for ESP Dust and 69 mm I.D. ×
168 m Pipe using Jones and Williams (2003) Model

Figure 6.15 shows that for the 69 mm I.D. × 168 m long pipe for ESP Dust, the model
results in significant over-prediction. For the larger diameter pipe for the same
powder (see Figure A2.6 in Appendix), the results show dramatic over-prediction.
For fly ash (Pan, 1992) and 69 mm I.D. × 168 m long pipe, the results again show
significant over-prediction. Due to such inaccurate response, the model was not
further pursued for the longer pipe (69 mm I.D. × 554 m long) for ESP dust and fly
ash (Pan, 1992) and for the "white powder". One possible reason for the inaccuracy
of the Jones and Williams (2003) model could be that the model was derived using
"back calculation" method, where "straight pipe" losses are obtained by subtracting
the losses due to the bends, vertical and initial acceleration from the total pipeline
pressure loss. As the procedure for accurately modelling these losses (especially the

relative contribution of bend loss, which can be substantial if dilute-phase test results were used to generate model and/or for a short pipe with many bends) are still not properly developed and validated, hence such "back calculation" technique may have introduced additional sources of inaccuracy, especially, when the model was derived based on the data of a short pipe, such as 50 m and having bends as many as nine.

6.4   Conclusions

None of the models were found to be consistent for accurately predicting the pressure drop under scale-up conditions of length or diameter for different powders, especially in dense-phase. The Stegmaier (1978) model provided mixed response: significantly over-predicting for the two different fly ash samples, but resulted in some under-prediction to reasonable good prediction for ESP dust (depending on the pipeline). Weber (1981) model consistently resulted in under-prediction for all the pipelines, with the margin of inaccuracy seeming to increase under greater scale-up conditions. Pan and Wypych (1998) model provided over-prediction for one sample of fly ash under diameter and length scale-up, but predicted very well for the other fly ash sample (for only length scale-up). The Jones and Williams (2003) model resulted in gross inaccuracy in nearly all cases. Therefore, it became apparent that further studies were to be conducted to understand better the flow mechanisms of fluidised dense-phase and to generate a more accurate model and/or test-design procedure, which could be used to accurately design industrial-scale fluidised dense-phase pneumatic conveying systems.

127

**CHAPTER 7: Modelling Solids Friction and Scale-up
Validation of Parameter Groupings**

7.1 Introduction

Previous investigations (Chapter 6) to examine the scale-up accuracy and stability of the different "existing" models for solids friction (Stegmaier, 1978; Weber, 1981; Pan and Wypych, 1998; Jones and Williams, 2003) by comparing the predicted and experimental pneumatic conveying characteristics (PCC) for two samples of fly ash, ESP dust and "white powder" have shown that the models generally can provide significant inaccuracy under significant scale-up conditions of diameter and/or length. Although the above findings demonstrated the limitations of the "existing" models (derived by other researchers), it was also appreciated that the investigation would have been more fair and comprehensive if new models have been derived using the conveying data of the same powders (i.e. fly ash, ESP dust and "white powder") and then evaluated under different diameter and length scale-up conditions. The very reason for which the design of a pneumatic conveying system is normally far more difficult compared to the single fluid flow is the design parameters of pneumatic conveying systems are significantly dependent on the powder/particle properties (such as the bulk and particle density, particle size, size distribution, shape, surface texture, air retention capabilities, permeability etc). A variation in any or a combination of these properties may potentially cause a significant change in the design (Wypych and Arnold, 1985). Therefore, it was felt that it would be more rational to examine the modelling procedure for its scale-up accuracy and stability (and not the model itself, which could be product specific). With this background, the aim of this chapter is to examine the accuracy of the existing design procedures/ modelling formats for solids friction (and their use of parameter groupings). Initial

investigations were carried out (during the first 12 months of the project) using the existing data of fly ash conveying in pipes of different diameters and lengths. Afterwards, similar evaluation work was extended using the test data of ESP dust and "white powder". The following section of this chapter presents results of such investigations using different modelling formats.

7.2   Modelling and scale-up evaluation

7.2.1   "General" power function format

It was considered that the total losses due to the conveying of solids-gas mixture through a pipe can be represented as the sum of individual losses due to the solids and gas only, as given by equation (2.1) (Barth, 1958). For the purpose of modelling, the "general" power function format provided in equation (7.1) was initially employed. This relatively simple format also has been used by other researchers, such as Wypych (1989), Jones and Williams (2003), Williams and Jones (2004) and Wypych et al. (2005).

$$\lambda_s = K \, (m^*)^a \, (Fr_m)^b \tag{7.1}$$

For the initial modelling work using fly ash data, two different sections of straight pipeline were selected for analysis and comparison: a section of straight horizontal pipe near the beginning of the pipelines, P9-P10; and a section of straight horizontal

section just before the vertical rise at the end of the pipelines, P11-P12, on the 69 mm

I.D. $\times$ 168 m long pipe (Figure 3.1). Initially to derive a model for λ_s, a manual

solution technique, based on the work of Wypych (1989) was used. As similar

manual based procedure was also employed by Jones and Williams (2003). From a

wide range (dilute- to fluidised dense-phase) of "straight pipe" steady state pressure

drop data obtained for the P9-P10 section and the subsequent calculations, a graph is

produced with the axes of equations (7.2) and (7.3). An example is shown in Figure

7.1.

$$Y = \lambda_s (m^*)^\sigma \qquad\qquad (7.2)$$

$$X = Fr_m \qquad\qquad (7.3)$$
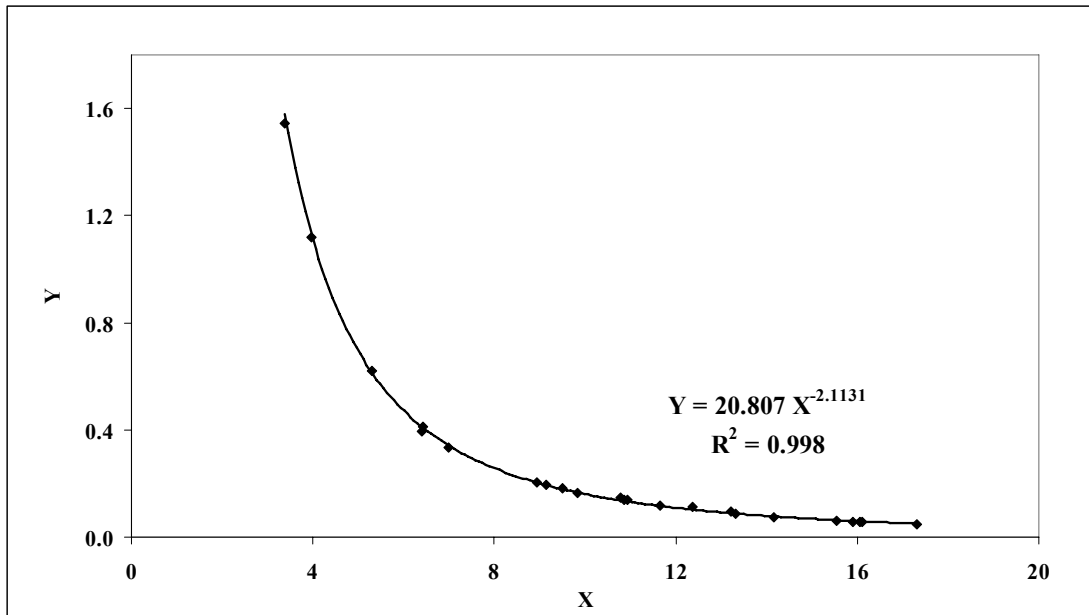
Figure 7.1: Axes used to Optimise Solution for Power Function (for K $\neq$ 1)

The data points are plotted using MS Excel 2003 and a power function trendline is added to the data. The equation of the trendline and the corresponding R^2 value are also displayed. The equation of the trendline is in the form:

$$Y = K\, X^z \tag{7.4}$$

where, K can be a variable or K = 1. In equation 7.2, σ is an unknown and its value was varied to obtain the optimal solution of the trendline. This was done by using two different methods depending on which form of K was required. To find the λ_s solution when K was an unknown (i.e. K $\neq$ 1), the value of σ was adjusted until the value of R^2 was maximised. During this process, the values of K and z in equation (7.4) continually changed. Once the optimum (maximum) values of R^2 was obtained, a substitution was made, resulting in:

$$\lambda_s\,(m^*)^\sigma = K\, Fr_m{}^z \tag{7.5}$$

or,

$$\lambda_s = K\,(m^*)^{-\sigma}\,(Fr_m)^z \tag{7.6}$$

which is the same form as equation (7.1). The optimal solution resulted in the following model for λ_s (when K $\neq$ 1):

$$\lambda_s = 20.807 \, (m^*)^{-0.71} \, (Fr_m)^{-2.11} \qquad [R^2 = 0.998] \qquad\qquad (7.7)$$

Experimental values of λ_s (calculated from test data) were compared with predicted values (using equation 7.7), as shown in Figure 7.2.
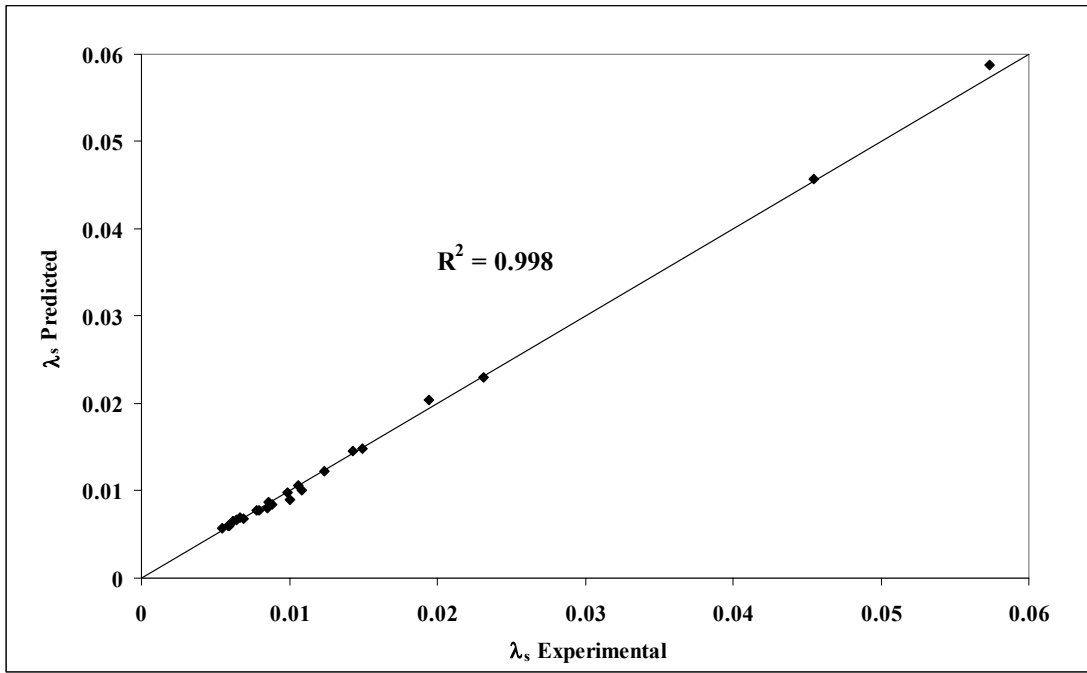
Figure 7.2: Solids Friction Factor – Predicted versus Experimental for Fly Ash and Model: $\lambda_s = 20.807 \, (m^*)^{-0.71} \, (Fr_m)^{-2.11}$

The high value of R^2 for the model suggests that the agreement between the experimental and predicted values of λ_s was very good (i.e. the correlation shows a "good fit").

To find the solution for λ_s when K=1, the value of σ is adjusted until the value of K in equation (7.4) is equal to 1. This resulted in the equation of the trendline being in the form;

$$Y = X^z \tag{7.8}$$

The plot between Y and X is shown in Figure 7.3.
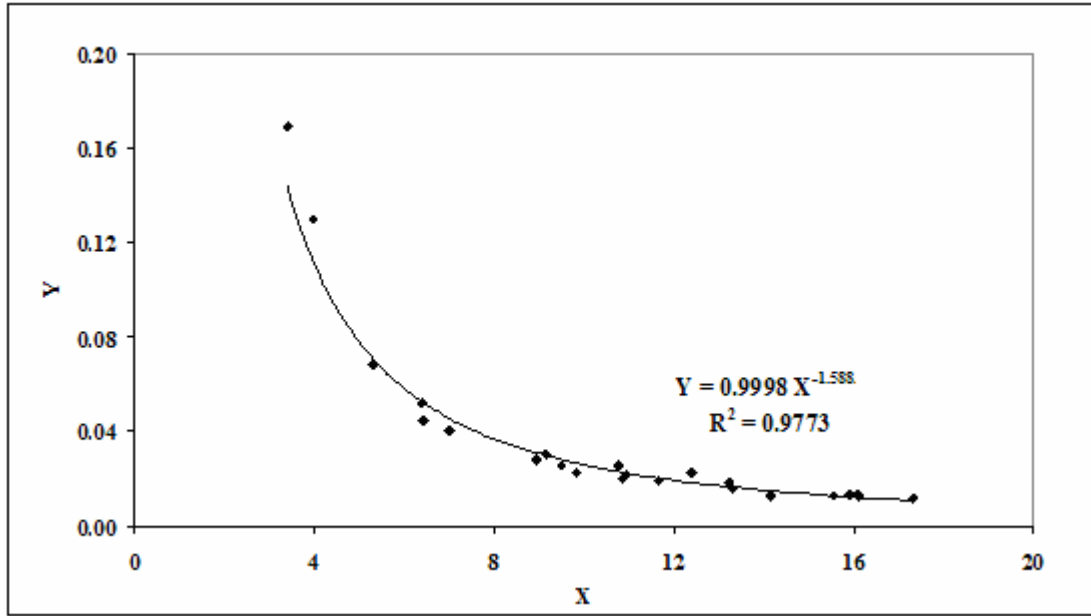
Figure 7.3: Axes used to Optimise Solution for Power Function (K = 1)

The maximum proximity up to which the value K could be forced to 1 was 0.9998. By approximating 0.9998 to 1, the following model for λ_s was obtained (i.e. when K = 1):

$$\lambda_s = (m^*)^{-0.23} (Fr_m)^{-1.59} \qquad [R^2 = 0.977] \tag{7.9}$$

134

Comparing the R^2 values of models given by equations (7.7) and (7.9), it can be seen that forcing K to 1 results in some decrement in the value of R^2. In fact, comparing Figures 7.1 and 7.3, it is quite evident that trendline with $K \neq 1$ criterion results in a superior "fit" to the data. Also it can be seen that the absolute numerical values of the exponents of m* and Fr_m in the λ_s models are larger for the case of $K \neq 1$ compared to $K = 1$.

A similar modelling procedure was pursued using the steady state "straight pipe" pressure drop data for fly ash (dilute- to fluidised dense-phase) obtained from the P11-P12 tapping points of the 69 mm I.D. × 168 m long pipe. The derived models for $K \neq 1$ and $K = 1$ conditions are given in equations (7.10) and (7.11), respectively.

$$\lambda_s = 1.998 \, (m^*)^{-0.36} \, (Fr_m)^{-1.66} \qquad [R^2 = 0.995] \qquad (7.10)$$

$$\lambda_s = (m^*)^{-0.257} \, (Fr_m)^{-1.54} \qquad [R^2 = 0.994] \qquad (7.11)$$

It was again found that the absolute numerical values of exponents of the power functions and R^2 are greater for the case when $K \neq 1$ than $K = 1$.

During this stage of the thesis, an attempt was made to form a liaison with Dr. F. Rizk of Germany, who had expressed interest in the modelling work. The same steady state "straight pipe" data obtained from P9-P10 and P11-P12 tapping points were provided

to him. Equations (7.12) and (7.13) are the models derived by Dr. Rizk using the P9-P10 and P11-P12 data set, respectively. He did not derive models in K = 1 format.

$$\lambda_s = 18.936 \, (m^*)^{-0.69} \, (Fr_m)^{-2.1} \tag{7.12}$$

$$\lambda_s = 1.377 \, (m^*)^{-0.3} \, (Fr_m)^{-1.6} \tag{7.13}$$

It can be seen that surprisingly, although the values of the "constants" and exponents of the models derived by Dr. Rizk were similar, but were not identical to those given in equations (7.7) and (7.10), even though the models were based on the same set of data. Hence it was decided to explore the cause of such difference. Instead of using the "manual" method for modelling, the "Regression" tool in the "Data Analysis" tool pack of Microsoft Excel 2003 was used as an alternative. It was found that the "constants" and exponents of the power function models obtained by the above method (i.e. using Microsoft Excel 2003) were identical to that derived by Dr. Rizk. This indicates that perhaps Dr. Rizk relied on the same procedure (i.e. use of Microsoft Excel instead of "manual" method). Potential of this "Regression" method (Microsoft Excel) was further examined by using it to derive models in K = 1 format (for both P9-P10 and P11-P12 data). It was found that the derived models using Microsoft Excel 2003 were very similar to those derived by the "manual" method, e.g. for the P11-P12 data, the model obtained by Microsoft Excel was given by;

$$\lambda_s = (m^*)^{-0.26} \, (Fr_m)^{-1.54} \qquad [R^2 = 0.999] \tag{7.14}$$

When compared with that derived by "manual method", given by equation (7.11), it can be seen that the exponents are almost identical. However, it must be noted that for some reason, Microsoft Excel seemed to provide greater values for R^2 compared to the "manual method". In any case, the "Regression" tool (Microsoft Excel 2003) was found to be a reliable means for deriving the models in power function formats. Also, is was believed that the method would prove significantly beneficial if additional parameter groupings were introduced in modelling (e.g ρ_m/ρ_s, d_s/D etc). It was decided that for all subsequent modelling work, the "Regression" tool of Microsoft Excel 2003 would be used. However, in the present case, only the "manually" obtained models (i.e. equations (7.7, 7.9 to 7.11) were selected for scale-up predictions. It was also decided that in spite of using this computer based approach regression technique, the predicted values of λ_s estimated by the derived "Regression" tool based model would be manually cross checked against the experimentally obtained values of λ_s to ensure that the derived correlations are sufficiently accurate in reality.

Another surprisingly finding needs to be highlighted is that that even though the product was the same (fly ash), the derived models were different depending on the selected pressure tapping point location. Similar observations were found when models were derived using the P9-P10 and P11$^+$-P12 data for "white powder" (equations 7.15 and 7.16, respectively). This may be attributed to the differences in prevailing local flow conditions for the respective pipe sections (Figures 5.6, 5.7, 5.19 and 5.20). It can be seen again that the absolute numerical values of exponents of the power functions are greater for the case when $K \neq 1$ compared to $K = 1$.

137

$$\lambda_s = 7.74\,(m^*)^{-0.301}\,(Fr_m)^{-2.09} \qquad\qquad [R^2 = 0.985] \qquad\qquad (7.15)$$

$$\lambda_s = (m^*)^{0.09}\,(Fr_m)^{-1.76} \qquad\qquad [R^2 = 0.998] \qquad\qquad (7.16)$$

Models derived from P9-P10 data of the 69 mm I.D. × 168 m long pipe for fly ash (i.e. equations 7.7 and 7.9, for both $K \neq 1$ and $K = 1$ formats, respectively) were evaluated for scale up accuracy and stability by using them to predict the total pipeline pressure drop for different pipelines (69 mm I.D. × 168 m, 105 mm I.D. × 168 m and 69 mm I.D. × 554 m) for various solids flow rates and comparing the predicted pneumatic conveying characteristics against the experimental plots. The Pan and Wypych (1998) model was used to predict the losses in the bends. Losses due to the verticals and initial acceleration were estimated using Marcus et al. (1990). The results are shown in the following figures (Figures 7.4 to 7.6). All the predicted PCC were limited to $Fr_i = 4$, as below this limit, flow instabilities were found to occur during the experimental program. This criterion has been used throughout this chapter for all the predicted PCC.
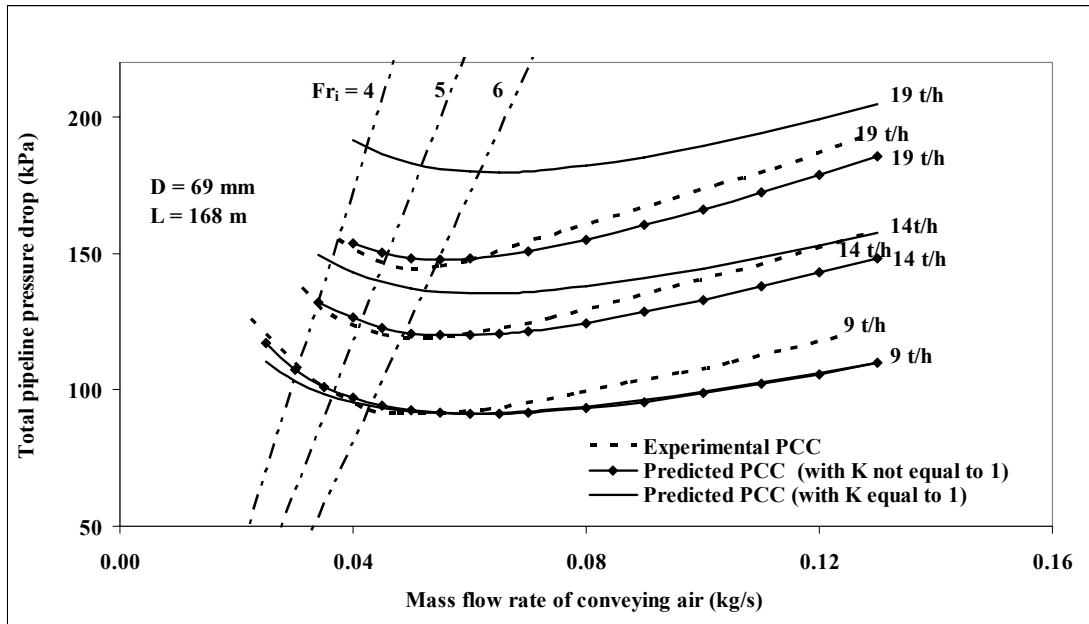
Figure 7.4: Experimental Versus Predicted PCC for Fly Ash and 69 mm I.D. × 168 m Pipe using Equations (7.7) and (7.9)
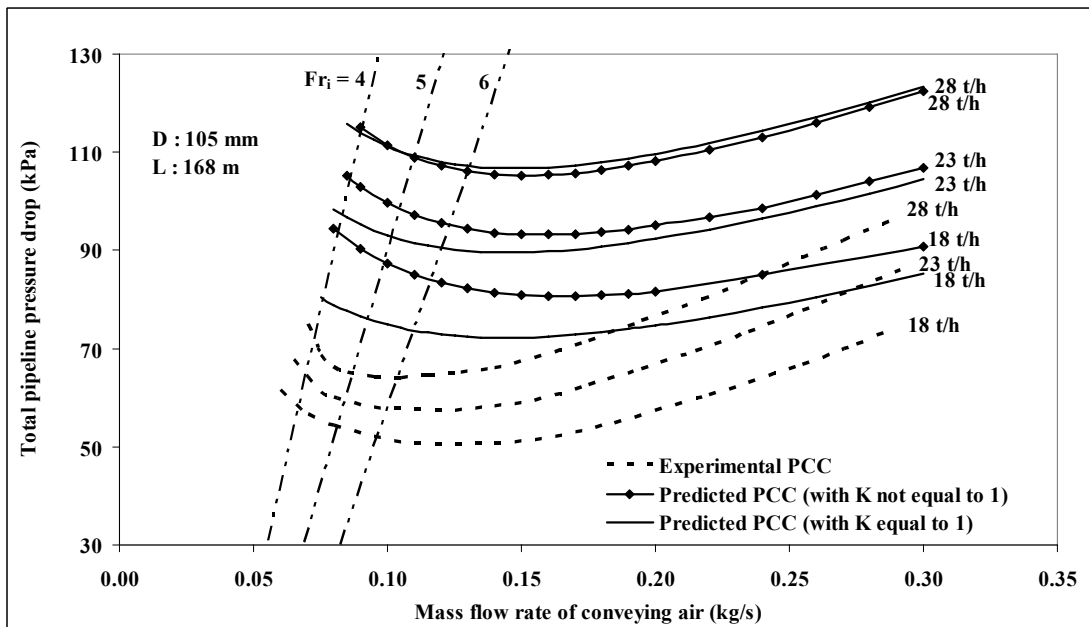
Figure 7.5: Experimental Versus Predicted PCC for Fly Ash and 105 mm I.D. × 168 m Pipe using Equations (7.7) and (7.9)
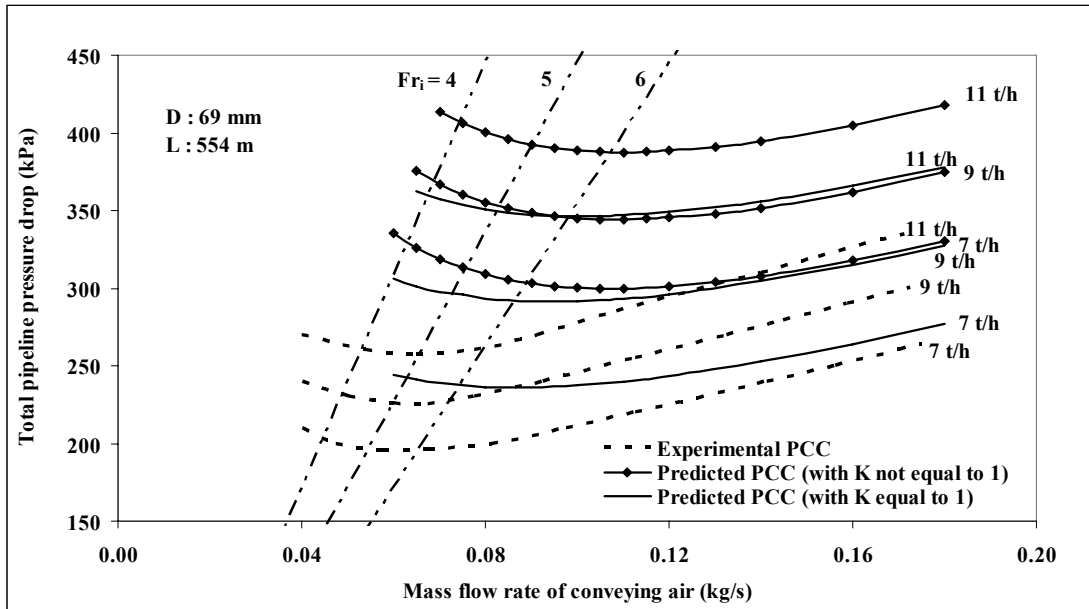
Figure 7.6: Experimental Versus Predicted PCC for Fly Ash and 69 mm I.D. × 554 m Pipe using Equations (7.7) and (7.9)

The results show that for the 69 mm I.D. × 168 m pipe (Figure 7.4), the model in K ≠ 1 format (equation 7.7) provides much better prediction, whereas model in K = 1 format (equation 7.9) results in considerable over-predictions. Both the models generate "U"-shaped predicted PCC. However, for diameter scale-up (105 mm I.D. × 168 m long pipe, see Figure 7.5), both the models (i.e. including the model given by equation 7.7, which was "excellent" for the smaller sized pipe) show significant over-predictions. This suggests that the "true" test of a model would only occur under scale-up conditions. Equation (7.9) appears to result in relatively better predictions. For significant length scale-up (69 mm I.D. × 554 m long pipe, see Figure 7.6), both the models show significant over-prediction, though the model given by equation (7.9) again results in relatively overall better predictions. For both diameter and

140

length scale-up, both the models show "U"- shaped predicted PCC. The location of pressure minimum curve (PMC) for the predicted PCC has considerably shifted to the right of the experimentally obtained PMC (though this is mainly contributed by the bend losses). Gradients of the predicted PCC (using both the models) were less than the experimental PCC. This, however, might have been significantly affected by the accuracy of the selected bend model.

Similar scale-up evaluations were conducted for fly ash using the models derived from P11-P12 tapping point data of the 69 mm I.D. × 168 m long pipe (i.e. models given by equation 7.10 and 7.11 in K ≠ 1 and K = 1 formats, respectively). Comparisons of experimental and predicted PCC are provided in Figures A3.1 to A3.3 (Appendix A3). The results again show significant over-predictions (especially for the larger diameter and longer pipes). The overall trend of the predicted PCC were similar to those previously shown in Figures 7.4 to 7.6.

To investigate the effect of pipe diameter and local air density on the modelling of λ_s, models were derived using the steady state "straight pipe" P9-P10 tapping point data of fly ash (for a wide range of flow conditions: dilute- to fluidised dense-phase) for the 105 mm I.D. × 168 m and 69 mm I.D. × 554 m long pipes. The derived models (in both K ≠ 1 and K = 1 formats) are given by equations (7.17) to (7.20). High R^2 values indicate "good fit" between the predicted and experimental data for which the models were derived.

Fly ash, P9-P10 data, 105 mm I.D. $\times$ 168 m long pipe:

$$\lambda_s = 10.2 \, (m^*)^{-0.685} \, (Fr)^{-2.04} \qquad [R^2 = 0.96] \qquad (7.17)$$

$$\lambda_s = (m^*)^{-0.32} \, (Fr)^{-1.61} \qquad [R^2 = 0.999] \qquad (7.18)$$

Fly ash, P9-P10 data, 69 mm I.D. $\times$ 554 m long pipe:

$$\lambda_s = 6.3 \, (m^*)^{-0.64} \, (Fr)^{-1.87} \qquad [R^2 = 0.992] \qquad (7.19)$$

$$\lambda_s = (m^*)^{-0.34} \, (Fr)^{-1.46} \qquad [R^2 = 0.999] \qquad (7.20)$$

It can be seen again that the absolute numerical values of exponents of the power functions are greater for the case when $K \neq 1$ compared to $K = 1$. The above models were evaluated for scale up accuracy and stability by using them to predict the total pipeline drop for different pipelines (69 mm I.D. $\times$ 168 m, 105 mm I.D. $\times$ 168 m and 69 mm I.D. $\times$ 554 m) for various solids flow rates and comparing the predicted pneumatic conveying characteristics against the experimental plots. The results are shown in the following figures (Figures 7.7 to 7.12).

Figure 7.7: Experimental Versus Predicted PCC for Fly Ash and 69 mm I.D. × 168 m Pipe using Equations (7.17) and (7.18)

Figure 7.8: Experimental Versus Predicted PCC for Fly Ash and 105 mm I.D. × 168 m Pipe using Equations (7.17) and (7.18)

Figure 7.9: Experimental Versus Predicted PCC for Fly Ash and 69 mm I.D. × 554 m Pipe using Equations (7.17) and (7.18)

Figure 7.10: Experimental Versus Predicted PCC for Fly Ash and 69 mm I.D. × 168 m Pipe using Equations (7.19) and (7.20)

Figure 7.11: Experimental Versus Predicted PCC for Fly Ash and 105 mm I.D. × 168

m Pipe using Equations (7.19) and (7.20)

Figure 7.12: Experimental Versus Predicted PCC for Fly Ash and 69 mm I.D. × 554

m Pipe using Equations (7.19) and (7.20)

The predicted PCC show some surprising results. For the 69 mm I.D. × 168 m pipe, the majority of models have resulted in under-predictions (this is in contrast to the previous predictions). Models with the K = 1 format seem to predict with better accuracy. Some unexpected improvements were found to occur when predicting for the larger and longer pipes. Although all the models still result in over-predictions for the 105 mm I.D. × 168 m long pipe, certainly better accuracy has been achieved (when compared to the results shown Figure 7.5 and A3.2). Similar improvements were observed when predicting for 69 mm I.D. × 554 m long pipe. In fact, equations (7.17) and (7.18) result in fairly accurate predictions. Equation (7.19) provides in slightly conservative predictions, whereas equation (7.20) shows significant over-predictions. However, the levels of over-prediction were certainly more stable (not as significant) compared to the earlier predictions for the same pipe (Figure 7.6 and A3.3).

An apparent cause for this improvement (i.e. reduction in the margin of over-prediction, in fact sometimes under-predicting) could be due to the models (equations 7.17 to 7.20) being derived using data sets obtained from "straight pipe" data of 105 mm I.D. × 168 m and 69 mm I.D. × 554 m long pipes (Figures 5.8 and 5.9, respectively), which showed relatively larger portions of dilute-phase region (compared to the previous models, which were obtained using the data set from the 69 mm I.D. × 168 m long pipe for fly ash and showed relatively less portions of dilute-phase and larger potions of dense-phase). From the "straight pipe" PCC

presented in Figures 5.8 to 5.9, it can be observed that the pressure drop in dilute-phase was lesser than that for dense-phase portion. Thus, the models derived using data sets having wider regions of dilute-phase data points could underestimate pressure drop when predicting for pipes displaying a relatively larger amount of dense-phase flow, e.g. in 69 mm I.D. × 168 m long pipe (Figure 7.7).

Similar modelling and scale-up evaluation work was further extended using the conveying data of ESP dust. Models in "general" format were derived using the steady state P9-P10 tapping point data of the 69 mm I.D. × 554 m long pipe for a wide range of flow conditions (dilute- to fluidised dense-phase). The derived models, in both K ≠ 1 and K = 1 formats, are given by equations (7.21) and (7.22), respectively. High R^2 values indicate "good fit" between predicted and experimental data from which the models were derived.

$$\lambda_s = 7.14 \, (m^*)^{-0.498} \, (Fr)^{-2.01} \qquad [R^2 = 0.995] \qquad (7.21)$$

$$\lambda_s = (m^*)^{-0.108} \, (Fr)^{-1.596} \qquad [R^2 = 0.998] \qquad (7.22)$$

It can be seen again that the absolute numerical values of exponents of the power functions are greater for the case when K ≠ 1 compared to K = 1. The above models were evaluated for scale up accuracy and stability by using them to predict the total pipeline drop for different pipelines (69 mm I.D. × 168 m, 105 mm I.D. × 168 m and 69 mm I.D. × 554 m) for various solids flow rates and comparing the predicted pneumatic conveying characteristics against the experimental plots. The results are

shown in the following figures (Figures 7.13 to 7.15). The Chambers and Marcus (1986) model was used to predict the losses in the bends. Losses due to the verticals and initial acceleration were estimated as per Marcus et al. (1990).
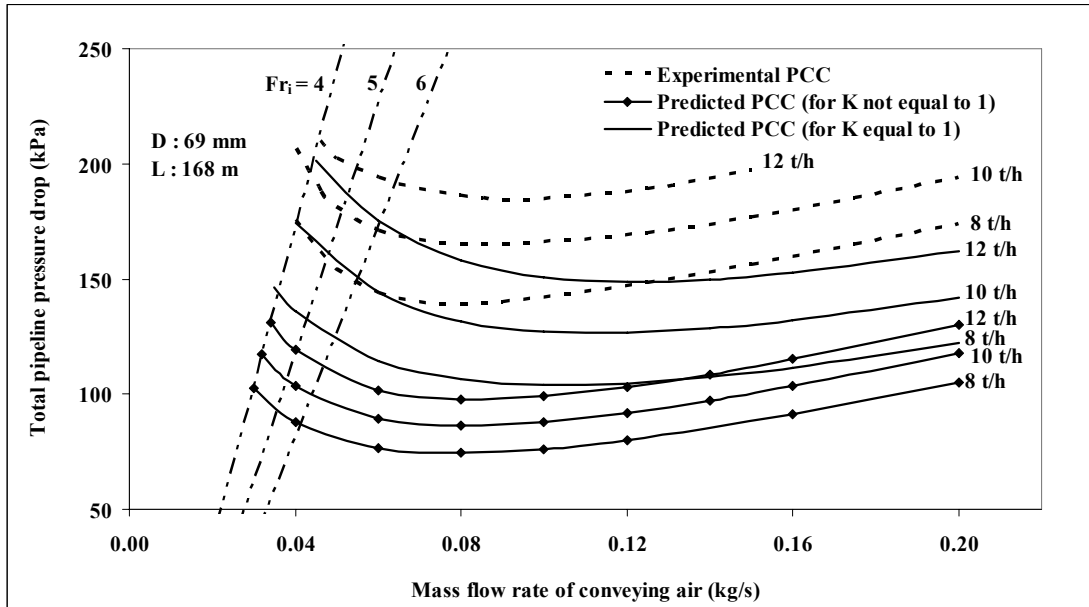
Figure 7.13: Experimental Versus Predicted PCC for ESP Dust and 69 mm I.D. × 168 m Pipe using Equations (7.21) and (7.22)
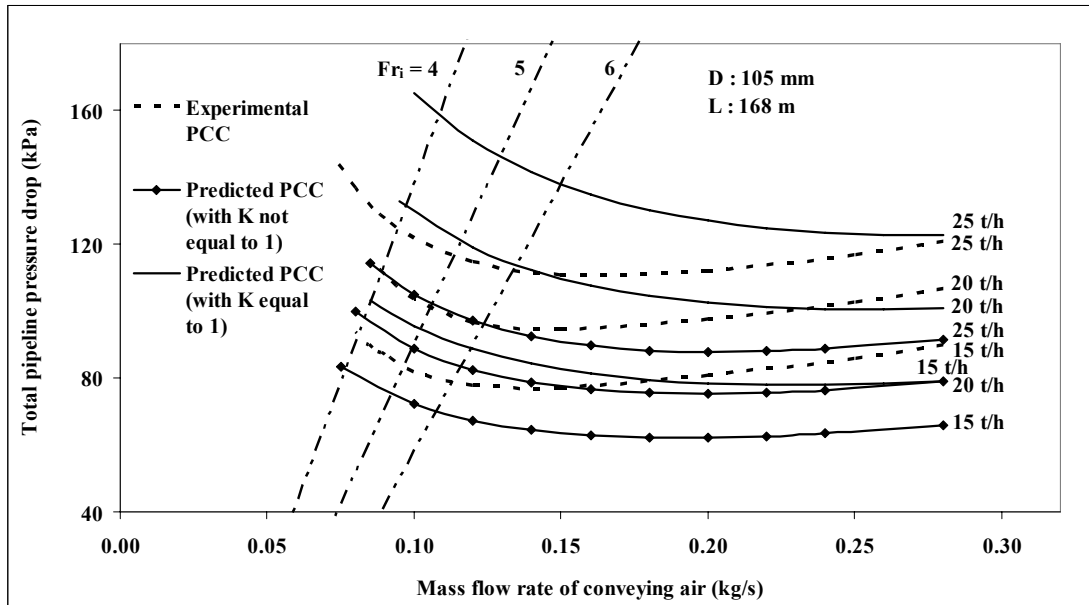
Figure 7.14: Experimental Versus Predicted PCC for ESP Dust and 105 mm I.D. ×

168 m Pipe using Equations (7.21) and (7.22)
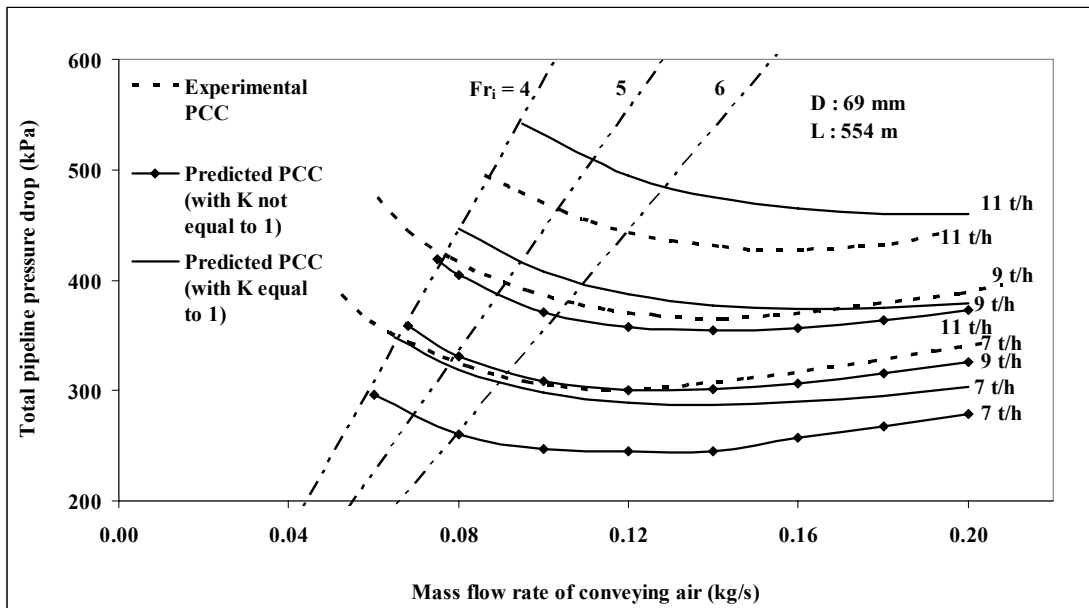
Figure 7.15: Experimental Versus Predicted PCC for ESP Dust and 69 mm I.D. ×

554 m Pipe using Equations (7.21) and (7.22)

The results show that for the 69 mm I.D. × 168 m pipe, the model given by equation (7.21) (i.e. for K ≠ 1) provides gross under-prediction, whereas equation (7.22) (i.e. for K = 1) results in reasonable estimations in dense-phase. However, for dilute-phase, equation (7.22) results in significant under-prediction. For both the 105 mm I.D. × 168 m and 69 the mm I.D. × 554 m long pipes, equation (7.21) provides considerable under-prediction, whereas equation (7.22) results in some over-prediction (for dense-phase). However, the margin of accuracy is much better than the previously obtained predictions for fly ash using the same model format. In fact, some over-prediction (as provided by equation 7.22 for the larger and longer pipes) can be considered desirable as this would provide some safety margin in design.

Prediction for "white powder" was not pursued, as the same was conveyed in only one pipeline (69 mm I.D. × 148 m long).

7.2.2 "Extended" power function format

It has been observed in the previous section that the "general" power format for solids friction factor were generally not capable of predicting pressure drop reliably (especially, under scale-up conditions). Therefore, it appeared that the dimensionless parameter groupings used in the "general" power function format do not adequately represent the dense-phase flow phenomenon. Also, it was a matter of concern that the derived models (e.g. equations 7.7 and 7.10) were different depending upon the pressure tapping location. Consequently, the subsequent predictions (e.g. under scale-

up conditions) were also considerably different depending on the selection of model. This seemed to be fundamentally incorrect, because the model for a particular product may be expected to be unique. It has been indicated in the literature (Wypych et al., 2005) that inclusion of additional parameter groups in power function expression (as given by equation 7.23) could result in obtaining one unique model for the solids friction factor (irrespective of the tapping location) and some improvement in predicting pressure drop under scale-up situations. However, since for a particular product and pipeline, the values of ρ_s, d_s and D are constant, they could not be considered for the purpose of correlation development. Therefore, the only "extension parameter" that could be included here is air density, as given in equation 7.24. This format was also used by Pan (1992) and Pan and Wypych (1998).

$$\lambda_s = K \, (m^*)^a \, (Fr_m)^b \, (\rho_m / \rho_s)^c \, (d_s/D)^d \tag{7.23}$$

$$\lambda_s = K \, (m^*)^a \, (Fr_m)^b \, (\rho_m)^c \tag{7.24}$$

From a wide range of (dilute- to fluidised dense-phase) "straight pipe" steady state pressure drop data for fly ash obtained for the P9-P10 and P11-P12 sections of the 69 mm I.D. × 168 m long pipe, the following models were derived (in both K ≠ 1 and K = 1 formats):

For the data obtained from P9-P10 tapping points;

$$\lambda_s = 14.5. \, (m^*)^{-0.63}(Fr_m)^{-2.01}(\rho_m)^{-0.207} \qquad [R^2 = 0.999] \tag{7.25}$$

$$\lambda_s = (m^*)^{-0.15}(Fr_m)^{-1.43}(\rho_m)^{-0.79} \qquad [R^2 = 0.999] \qquad (7.26)$$

For the data obtained from P11-P12 tapping points;

$$\lambda_s = 1.85 \cdot (m^*)^{-0.353}(Fr_m)^{-1.66}(\rho_m)^{-0.071} \qquad [R^2 = 0.999] \qquad (7.27)$$

$$\lambda_s = (m^*)^{-0.25}(Fr_m)^{-1.5}(\rho_m)^{-0.079} \qquad [R^2 = 0.999] \qquad (7.28)$$

It can be seen again that the absolute numerical values of exponents of the terms m^* and Fr_m are greater for the case when $K \neq 1$ than $K = 1$. High R^2 values for all the above models indicate the agreements between the experimental and predicted values of λ_s are very good (within the data range from which the models were derived). However, it is again found that even after including the ρ_m term, the values of the "constants" and exponents of the power function based models for λ_s are quite different depending on the location of tapping points (thus, addition of only ρ_m did not seem to be adequately capable of deriving unique models for λ_s irrespective of the location of pressure tapping points in the pipelines). Nonetheless, the derived models were evaluated for scale-up accuracy and stability (mainly to explore if inclusion of the ρ_m term in the model could improve the accuracy of prediction) by using them to predict the total pipeline drop for different pipelines (69 mm I.D. × 168 m, 105 mm I.D. × 168 m and 69 mm I.D. × 554 m) for various solids flow rates for fly ash and comparing the predicted and experimental PCC. The results are for the models given by equations (7.25) and (7.26) are shown in Figures 7.16 to 7.18. Prediction for the models given by equations (7.27) and (7.28) are displayed in Figures A3.4 to A3.6

(Appendix A3). The Pan and Wypych (1998) model was used to predict the losses in the bends. Losses due to the verticals and initial acceleration were estimated using Marcus et al. (1990).

Figure 7.16: Experimental Versus Predicted PCC for Fly Ash and 69 mm I.D. × 168 m Pipe using Equations (7.25) and (7.26)
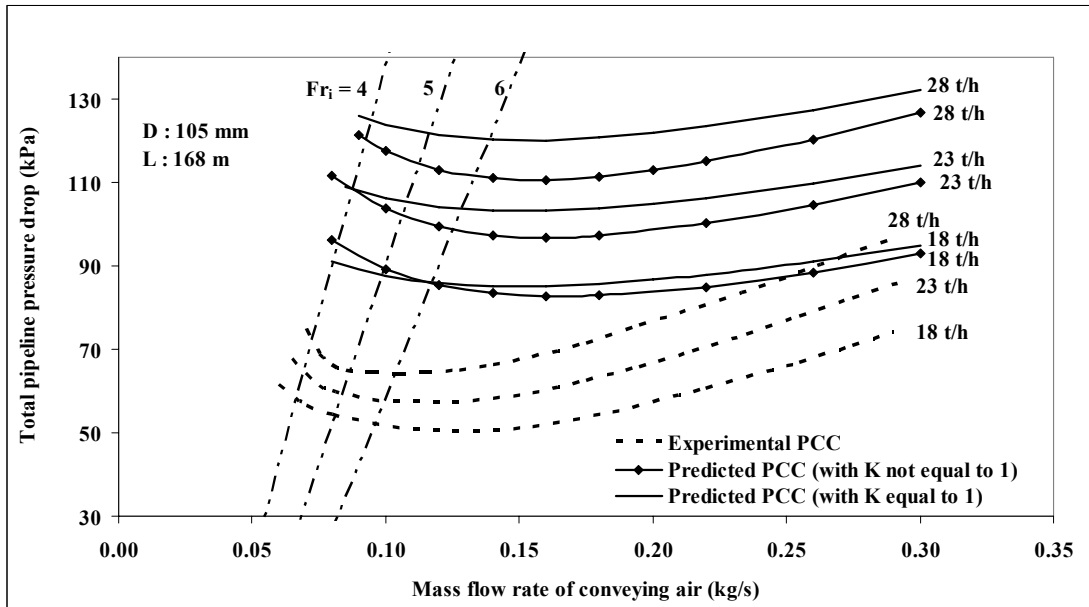
Figure 7.17: Experimental Versus Predicted PCC for Fly Ash and 105 mm I.D. × 168

m Pipe using Equations (7.25) and (7.26)
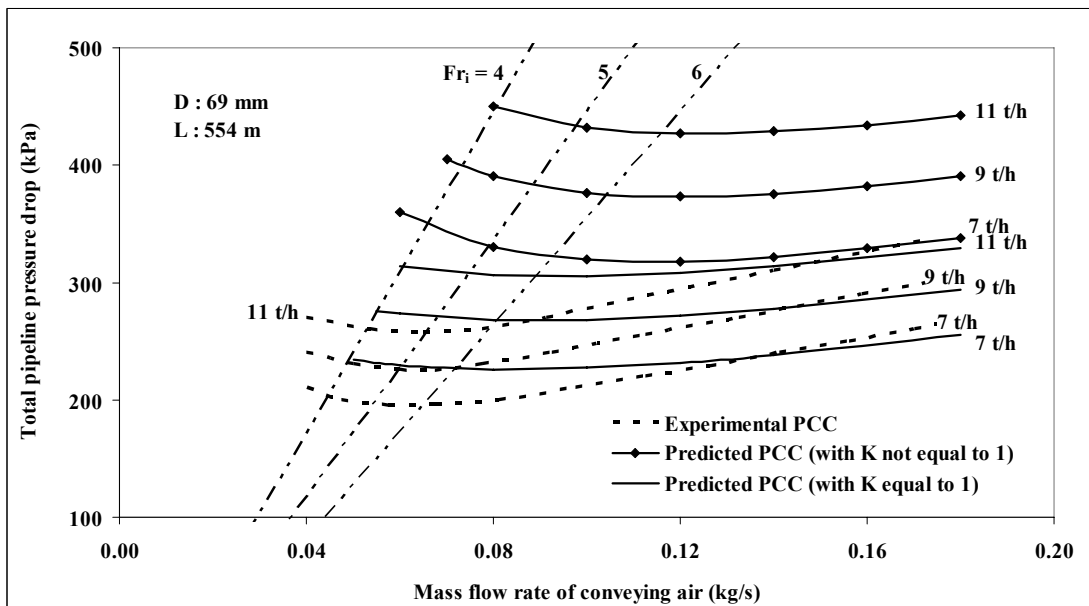
Figure 7.18: Experimental Versus Predicted PCC for Fly Ash and 69 mm I.D. × 554

m Pipe using Equations (7.25) and (7.26)

Figure 7.16 shows that for the 69 mm I.D. × 168 m long pipe, equation (7.25) (i.e. model in K ≠1 format) provides reasonably good prediction for dense- to dilute-phase, whereas the model given by equation (7.26) (i.e. model in K = 1 format) result in considerable over-prediction. The shape of the predicted PCC using equation (7.26) is rather horizontal (i.e. not "U" shape). Also, for both the models, the predicted PCC in dilute-phase have a lesser gradient compared to the experimental PCC. This, however, might have been significantly affected by the accuracy of the selected bend model. For the larger diameter pipe (105 mm I.D. × 168 m long), Figure 7.17, both the models result in significant over-prediction, with equation (7.25) (i.e. model in K ≠ 1 format) displaying relatively slightly better predictions. Both the models produce rather horizontal shaped PCC and the predicted PMC has shifted considerably to the right of the experimentally obtained PMC. For the longer pipe (69 mm I.D. × 554 m), see Figure 7.18, model given by equation (7.25) (i.e. for K ≠ 1) provides significant over-predictions. However, equation (7.26) (i.e. for K = 1) results in reasonably good predictions. Both the models produce rather horizontal shaped PCC, with the locations of predicted PMC being rather difficult to establish.

For the models given by equations (7.27) and (7.28) (i.e. models derived using P11-P12 data, in K ≠ 1 and K = 1 formats, respectively), prediction for the 69 mm I.D. × 168 m long pipe (Figure A3.4) shows that equation (7.28) has resulted in considerable over-predictions, whereas equation (7.27) provides relatively better predictions (though still some over-predictions exist). For diameter and length scale-up (Figure A3.5 and A3.6, respectively) both the models result in considerable to

significant over-prediction (especially, the amount of inaccuracy is greater for equation (7.28). Both the models produce rather horizontal shaped PCC, with the locations of predicted PMC being rather difficult to establish.

Similar investigations were further carried out for ESP dust. Using the "straight pipe" pressure loss data from P9-P10 tapping points on the 69 mm I.D. × 554 m long pipe, the following models for λ_s were derived (in both K $\neq$ 1 and K =1 formats):

$$\lambda_s = 19.08 \, (m^*)^{-0.88} \, (Fr_m)^{-2.39} (\rho_m)^{0.52} \qquad [R^2 = 0.998] \qquad (7.29)$$

$$\lambda_s = (m^*)^{-0.12} \, (Fr_m)^{-1.6} (\rho_m)^{0.03} \qquad [R^2 = 0.999] \qquad (7.30)$$

It can be seen that again the absolute numerical values of exponents of the terms m* and Fr_m are greater for the case when K $\neq$ 1 than K = 1. The high values of R^2 indicated "good fit". The models were evaluated for scale-up accuracy and stability by using them to predict the total pipeline drop for different pipelines (69 mm I.D. × 168 m, 105 mm I.D. × 168 m and 69 mm I.D. × 554 m) for various solids flow rates and comparing the predicted and experimental PCC. The results are shown in Figures 7.19 to 7.21. The Chambers and Marcus (1986) model was used to predict the losses in the bends.

Figure 7.19: Experimental Versus Predicted PCC for ESP Dust and 69 mm I.D. ×

168 m Pipe using Equations (7.29) and (7.30)

Figure 7.20: Experimental Versus Predicted PCC for ESP Dust and 105 mm I.D. ×

168 m Pipe using Equations (7.29) and (7.30)

Figure 7.21: Experimental Versus Predicted PCC for ESP Dust and 69 mm I.D. × 554 m Pipe using Equations (7.29) and (7.30)

The results show that for all the three pipelines, equations (7.29) (i.e. model in the format K ≠ 1) produces dramatic under-prediction. For the 69 mm I.D. × 168 m long pipe, equation (7.30) (i.e. for K = 1), provides reasonably good prediction for dense-phase, however, considerable under-prediction towards the dilute-phase region. The model results in some over-prediction for dense-phase for the larger diameter pipe (see Figure 7.20), however, predicts quite well for dilute-phase. Surprisingly, the model predicts quite well for the longer pipe (69 mm I.D. × 554 m) for dense- to dilute-phase.

Afterwards, modelling was carried out for "white powder" using the "straight pipe" pressure loss data from P9-P10 and P11$^+$-P12 tapping locations. The derived models are given by equations 7.31 to 7.34 (in both K $\neq$ 1 and K = 1 formats).

Based on P9-P10 data:

$$\lambda_s = 5.37(m^*)^{-0.076}(Fr)^{-1.95}(\rho)^{-0.69} \qquad\qquad [R^2 = 0.985] \qquad\qquad (7.31)$$

$$\lambda_s = (m^*)^{0.28}(Fr)^{-1.66}(\rho)^{-0.85} \qquad\qquad [R^2 = 0.999] \qquad\qquad (7.32)$$

Based on P11$^+$-P12 data:

$$\lambda_s = 0.904\,(m^*)^{0.17}(Fr)^{-1.5}(\rho)^{-0.51} \qquad\qquad [R^2 = 0.998] \qquad\qquad (7.33)$$

$$\lambda_s = (m^*)^{0.15}(Fr)^{-1.5}(\rho)^{-0.496} \qquad\qquad [R^2 = 0.999] \qquad\qquad (7.34)$$

Again, it is found that the models are different depending on the location of tapping points. Scale-up evaluation for "white powder" was not pursued, as the same was not conveyed in larger/longer pipes.

Thus, it is evident that the inclusion of ρ_m term in the power function equation for λ_s, has not resulted in achieving a better modelling procedure. Some improvements in predictions have been noticed for certain product and pipeline, but the improvements are not consistent for a wide range of flow conditions and some unexpected inaccuracy may occur. Also, inclusion of the ρ_m term did not result in obtaining

unique model for a particular powder, i.e. the exponents and "constant" terms of the models were still dependent on the location of pressure tapping points in the pipeline. Hence, further efforts were pursued in search of establishing a reliable modelling procedure.

7.2.3 *"Back Calculation" method*

To avoid the issue of adopting a modelling procedure that depended on the position of pressure tapping points (as discussed previously), an alternative modelling and design approach was attempted, known as the "back calculation" method (Jones and Williams, 2003; Williams and Jones, 2004). The "back calculation" approach of modelling involves indirect estimation of the "straight pipe only" pressure loss by subtracting bends, verticals and initial acceleration losses from the total pipeline pressure loss. The P8 transducer data (Figure 3.1) were recorded as the total pipeline pressure drop for the 69 mm I.D. × 168 m long pipe. Bend loss was calculated using the Chambers and Marcus (1986) model, as provided by equation (2.14). The above bend model was also used by other researchers (Jones and Williams, 2003) for deriving expressions for solids friction factor using "back calculation" method. The bend loss factor was considered as 0.5 (Jones and Williams, 2003). Vertical and initial acceleration losses were calculated as per Marcus et al. (1990). From the "straight pipe only" data obtained by such "back calculation" approach, power function based model for λ_s was derived for fly ash, given by equations 7.35 and 7.36 (in $K \neq 1$ and $K = 1$ formats, respectively). Again, the high values of R^2 suggested the

agreements between the experimental and predicted values of λ_s were very good (i.e. the correlation showed "good fit").

$$\lambda_s = 13.059 \, (m^*)^{-0.73} \, (Fr_m)^{-1.79} \qquad\qquad [R^2 = 0.989] \qquad\qquad (7.35)$$

$$\lambda_s = (m^*)^{-0.34} \, (Fr_m)^{-1.36} \qquad\qquad [R^2 = 0.999] \qquad\qquad (7.36)$$

It can be seen that again the absolute numerical values of exponents of the terms m* and Fr_m are greater for the case when $K \neq 1$ than $K = 1$. The above models were evaluated for scale-up accuracy and stability by using them to predict the total pipeline drop for the larger and longer pipelines (105 mm I.D. × 168 m and 69 mm I.D. × 554 m) for various solids flow rates and comparing the predicted and experimental PCC. Predictions were not pursued for the 69 mm I.D. × 168 m long pipe, because as the models were derived using the experimental total pipeline pressure drop data of this very pipe, hence it was expected that the predicted total pipeline PCC would have matched with the experimental PCC quite well. The Chambers and Marcus (1986) model was used to estimate the losses due to the bends (as employed by Jones and Williams, 2003). The results are shown in Figures 7.22 and 7.23.
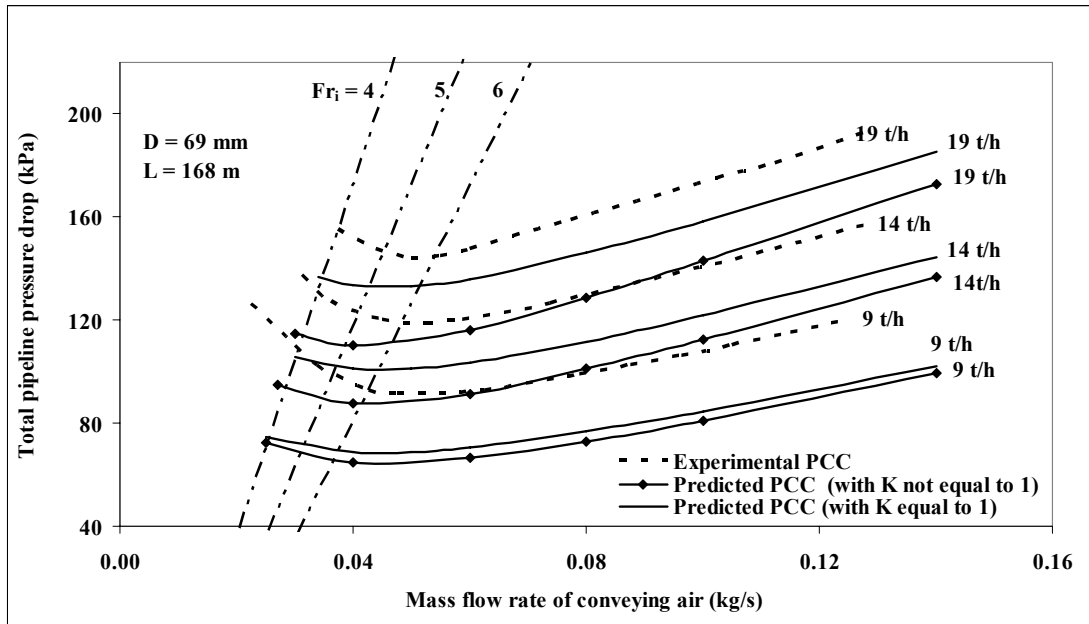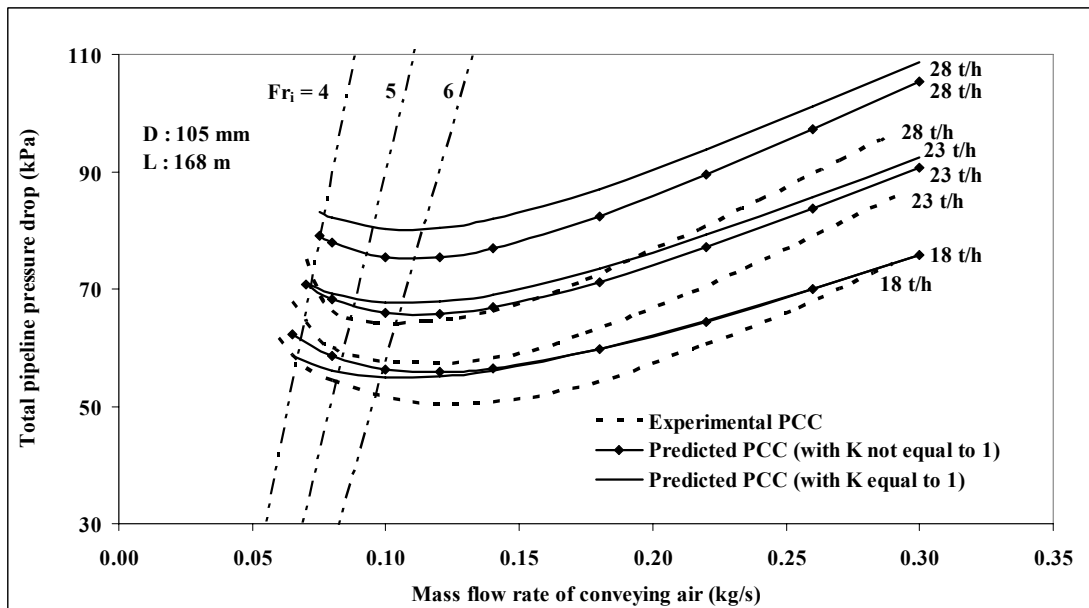
Figure 7.22: Experimental Versus Predicted PCC for Fly Ash and 105 mm I.D. × 168 m Pipe using Equations (7.35) and (7.36)
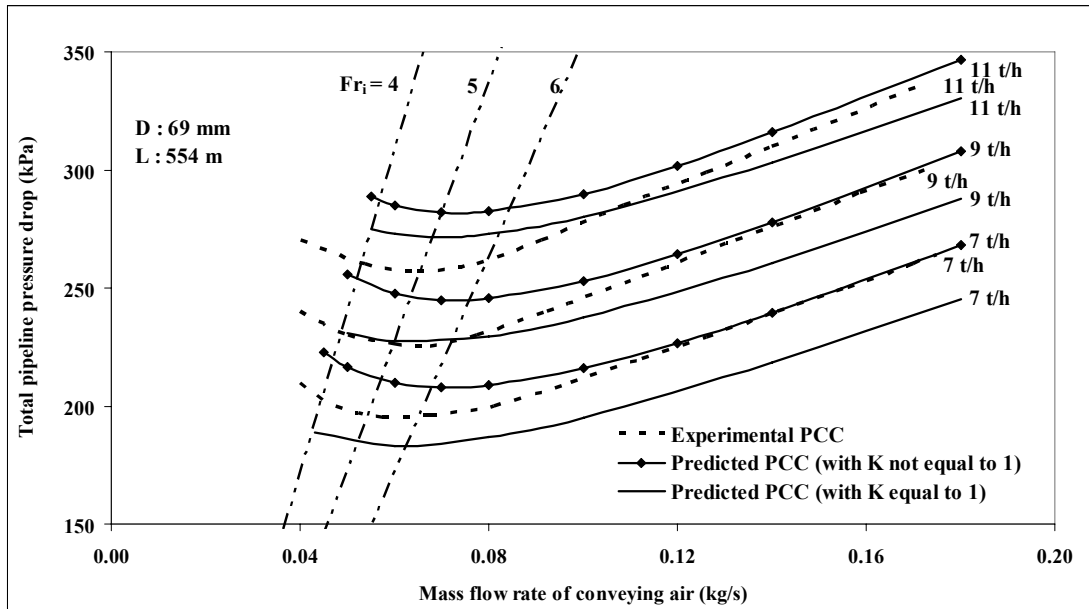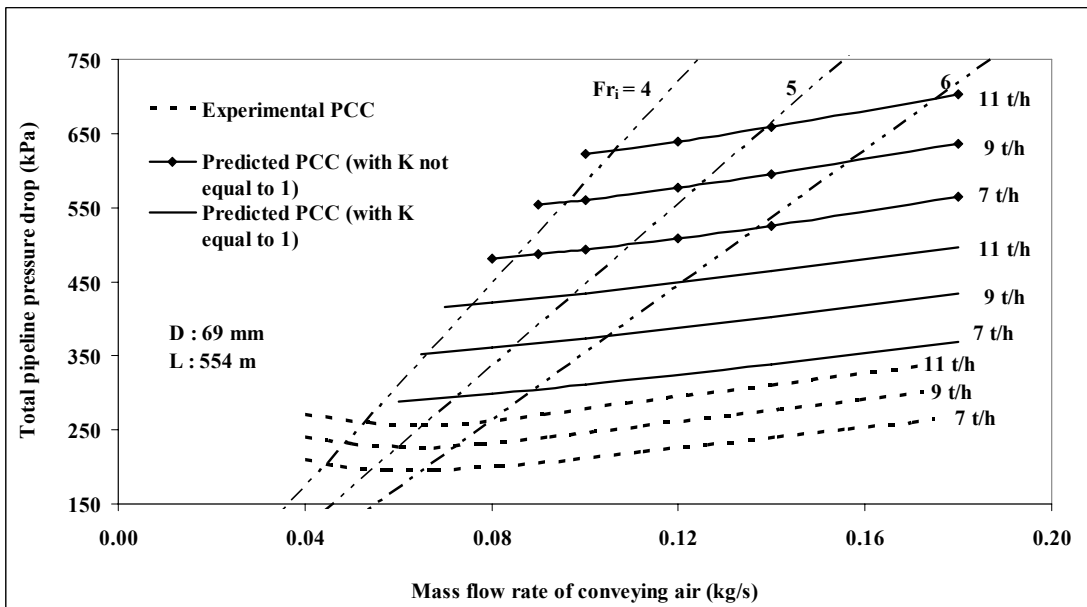

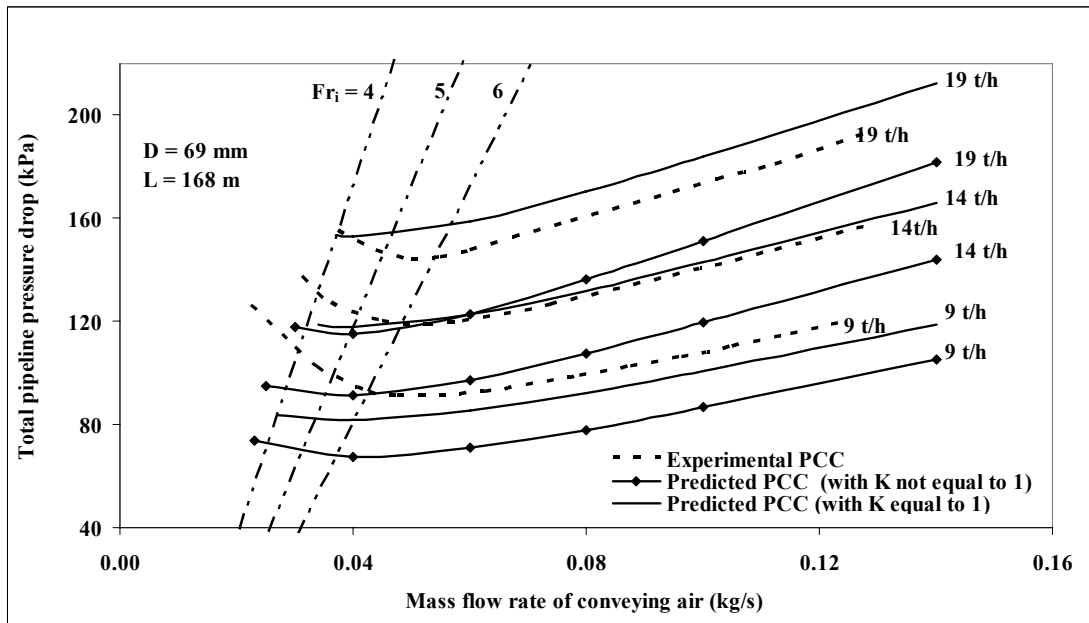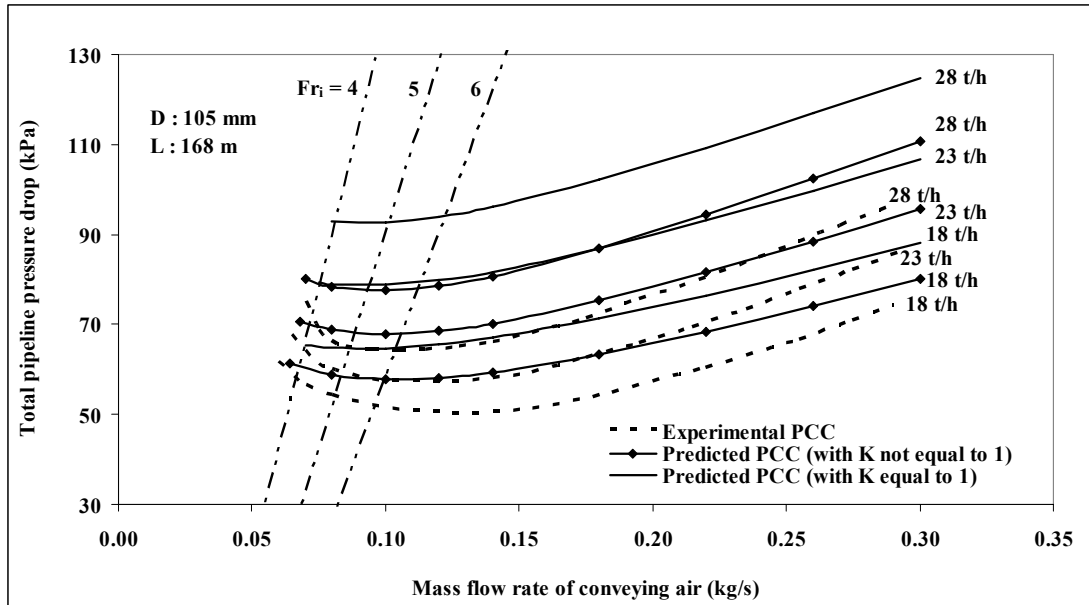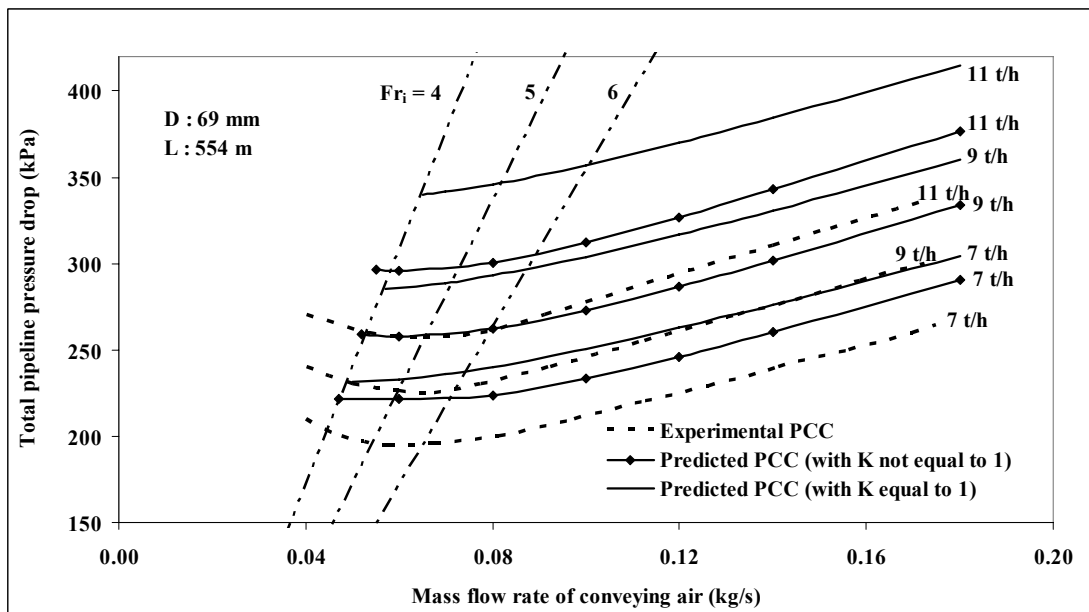**Figure 7.23:** Experimental Versus Predicted PCC for Fly Ash and 69 mm I.D. × 554 m Pipe using Equations (7.35) and (7.36)

The results show that for the 105 mm I.D. × 168 m long pipe (Figure 7.22), the models over-predict the experimental PCC quite considerably. The model provided by equation (7.36) (i.e. for K = 1), results in relatively better predictions. The predicted PCC do not show any "U"-shaped trend (the values of predicted PCC continue to decrease with decrease in air flow rates at low Fr_i region). For the 69 mm I.D. × 554 m long pipe, equation (7.35) (i.e. model for K ≠ 1) results in dramatic over-prediction. Using equation (7.36) (i.e. for K = 1), relatively better predictions are obtained (though still significant over-predictions exist).

Similar investigations were further carried out for ESP dust. Using the total pipeline pressure loss data for the 69 mm I.D. × 168 m long pipe, the following models for λ_s were derived (in both K ≠ 1 and K =1 formats) using "back calculation" method:

$$\lambda_s = 7.16 \, (m^*)^{-0.536} \, (Fr_m)^{-1.677} \qquad\qquad [R^2 = 0.994] \qquad\qquad\qquad (7.37)$$

$$\lambda_s = (m^*)^{-0.212} \, (Fr_m)^{-1.333} \qquad\qquad\quad [R^2 = 0.999] \qquad\qquad\qquad (7.38)$$

It can be seen that again the absolute numerical values of exponents of the terms m^* and Fr_m are greater for the case when K ≠ 1 than K = 1. The high values of R^2 indicated "good fit". The above models were evaluated for scale-up accuracy and stability by using them to predict the total pipeline drop for the larger and longer pipelines (105 mm I.D. × 168 m and 69 mm I.D. × 554 m) for various solids flow rates for and comparing the predicted and experimental PCC. Again, predictions were not pursued for the 69 mm I.D. × 168 m long pipe. Chambers and Marcus (1986)

163

model was used to estimate the losses due to the bends. The results are shown in Figures 7.24 to 7.25.
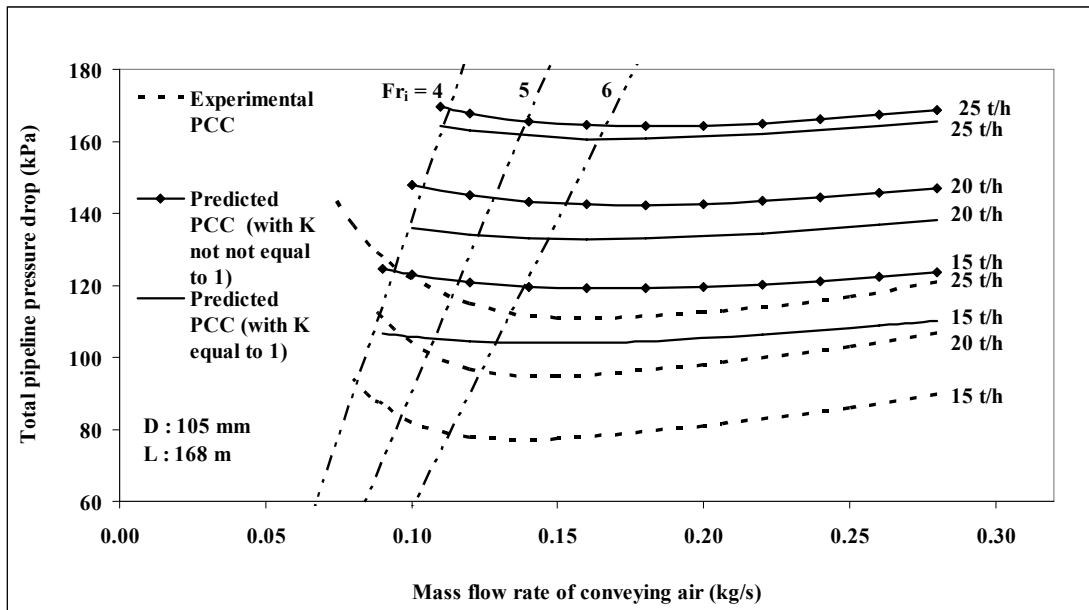
Figure 7.24: Experimental Versus Predicted PCC for ESP Dust and 105 mm I.D. × 168 m Pipe using Equations (7.37) and (7.38)
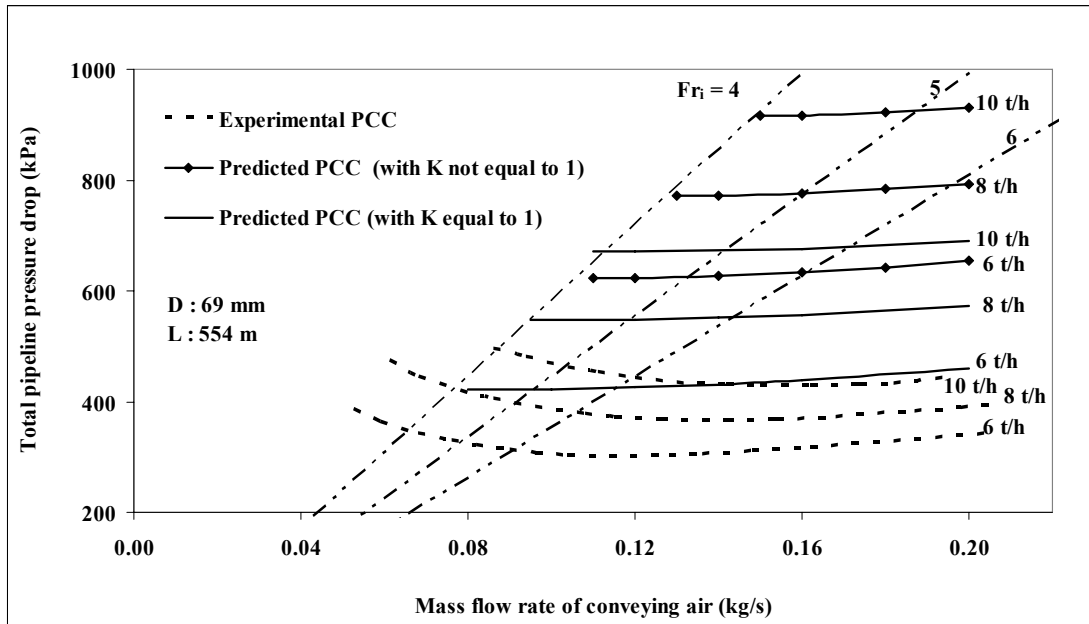
Figure 7.25: Experimental Versus Predicted PCC for ESP Dust and 69 mm I.D. × 554 m Pipe using Equations (7.37) and (7.38)

The results show that for the 105 mm I.D. × 168 m long pipe (Figure 7.24), the models over-predict the experimental PCC quite significantly (especially, for the higher solids flow rates). The shapes of the predicted PCC also were rather horizontal. For the 69 mm I.D. × 554 m long pipe, equation (7.37) (i.e. model for K ≠ 1) results in dramatic over-prediction. Using equation (7.38) (i.e. for K = 1), relatively better predictions are obtained (though still significant over-predictions exist).

The amount of inaccuracy obtained using the "back calculation" approach was found to be generally larger than the methods using "straight pipe" data (described previously in subsections 7.2.1 and 7.2.2). Because the accuracy of the "back

calculation" approach depends to a large extent on the validity and accuracy of the bend models (which in itself is an undeveloped area to date) used during the modelling of solids friction factor (especially from a test rig is short in length and having many bends), this approach is more prone to generating a larger amount of inaccuracy under scale-up conditions, as compared to the "straight pipe" method. Another point of concern or source of potential error is: since in "back calculation" method, the estimation of bend loss during modelling stage (for subtracting the bend losses from total pipeline losses) is based on the average density and velocity for the whole pipe multiplied by the number of bends in line (Jones and Williams, 2003), the estimated total bend loss in this method is less than what is obtained by calculating the loss for each bend separately (but this can not be done unless model for straight pipe loss is derived). As example: the estimated bend loss by grouping all bends together for $m_f = 0.13$ kg/s, $m_s = 18$ t/h for the 69 mm I.D. × 168 m pipe with fly ash is 25 kPa, however if losses in each bend were calculated separately and added, it would come 35 kPa (also refer to Table 6.1). Of course one can still argue about the accuracy of the bend model itself, but certainly calculating for each bend is a relatively more accurate method than grouping all bends together. As a result of this, the estimated total straight pipe loss for the pipe (which is obtained by subtracting total bend, vertical and acceleration loss from total pipeline loss) in back-calculation method of modelling is of higher value than what it should be in reality. As a result, models derived from this higher value of straight pipe loss will have an inherent tendency of over-predicting. An exercise was also carried out by altering the bend loss factor $B = 0.5$ to $B = 0.2$ for fly ash. It was found that the resultant model is very

similar to the model with B = 0.5 (Equation 7.36). The new exponents for m* and Fr_m are -0.35 and -1.33, respectively. As a result, this model was not evaluated. These exponents are very similar to those of equation 7.36 due to the under-estimation of total bend losses by the grouping method. This is because the estimated bend loss by grouping method is under-predicting the bend loss (as already discussed), hence a factor of change on this (e.g. B = 0.5 to B = 0.2) will not have scope to cause much change to the total straight pipe loss and the solids friction model derived from it. This again points out that more number of bends in test rig (in a short pipe, such as Jones and Williams, 2003), the more is the chance of having these uncertainties in calculating the correct straight pipe loss for modelling.

From the results of the various evaluation work shown (subsection 7.2.1 to 7.2.3), it appears that models derived with the K = 1 format are generally more stable than the models derived with the K ≠ 1 format, especially under significant scale-up condition. This seems to support the preliminary observations of Wypych et al. (2005). This could be due to the higher absolute values of the exponents of Froude number in the λ_s models for the K ≠ 1 compared to the K =1 format. This could make the models in K ≠ 1 format more sensitive to the changes in Froude number when the models extrapolate beyond the experimental data range of Froude number within which they were originally derived, thus increasing their chance of instability. It was decided that for all subsequent modelling work in this thesis, the K = 1 format would be used.

7.2.4 Weber (1991) method

Weber (1991) suggested that the pressure drop of the solids-air mixture is integral in nature, i.e. the pressure drop due to air-only and that due to the solids-only are difficult to separate individually, as represented by Barth (1958), and suggested a combined friction factor for solids and air mixture (λ_T), provided by equation 2.25. Since Weber (1991) did not validate his method under scale-up conditions of diameter and length, the same is being pursued here. Using the steady state "straight pipe" pressure drop data obtained from the P9-P10 and P11-P12 tapping points for the 69 mm I.D. × 168 m long pipe for fly ash conveyed over a wide range of flow conditions (dilute- to fluidised dense-phase), the following models for λ_T were derived using the dimensionless groupings used by Weber (1991):

Based on P9-P10 data:

$$\lambda_T = (m^*)^{0.73} \ (Fr_m)^{-1.5} \qquad\qquad [R^2 = 0.991] \qquad\qquad (7.39)$$

Based on P11-P12 data:

$$\lambda_T = (m^*)^{0.71} \ (Fr_m)^{-1.46} \qquad\qquad [R^2 = 0.999] \qquad\qquad (7.40)$$

The high values of R^2 indicated "good fit". The model given by equation (7.39) was evaluated for scale-up accuracy and stability by using it to predict the total pipeline drop for the larger and longer pipelines (viz. 69 mm I.D. $\times$ 168 m, 105 mm I.D. $\times$ 168 m and 69 mm I.D. $\times$ 554 m) for various solids flow rates for and comparing the predicted and experimental PCC. Since the models have similar values of exponents for the dimensionless groupings, it was considered adequate to only evaluate equation (7.39). Pan and Wypych (1998) model was used to estimate the losses due to the bends. The results are shown in Figures 7.26 to 7.28.
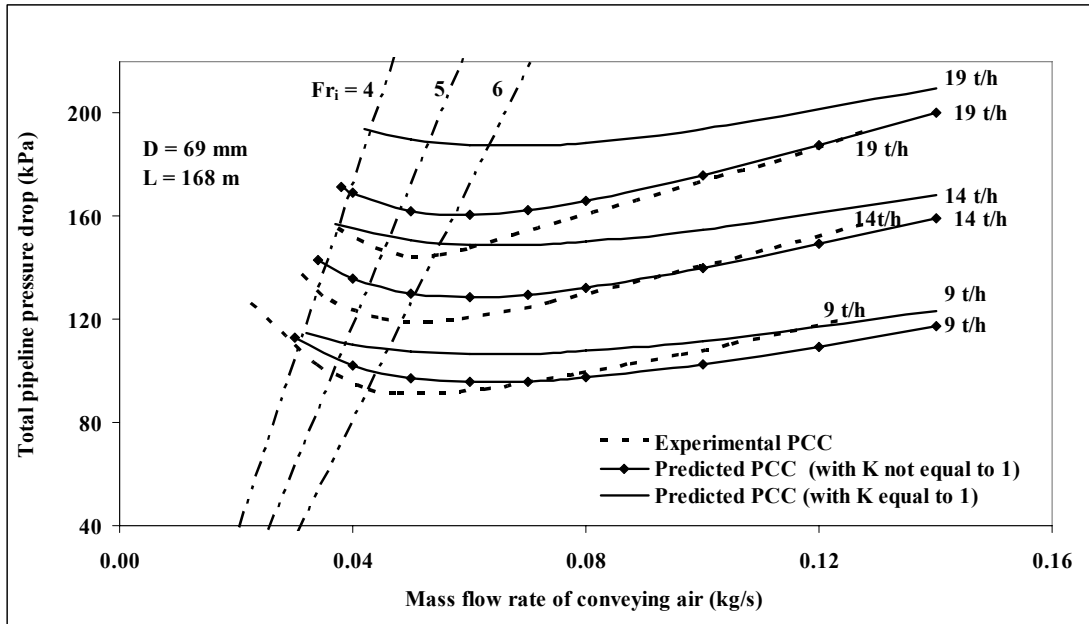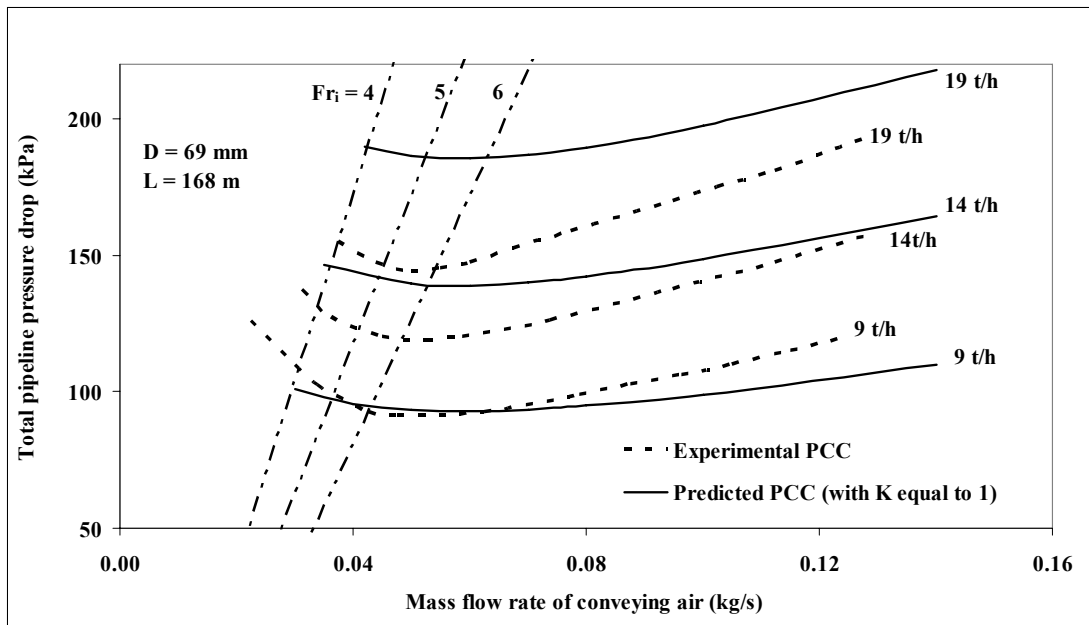

Figure 7.26: Experimental Versus Predicted PCC for Fly Ash and 69 mm I.D. $\times$ 168 m Pipe using Equation (7.39)
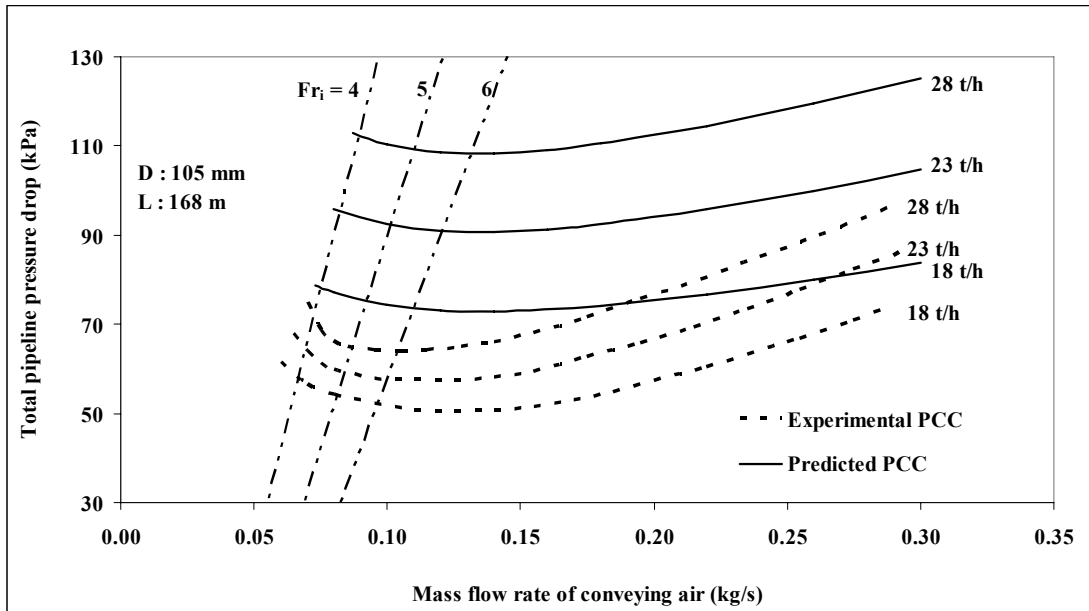
Figure 7.27: Experimental Versus Predicted PCC for Fly Ash and 105 mm I.D. × 168 m Pipe using Equation (7.39)
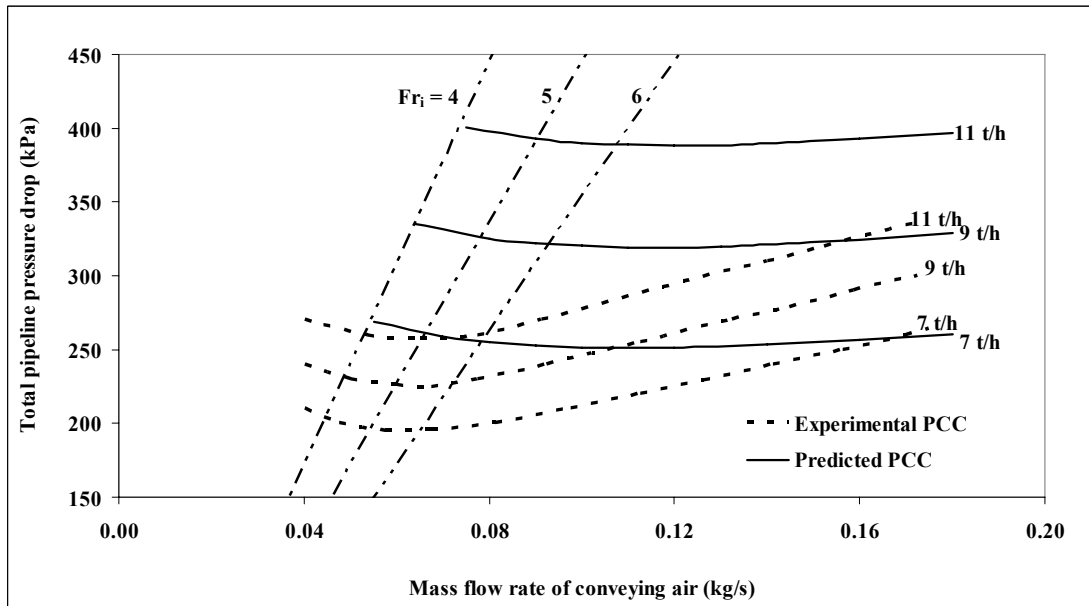
Figure 7.28: Experimental Versus Predicted PCC for Fly Ash and 69 mm I.D. × 554 m Pipe using Equation (7.39)

170

Figure 7.26 shows that for the 69 mm I.D. × 168 m pipe, the higher solids flow rates (especially, the 19 t/h line) result in considerable over-predictions. However, good predictions are obtained for m_s = 9 t/h (especially, for dense-phase). For diameter scale-up (Figure 7.27), the model results in significant over-prediction. The predicted PCC do not display sharp "U"-shaped trends (similar to the experimental PCC). For the 69 mm I.D. × 554 m long pipeline, Figure 7.27, the model results in significant over-prediction. Also, the trends of the predicted PCC are not "U"-shaped. The predicted pressure drop values continue to decrease (although very slightly) with increase in air flow rates even at high air velocity range. Further modelling and prediction work using this method were not pursued for ESP dust and "white powder".

7.2.5   "K" method (Datta and Ratnayaka 2003, 2005)

In recent years, a new approach of modelling has been employed by some researchers (Datta and Ratnayaka 2003, 2005), where the solids-air mixture has been considered as a single phase (instead of treating solids and air separately). The total pressure drop due to solids-air mixture was represented using a combined "pressure drop coefficient" ("K") and the concept of "suspension density", as given by equations (7.41) and (7.42).

$$\Delta P_T = K\, \rho_{sus}\, L/D\, V^2_{entry}/2 \tag{7.41}$$

$$\rho_{sus} = (M_s + M_f)/(V_s + V_f) \tag{7.42}$$

The above procedure was reported (Datta and Ratnayaka 2003, 2005) to have resulted in reasonably good agreement between estimated values and the researchers' own data. However, the models were not tested under significant scale-up conditions. Hence, there is a requirement to properly evaluate the validity of the same (under significant length/diameter scale-up conditions). Based on the steady state "straight pipe" pressure drop data of fly ash obtained from P9-P10 tappings for 69 mm I.D. × 168 m and 105 mm I.D. × 168 m pipes and P11-P12 tappings for 69 mm I.D. × 168 m pipe, the following models for pressure drop coefficient were derived. The correlation coefficient (R^2) values (between "K" and "V^2_{entry}") were reasonably high (0.94, 0.97, 0.95), indicating a fairly good functional relationship.

Based on P9-P10 data; 69 mm I.D. × 168 m long pipe:

$$K = 0.1835 \, (V^2_{entry})^{-0.66} \tag{7.43}$$

Based on P9-P10 data; 105 mm I.D. × 168 m long pipe:

$$K = 0.1177 \, (V^2_{entry})^{-0.58} \tag{7.44}$$

Based on P11-P12 data; 69 mm I.D. × 168 m long pipe:

$$K = 0.1373 \, (V^2_{entry})^{-0.60} \tag{7.45}$$

"K" is expressed as a function of "V_{entry}", because similar functional representations of "K" were employed by (Datta and Ratnayaka 2003, 2005). It should be noted that the derived models were different depending on the pipe diameter and location of tapping points (for the same pipe), even for the same product (fly ash).

The above models were evaluated for scale-up accuracy by using them to predict the total pipeline drop for different pipes (69 mm I.D. × 168 m, 105 mm I.D. × 168 m and 69 mm I.D. × 554 m) for various solids flow rates and comparing the predicted pneumatic conveying characteristics against the experimental plots. To estimate the losses occurring in the bends, the bend model derived by Pan and Wypych (1998) was used. Typical results using the model given by equation (7.43) are shown in the following figures (Figures 7.29 to 7.31). Comparison between experimental and predicted PCC using the other models (equations 7.44 and 7.45) are provided in Figures A3.7 to A3.12 (Appendix A3).
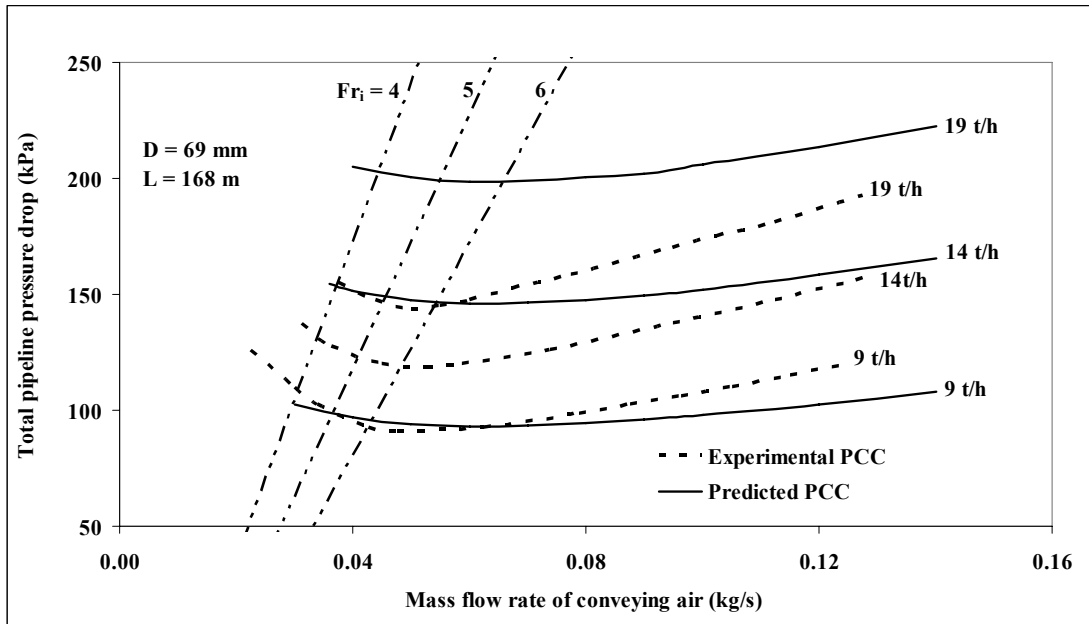
Figure 7.29: Experimental Versus Predicted PCC for Fly Ash and 69 mm I.D. × 168 m Pipe using Equation (7.43)
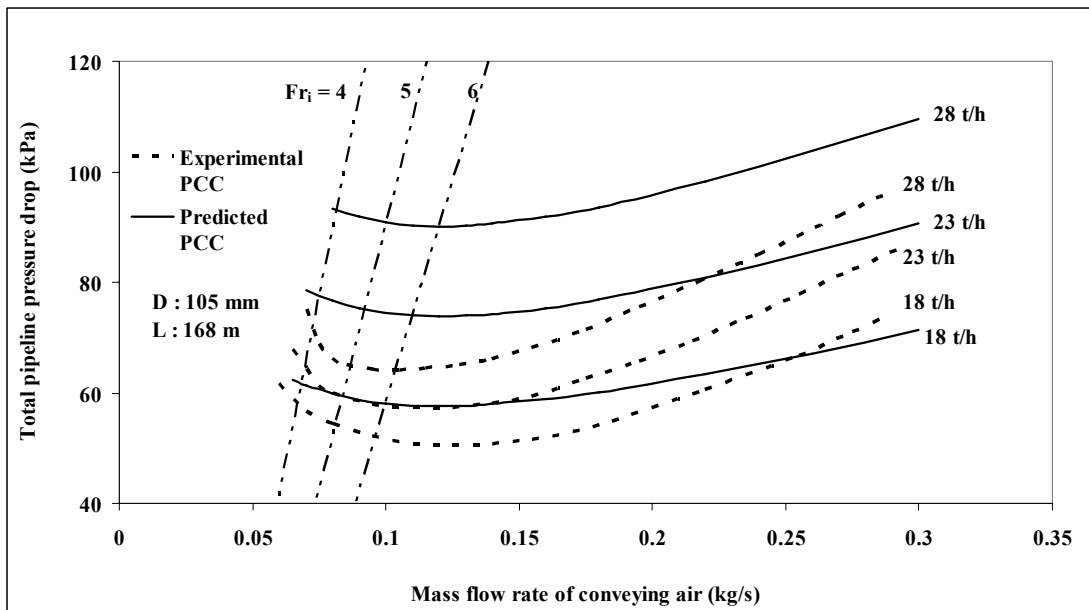
Figure 7.30: Experimental Versus Predicted PCC for Fly Ash and 105 mm I.D. × 168 m Pipe using Equation (7.43)

174
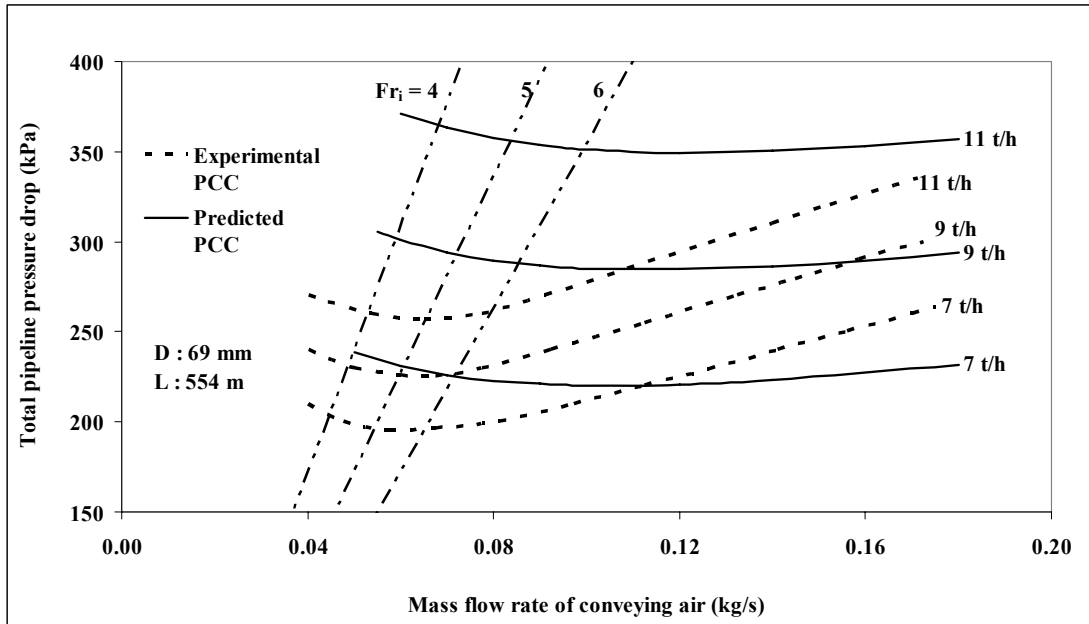
Figure 7.31: Experimental Versus Predicted PCC for Fly Ash and 69 mm I.D. × 554 m Pipe using Equation (7.43)

The results show that none of the models are generally capable of consistently predicting the pressure drop accurately for the various scale-up conditions. For the 69 mm I.D. × 168 m pipe, equation (7.43) provides significant over-predictions, whereas equations (7.44) and (7.45) result in relatively better predictions (though the nature or trend of the predicted PCC was not typically "U"-shaped). Under diameter scale-up condition (i.e. for the 105 mm I.D. × 168 m long pipe), again equation (7.43) results in significant over-predictions, whereas equations (7.44) and (7.45) result in some improvements. For significant length scale-up condition (i.e. for 69 mm I.D. × 554 m long pipe), all the models provide significant over-predictions. Also, the

"downwards" trend of the predicted PCC using equation (7.43) was inappropriate for the 69 mm I.D. × 554 m long pipe.

Similar investigations were further carried out for ESP dust. Using the steady state "straight pipe" pressure loss data from P9-P10 tapping points on the 69 mm I.D. × 554 m long pipe, the following model was derived:

$$K = 0.468 \ (V^2_{entry})^{-0.754} \tag{7.46}$$

The value of R^2 obtained for the above model was 0.986, indicating good strength of relationship. The above model was evaluated for scale-up accuracy by using it to predict the total pipeline drop for different pipes (69 mm I.D. × 168 m, 105 mm I.D. × 168 m and 69 mm I.D. × 554 m) for various solids flow rates and comparing the predicted and experimental PCC. Chambers and Marcus (1986) model was used to estimate the losses occurring in the bends. Results are shown in the following figures (Figures 7.32 to 7.34).
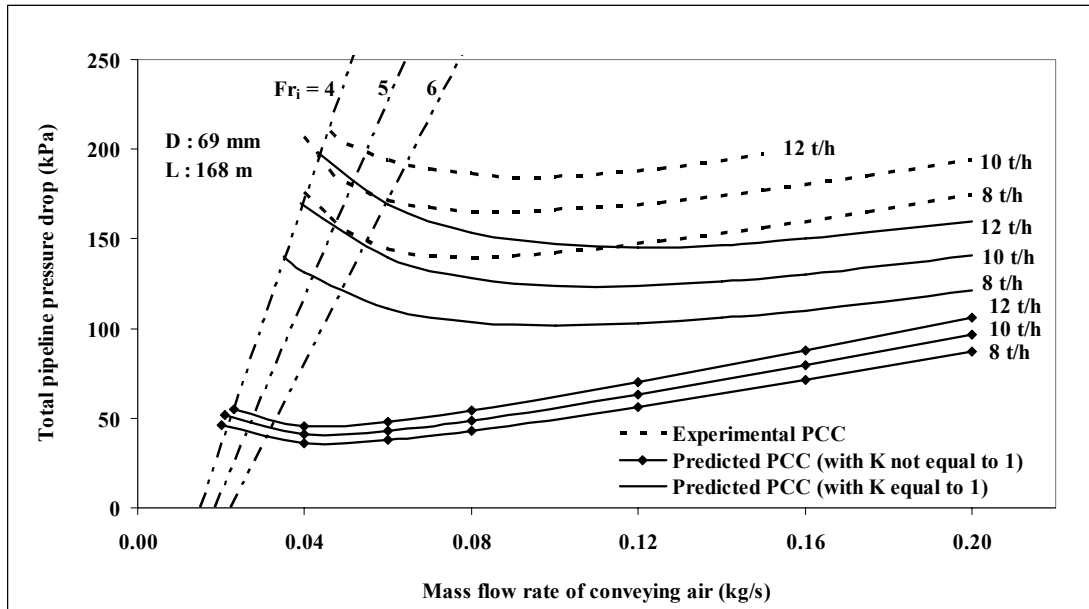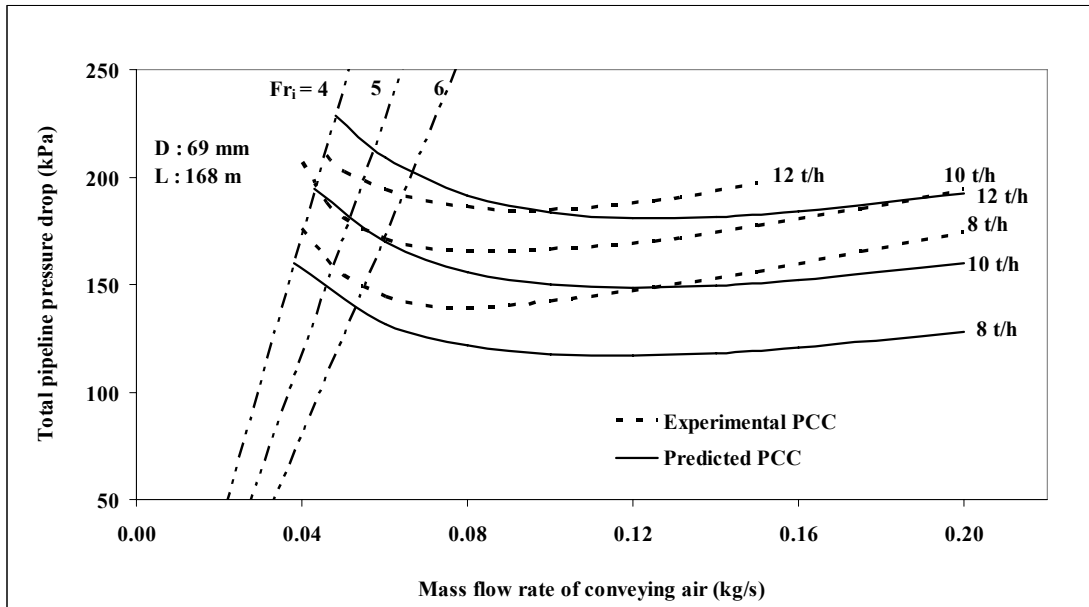
Figure 7.32: Experimental Versus Predicted PCC for ESP Dust and 69 mm I.D. ×
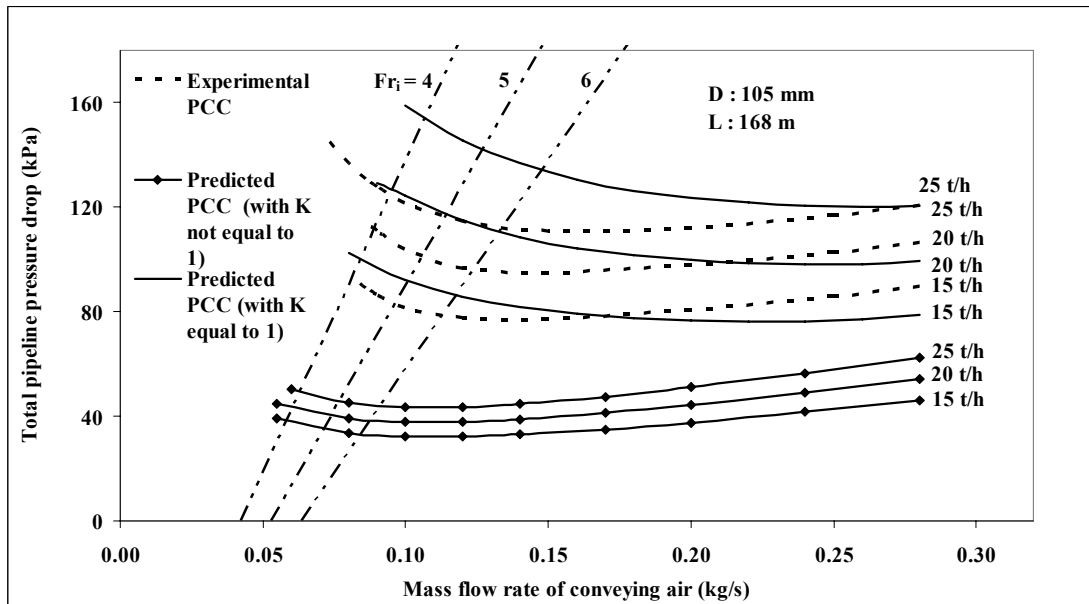
168 m Pipe using Equation (7.46)
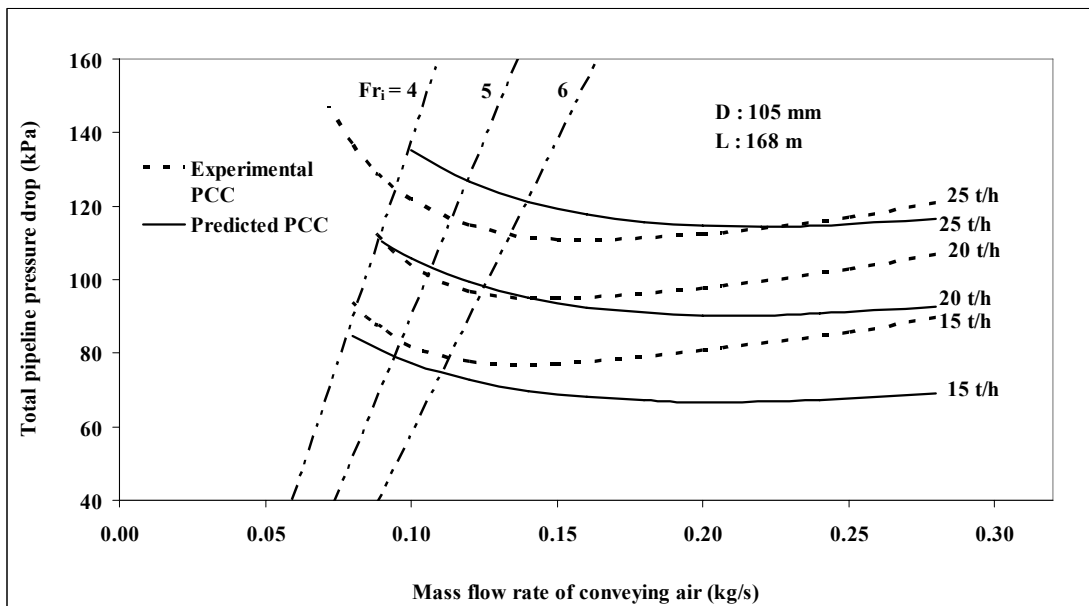
Figure 7.33: Experimental Versus Predicted PCC for ESP Dust and 105 mm I.D. ×
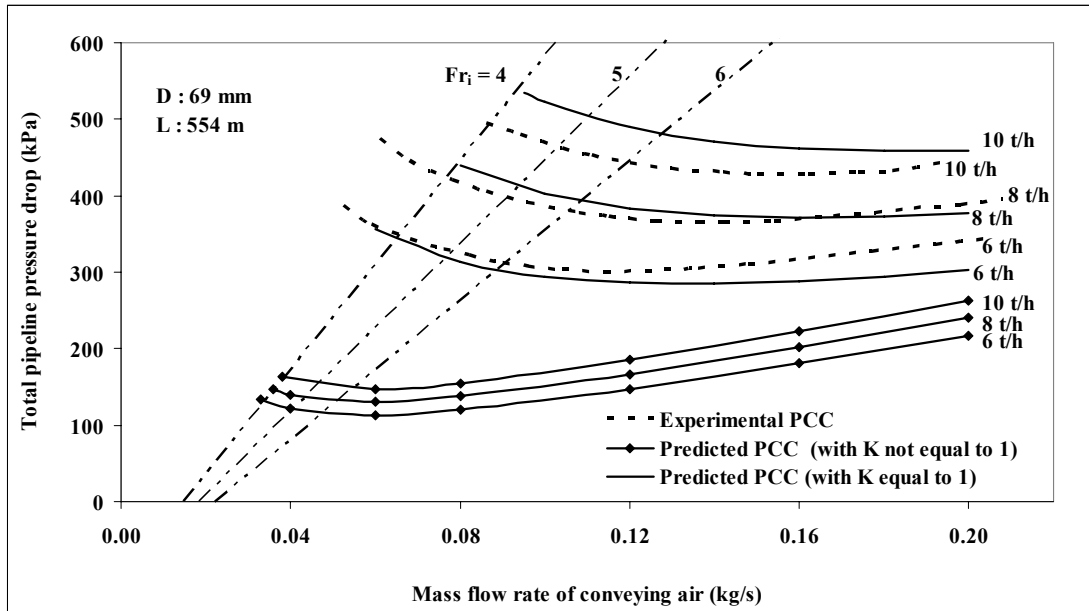
168 m Pipe using Equation (7.46)
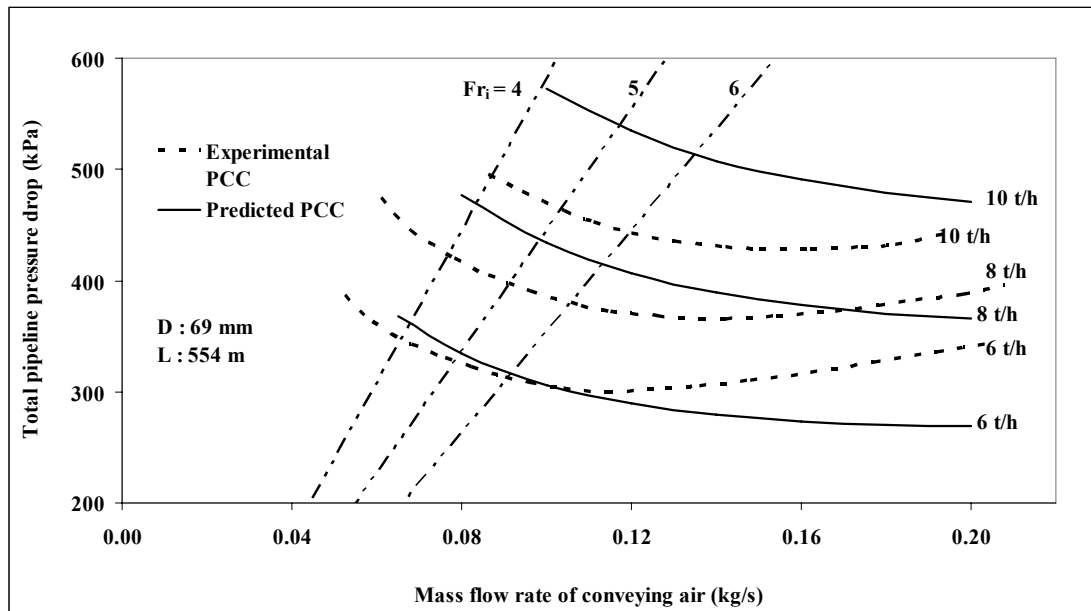
Figure 7.34: Experimental Versus Predicted PCC for ESP Dust and 69 mm I.D. ×
554 m Pipe using Equation (7.46)

Results show that surprisingly, for all the pipelines, good predictions are obtained for
dense-phase regime. Although there are some over-predictions for the 69 mm I.D. ×
554 m long pipe for the higher solids flow rate line (m_s = 10 t/h), but this may be
considered within acceptable design limits. However, the model starts to produce
under-prediction towards the dilute-phase region (especially, for lower solids flow
rates).

It is in fact quite interesting to note that for many of the modelling formats (discussed
in this chapter), a particular parameter grouping, which would result in significant
over-prediction for fly ash, has unexpectedly provided significant under-prediction
for ESP dust and even to guess the trend of the predicted PCC (i.e. whether to expect

under- or over-prediction) using a particular model format is a significantly difficult task.

7.2.6   *Parameter groupings for strand conveying (Wirth and Molerus, 1983)*

Wirth and Molerus (1983) had developed an expression for pressure drop for strand conveying by introducing a dimensionless "friction number" term, as given in the following:

$$Fri = V/ [(\rho_s/ \rho) (1 - \rho_s/ \rho) (1 - \varepsilon) D g f_r]^{0.5} \tag{7.47}$$

They also included another parameter grouping: $\rho/\{\rho_s(1-\varepsilon)\}$. Their approach was considered worthwhile for modelling, as for the dense-phase conveying of fine powders, experimentally it has been observed that there exists a dense non-suspension layer at the bottom of pipe, on top of which a dilute-phase suspension flow occurs, resembling a strand. Wirth and Molerus (1983) did not validate their model under scale-up conditions.

Using the steady state "straight pipe" pressure drop data obtained from the P9-P10 and P11-P12 tapping points for the 69 mm I.D. × 168 m long pipe for fly ash conveyed over a wide range of flow conditions (dilute- to fluidised dense-phase), models for λ_s were derived by representing straight pipe pressure loss as per Barth (1958). The models are given by equations (7.48) and (7.49).

Based on P9-P10 data:

$$\lambda_s = (m^*)^{-0.51} (Fri)^{-1.87} (\rho/(\rho_s(1-\epsilon))^{0.43} \qquad [R^2 = 0.999] \qquad (7.48)$$

Based on P11-P12 data:

$$\lambda_s = (m^*)^{-0.278} (Fri)^{-1.54} (\rho/(\rho_s(1-\epsilon))^{0.598} \qquad [R^2 = 0.999] \qquad (7.49)$$

where, $\epsilon = 1 - (\rho_{bl}/\rho_s)$; the value of wall friction angle was determined as 16.5 degree using Jenike shear tests. The high values of R^2 indicated "good fit". It is again observed that the models derived from P9-P10 and P11-P12 data are different. The models were evaluated for scale-up accuracy and stability by using them to predict the total pipeline drop for the larger and longer pipelines (69 mm I.D. × 168 m, 105 mm I.D. × 168 m and 69 mm I.D. × 554 m) for various solids flow rates and comparing the predicted and experimental PCC. The Pan and Wypych (1998) model was used to estimate the losses due to the bends. The predictions for equation (7.48) are shown in Figures 7.35 to 7.37. Results using equation (7.49) are provided in Figures A3.13 to A3.15 (in Appendix A3).

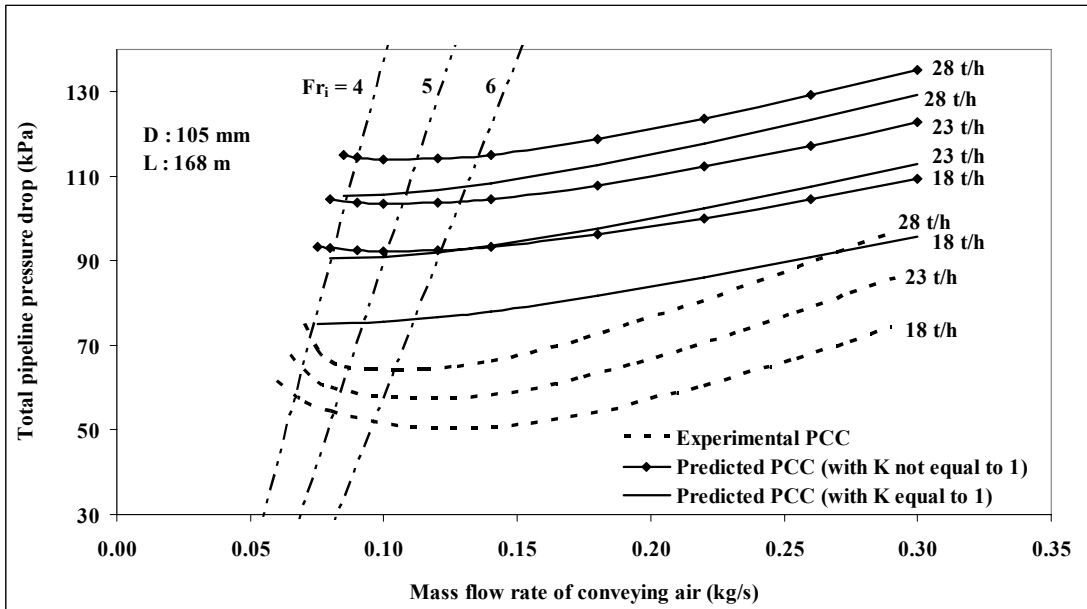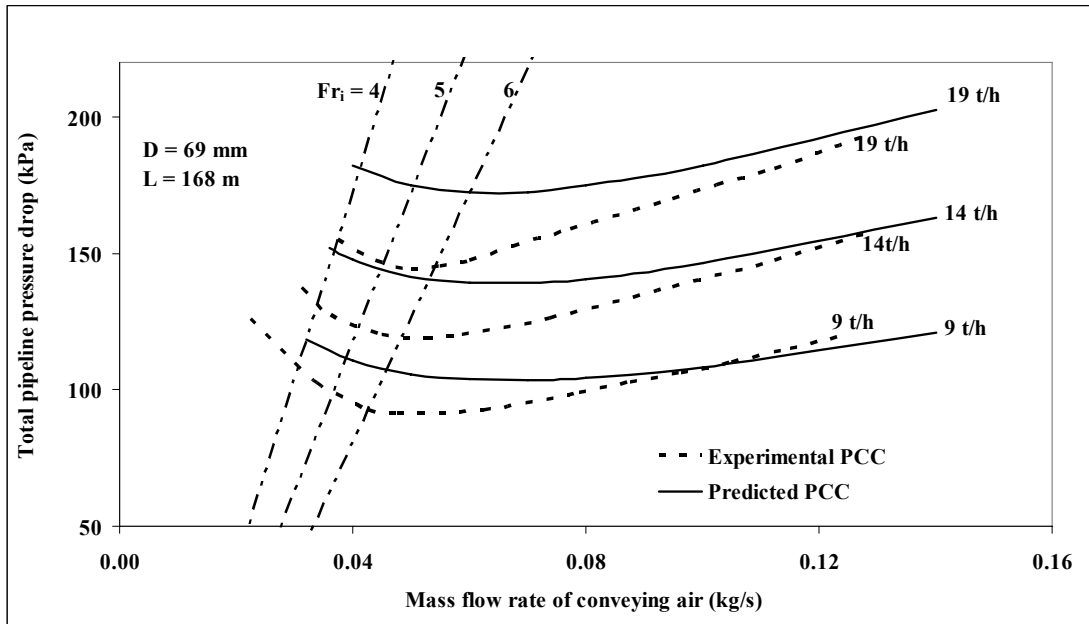**Figure 7.35:** Experimental Versus Predicted PCC for Fly Ash and 69 mm I.D. × 168 m Pipe using Equation (7.48)
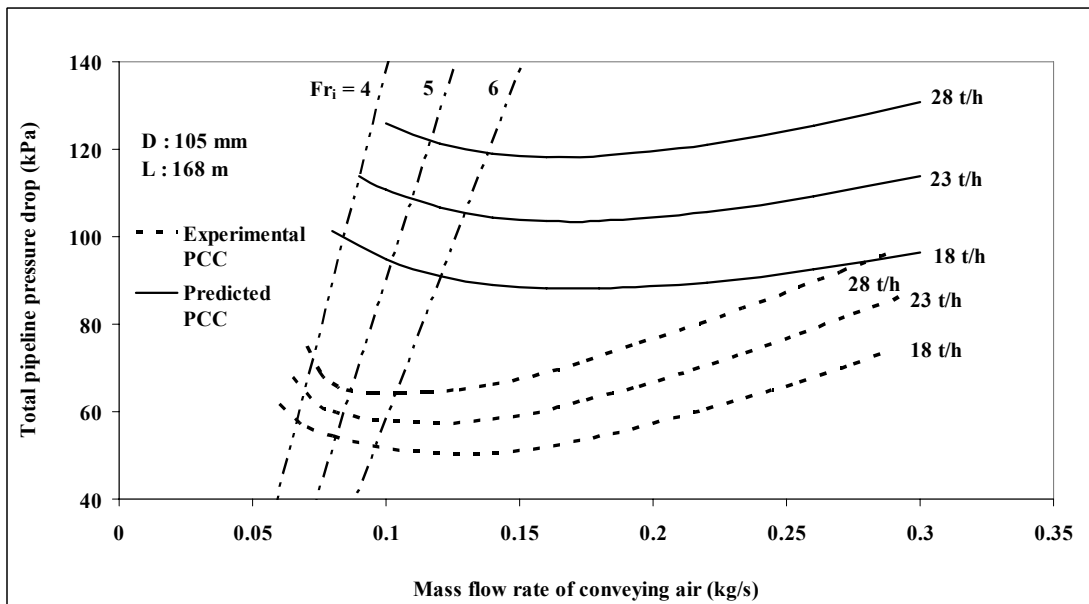
Figure 7.36: Experimental Versus Predicted PCC for Fly Ash and 105 mm I.D. × 168 m Pipe using Equation (7.48)
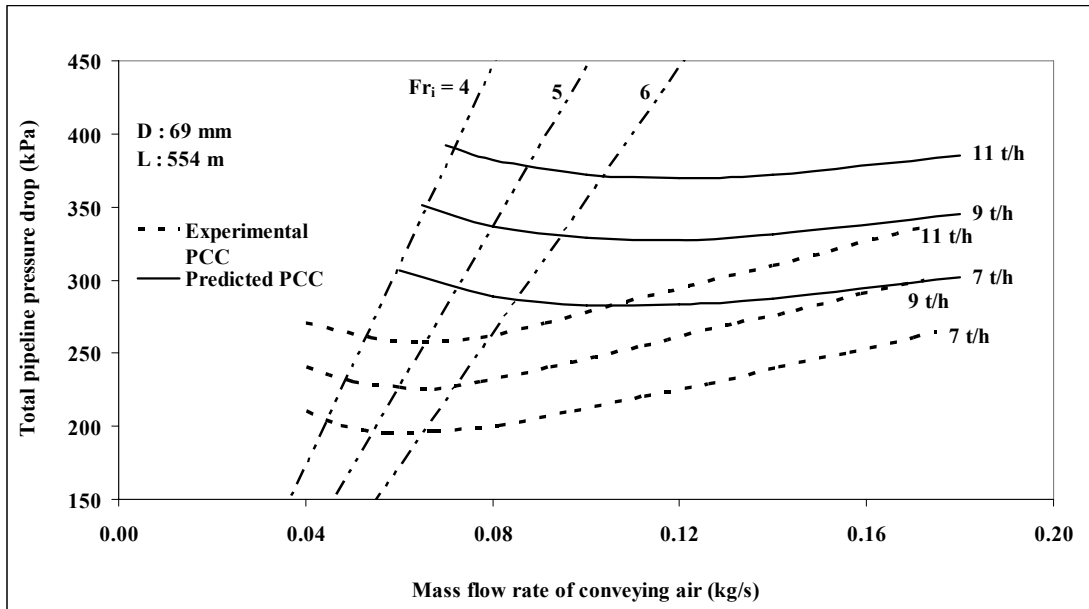
Figure 7.37: Experimental Versus Predicted PCC for Fly Ash and 69 mm I.D. × 554 m Pipe using Equation (7.48)

Figure 7.35 shows that for the 69 mm I.D. × 168 m long pipe, equation (7.48) provides some over-prediction. However, the model seems to predict fairly well towards the dilute-phase (though the gradients of the predicted PCC are somewhat less than those for the experimental PCC in the dilute-phase). For the larger and longer pipes, as shown in Figures 7.36 and 7.37, respectively, the model results in significant over-prediction (especially, in dense-phase). Also, the predicted PCC do not provide "U"-shaped trend. The predicted PCC using equation (7.49) provide similar trends, however, with relatively better accuracy for prediction (i.e. the margin of over-prediction has reduced).

A similar exercise was further carried out for ESP dust. Using the "straight pipe" pressure loss data from P9-P10 tapping points on the 69 mm I.D. × 554 m long pipe the following model was derived:

$$\lambda_s = (m*)^{-0.187} (Fri)^{-1.697} (\rho f/(\rho s(1-\varepsilon)))^{0.627} \qquad [R^2 = 0.999] \qquad (7.50)$$

The value of wall friction angle was determined as 25.8 degree (using Jenike shear tests) for the above model. The model was evaluated for scale-up accuracy and stability by using it to predict the total pipeline drop for the larger and longer pipelines (69 mm I.D. × 168 m, 105 mm I.D. × 168 m and 69 mm I.D. × 554 m) for various solids flow rates and comparing the predicted and experimental PCC. The Chambers and Marcus (1986) model was used to estimate the losses due to the bends. The results are shown in Figures 7.38 to 7.40.
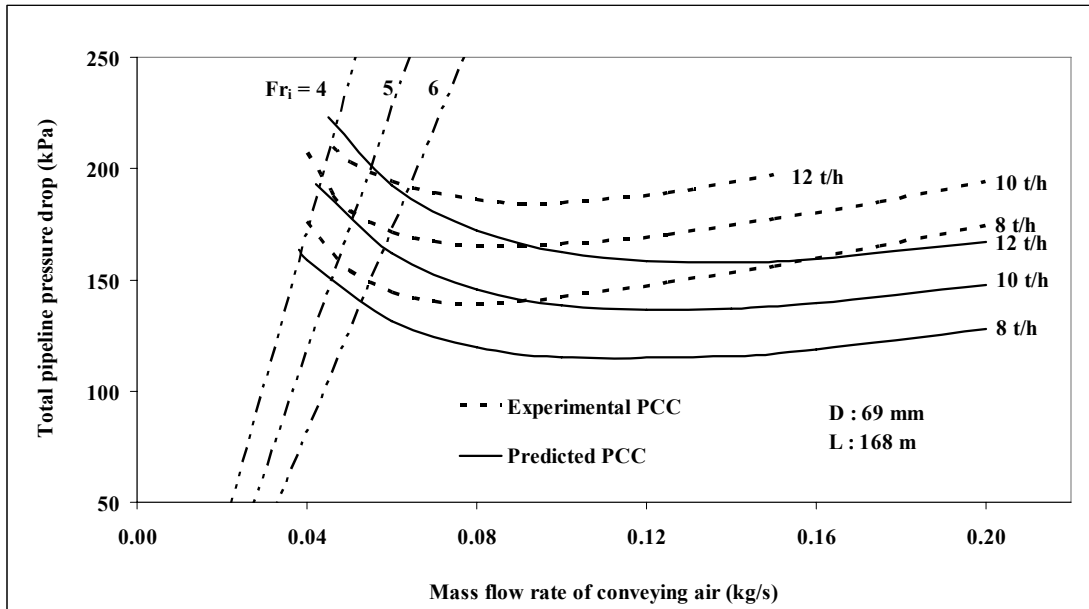
Figure 7.38: Experimental Versus Predicted PCC for ESP Dust and 69 mm I.D. ×
168 m Pipe using Equation (7.50)
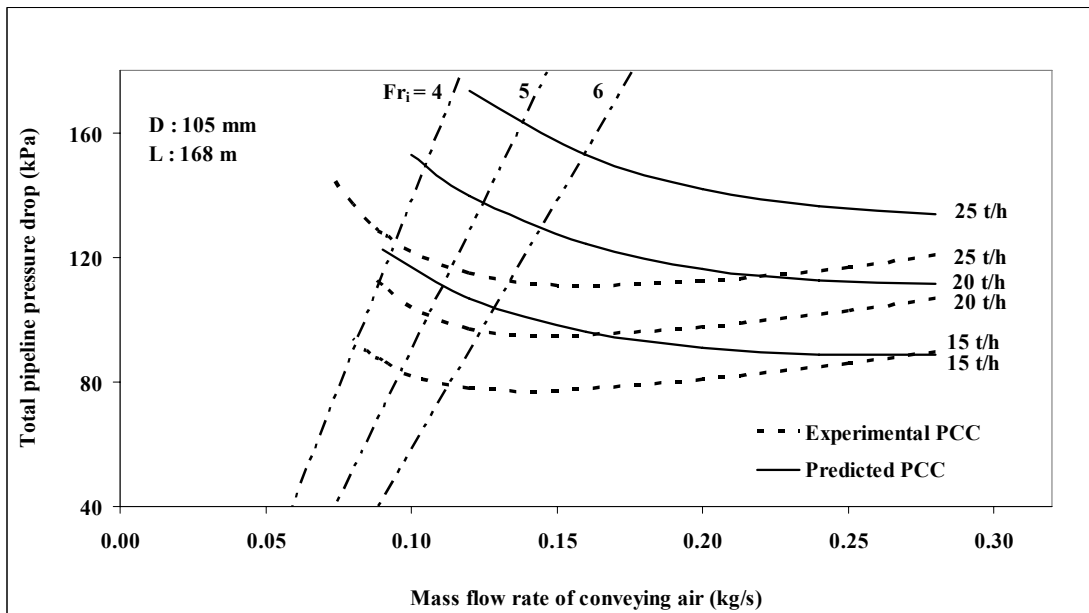
Figure 7.39: Experimental Versus Predicted PCC for ESP Dust and 105 mm I.D. ×
168 m Pipe using Equation (7.50)
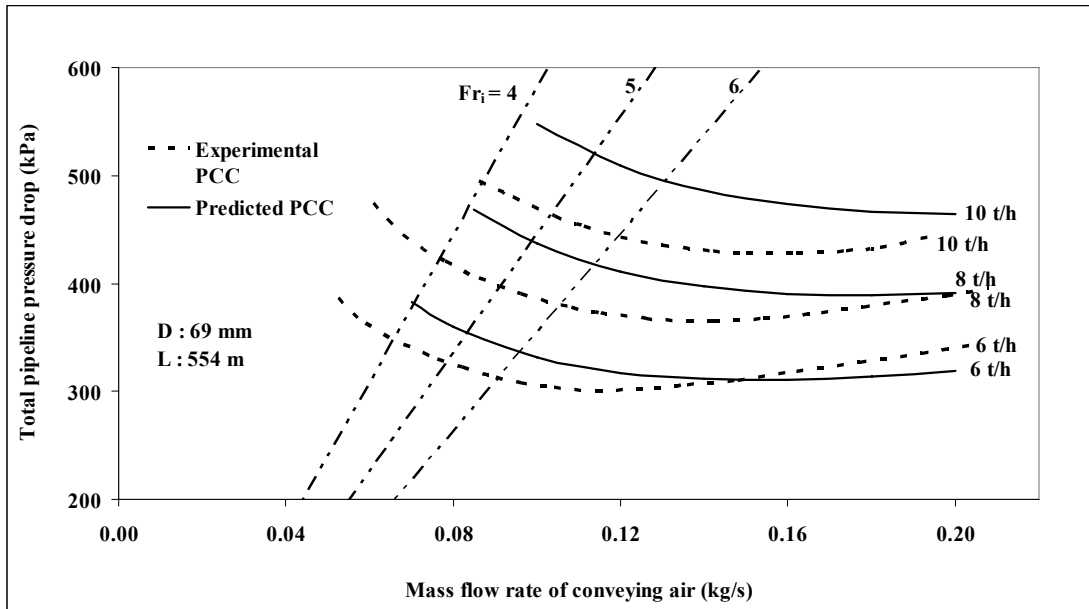
Figure 7.40: Experimental Versus Predicted PCC for ESP Dust and 69 mm I.D. × 554 m Pipe using Equation (7.50)

Figure 7.38 shows that for the 69 mm I.D. × 168 m long pipe, the model predicts very well for dense-phase region. However, the model results in considerable under-prediction towards the dilute-phase regime. For the 105 mm I.D. × 168 m long pipe, the model provides considerable over-predictions for dense-phase, however, results in relatively better prediction towards the dilute-phase. Surprisingly, the model results in quite good predictions for the longer pipe (69 mm I.D. × 554 m), Figure 7.40, for dense- to dilute-phase.

7.3   Further studies to identify suitable parameters groupings and conclusions

It has been demonstrated that the various existing design procedures are generally not capable of proving accurate predictions under scale-up conditions of diameter and/or length. It appears that the parameter groupings which are frequently used in modelling solids friction (such as m*, Fr), are inappropriate and/or insufficient to adequately represent the turbulent (and complex) flow phenomenon of dense-phase pneumatic conveying of powders. As a result, a need for further studies was realised. Some initial investigation into dimensional analysis were undertaken to explore if some appropriate parameter groupings could be generated. The work of Duckworth (1977) on dilute-phase (suspension flow) was studied. It was found that he ended up with a number of dimensionless numbers, such as Re, Fr, m*, ρ/ρ_s, d/D etc. However, the physical significance of all of these parameter groupings could not be totally appreciated for dense-phase solids-gas flows. It had been already found the power function based models λ_s models that use some of the above parameters (such as m*, Fr, ρ) generally resulted in inaccurate predictions under scale-up situations. Flow visualisation using 1-m long "sight glass" (Figure 3.5) for "white powder" conveyed through the 69 mm I.D. × 148 m long pipe has shown quite clearly that different flow mechanisms exist for dense- and dilute-phase. Hence, it was thought that different parameter groupings would perhaps be needed for dense- and dilute-phase to adequately describe the flow phenomenon occurring in the respective phases. For the above purpose, dimensional analysis was considered to be inappropriate. This is because starting with same fundamental physical variables, one would end up getting

the same set of dimensionless groupings, irrespective of whether it is dilute or dense-phase, as up to the stage of forming dimensionless parameter groupings, the very nature of dimensional analysis does not take into account the physical contribution of various variables for a particular condition of flow (dilute/dense).

With no rewards forthcoming, it was considered that dimensional analysis/ dynamic similarity are best suited to areas where they unquestionably have significant contributions to make, such as modeling of pumps, ships etc. Bradley (1990) also had reached similar conclusion. It was appreciated that further investigations would need to be conducted into new avenues (such as the subject of fluidisation) to explore any parameter grouping that might have been used to represent pressure drop and scaling relationships of fluidised beds. Though the fluidised beds are generally vertically oriented, whereas the present study aims at modelling horizontal flow of powders through pipes, it was nonetheless considered worthwhile to explore if some suitable model/parameter grouping(s) could show promise in accurately estimating pressure drop across a fluidised bed. Such model/parameter grouping(s) may also be applicable for horizontal pneumatic conveying under fluidised dense-phase (perhaps with some possible modifications, as required), as essentially a fluidised bed and dense-phase pneumatic conveying of powders, both deal with powders/ particles under "fluidised" conditions. Report on such studies and some additional explorations into related subjects, such as solids-gas turbulence/ "two-way coupling", are provided in Appendix A3.

CHAPTER 8: Evaluation of "System" Approach

8.1 Introduction

It has been already demonstrated in the previous chapters (Chapters 6 and 7) that the existing design techniques using "micro" or "component" approach (where models of solids friction are normally represented in terms of different dimensionless parameter groupings such as m*, Fr etc) are generally not capable of providing reliable scale-up predictions. Hence, it was considered worthwhile exploring the usefulness of "macro" or "system" approach for scale-up applications. "System" approach consists of initially generating test rig PCC for a product and then applying suitable scale-up equations to determine the pressure drop characteristics for the proposed plant (Mills, 1982; Wypych and Arnold, 1987). A first look at the method did not appear to be very convincing that it could provide accurate predictions as it does not seem to be addressing fundamental flow phenomenon, such as particle-particle/wall interactions. However, it was noted that this approach has been in existence for more than two decades (Mills, 1982 to Wypych and Arnold, 1987 to Mills, 2004). Hence, it was suspected that the method might have worked reasonably well under certain conditions. In fact, Wypych and Arnold (1987) have reported that "system" approach may be useful for assisting with "general system design and feasibility studies". However, in spite of its apparent popularity, the validity of this method has not been adequately tested till date for a wide range of flow and pipe layout conditions. The aim of this chapter is to evaluate the "system" approach under scale-up conditions of diameter and length for different products to provide some guidance to the engineers and researchers involved in designing industrial plants using this method.

8.2   Scale-up models in "system" approach

It was found in the literature that different versions of scale-up models had been proposed by previous researchers. It was considered worthwhile to conduct a through review of the different methods.

8.2.1   Original scale-up models (Mills et. al, 1982)

Scaling up using a "system" approach was originally proposed by Mills et al. (1982). Fine "pulverised fuel ash" was conveyed for a wide range of product flow rates through a 50 mm I.D. × 100 m long pipe having thirteen 90 degree bends. The derived PCC were then scaled-up to predict the conveying characteristics for 50 mm I.D. × 150 m, 75 mm I.D. × 150 m and 100 mm I.D. × 150 m long pipes using the following scale-up laws:

For constant air mass flow rate per unit area and pressure drop due to product,

Length scale-up: $m_{s2} = m_{s1} (L_1/L_2)$;   (8.1)

Diameter scale-up: $m_{s2} = m_{s1} (D_2/D_1)^2$ (8.2)

The original scale-up relationships were later presented as "generalised scale-up equations" (Wypych and Arnold, 1987):

$$m_{f2} = m_{f1} \, (D_2/D_1)^2 \tag{8.3}$$

$$m_{s2} = m_{s1} \, (L_1/L_2) \, (D_2/D_1)^2 \tag{8.4}$$

$$\Delta P_{T2} = \Delta P_{T1} + \Delta P_{f1} \, \{(L_2/L_1) \, (D_1/D_2) - 1\} \tag{8.5}$$

The work of Mills et al. (1982), however, seems to have the following limitations:

- The method does not provide any justification (or reference) for the derivation of his scale-up relationships.

- The method considers straight pipe length (e.g. L_1 and L_2) in scale-up laws but makes no allowance for the losses due to bends (and verticals). Mills, however, later seems to suggest that the bend losses can be significant and need to be considered properly (Mills, 2004).

- The method does not provide a comparison between predicted and experimental PCC. It would have been useful to evaluate the accuracy of the scale-up laws had the results of any such comparison study been made available.

8.2.2 *Scale-up laws presented by Wypych and Arnold (1987)*

To investigate the original work of Mills et al. (1982), Wypych and Arnold (1987) conveyed fly ash and cement mixture, PVC powder and screened coke through test

rigs of different diameters and lengths. For ease of reference, the layout details of the pipes are provided in Table 8.1.

Table 8.1: Pipe layout details of Wypych and Arnold (1987)

'Please see print copy for image'

For evaluating the diameter scale-up criteria of Mills et al. (1982), fly ash and cement mixture were conveyed through test rigs A and B. The derived PCC obtained from rig A were scaled-up to rig B and were compared with experimental data. It was found that for diameter scale-up, the criteria proposed by Mills et al. (1982) resulted in significant over-predictions. Wypych and Arnold (1987) modified the exponent of the diameter ratio given in equation (8.2) to a value of 2.8 and demonstrated more accurate predictions for diameter scale-up. The modified equation is presented in equation (8.6).

$$m_{s2} = m_{s1} \, (L_1/L_2) \, (D_2/D_1)^{2.8} \tag{8.6}$$

The merit of the above work lies in the fact that both test rigs A and B had almost identical layouts (with the same pipe lengths, number, type and location of bends). Thus it could be expected that any uncertainties arising due to bend effect would be minimised as much as possible and the difference between the PCC of test rig A and B would be primarily due to the effect of diameter. However, it would have been better if Wypych and Arnold (1987) had presented results from other products conveyed in fluidised dense-phase (although PVC powder was tested, but it was conveyed only in dilute-phase).

To examine the length scale-up criteria of Mills et al. (1982), screened coke was conveyed through test rigs C and D. Comparing the predicted PCC of test rig D (obtained from scaling up the experimental PCC of test rig C), it was concluded (Wypych and Arnold, 1987) that the Mills length scale-up criteria (equation 1) were reasonable. However, this part of the work seems to have the following uncertainties:

- It would have been prudent not to use the data of short pipes having 25 m and 71 m lengths (and having many bends) for evaluating the length scale-up criteria. Although an equivalent length of 4 m per bend was added by Wypych and Arnold (1987), the issue of bend loss could be far more complex than this simple assumption. In fact, Pan (1992) and Pan and Wypych (1998) had presented bend loss in terms of the conditions at the outlet of each bend. Thus, it is possible that the inability of estimating bend loss accurately may have led

Wypych and Arnold (1987) to an incorrect conclusion regarding the validity of length scale-up criteria.

- Wypych and Arnold (1987) did not test the length scale-up criteria on products which were conveyed in fluidised dense-phase (e.g. fly ash and cement mixture). They used the conveying data of screened coke (slugging) and PVC powder (dilute-phase only).

Wypych and Arnold (1987) further suggested that for an improvement, the following equation should be used:

$$m_{s2} = m_{s1} \, (L_1'/L_2') \, (D_2/D_1)^{2.8} \tag{8.7}$$

Where, L_1' and L_2' represents the adjusted values of L_1 and L_2 to allow for any differences between the number and type of bends used in the test rig and the actual plant. It seems that Wypych and Arnold (1987) had actually intended to include some adjustment factor to account for the losses in the verticals as well. For the verticals, a length of $2L_v$ was suggested to be added with L_h. This adjustment for vertical loss ($2L_v$) is believed to have come from work of Marjanovi´c, P who studied pressure drop in vertical pipes in much details, such as Marjanovi´c, P (1982). This is also stated in Mills (2005). It appears that the suggested adjustment value to account for bend losses was an additional 4 m length that should be added for the presence of each bend in the line.

8.2.3 Recent scale-up laws by Mills (Mills, 2004)

Recently, Mills (2004) had attempted to re-establish the validity of the "system" approach by certain modifications of his original work (Mills et al., 1982). For length scale-up criteria, he suggested the following equation:

$$m_{s2} = m_{s1} \ (L_{e1}/L_{e2}) \tag{8.8}$$

$$\text{Where, } L_e = L_h + 2L_v + Nb_e \tag{8.9}$$

It seems that the term "L_e" is actually same as $L^{'}$ (Wypych and Arnold, 1987). It is interesting to note that the suggested adjustment factor by Mills (2004) for the verticals actually matches with that previously suggested by Wypych and Arnold (1987). For diameter scale-up, it was found that Mills (2004) did not employ the improved diameter scale-up criteria suggested by Wypych and Arnold (1987) and had reused his original relationship (equation 8.4). Much similar to the shortcomings of his original work (Mills, 1982), this latest work of Mills (2004), seems to have the following limitations:

- No basis was provided for the derivation or justification of the scale-up relations.

- A comparison between predicted and experimental PCC for significant length and/or diameter scale-up conditions was not provided. As a result, it is difficult to evaluate the accuracy of the Mills' method.

- To estimate the equivalent lengths for bend losses, Mills (2004) seemed to have suggested using the bend loss data of conveying of barites through a 90 degree bend, having a $2R_B/D$ ratio of 24 and a pipe bore of 53mm to represent other products and bend geometries. However, as the pressure drops in bends have been previously found to depend on the bend geometry and type of product (Pan, 1992), it is doubtful that the barites data are valid for other cases.

Therefore, it seems that the existing methods of scale-up using the "system" approach contain several uncertainties and scale-up investigation need to be carried out for a evaluation of this method. This has been attempted in the following.

8.3   Scale-up evaluation of "system" approach

8.3.1   Evaluation of existing diameter scale-up criteria

The total pipeline PCC obtained by conveying fly ash and ESP dust through the 69 mm I.D. × 168 m pipe over a wide range of air and solids flow rate shown in Figures

5.1 and 5.14 respectively were scaled-up to predict the total PCC for the 105 mm I.D. × 168 m pipe using the different suggested criteria for diameter scale-up of Mills (2004) and Wypych and Arnolds (1987) (i.e. applying equations 8.2 and 8.7 respectively). Equivalent pipe lengths and air only losses were estimated (for both methods) as per Mills (2004). The predicted PCC were then compared with the experimental plots and are shown in Figures 8.1 and 8.2. Comparisons have been shown for only the highest and lowest solids flow rates, which are indicated on each figure. Other intermediate solids flow lines had similar trends. All the predictions were limited to a minimum inlet Froude number of 4, as below this range flow instabilities had been reported to occur during the experimental program.

'Please see print copy for image'

Figure 8.1: Experimental versus predicted PCC for fly ash and 105 mm I.D. × 168 m pipe using diameter scale-up criteria of Mills (2004) and Wypych and Arnold (1987)

Figure 8.2: Experimental versus predicted PCC for ESP dust and 105 mm I.D. ×
168 m pipe using diameter scale-up criteria of Mills (2004) and Wypych and Arnold
(1987)

The results show that for both fly ash and ESP dust, the criteria suggested by Mills
(2004) provide gross over-predictions, whereas the criteria of Wypych and Arnold
(1987) provide a significant improvement. Although there still exists some over-
prediction in the dense-phase region, this could be considered as within acceptable
margins for design. This supports the claim of Wypych and Arnold (1987) scale-up
factor of 2.8 instead of 2. Towards the dilute-phase region, the predicted PCC (as per
Wypych and Arnold, 1987) match with the experimental plots quite well. It should be

noted that in this analysis, both the 69 mm I.D. × 168 and 105 mm I.D. × 168 pipes had similar pipe layouts (with number, type and location of bends being identical), thus eliminating the chances of introducing uncertainties due to the effect of bends as far as possible.

8.3.2   Evaluation of existing length scale-up criteria

For evaluating the length scale-up criteria, the PCC shown in Figures 5.1 and 5.14 were scaled-up to predict the total pipeline PCC for the 69 mm I.D. × 554 m pipe (for both fly ash and ESP dust) using the suggested criteria of Mills (2004) for length scale-up, i.e. applying equation (8.8). Wypych and Arnold (1987) did not provide any improved criteria for length scale-up. Hence, an evaluation using the Mills' method (Mills, 2004) was considered as sufficient. Equivalent pipe lengths and "air only" losses were estimated as per Mills (2004). The predicted PCC were compared with the experimental data and the results are shown in Figures 8.3 and 8.4. Comparisons have been shown for only the highest and lowest solids flow rates. The intermediate solids flow rate lines displayed similar trends.

‘Please see print copy for image’

Figure 8.3: Experimental versus predicted PCC for fly ash and 69 mm I.D. × 554 m pipe using Mills' length scale-up criteria (Mills, 2004)

‘Please see print copy for image’

Figure 8.4: Experimental versus predicted PCC for ESP dust and 69 mm I.D. × 554 m pipe using Mills' length scale-up criteria (Mills, 2004)

Comparing the predicted and experimental PCC for both products, it is observed that the suggested criteria of Mills (2004) for length scale-up provide some under-prediction, especially in dense-phase. The level of under-prediction may be considered acceptable for fly ash, but perhaps not for ESP dust. One could argue that the inaccuracy is due to effect of incorrect estimation of bend losses (e.g. the 69 mm I.D. × 554 m long pipe had 17 bends). However, it needs to be appreciated that had the bend issue been the only cause of concern, most of the inaccuracy would have been observed in the dilute-phase region (where the losses due to bends are more significant). Instead, it is found that the under-predictions are more prominent towards the dense-phase regime. In fact, this is similar to the trend of inaccuracy being shown for the cases of diameter scale-up (Figure 8.1 and 8.2), where most of the inaccuracies were also observed in the dense-phase region (however, the results were over-predicting). Thus, it appears that the existing methods of scale-up using the "system" approach (especially, the length scale-up criteria) are inaccurate in the dense-phase region.

To separately evaluate the validity of the "system" approach (especially, the length scale-up criteria) for dilute-phase, PCC obtained by Pan (1992) for the dilute-phase conveying of pulverised coal through a 69 mm I.D. × 172 m long pipe (having 5 × 90 degree bends) were scaled up to the 69 mm I.D. × 553 m long pipe (having 17 × 90 degree bends) using the length scale-up criteria of Mills (2004). Figure 8.5 shows the predicted PCC compared with the experimental plots.

‘Please see print copy for image’

Figure 8.5: Experimental versus predicted PCC for pulverised coal (Pan, 1992) and 69 mm I.D. × 554 m pipe using Mills' length scale-up criteria (Mills, 2004)

The results show that for m_s = 2.5 kg/s, the predictions are excellent. However, there are slight under-predictions for m_s = 0.5 and 1.5 kg/s, but the trends of the predicted PCC match well the experimental plots. Overall, the predictions are fairly accurate. Thus, it seems that "system" approach is more valid for the case of dilute-phase rather than dense-phase. One probable reason for this could be that in dilute-phase, the powders are suspended in air, thus there is relatively less chance of powder to powder (and perhaps even powder to wall) interactions. Thus the flow would be dominated by the air turbulence, which is relatively simple to model. However, for dense-phase, the particles are vigorously in contact with each other and with the wall in the non-suspension part of flow. This would bring particle-to-particle/wall interactions into play, which could be expected to be governed by various particle properties (such as

particle size, shape, cohesiveness, surface roughness/texture etc), making the dense-phase flow as far more product dominant and complex to be tackled compared to dilute-phase. This could be further illustrated by the help of Figure 5.17, which shows the "straight pipe" PCC for the conveying of ESP dust through the P9-P10 tapping locations of the 69 mm I.D. $\times$ 554 m pipe. In the dilute-phase region, i.e. to the right of PMC (Marcus et al., 1990) (i.e. approximately to the right of the $Fr_m = 10$ line), the conveying characteristics are rather flat, apparently indicating no drastic change in flow mechanism in dilute-phase. However, to the left of PMC (dense-phase region), the pressure drop characteristics start to have an upward trend with a decrease in m_f, thus indicating the significant contribution of enhanced particle-particle/wall interactions. Hence it appears that the relatively complex interactions in dense-phase flow may be difficult to model using simple relationships (such as the "system" approach), which do not fundamentally address particle-particle/wall interactions.

8.4   Effect of bends on the accuracy of the "system" approach

The evaluation work presented before (Figures 8.1 to 8.5), was for cases where the test and scale-up pipes had same layouts (for diameter scale-up) or same pipe length to bend ratio (for length scale-up). Thus, it may be expected that the issue of inaccuracies arising due to the incorrect estimation of bend losses is minimised. However, a practical situation may arise where the test set up contains too many bends (e.g. due to lack of availability of outdoor space to run decent straight lengths

of pipes) and scale-up (e.g. for a long pipe, having a much higher value of pipe length to bend ratio) needs to be done. It was considered worthwhile evaluating the validity of the "system" approach under such rigorous conditions. The PCC obtained by Pan (1992) for conveying fly ash through pipeline I (L_h = 96 m, L_v = 6 m, 9 × 90 degree bends) and pipeline II (L_h = 129 m, L_v = 6 m, 9 × 90 degree bends) (Pan, 1992) were scaled up to predict PCCs for pipeline A2 (L_h = 547 m, L_v = 6 m, 17 × 90 degree bends) (Pan, 1992). Figure 8.6 compares the predicted and experimental PCC. Scale-up relationships were used as per Wypych and Arnold (1987). Equivalent lengths and air-only pressure losses were calculated as per Mills (2004).

'Please see print copy for image'
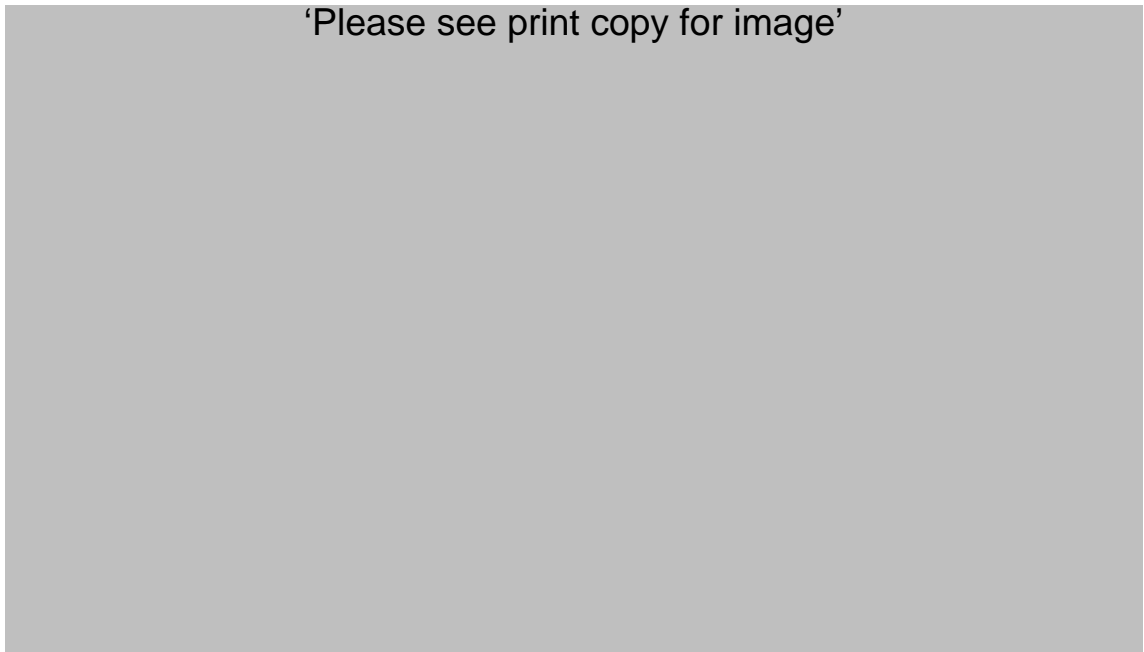
Figure 8.6: Experimental versus predicted PCC for fly ash (Pan, 1992) and 69 mm I.D. × 554 m pipe using scale-up criteria of Wypych and Arnold (1987)

The results show that the predicted PCC are grossly under-predicting the experimental PCC. In fact, the scaled-up PCC obtained using pipe-I data resulted in greater under-predictions than those obtained from the pipe-II data. This could be due to the bend effect being more significant in pipe-I than pipe-II (due to pipe-I being shorter in length than pipe-II, but having the same number of bends). This exercise cautions the designer while using the "system" approach for scale-up in cases where the pipe length to bend number ratios of the test rig and the proposed plant are considerably different.

8.5   Conclusions

The Mills' procedure (Mills, 2004) for scaling-up diameter has shown significant over-prediction when estimating the total pipeline pressure drop. The suggested criteria of Wypych and Arnold (1987) for scaling-up of diameter, were found to provide significant improvements. Existing procedures for scaling-up length (Mills, 2004) do not seem to be valid for the dense-phase region. Comparisons between experimental and predicted PCC have shown considerable under-prediction for significant length scale-up conditions in dense-phase. However, it was found that the existing length scale-up criteria (Mills, 2004) works quite well for dilute-phase. The accuracy of the "system" approach seems to be largely dependent on the system layout. It appears that the issue of pressure drop in bends has not been properly addressed. Scaling-up when the length/bend ratio of the test rig and proposed plant are quite different, have resulted in gross inaccuracy. This should serve a warning to

the engineers and researchers involved in designing industrial plants using the "system" approach.

CHAPTER 9: Prediction of Minimum Transport Boundary

9.1 Introduction

For reliably designing optimal industrial plants, the accurate prediction of the minimum transport or capacity limitation boundary for the dense-phase pneumatic conveying of powders through a given pipeline system is of significant importance. Such information affects the determination of maximum solids loading and the proper sizing of the conveying pipeline. Some fundamental transport boundary models based on powder mechanics have been developed for the low-velocity slug-flow of granular products (Wypych and Yi, 2003). However, the dense-phase conveying of powders involves far more complex interaction between the particles, carrier gas and pipe/bend wall, and most models to date have been largely empirical (Mills et al., 1982; Mills, 2004; Mills, 2004a). Preliminary investigation by Wypych et al. (2005) has shown that such models have been based on certain products and pipeline conditions, and have not been tested properly under important criteria, such as scale-up accuracy. With this background, the objectives of this chapter are to:

- Evaluate the existing techniques for predicting minimum transport boundary.

- If the above is found to be inadequate, develop an improved method for accurately representing minimum transport boundary, especially under scale-up conditions.

For powders suitable for fluidised dense-phase conveying, the flow transition from suspension to non-suspension mode is relatively gradual, i.e. without any sudden

changes in flow mechanism causing instability, unlike the low-velocity slug-flow of granular products (Wypych and Yi, 2003, Marcus et al., 1990). A typical characteristic of fluidised dense-phase conveying is shown in Figure 9.1. A reduction in gas flow rate beyond the good "steady state" dense-phase region would cause the formation of unsteady dunes, characterised by enhanced pressure fluctuations. A further decrease of gas flow would cause a build-up of product along the line in the form of deposits. This would result in an inability of the system to attain a consistent steady-state conveying condition (i.e. the pressure signal would continue to gradually increase with time). This limit has been considered as the "minimum transport boundary" in the present study and is represented by the "Unstable Boundary" shown in Figure 9.1. A further reduction in gas flow rate would cause a flow blockage, indicated by a rapid increase in pressure.
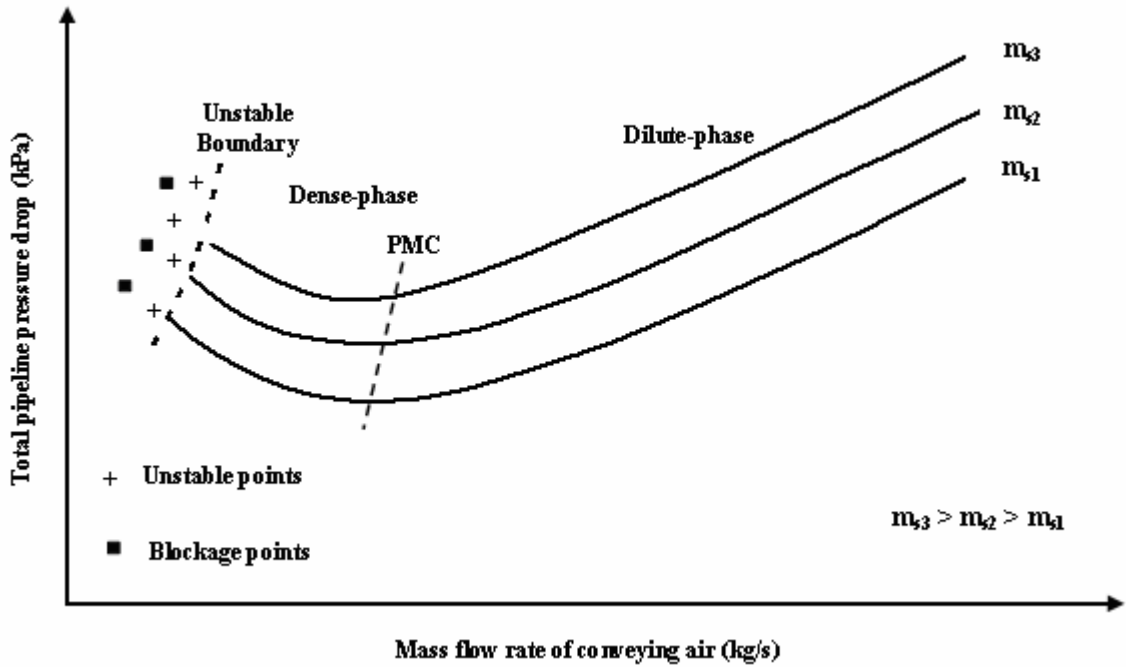
Figure 9.1: Typical Pneumatic Conveying Characteristics (PCC) of fluidised dense-phase conveying, showing minimum transport boundary

9.2. Evaluation of existing method(s)

Mills (2004) conveyed cement through a 81 mm I.D. × 95 m test rig and obtained the PCC as reproduced in Figure 9.2a. From this conveying data, Mills (2004) presented a graph of V_i versus m* (Figure 9.2b) to represent the minimum conveying conditions for the given material. This form of representation looks similar to that provided by in Mills' in his earlier work (Mills et al., 1982).

‘Please see print copy for image’

Figure 9.2: Deign data for pneumatic conveying of cement: a) PCC for 81 mm I.D. × 95 m test rig, 9 bends; b) Minimum velocity relationship (Mills, 2004)

Mills (2004) did not show any blockage/unstable points or boundaries in his PCC. The PCC shown in Figure 9.2a is transformed in Figure 9.3 by plotting total pipeline pressure drop against air mass flow rate, constant pipe inlet air velocity lines superimposed on the plots.

'Please see print copy for image'

Figure 9.3: PCC for cement conveying through 81 mm I.D. × 95 m test rig, 9 bends (Mills, 2004), with constant V_i lines and unstable boundary curve

It is interesting to note that the conveying characteristics for m_s = 10 t/h finishes at the V_i = 7 m/s line, whereas higher solids flow lines were extended to 3.5 to 4 m/s (approx). Mills (2004) did not show blockage/unstable point in his presentation. As a result, it is unclear which boundary was used by Mills (2004) to depict the minimum transport criteria as shown in Figure 9.2b. To investigate this, an assumed unstable boundary (A-B) is drawn in Figure 9.3, passing through the extreme left points of all the different m_s lines. These end points have been superimposed on Figure 9.2b, as shown in Figure 9.4, which shows that the selected points are located quite well on the curve representing the minimum conveying conditions. This indicates that Mills had also considered curve A-B to represent the minimum conveying condition.
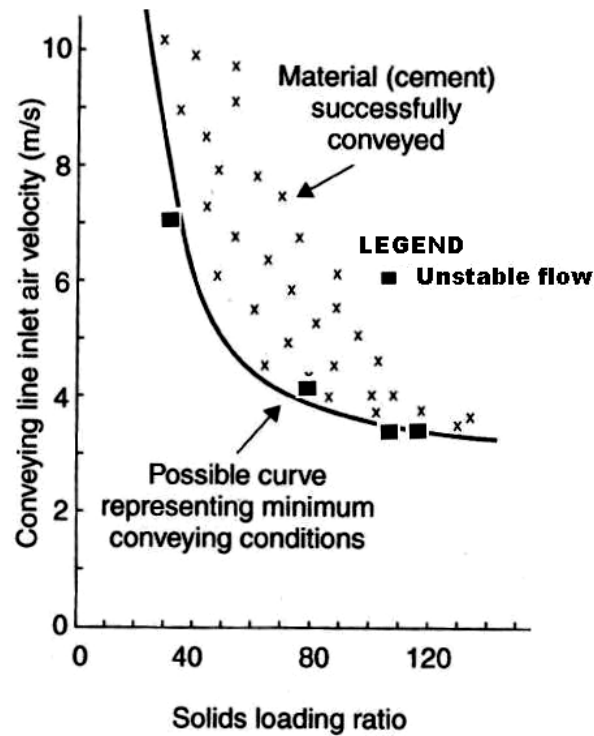
Figure 9.4: Verification of the "assumed boundary" shown in Figure 9.3

In the same reference (Mills, 2004), Mills has provided another example of representing the minimum conveying boundary by conveying cement through a different test rig (53 mm I.D. × 101 m; 17 × 90 degree bends; top discharge blow tank). It appears that the same work has also been presented in (Mills, 2004a). The PCC showed by Mills (2004a) has been reproduced in Figure 9.5, with constant V_i lines superimposed on the PCC. The relationship between V_i and m*, as represented by Mills (2004, 2004a) are shown in Figure 9.6.

'Please see print copy for image'

Figure 9.5: PCC for cement conveying through 53 mm I.D. × 101 m test rig (Mills 2004a), with constant V_i lines superimposed
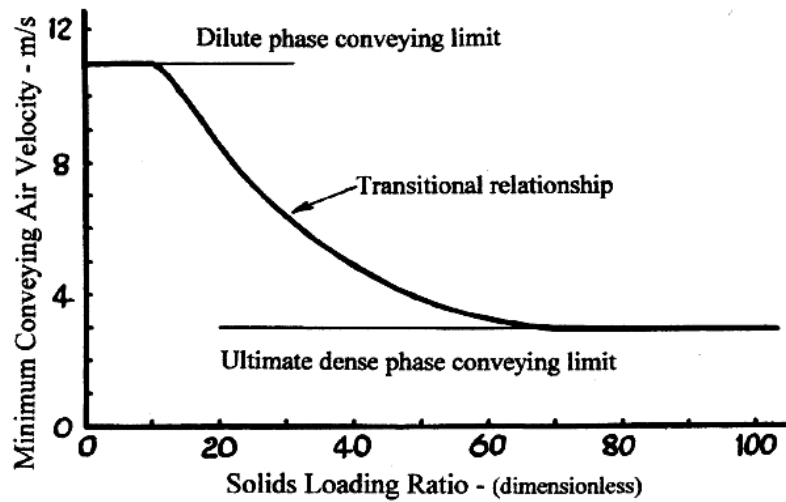
Figure 9.6: Minimum velocity relationship (Mills, 2004, 2004a)

It is to be noted that in Figure 9.5, Mills (2004a) had shown only one point representing pipeline blockage, with V_i = 3.7 m/s. However, Mills (2004a) have

214

proposed V_i = 3 m/s as the lower dense-phase conveying boundary. It is the view of the authors that it would have been far more convincing if Mills (2004a) had obtained and shown additional blockage points to prove or disprove this boundary. Mills has extended the 16 t/h PCC to the left of the blockage point, up to 3 m/s air velocity line. It is not clear how it was possible to extend a PCC to the left of a blockage point. A horizontal line has been drawn at both the 3 m/s and 11 m/s minimum conveying air velocity values (Figure 9.6) and Mills (2004, 2004a) had added a transitional relationship between the two limits. It is difficult to find an explanation for the location and shape of the transitional curve. In fact, Mills (2004a) had mentioned that such relationship is "by no means definitive", as difficult experimental work would be required in its determination.

The above work of Mills (Mills et al., 1982; Mills, 2004; Mills, 2004a) concentrates on cement conveying. Therefore, there is a need to develop minimum transport criteria for dense-phase conveying using test data of other powders. Also, the authors believed that the above criteria had to be validated under significant scale-up conditions of diameter and length. With this aim, the author of this thesis has conducted further investigations using his own data. ESP dust was conveyed through the 69 mm I.D. × 168 m test rig (Figure 3.1). Figure 9.7 shows the PCC with the lower dense-phase conveying boundary marked as curve C-D. There were several data points to the left of this curve where unstable conditions were obtained (e.g. fluctuating and "non-linear" flow of material into receiving bin). The safe conveying

215

air velocity at this boundary is approximately 3 m/s and the corresponding Froude number is 3.6.
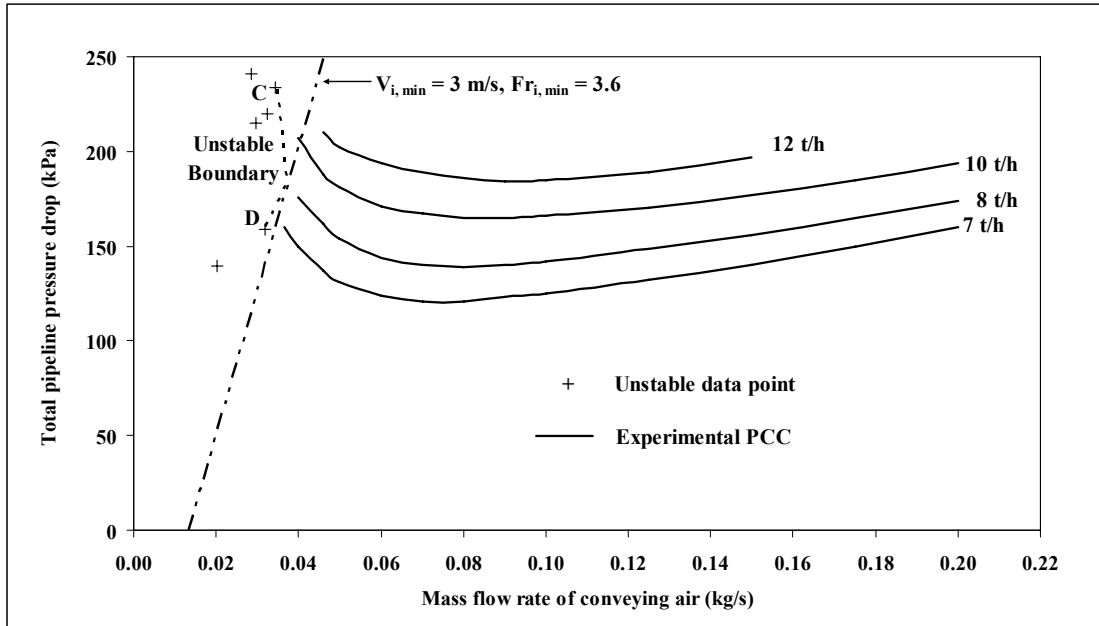
Figure 9.7: PCC for ESP dust for 69 mm I.D. × 168 m pipe

The unstable boundary C-D is plotted in Figure 9.8 using the Mills' format, denoted as C^+-D^+, showing the relationship between V_i and m*.
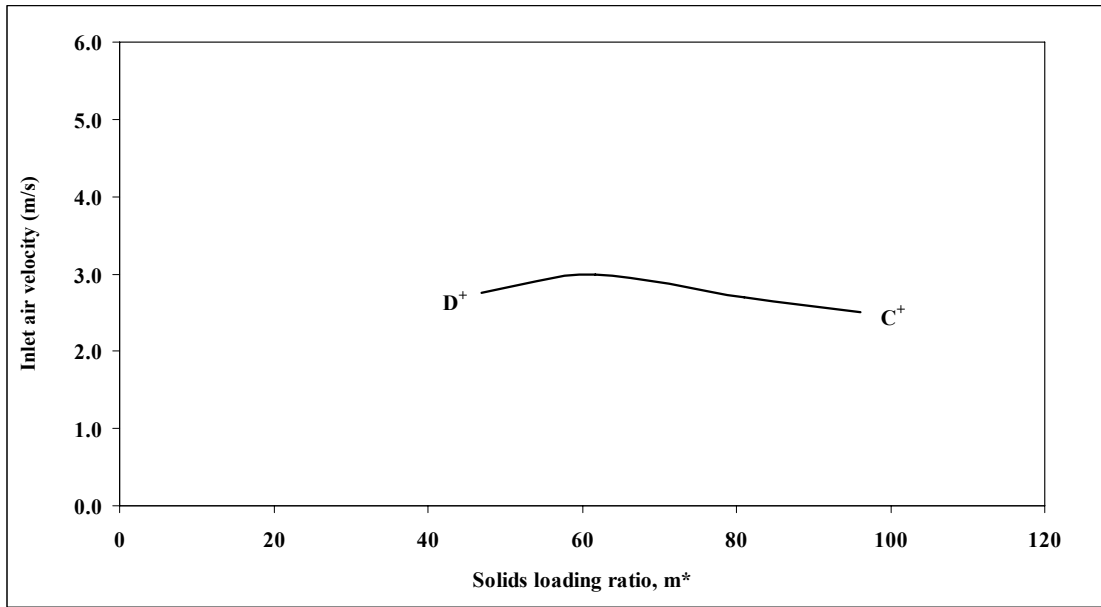
Figure 9.8: Minimum conveying conditions for ESP dust for 69 mm I.D. × 168 m pipe

It can be seen that the trend of relationship shown in Figure 9.8 is quite different to that obtained by Mills (Figure 9.2b, 9.6). The V_i versus m* plot is much flatter compared to the Mills' representations. In fact, with an increase in m* from 47 to 62, V_i increases from 2.8 to 3 m/s, however, with a further increase in m*, from 62 to 96, V_i drops to 2.5 m/s. The difference in trends could be attributed to the nature of PCC shown in Mills representations (e.g. Figure 9.5), especially in the lower solids feed rate lines, where higher values of V_i need to be maintained as per Mills (2004a) (Figure 9.5). The reason for this is not very clear. Some system or hardware limitation also may be involved here (e.g. certain size of top-discharge blow tank limiting achievable air flow rates and feed/conveying rates).

To investigate the effect of pipe diameter on the determination of minimum conveying air velocity, the data obtained using ESP dust in 105 mm I.D. × 168 m pipe are used. Figure 9.9 shows the PCC obtained from these tests with the lower dense-phase conveying boundary marked as E-F. The minimum conveying air velocity at this boundary is 3.7 m/s and the corresponding Froude number is 3.6.
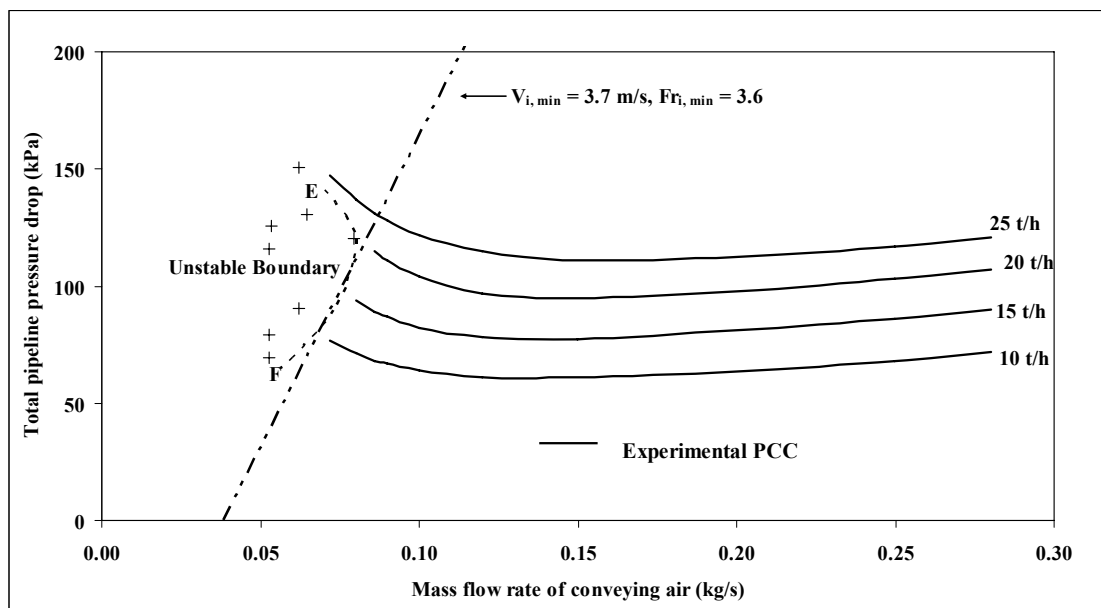
Figure 9.9: PCC for ESP dust for 105 mm I.D. × 168 m pipe

The unstable boundary E-F is also represented using Mills' format, as shown in Figure 9.10.
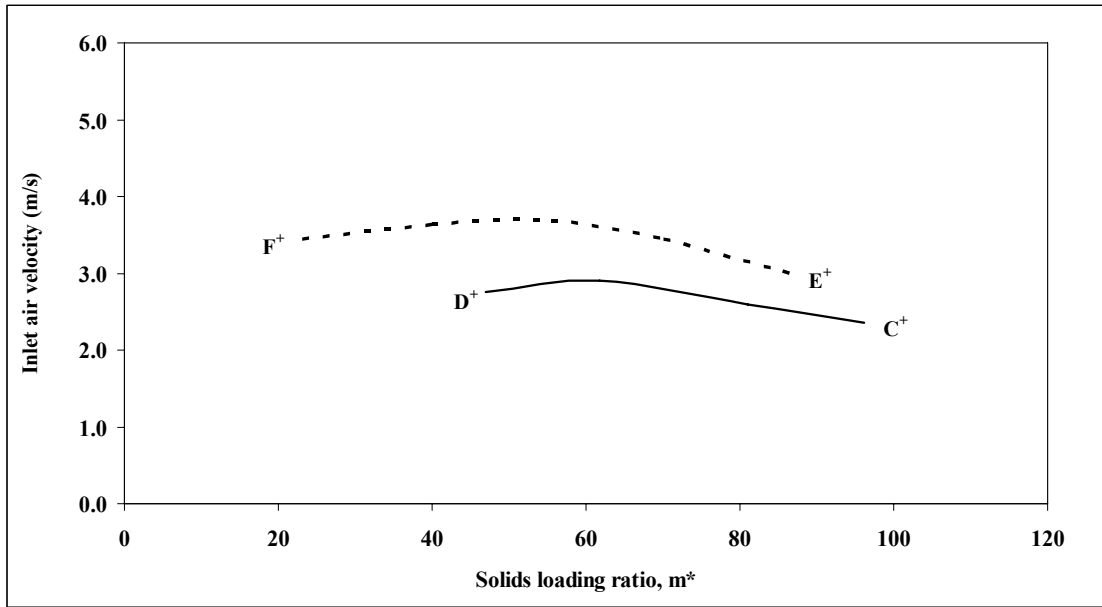
Figure 9.10: Minimum conveying conditions for ESP dust for 69 and 105 mm I.D. × 168 m pipe

C^+-D^+ and E^+-F^+ lines are for 69 × 168 m and 105 mm I.D. × 168 m pipes, respectively. From Figure 9.10 it is evident there is a difference in the requirement of the minimum conveying air velocity for the 69 and 105 mm I.D. pipes, thus indicating an influence of pipe diameter on the minimum transport criteria. This demonstrates that representation of minimum V_i as a function of m* may not be adequate under diameter scale-up conditions and pipe diameter term needs to be incorporated in the minimum V_i criteria. This seems to support the conclusion of Yi et al. (1998), where various existing correlations for minimum conveying velocity relationships for dilute-phase flow were studied.

Figure 9.11 plots the Froude number versus m* for both sets of data. As the minimum Froude number is 3.6 for both sets of data, see Figure 9.7 and Figure 9.9, this

indicates that $Fr_{min} = 3.6$ can be used for scale-up purposes for this material (i.e. in terms of pipe diameter).
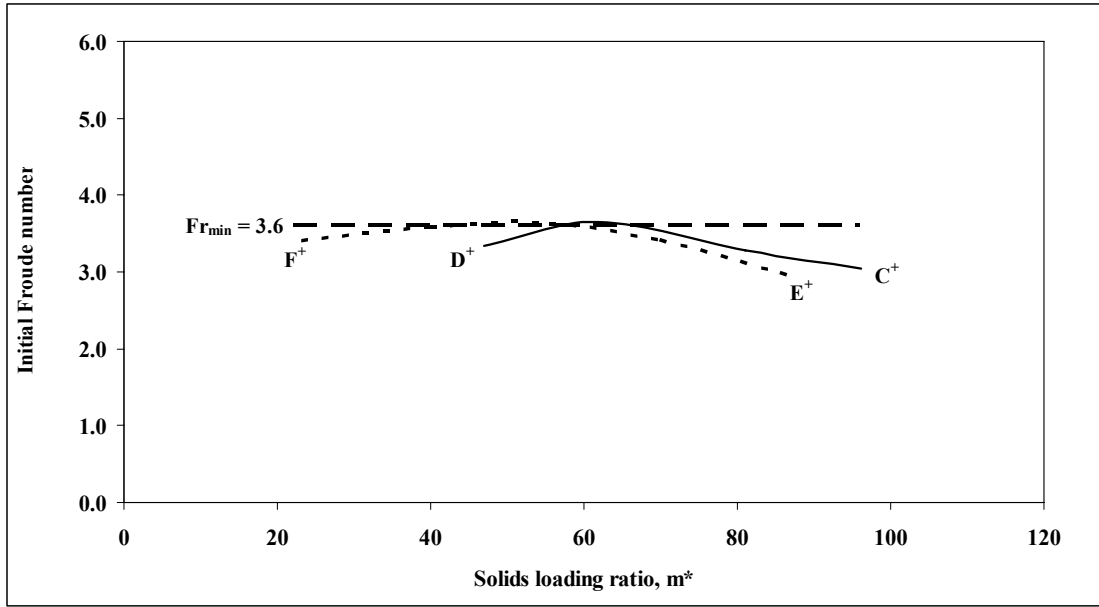
Figure 9.11: Comparison of Froude number for both sets of ESP dust data for 69 and 105 mm I.D. × 168 m pipes

To investigate the effect of pipe length on the determination of minimum conveying air velocity, the PCC for long distance conveying (69 mm I.D. × 554 m) of ESP dust is shown in Figure 9.12. It is observed that there is a reduction of the minimum Fr_i requirement for the longer pipeline (e.g. $Fr_{i, min}$= 3 for 554 m pipe, whereas $Fr_{i, min}$= 3.6 for the 168 m long pipe for ESP dust). Decrease in the value of $Fr_{i, min}$= 3 with an increase in pipe length (i.e. increase in air density) was also mentioned by Wypych and Arnold (1989).
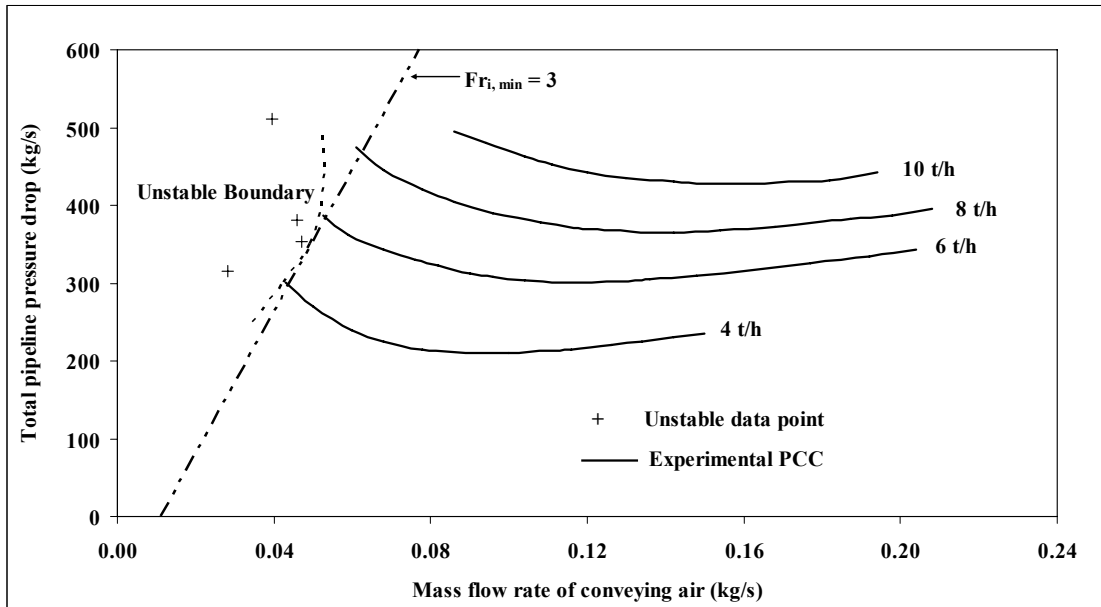
Figure 9.12: PCC for ESP dust for 69 mm I.D. × 554 m pipe

9.3. Representation of minimum transport

Conveying characteristics for fly ash (sample 1) in pipes of different diameter and length (69 mm I.D. × 168 m, 105 mm I.D. × 168 m, 69 mm I.D. × 554 m) are shown in Figures 9.13 to 9.15. The fly ash conveyed by Wypych et al. (2005) is being referred to here as "sample 1". Lines of constant Froude number at the entry to the pipe have been superimposed on the PCC.
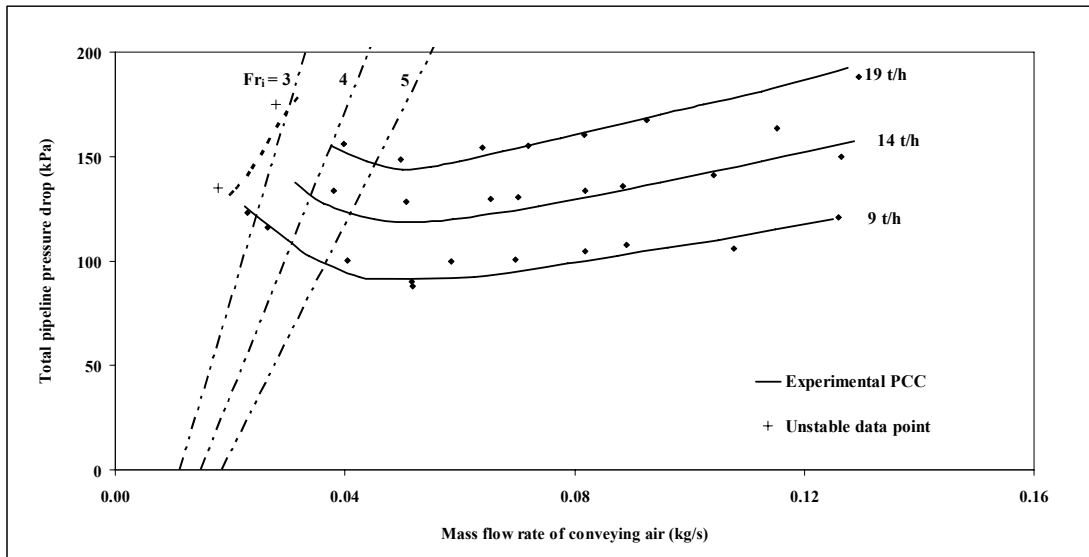
Figure 9.13: PCC for fly ash (Sample 1) for 69 mm I.D. × 168 m pipe
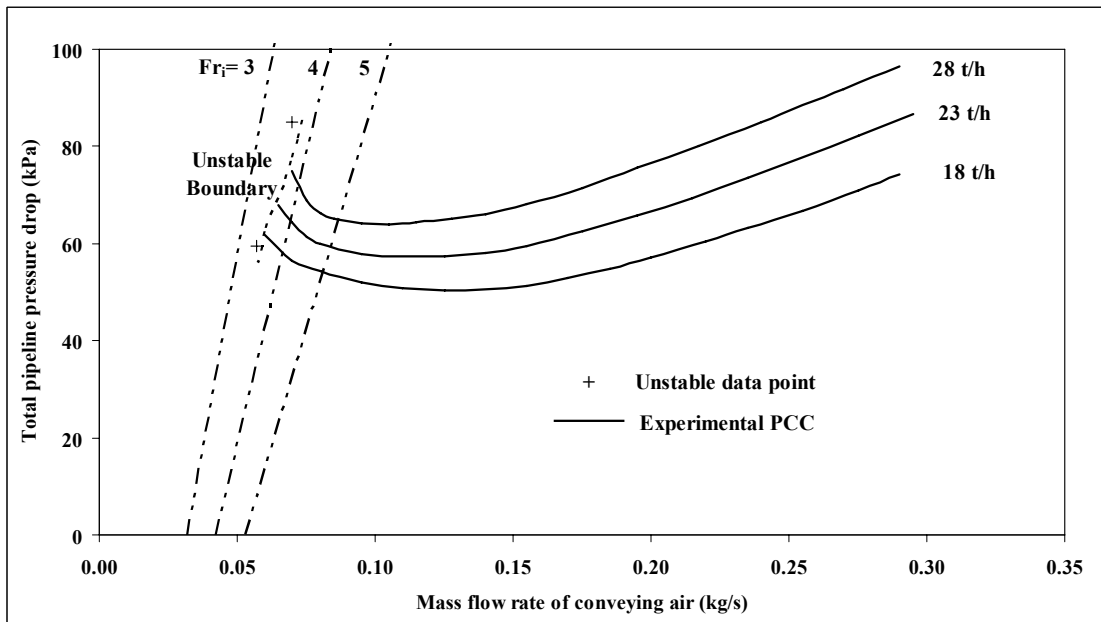
Figure 9.14: PCC for fly ash (Sample 1) for 105 mm I.D. × 168 m pipe
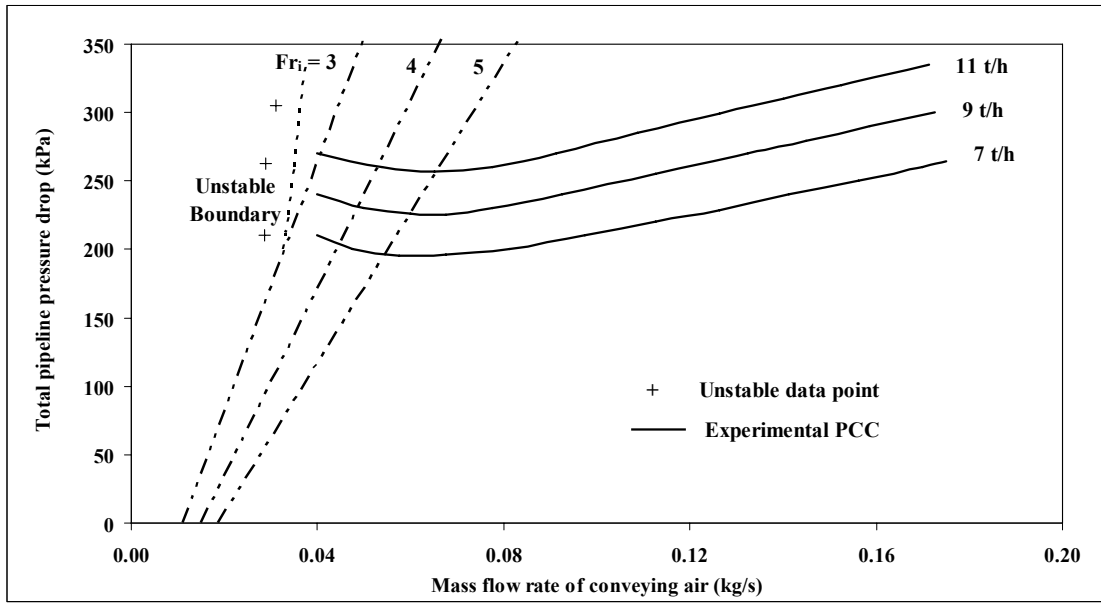
Figure 9.15: PCC for fly ash (Sample 1) for 69 mm I.D. × 554 m pipe

The results show that for the 168 m long pipes (69 and 105 mm I.D.), the unstable boundaries lie within the inlet Froude number range of 3 to 4. However, for the longer pipeline (554 m), there is a shift of $Fr_{i, min}$ to the left of the $Fr_i = 3$ line. This phenomenon of reduction of $Fr_{i, min}$ with increase in pipe length is similar to that previously shown for the case of ESP dust.

In previous testing by Wypych (1989), a pneumatic conveying rig was used to convey and compare a variety of power station fly ash samples, their physical properties displayed in Table 1. The product was fed into the system via a 0.425 m^3 bottom-discharge blow tank, the pipeline having the attributes shown in Table 2.

Table 9.1: List of product samples and physical properties (Wypych, 1989)

'Please see print copy for image'
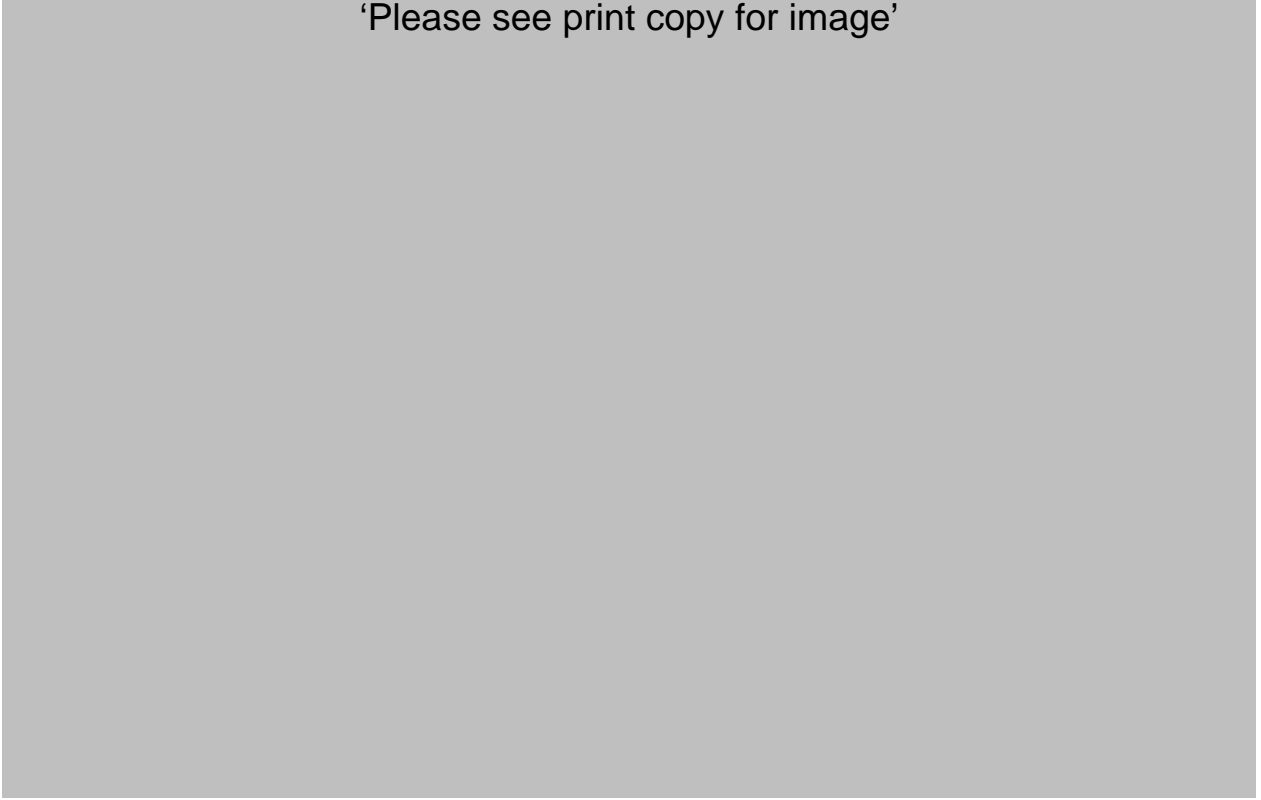
Table 9.2: Pipeline details for test rig (Wypych, 1989)

'Please see print copy for image'

After sufficient tests were performed for a wide range of air mass flow rates and solids mass flow rates, PCC were generated for each fly ash sample. These PCC have been converted into the three graphs shown in Figure 9.16 a, b and c. Each graph plots the curves for the same solids mass flow rate of each sample of fly ash: m_s = 3, 2

and 1 kg/s. The curves on each graph vary widely in the dense-phase regime, resulting from different product characteristics. At the left most point of each curve is a circle, which represents the boundary location for the reliable transport limit (defined by unstable flow and/or blockage conditions, Wypych, 1989).Three initial Froude number lines have been added to each graph representing $Fr_i = 3$, 4 and 5. On further inspection, it is fair to say that on the whole, the reliable transport limit boundary for most of the fly ash samples falls in the region $Fr_{i,\ min} = 3$ to 5. This agrees well with the $Fr_{i,\ min} = 3$ to 4 obtained for the fly ash (sample 1) tested in significantly larger rigs (Figures 9.13 to 9.15).

'Please see print copy for image'
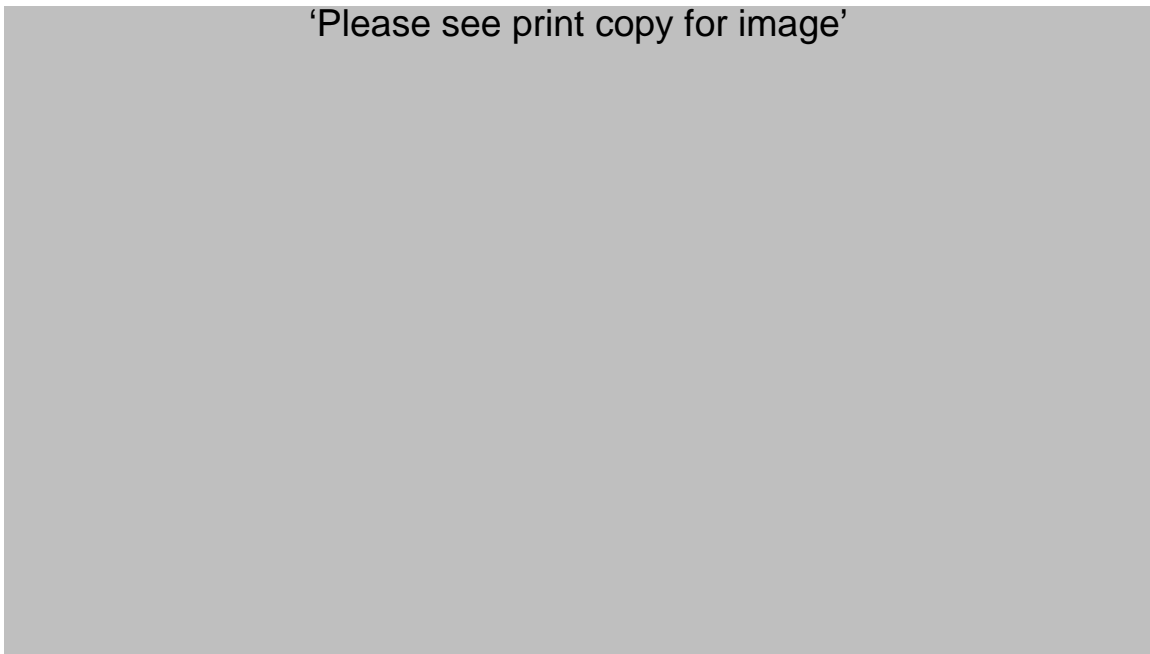
Figure 9.16a: Comparison of PCC for fly ash through 52 mm I.D. × 71 m pipe, $m_s = 3$ kg/s (Wypych, 1989)

'Please see print copy for image'

Figure 9.16b: Comparison of PCC for fly ash through 52 mm I.D. × 71 m, $m_s = 2$

kg/s (Wypych, 1989)

'Please see print copy for image'

Figure 9.16c: Comparison of PCC for fly ash through 52 mm I.D. × 71 m, $m_s = 1$

kg/s (Wypych, 1989)

Minimum transport criteria were further investigated for pulverised coal (ρ_s = 1600 kg/m^3; ρ_{bl} = 760 kg/m^3; d_{50} = 30 μm) (Wypych et al., 1990), "white powder" and cement (Mills, 2004; Mills 2004a), as shown in the Figures 9.17 to 9.20. The unstable boundary for pulverised coal and "white" powder are found to lie within Fr_i range of 4 to 6 and 4 to 5, respectively. The unstable boundaries for cement were not shown by Mills (2004, 2004a). Nevertheless, the lowest air flow rate points of the PCC (Mills, 2004; Mills 2004a) were found to lie within the Fr_i = 4 to 5 range.

'Please see print copy for image'
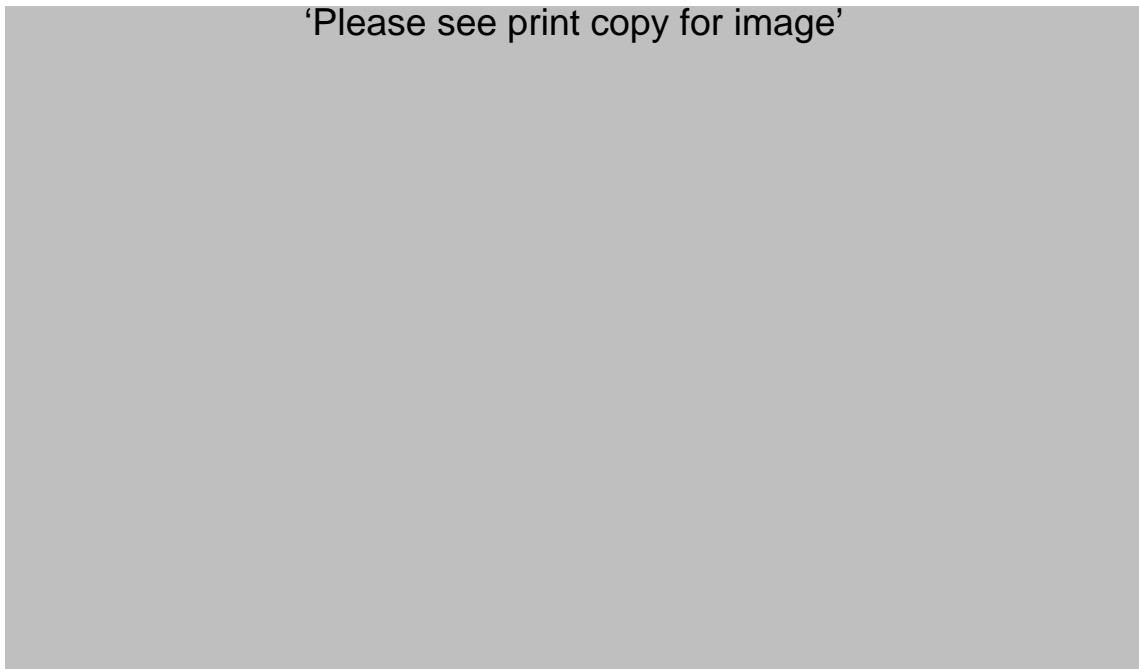
Figure 9.17: PCC for pulverised coal for 52 mm I.D. × 71 m pipe (see Table 2) (Wypych et al., 1990)
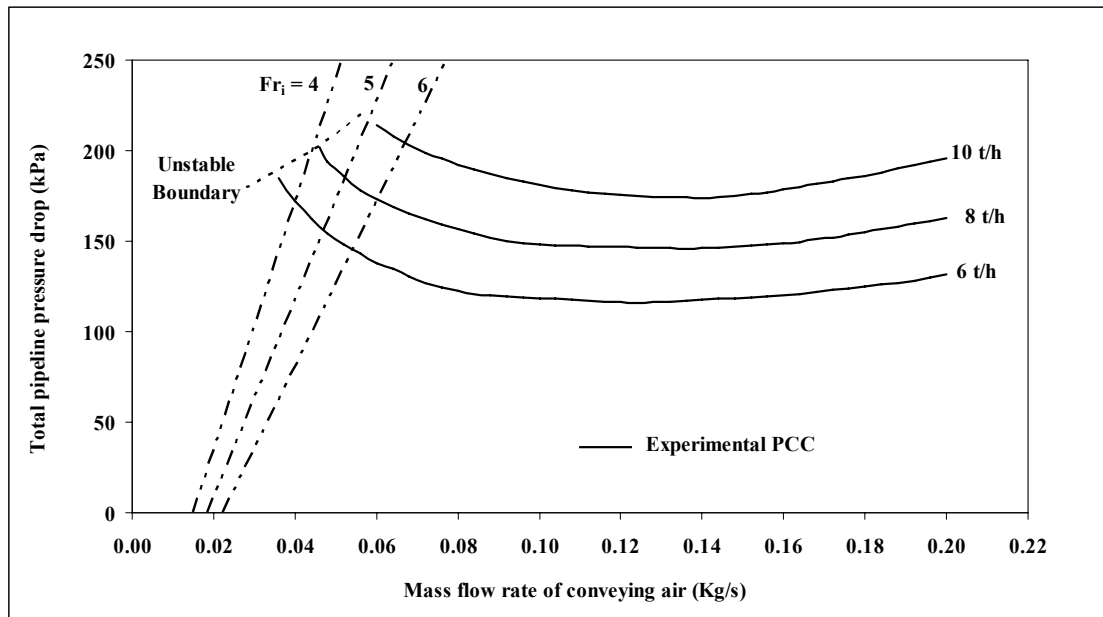
Figure 9.18: PCC for "white powder" for 69 mm I.D. × 148 m pipe

'Please see print copy for image'
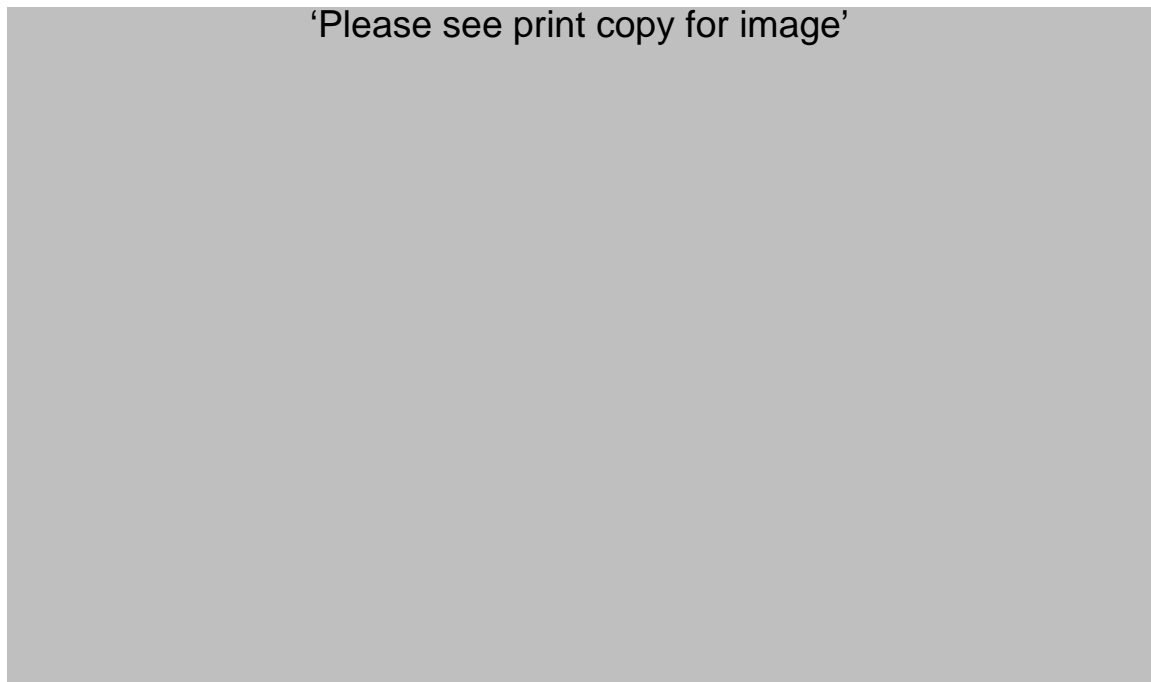
Figure 9.19: PCC for cement for 81 mm I.D. × 95 m test rig (Wypych, 2004)

Figure 9.20: PCC for cement for 53 mm I.D. × 101 m test rig (Mills, 2004a)

Table 9.3 summarises all the $Fr_{i, min}$ findings obtained in this study.

Table 9.3: Summary of $Fr_{i, min}$ and $V_{i, min}$ for various products

Powder	d_{50} (μm)	ρ_s (kg/m³)	ρ_{bl} (kg/m³)	D (mm)	L (m)	$Fr_{i, min}$	$V_{i, min}$ (m/s)
ESP Dust	7	3637	610	69	168	3.6	3
				69	554	3.0	2.5
				105	168	3.6	3.7
Fly Ash (Sample 1)	30	2300	700	69	168	3.2	2.6
				69	554	2.9	2.4
				105	168	3.6	3.7
Tallawarra fly ash (Wypych, 1989)	20	2350	500	52	71	4.0	2.9
Eraring fly ash (Wypych, 1989)	27	2160	880	52	71	5.0	3.6
Munmorah fly ash (Wypych, 1989)	25	2100	650	52	71	3.0	2.1
Vales Point fly ash (Wypych, 1989)	19	2130	700	52	71	4.5	3.2
Gladstone fly ash (Wypych, 1989)	18	2250	1030	52	71	4.5	3.2
Wallerawang fly ash (Wypych, 1989)	12	2195	455	52	71	3.5	2.5

Table 9.3 (contd.): Summary of $Fr_{i, min}$ and $V_{i, min}$ for various products

Powder	d_{50} (μm)	ρ_s (kg m^{-3})	ρ_{bl} (kg m^{-3})	D (mm)	L (m)	$Fr_{i, min}$	$V_{i, min}$ (m/s)
Liddell fly ash (Wypych, 1989)	13	2415	640	52	71	5.0	3.6
Pulverised coal (Wypych et al., 1990)	30	1500	760	52	71	< 5.7	< 4.1
"White powder"	55	1600	620	69	148	< 5.0	< 4.1
Cement (Mills, 2004)	14	3060	1070	81	95	4 to 5	3.6 to 4.5
Cement (Mills, 2004a)	14	3060	1070	53	101	4 to 5	2.9 to 3.6

At a later stage of the project, it was decided that air velocity values corresponding to $Fr_{i, min}$ should be included in Table 9.3 for a fair comparison between $Fr_{i, min}$ and $V_{i, min}$ towards representing the minimum transport criteria. The same has been done here.

Based on Table 9.3, the following comments and conclusions can be made.

(a) Based on the conveying data of ESP dust and fly ash (Wypych et al., 2005) conveyed through the 168 m long pipelines and pipe I.D. increasing from 69 to 105 mm, there is an increment in the requirement for $V_{i, min}$ with increase in

pipe diameter (e.g. $V_{i,\,min}$ = 3.0 to 3.7 for the ESP dust and $V_{i,\,min}$ = 2.6 to 3.7 for the fly ash). The numerical range of variation of $Fr_{i,\,min}$ with change in pipe diameter/length (for the same product) is smaller than that of $V_{i,\,min}$.

(b) For both the ESP dust and fly ash conveyed through the 69 mm I.D. pipeline from 168 to 554 m in length, there is a clear reduction in the requirement for $Fr_{i,\,min}$ (e.g. $Fr_{i,\,min}$ = 3.6 to 3.0 for the ESP dust and $Fr_{i,\,min}$ = 3.6 to 2.9 for the Fly ash). The main difference between the PCC for the 168 and 554 m long pipelines is the operating pressure or air density. From these results and comparisons, it appears that $Fr_{i,\,min}$ (and hence, operating Fr_i) can be reduced for higher air densities. Some evidence of this can be found in the literature, such as the relationship determined by Roski (1987), where $Fr_{i,\,min} \propto \rho_f^{-0.15}$ for a given powder and solids loading. However, it should be noted also that the maximum solids loadings decrease and the minimum air mass flow rates increase for the longer conveying distance.

(c) $Fr_{i,\,min}$ and $V_{i,\,min}$ both vary for change of products. For all the powders listed in Table 3, the minimum Froude number requirement at the pipe inlet can be represented by the range $Fr_{i,\,min} \approx 3.0$ to 5.7 (for D = 52 to 105 mm and L = 71 m to 554 m). Also, it appears that if a powder has "good" dense-phase characteristics, then $Fr_{i,\,min} \approx 5$ would provide a good initial indication of minimum transport conditions. With a 20% safety margin, the corresponding operating $Fr_i \approx 6$.

232

It should be noted that these results and conclusions are relevant only to blow tank feeders that have reliable and consistent discharge and an efficient method of aeration/fluidisation (e.g. fluidising-discharge-cone). Blow tanks with poor control/aeration may feed the pipeline unreliably and deteriorate conveying performance (and higher values of $Fr_{i, min}$ may be required).

Significance of Froude Number

Traditionally, the Froude Number is a dimensionless parameter measuring the ratio of the inertia force on an element of fluid to the weight of the fluid element (i.e. the inertial force divided by gravitational force), and has been used in open channel flow and wave and surface behaviour calculations in particular. In the context of minimum conveying, the Froude number for a given powder can be considered to represent the inertial (driving) forces needed for a certain gravitational force (or "mixture" weight or solids loading). Other pneumatic conveying researchers also have found Froude number a useful parameter to represent minimum conveying, such as Roski (1987) and Weber (1981).

9.4. Extended work on minimum transport criteria

In the later stages of thesis, the work was extended with the help of various other product and pipeline data obtained from the previous work of other researchers. Their PCC were re-plotted, with lines corresponding to Froude number at pipeline inlet superimposed on PCC. These are shown in Figures 9.21 to 9.32. Some product properties, pipeline lengths and diameters, values of $Fr_{i,\,min}$ and $V_{i,\,min}$ are provided in Table 9.4. It is to be noted that in the original source of these PCC (except Wypych, 1993) the unstable data points were not shown. The left most points on the solids flow lines were considered to represent the unstable boundary line for the purpose of this work.

'Please see print copy for image'
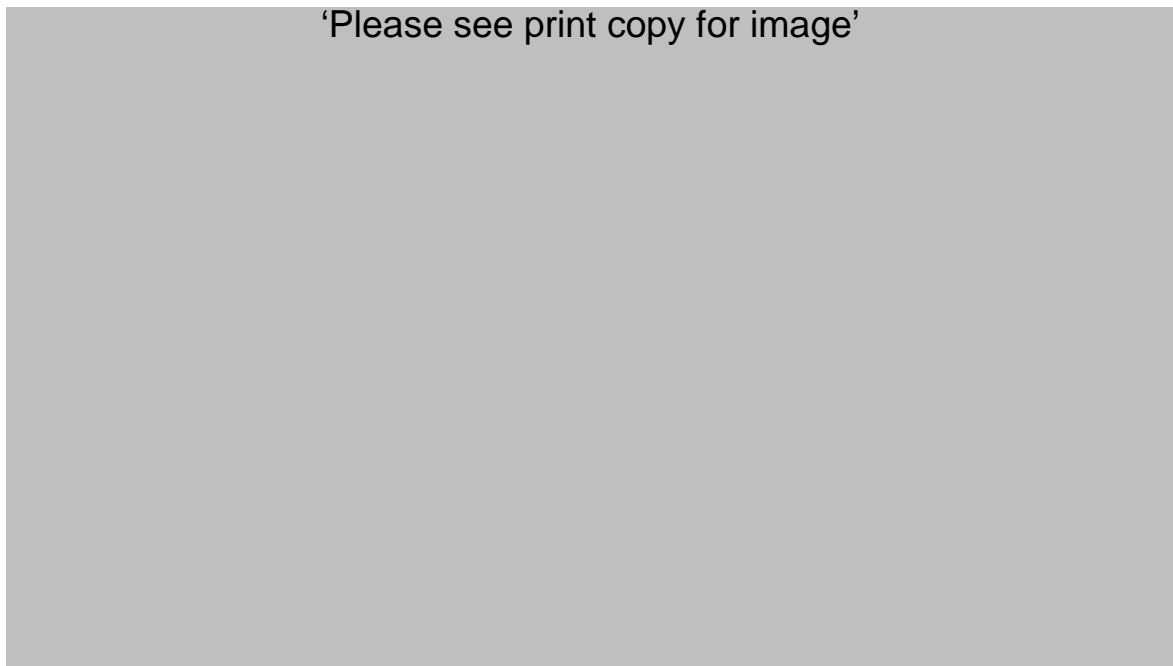
Figure 9.21: PCC for cement and fly ash mixture for 60 mm I.D. × 168 m test rig (Wypych, 1989)

‘Please see print copy for image’

Figure 9.22: PCC for cement and fly ash mixture for 105 mm I.D. × 168 m test rig (Wypych, 1989)

‘Please see print copy for image’

Figure 9.23: PCC for fly ash for 52.5 mm I.D. × 102 m test rig (Pan, 1992)

'Please see print copy for image'

Figure 9.24: PCC for fly ash for 69 mm I.D. × 168 m test rig (Pan, 1992)

'Please see print copy for image'
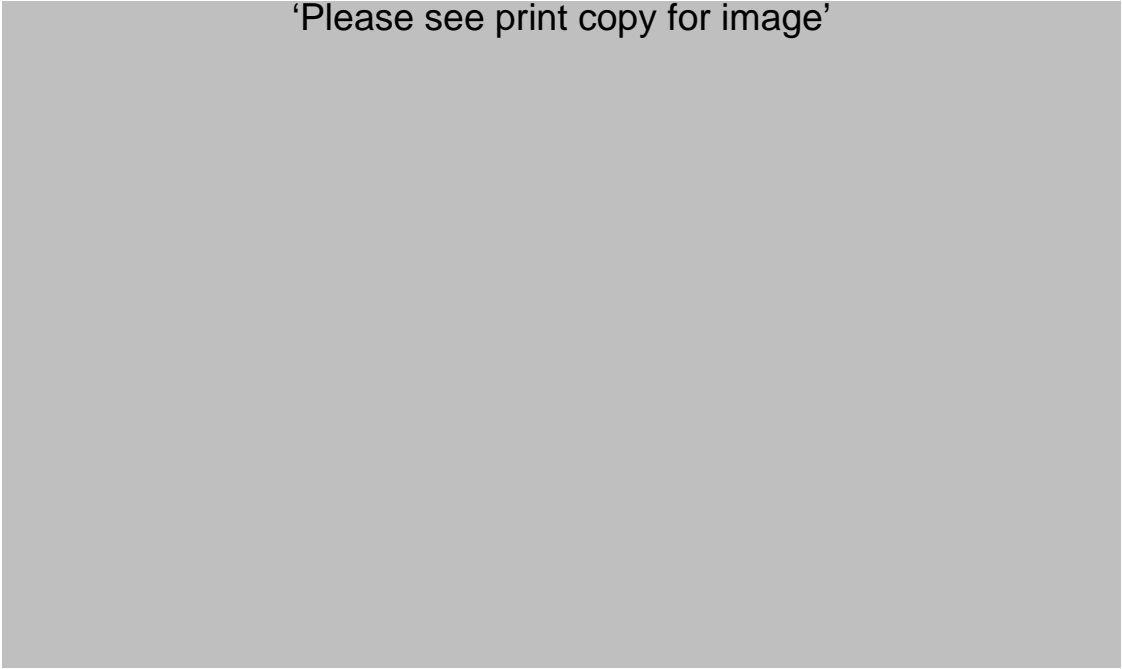
Figure 9.25: PCC for fly ash for 69 mm I.D. × 554 m test rig (Pan, 1992)

'Please see print copy for image'
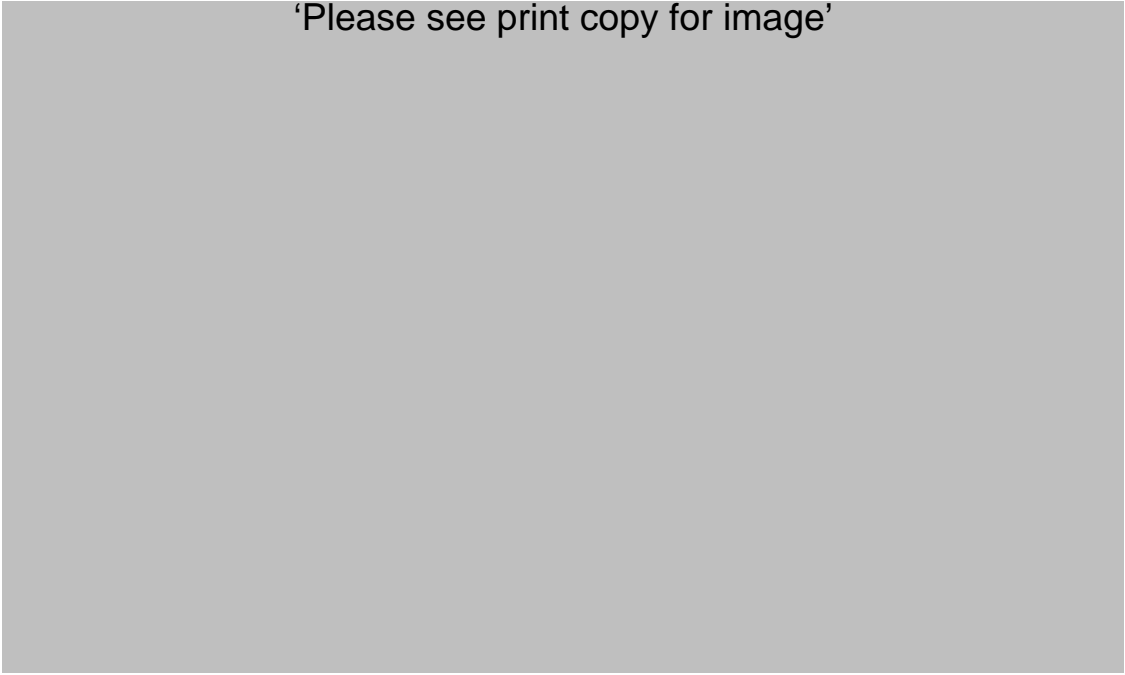
Figure 9.26: PCC for cement for 69 mm I.D. × 168 m test rig (Wypych and Arnold, 1984)

'Please see print copy for image'

Figure 9.27: PCC for fly ash (sample 1) for 69 mm I.D. × 554 m test rig (Pan and Wypych, 1998)

'Please see print copy for image'

Figure 9.28: PCC for fly ash (sample 2) for 105 mm I.D. × 168 m test rig (Pan and

Wypych, 1998)

'Please see print copy for image'

Figure 9.29: PCC for fly ash (sample 3) for 69/81 mm I.D. × 945 m test rig (Pan and

Wypych, 1998)

‘Please see print copy for image’

Figure 9.30: PCC for fly ash (sample 4) for 52.5 mm I.D. × 70 m test rig (Pan and Wypych, 1998)

‘Please see print copy for image’

Figure 9.31: PCC for fly ash for 52 mm I.D. × 71 m test rig (Wypych, 1993)

'Please see print copy for image'

Figure 9.32: PCC for pulverised coal for 52 mm I.D. × 25 m test rig (Wypych, 1989)

Table 9.4: Summary of $Fr_{i, min}$ and $V_{i, min}$ for various products (extended list)

Powder	d_{50} (μm)	ρ_s (kg/m³)	ρ_{bl} (kg/m³)	D (mm)	L (m)	$Fr_{i, min}$	$V_{i, min}$ (m/s)
Fly ash (89%), cement (11%) by weight mix (Wypych, 1989)	19	2130	700	60	168	7	5.4
	20	3100	950	105	168	7	7.1
Fly ash (Pan, 1992)	16	2197	634	52.5	102	3	2.2
				69	168	3	2.5
				69	554	5	4.1
Cement (Wypych and Arnold 1984)	20	3100	950	69	168	3.5	2.9
Fly ash 1st sample (Pan and Wypych, 1998)	16	2197	634	69	554	5.2	4.3
Fly ash 2nd sample (Pan and Wypych, 1998)	12	2215	955	105	168	1.2	1.2
Fly ash 3rd sample (Pan and Wypych, 1998)	3.5	2540	670	69/81	945	3.5	2.9
Fly ash 4th sample (Pan and Wypych, 1998)	58	2180	730	52.5	70	5	3.6
Fly ash (Wypych, 1993)	27	2100		52	71	2.5	1.8
Pulverised coal (Wypych, 1989)	30	1600	760	52	25	2	1.4

Table 9.4 shows that for same product, fly ash and cement mixture (Wypych, 1989) and fly ash (Pan, 1992), diameter scale-up causes higher requirement for minimum transport velocity. For pipe diameter increase from 60 to 105 mm for fly ash and cement mixture, $V_{i, min}$ has increased from 5.4 to 7.1 m/s, whereas $Fr_{i, min}$ has remained the same ($Fr_{i, min} = 7$). Similar for the case of fly ash (Pan, 1992), increase in pipe diameter from 52.5 to 69 mm has caused a requirement for higher minimum conveying air velocity (an increment of 2.2 to 2.5 m/s), whereas $Fr_{i, min}$ has remained the same ($Fr_{i, min} = 3$). These findings are similar to that obtained previously for fly ash and ESP dust (Wypych et al. 2005) – see Table 9.3. However, contrary to Table 9.3, fly ash (Pan, 1992) in Table 4 shows higher requirement in the value of $Fr_{i, min}$ for length scale-up (an increment in pipe length from 168 to 554 m, diameter remaining same as 69 mm, has caused an increase of $Fr_{i, min}$ from 3 to 5. Same as Table 9.3, Table 9.4 shows the numerical range of variation of $Fr_{i, min}$ with change in pipe diameter/length (for the same product) is smaller than that of $V_{i, min}$. It can be seen that the requirement of $Fr_{i, min}$ vary from minimum 1.2 to maximum 7 and $V_{i, min}$ vary from minimum 1.2 m/s to maximum 7.1 m/s depending on the powder. It should be noted that $Fr_{i, min} = 1.2$ ($V_{i, min} = 1.2$ m/s) for fly ash 2nd sample (Pan and Wypych, 1998) appears to be considerably (and surprisingly) low, especially for the 105 mm I.D pipe. However, low $Fr_{i, min}$ value is also obtained with pulverised coal (Wypych, 1989), with $Fr_{i, min} = 2$. In any case, even if too low value of $Fr_{i, min}$ ($Fr_{i, min} = 1.2$) is ignored, still the variation of $Fr_{i, min}$ ($Fr_{i, min} = 2$ to 7) remains considerably higher than that presented in Table 9.3 ($Fr_{i, min} = 2.9$ to 5.7). This suggests that $Fr_{i, min} = 6$ (with 20% margin) criteria proposed based on Table 9.3 does not apply to the products listed in Table 9.4.

9.5. Conclusions

Based on the experimental data of various powders conveyed over a wide range of pipe lengths and diameters, it is found that with increase in pipe diameter, the requirement of minimum conveying air velocity increases. To capture the pipe diameter effect, a Froude number based approach has been introduced to reliably represent the minimum transport boundary. This has shown some promise in that with increase in pipe diameter for a particular powder has not changed the requirement of minimum Froude number values for three products and insignificant change for another product. The minimum air velocity and Froude number requirement both vary quite considerably depending on the powder. More efforts are needed to establish a unified criteria to represent minimum transport condition for a wide range of products and pipelines.

CHAPTER 10: Development of New Design Procedure

10.1   Dense-phase flow phenomena

With the various existing design methods clearly demonstrating the inability to derive models, which are accurate and robust under significant scale-up conditions (Chapters 6, 7 and 8), there is a need to properly investigate the validity of the dimensionless parameter groupings, which are frequently employed in the existing modelling methods (such as m* and Fr), by assessing their suitability from a physical point of view (i.e. through proper understanding of all the particle and wall interactions, especially for dense-phase conveying). The aim is to derive a reliable modelling and scale-up procedure for the accurate prediction of pressure drop for dense-phase pneumatic conveying of powders. To achieve the above, attempts were made to visualise the flow phenomena through the 1-m long sight glass during the conveying trials of "white powder". Figure 10.1 shows the complex flow phenomenon as observed through the sight glass. Because of the difficulties to get decent quality picture of flow through sight glass (as the glass gets coated by powder), a handmade drawing of typical non-suspension flow is provided. There was a considerable gradient of solids concentration across the pipe diameter, a dense non-suspension layer of product being conveyed along the bottom portion of the pipe and on top of this layer, a dilute-phase suspension flow was prevalent. However, the interface between the non-suspension and suspension layers was not very distinct. Most of the product flow appeared to occur through the non-suspension layer. This non-suspension layer seemed to have a wavy/liquid type appearance with a turbulent top surface, where a rapid mass exchange of solids with the upper dilute-phase flow took place. Similar flow phenomenon was also observed when milk powder was conveyed

through a 105 mm I.D test rig. With an increase in conveying air flow rate, the thickness of the non-suspension layer decreased (with more and more products going into the suspension flow), ultimately resulting in the disappearance of the non-suspension layer, with the suspension flow (dilute-phase) occurring through the whole cross section of the pipe. Recent work of other researchers using Electrical Capacitance Tomography (ECT) technique to analyse the flow structure of dense-phase conveying of fine powders (Jones et al., 2008; Williams et al., 2008) have indicated similar flow mechanisms.
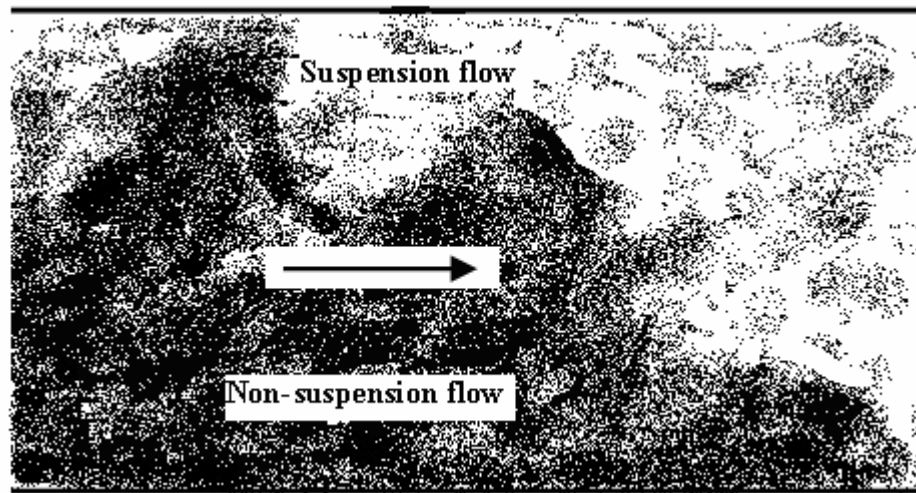
Figure 10.1: Two-Layer Flow of Fine Powders in Dense-Phase

In an attempt to evaluate the suitability of the currently used dimensionless groupings towards adequately representing the flow phenomena of the dense non-suspension liquid-like-layer of powders (Figure 10.1), some justification for the use of the m* term (such as in equations 6.1 and 7.7) can be imagined, e.g. an increase in mass flow rate of solids would cause an increase in the particle/particle/wall (inelastic)

246

interactions causing higher energy losses. However, it is difficult to justify the use of the Froude number term to model particle-particle/wall interactions for a non-suspension layer. By definition, Froude number is the ratio of inertia to gravity force and finds application in estimating the resistance of ship movement due to wave action (Streeter and Benjamin, 1979; Daugherty et al., 1989). Therefore, the Froude number based approaches could be imagined to be valid for dilute-phase/suspension flow conditions, where the gravity force of the particles are to be overcome by providing sufficient inertia force to keep particles in suspension. Bradley (1990) also raised similar scepticism over the use of Froude number term. Bradley (1990) could not provide any model for solids friction factor as his work mainly concentrated on investigating the pressure drop caused by bends with a limited focus on modelling pressure loss through straight pipes.

Therefore, it appears that for adequately representing the dense-phase flow mechanism, it is necessary to accurately model each of the non-suspension and suspension flow phenomena. A pure dilute-phase model which has been reported to provide good predictions for dilute-phase flow for different pipeline configurations is the "Weber-A4" model (Wypych et al., 1990). This model separates the total solids friction loss into two individual loss components – losses due impact and friction between particle-particle/air/pipe wall interactions and that due to keeping the particles in suspension. The model, as expressed by Wypych et al. (1990), is given by equation (10.1)

$$\lambda_s = \lambda_s{}^* \, C/V + 2\beta_0/[(C/V) \, Fr^2] \qquad\qquad (10.1)$$

where, $\beta_0 = w_{f0}/V$ and w_{f0} is the free settling velocity of an isolated particle. This appears to refer to a condition of very dilute-phase at which each particle may be thought of being sufficiently distant from other particles (i.e. a single particle is not influenced by the presence of its surrounding particles). Perhaps for this reason, the above model seems to have performed well for purely dilute-phase conditions only (and not for dense-phase). Hence, it appears logical, that this model could be applied to the suspension flow shown in Figure 10.1. However, due to the turbulent nature of the transition zone between the non-suspension and suspension flows (as confirmed by the sight glass observations), it is believed that the settling phenomenon of particles will be influenced by the presence of the neighbouring particles. Thus, it became apparent that perhaps replacing the β_0 term by β in equation (10.1) would be more appropriate for this region, where $\beta = w_f/V$ and w_f is the settling velocity of a particle in a cloud. Interestingly, it was found that some researchers (Rizk, 1976; Marcus et al., 1990) have indeed used the term $\beta = w_f/V$ instead of β_0 in the "Weber-A4" format (even for dilute-phase conditions). It must be noted though that in such work (Rizk, 1976; Marcus et al., 1990), the model was only applied to coarse particle conveying. Nevertheless, it was decided that in the present study, this model format (Rizk, 1976; Marcus et al., 1990) would be employed for fine powders (such as fly ash and ESP dust to model the pressure drop under suspension flow conditions to evaluate its applicability. The format will be referred to as the "modified Weber-A4" model in the subsequent portions of this study.

At this stage it was felt also that if the "modified Weber-A4" model could adequately describe the lower velocity regions of dilute-phase, it would be interesting to investigate the response of the model when extended even further into the dense-phase regime. This approach of extending the "modified Weber-A4" model into dense-phase makes an underlying assumption that the entire flow occurring in dense-phase can be treated as a pseudo-suspension flow. This assumption may be reasonable for the current case of fluidised dense-phase conveying of powders, which are air retentive. In any case, it was considered worthwhile to see how much overall improvement could be achieved using the "modified Weber-A4" method. Details of the modelling and results of predictions using this approach for the entire range of dense-to-dilute phase for fly ash and ESP dust are provided in section 10.2.1 of this thesis.

A more direct approach for modelling dense-phase flow was also envisaged and evaluated by assigning a single fluid friction factor type term for the non-suspension layer which has a liquid/wavy type appearance (at the bottom of pipe) and by modelling the suspension flow (blowing over the top of non-suspension layer) using the "modified Weber-A4" approach. The additional challenge with this approach is to assign a suitable friction term for the non-suspension layer, which can adequately represent the turbulent flow conditions. Of course, this would add to the complexity of modelling and predictions, but nonetheless as this two-layer based method seems to address the physical flow conditions much better compared to the earlier methods (e.g. various m*, Fr based power function type models shown in Chapters 6 and 7 and even the "modified Weber-A4" method described in this chapter), it was decided to

249

properly evaluate the potential of this approach. This method will be referred to as the "two-layer" model in the subsequent portions of this chapter. Details of the modelling and results of predictions using this technique for the entire range of dense-to-dilute phase for fly ash and ESP dust are provided in section 10.2.2 of this study.

10.2 Modelling and scale-up prediction of pressure drop

10.2.1 "Modified Weber-A4" model

The additional considerations involved in "modified Weber-A4" modelling compared to the "Weber-A4" approach represented by Wypych et al. (1990) are given below:

a) Determination of w_f using the following relations (Marcus et al., 1990),

$$w_f = K_1\, w_{f0} \tag{10.2}$$
$$K_1 = [\{(V\text{-}C)/w_{f0}\}^2\, 2\, (C/V)/(\lambda_s\, Fr^{*2})]^{0.5} \tag{10.3}$$

b) "Weber-A4" approach (Wypych et al., 1990) uses the value of C/V as close to unity for a range of Froude numbers in the dilute-phase. However, since the "modified Weber-A4" is being applied to the dense-phase conditions, it was considered that at low superficial air velocity range, the value of C/V would be less than that of dilute-phase. It was assumed that the value of C/V decreases linearly with

decrease in the value of Froude number of flow within the following boundary conditions:

C/V = 0.99 at Fr = 60   (10.4)

C/V = α (α <0.99) at Fr = 4   (10.5)

The lower limit of Fr was selected as 4 as flow instabilities were found to occur below this range during the experimental program. The upper limit of Fr was selected as 60, because Fr = 60 corresponds to m_f = 0.22 and 0.6 kg/s for the 69 and 105 mm I.D pipes, respectively, which are higher than the maximum m_f conditions through the pipes considered in this study. One must not forget that in the absence of experimentally determined particle velocity (C) values for different Fr number values between 4 and 60 to plot a trend, a linear relationship trend was assumed. As a result of this, the C/V value determined using equations 10.4 and 10.5 corresponding to the onset of suspension flow may be somewhat less than 1 (e.g. 0.91 for this fly ash corresponding to 12 m/s, assuming 12 m/s as pickup velocity), but the method was considered worth trying as an initial trial.

Using the straight pipe data obtained from P9-P10 static pressure measurements of the 69mm I.D and 168 m pipe for a wide range (dilute-to-fluidised dense-phase) of steady state conveying conditions of fly ash and by assigning a value of "α" as 0.9 (as an initial guess), K_1 values were calculated for each of the data points. It was found that the values of w_f (i.e. in effect K_1) are different for the different data points. Therefore, in order to accurately estimate the variation of K_1 over a wide range of flow conditions for the purpose of modelling and prediction, it is necessary that K_1 be expressed as a function of some easily measured/calculated system parameter(s). It was found that Rizk (1976), in his study of coarser particles, had expressed the variation of β in terms of Fr. Likewise, in the present study, K_1 and β were expressed as functions of Fr, as shown in Figures 10.2 and 10.3 respectively.
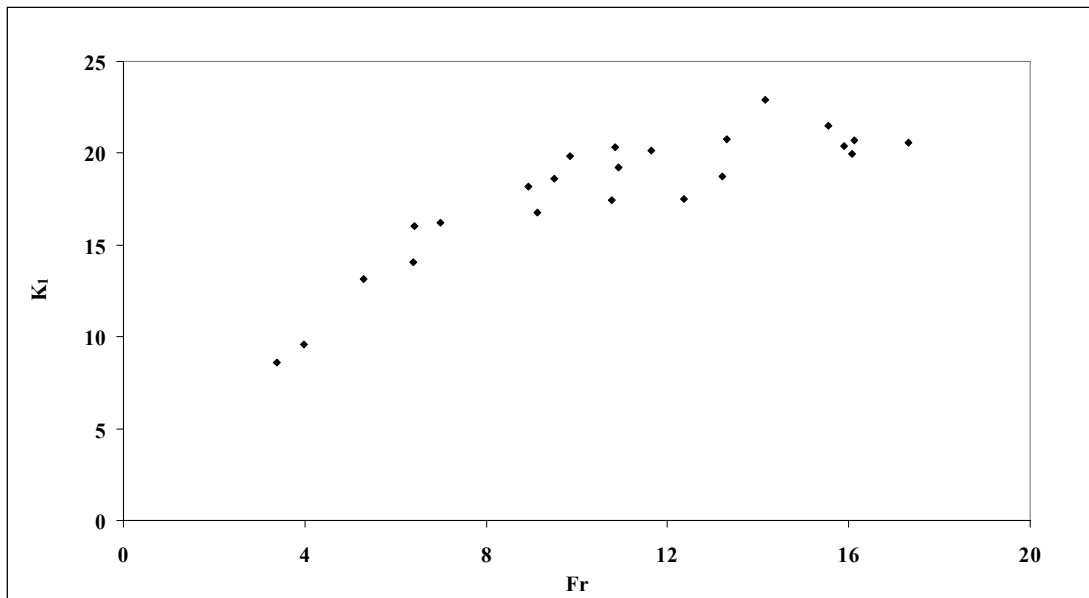
Figure 10.2: K_1 Versus Fr for Fly Ash for 69 mm I.D. × 168 m Pipe
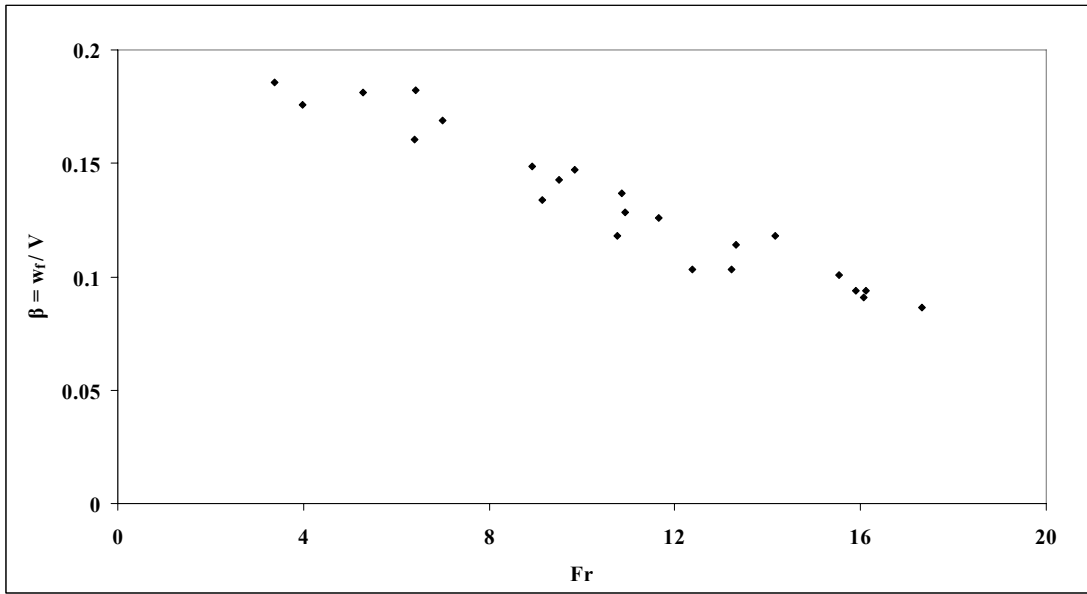
Figure 10.3: β Versus Fr for Fly Ash for 69 mm I.D. × 168 m Pipe

The trend of increase in the value of β with decreasing Fr is similar to that obtained by Rizk (1976). Although some trends seem to exist, the plots still were considered to be somewhat scattered. To improve the correlation, the factor contributing to the losses due to the suspension in the expression of λ_s (i.e. the $2\beta/[(C/V) \, Fr^2]$ term) has been plotted against Fr, as shown in Figure 10.4.
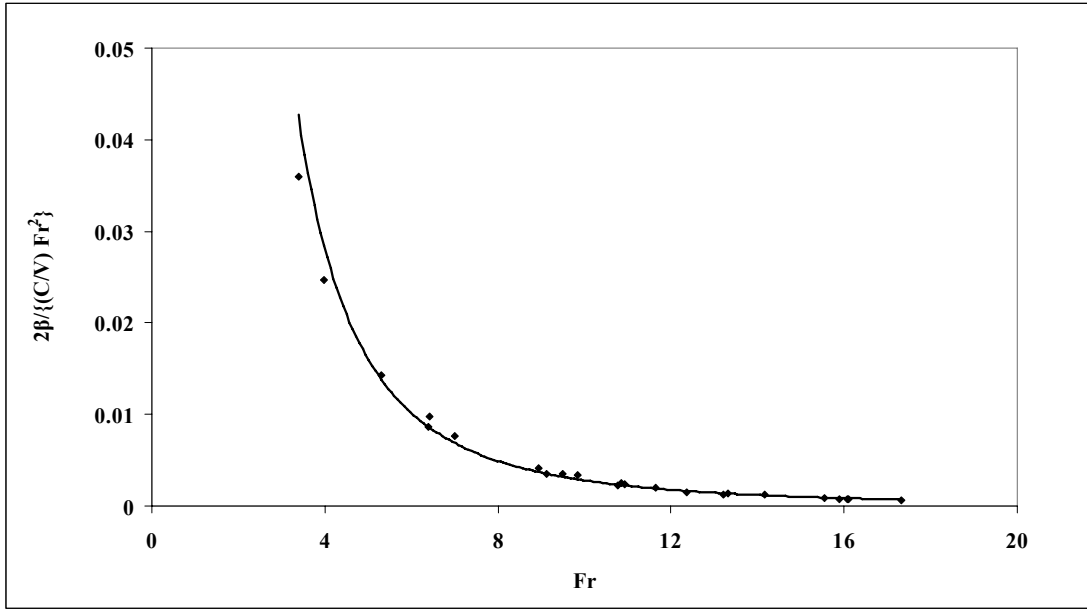
Figure 10.4: $2\beta/[(C/V)\ Fr^2]$ Versus Fr for Fly Ash for 69 mm I.D. $\times$ 168 m Pipe

It is quite apparent that the strength of correlation between $2\beta/[(C/V)\ Fr^2]$ and Fr is greater than those between K_1, β and Fr. As a result, it was decided that variation of w_f would best be expressed by correlating $2\beta/[(C/V)\ Fr^2]$ with respect to Fr. It was also decided that for the trend shown in Figure 10.4, power function type relationships would perhaps be the most appropriate. Similar trend was obtained for the case of ESP dust, which is shown in Figures A4.1 (Appendix A4.1). Using the regression tool of the data analysis tool-pack of Microsoft Excel 2003, the following relationships were derived:

$$2\beta/[(C/V)\ Fr^2] = (Fr)^{-2.55} \qquad [R^2 = 0.99] \qquad (10.6)$$

Selecting a data point towards the dilute-phase range for the set of P9-P10 data for fly ash, the value of λ_s^* was determined as 0.0054 (using the procedure mentioned in

254

Wypych et al., 1990 and Marcus et al., 1990). Appendix A4.2 provides an example of the EXCEL calculations involved in the modelling.

Using $\lambda_s^* = 0.0054$ and equations (10.4) and (10.5) to calculate C/V ratio and equation (10.6) to represent the variation of w_f for a wide range of flow conditions (dilute-to-fluidised dense-phase), total pipeline pressure drop was calculated for various air and solids mass flow rates. To calculate bend pressure drop, the Chambers and Marcus (1986) model was used. This model was used by other researchers in the past to estimate bend loss for fine powders (Jones and Williams, 2003; Williams and Jones, 2004). This model will be used in all the cases of estimation of bend loss in this chapter. Reason for choosing this model in this chapter is provided in Chapter 11. Appendix A4.3 provides an example of the "macro" based EXCEL programming (using iterative solution methods) for the 69 mm I.D. × 168 m Pipe.

Figure 10.5 compares the predicted pneumatic conveying characteristics (PCC) using "modified Weber-A4" method with the experimental plots. The predicted PCC using only "Weber-A4" model (Wypych et al., 1990) have been superimposed on the plots.
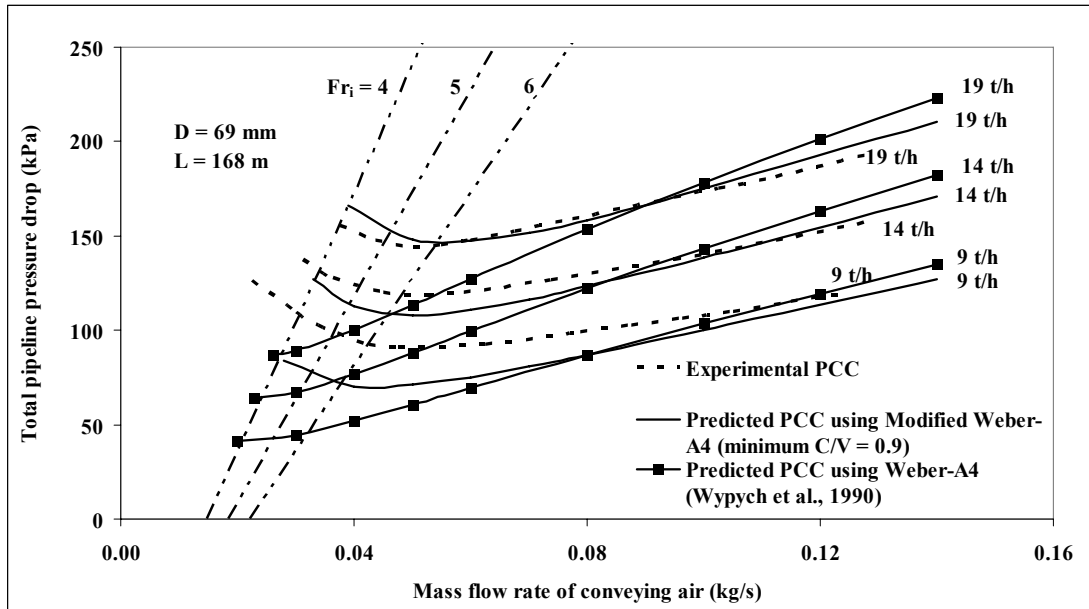
Figure 10.5: Experimental Versus Predicted PCC for Fly Ash and 69 mm I.D. × 168 m Pipe using "Modified Weber-A4" Model ($\alpha = 0.9$)

The results show that: the "Weber-A4" model (Wypych et al., 1990) is unsuitable for the dense-phase region (with predicted values of pressure drop decreasing with decreasing in air mass flow rate); the "modified Weber-A4" approach predicts quite well for dense-phase ("U"-shaped PCC follows the experimental PCC); both the "modified Weber-A4" and "Weber-A4" (Wypych et al., 1990) models provide similar predictions in dilute-phase.

The above steps were then repeated using $\alpha = 0.8$ and 0.95. It was found that for $\alpha = 0.95$, the model provided under-predictions, whereas selecting $\alpha = 0.8$ resulted in considerable over-predictions (as shown in Figure A4.2, Appendix A4.1). The above results suggested that for this sample of fly ash, $\alpha = 0.9$ would be the most accurate selection. Hence, using this value of α (i.e. $\alpha = 0.9$), the total pipeline pressure drop

256

was calculated for larger and longer pipeline (viz. 105 mm I.D. × 168 m and 69 mm I.D. × 554 m). Figure 10.6 and 10.7 compare the predicted and experimental PCC.
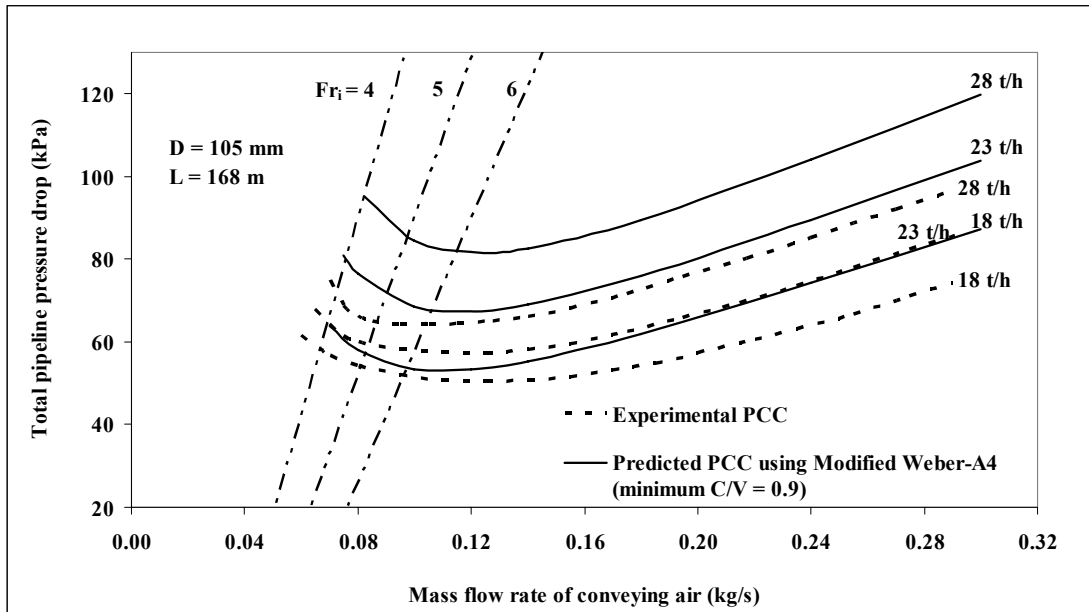
Figure 10.6: Experimental Versus Predicted PCC for Fly Ash and 105 mm I.D. × 168 m Pipe using "Modified Weber-A4" Model (α = 0.9)
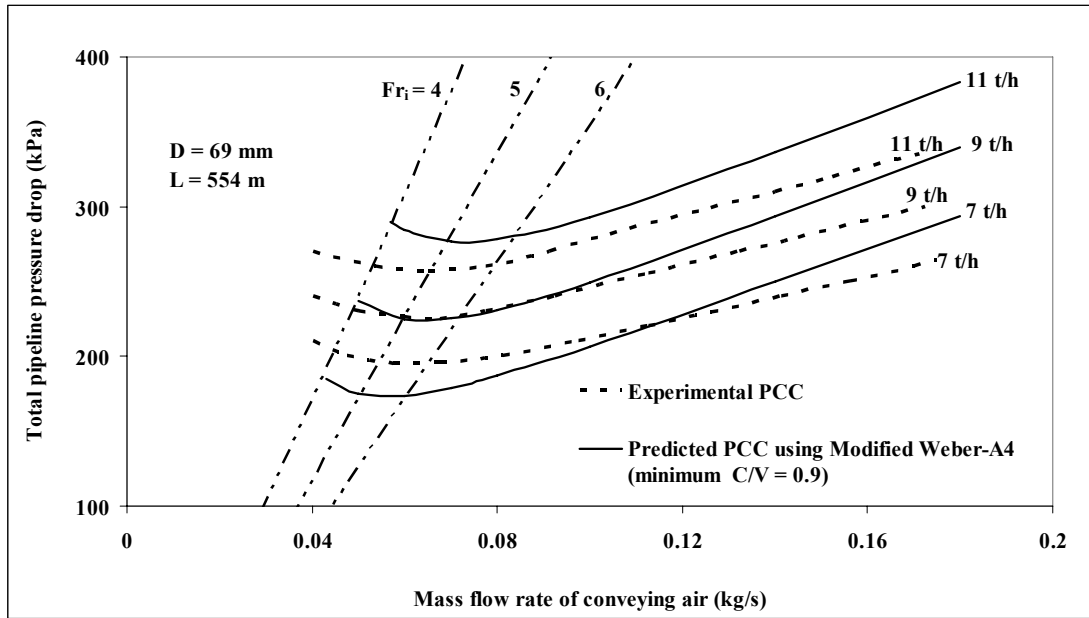
Figure 10.7: Experimental Versus Predicted PCC for Fly Ash and 69 mm I.D. × 554 m Pipe using "Modified Weber-A4" Model ($\alpha = 0.9$)

The results show some over-prediction for diameter scale-up (Figure 10.6). However, comparing the predictions obtained using existing modelling and scale-up procedures (such as Figures 6.10 and 7.5) for the same pipe, it must be said that the overall accuracy of predictions has increased substantially. For the case of length scale-up (Figure 10.7), the predicted and experimental PCC match quite well.

The above procedure was then applied for ESP dust and another fly ash sample (Pan, 1992). By comparing the predicted and experimental PCC for the 69 mm I.D. × 168 m pipe, the optimum values of α for ESP dust and fly ash (Pan, 1992) were obtained as 0.5 and 0.75, respectively. The derived relationships between $2\beta/[(C/V)\,Fr^2]$ and Fr

are given in equations (10.7) and (10.8) for ESP dust and fly ash (Pan, 1992),
respectively.

$$2\beta/[(C/V) \, Fr^2] = (Fr)^{-1.897} \qquad [ESP \, Dust, \, R^2 = 0.98] \qquad (10.7)$$

$$2\beta/[(C/V) \, Fr^2] = (Fr)^{-2.294} \qquad [Fly \, Ash, \, Pan \, (1992), \, R^2 = 0.99] \qquad (10.8)$$

In order to calculate the values of λ_s* for ESP dust and fly ash (Pan, 1992), points
towards dilute-phase region of corresponding "total" pipe PCC for 69 mm I.D. × 168
m pipes were used as the "straight pipe" data between two tapping points for these
powders (such as the P9-P10 "straight pipe" PCC obtained from the 69 mm I.D. ×
554 m pipe for ESP dust) consisted mainly of a wide dense-phase region with only a
narrow region of transition phase (Figure 5.17). For estimating λ_s*, losses due to
bends (Chambers and Marcus, 1986), verticals (Marcus et al., 1990) and acceleration
(Marcus et al., 1990) were subtracted from the total pipe pressure drop to determine
the losses only due to straight pipe portions of the pipe. The values of λ_s* determined
for ESP dust and fly ash (Pan, 1992) were 0.0086 and 0.006, respectively.

Using the relationships provided in equations (10.7) and (10.8), scale-up predictions
were obtained for the larger/longer pipes, such as 105 mm I.D. × 168 m and 69 mm
I.D. × 554 m ESP dust and 69 mm I.D. × 554 m fly ash (Pan, 1992). Fly ash (Pan,
1992) was not conveyed in a larger diameter pipe. Figures 10.8 to 10.10 show the
comparisons between the predicted and experimental PCC.
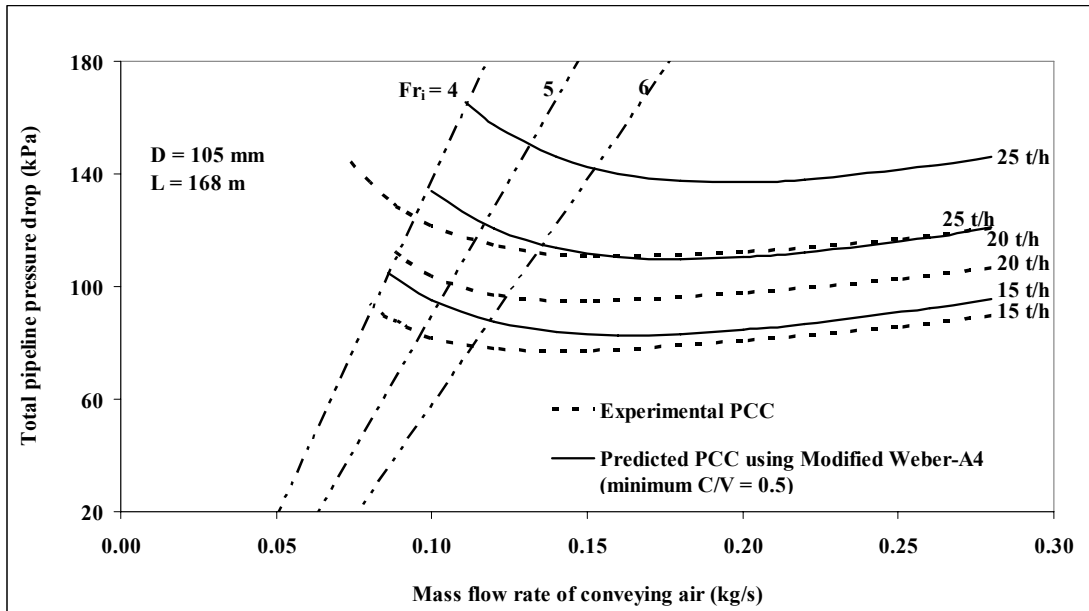
Figure 10.8: Experimental Versus Predicted PCC for ESP Dust and 105 mm I.D. × 168 m Pipe using "Modified Weber-A4" Model (α = 0.5)
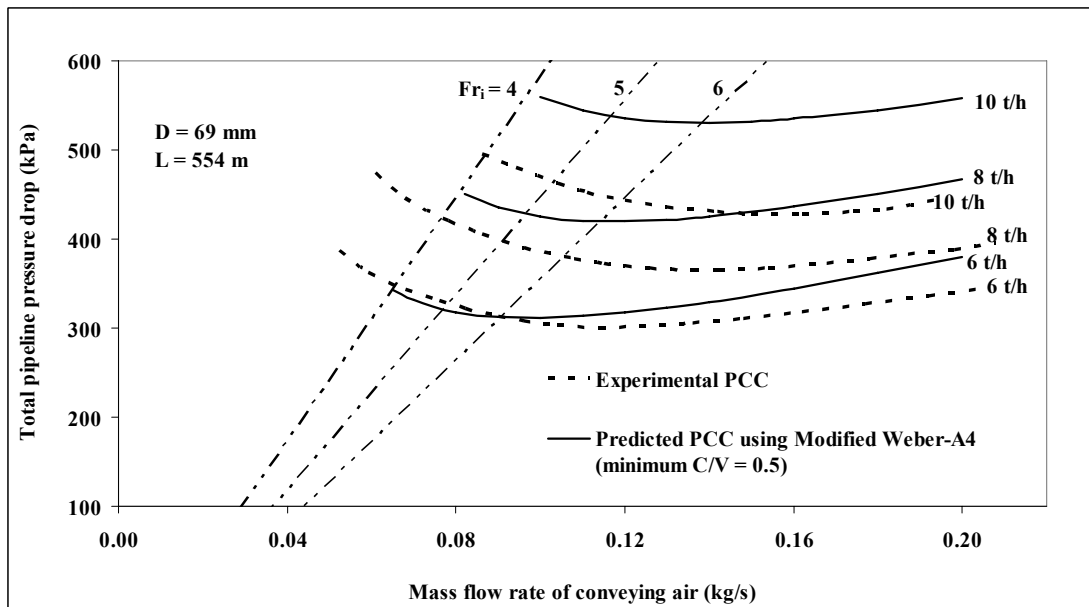
Figure 10.9: Experimental Versus Predicted PCC for ESP Dust and 69 mm I.D. × 554 m Pipe using "Modified Weber-A4" Model (α = 0.5)

'Please see print copy for image'

Figure 10.10: Experimental Versus Predicted PCC for Fly Ash (Pan, 1992) and 69 mm I.D. $\times$ 554 m Pipe using "Modified Weber-A4" Model ($\alpha = 0.75$)

The results show some over-prediction for diameter scale-up for ESP dust (Figure 10.8). For the case of length scale-up, the predicted and experimental PCC match quite well (Figure 10.9 and 10.10) for both ESP dust and fly ash (Pan, 1992). Although there are some over-predictions for the solids flow rate of 10 t/h for ESP dust (Figure 10.9) and some under-prediction for 2 kg/s for fly ash (Pan, 1992) (Figure 10.10), these deviations may be considered within acceptable limits, especially for design.

Afterwards, a similar design procedure ("Modified Weber-A4") was pursued for the following cases:

a) Evaluation for diameter scale-up for cement and fly ash mixture (Wypych, 1989) by scaling up experimental PCC of 60 mm I.D. × 168 long pipe to 105 mm I.D. × 168 long pipe and comparing the predicted and experimental PCC (i.e. diameter scale-up from 60 to 105 mm I.D.).

b) Evaluation for length scale-up for pulverised brown coal (Pan, 1992) by scaling up experimental PCC of 69 mm I.D. × 168 long pipe to 69 mm I.D. × 554 long pipe and comparing the predicted and experimental PCC (i.e. length scale-up from 168 to 554 m).

c) Evaluation for diameter and length scale-up for pulverised brown coal (Pan, 1992) by scaling up experimental PCC of 69 mm I.D. × 168 long pipe to 69/81/105 mm I.D. × 1208 m long stepped-diameter pipe and comparing the predicted and experimental PCC (i.e. diameter scale-up from 69 to 81 to 105 mm and length scale-up from 168 to 1208 m).

The results are displayed in the following figures (Figures 10.11 to 10.13). The experimental PCC suggest that the powders were conveyed in the Fr_i range from 6 to 10 (rather high). The same range of were Fr_i maintained while predicting the PCC (i.e. the predicted PCC were not initiated from the value of Fr_i as low as 4).

'Please see print copy for image'

Figure 10.11: Experimental Versus Predicted PCC for Fly Ash and Cement Mixture (Wypych, 1989) and 105 mm I.D. × 168 m Pipe using "Modified Weber-A4" Model (α = 0.9)

'Please see print copy for image'

Figure 10.12: Experimental Versus Predicted PCC for Pulverised Brown Coal (Pan, 1992) and 69 mm I.D. × 554 m Pipe using "Modified Weber-A4" Model (α = 0.6)

'Please see print copy for image'

Figure 10.13: Experimental Versus Predicted PCC for Pulverised Brown Coal (Pan, 1992) and 69/81/105 mm I.D. × 1208 m Pipe using "Modified Weber-A4" Model (α = 0.6)

The results show that for diameter scale-up with fly ash cement mixture (Figure 10.11), good predictions are obtained towards the dense-phase. However, the model results in considerable amount of over-prediction in the dilute-phase. For length scale-up with pulverised coal (Figure 10.12), the predictions are "excellent" for the whole range of air flow rates. For the stepped-diameter pipe, i.e. for both diameter and length scale-up (Figure 10.13), the results again show reasonably good predictions. Some over-predictions and some under-predictions exist for the 2 and 1 kg solids flow rate lines, respectively, but considering the extent of scale-up, this may be considered acceptable.

10.2.2 "Two-layer" model

Another modelling procedure being proposed here is based on the actual flow condition in dense-phase (i.e. considering the presence of a non-suspension layer), as shown in Figure 10.1. It was considered that as the interface between the non-suspension and suspension layers are not very distinct under real flow conditions and also the height of the non-suspension layer keeps on fluctuating (i.e. dune type appearance) due to the highly turbulent nature of flow, it would be extremely difficult to model such a flow phenomenon without making certain simplified assumptions, which are as mentioned below:

a) There exists a clear boundary/interface between the non-suspension and suspension layers. A simplified diagram of the flow structure would be as shown in Figure 10.14. The interface is shown by the horizontal "dashed" line, even though recent studies using ECT (Jones et al., 2008; Williams et al., 2008) have indicated that its actual profile is curved.
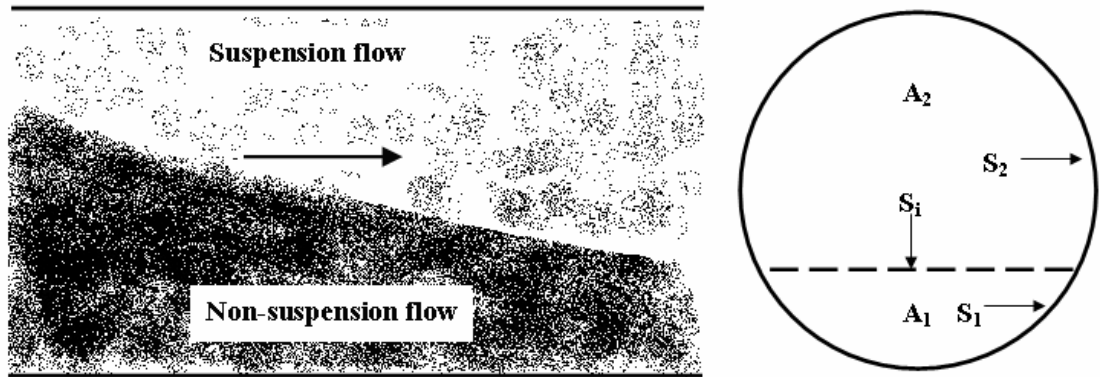
Figure 10.14: Simplified Structure of Two-Layer Flow of Fine Powders in Dense-Phase

b) Only a trivial amount of air flow is consumed in fluidising the non-suspension layer. Thus, almost the entire amount of the conveying air flow (m_f) passes through the suspension layer. For the purpose of calculation, all the air is considered passing through the top layer.

c) The non-suspension layer behaves like a liquid/pseudo-fluid, having uniform (average) values of apparent density and viscosity across the thickness of the non-suspension layer (at any particular location and also along the pipe). This means that even as the air flow rate and/or velocity increases, no extra air gets entrapped into the non-suspension layer to cause a variation of its rheological properties. Recent studies using ECT (Jones et al., 2008; Williams et al., 2008) have indicated variations in bulk-density across the thickness of the non-suspension layer. However, the more simplified approach of using an "average" condition is being pursued in this study.

d) At the minimum conveying conditions (blockage/flow instability), i.e. for Fr = 4, $m_{s\,(non-sus)} = m_s$ and $m_{s\,(sus)} = 0$. In the dense-to dilute transition zones of the PCC, i.e. for Fr = 10, $m_{s\,(non-sus)} = 0$ and $m_{s\,(sus)} = m_s$. Note: the value of Fr for dense-to-dilute transition has been assumed as 10. The respective increase and decrease in the amount of $m_{s\,(sus)}$ and $m_{s\,(non-sus)}$ is assumed to be linearly proportional to the increase in local Fr values. However, one should note that a proper study of change in thickness is a matter of further research. Plots of calculated values of $m_{s(sus)}$ and $m_{s(non-sus)}$ in relation to Froude number based on the assumption (d) for ESP dust data are provided in Appendix A4.4.

e) The non-suspension layer is conveyed at a velocity ($V_{non-sus}$) equal to the superficial air velocity (V). The actual air velocity in the suspension layer is V_1 (where, $V_1 > V$).

With the help of the above assumptions, the flow phenomenon can be modelled using two-layer modelling procedure similar to the case of slurry flow (Shook and Roco, 1991; Giles et al., 1991; Giles and Shook, 2000). It was found that Mason and Levy (2001) had adopted a similar approach to model the dense-phase pneumatic conveying of cement. However, their design procedure was not validated under significant length and/or diameter scale-up conditions.

Due to the velocity difference between the two layers ($V_1 > V$), interfacial stress exists between the two layers (Shook and Roco, 1991; Giles et al., 1991; Giles and Shook,

2000). Using force balance for the pipe as a whole, the following relations can be established (Shook and Roco, 1991; Giles et al., 1991; Giles and Shook, 2000):

$$\Delta P = (L/A) \, (\tau_1 S_1 + \tau_2 S_2) \tag{10.9}$$

$$\tau_1 = 0.5 \, (\lambda_{non\text{-}sus}) \, (\rho_{non\,sus}) V^2 \tag{10.10}$$

From the famous Barth (1958) equation (given in equation 2.1), for the suspension layer:

$$\tau_2 = 0.5 \, (\lambda_f + m^* \lambda_{sus}) \, \rho \, V_1^2 \tag{10.11}$$

The value of λ_{sus} can be determined using the "modified Weber A4" method described in section 10.2.1 for the calculation of λ_s. However, it must noted that λ_{sus} needs to calculated based on the actual air velocity condition in the suspension layer (V_1). $\rho_{non\,sus}$ has been considered equal to ρ_{bl}, since it was assumed that very little amount of the conveying air gets actually added into the non-suspension layer. Calculation for both the layers is performed based on the hydraulic diameter of each layer (Shook and Roco, 1991).

The major task which still remains is to assign suitable dimensionless parameter groupings to adequately represent $\lambda_{non\text{-}sus}$. The friction factor for single-phase turbulent flow is generally represented in terms of Reynolds number of flow and relative roughness of the pipe wall (Swamee and Jain, 1976). Since the non-suspension layer has been considered having a liquid-type appearance, it was decided

that $\lambda_{non-sus}$ would be represented as a function of Reynolds number for the non-suspension layer, as expressed in equation (10.12).

$$\lambda_{non-sus} = \text{function of } (\rho_{bl} \, V \, D_{h \, (non-sus)} / \, \mu_{non-sus}) \qquad (10.12)$$

The only unknown term in the equation (10.12) is $\mu_{non-sus}$. Reviewing the relevant literature (Gibilaroa, 2001; King, 1981; Anjaneyulu and Khakhar, 1995; Rees et al., 2005; Colafigli) on the apparent viscosity of gas-fluidised beds seems to suggest that at conditions close to minimum fluidisation, the apparent viscosity of the fluidised bed varies within the range of 0.1-2 Pas (for fine to coarse material). Therefore, in this study, the value of $\mu_{non-sus}$ has been considered as 0.5 Pas as an initial guess.

The next stage of the modelling procedure was to develop a relationship for $\lambda_{non-sus}$. Equating the values of P9-P10 "straight pipe" pressure loss of fly ash and ESP dust with the ΔP term of equation (10.9) and by estimating λ_s using "modified Weber-A4" approach, values of $\lambda_{non-sus}$ were calculated using equation (10.10). It was found that for values of Fr higher than 5 (approx), the values of $\lambda_{non-sus}$ became negative. This suggests the existence of the non-suspension layer only within the Froude number range of 4 to 5. This range seems to be quite narrow (especially considering that flow visualisation of "white power" showed the existence of a non-suspension layer almost up to local Froude number of 10). This apparent discrepancy could be attributed to the various sensitive calculation procedure involved in the estimation of $\lambda_{non-sus}$ (e.g. pre-estimation of λ_{sus}, $D_{h \, (non-sus)}$ etc). It was found that the number of experimental data points for fly ash available within the range 4<Fr<5 were not adequate for use

269

for modelling purpose. Hence, further modelling and scale-up evaluation were not pursued for fly ash. Fortunately, comparatively larger number of data points existed for ESP dust within the above range of Fr. To test the strength of relationship between the values of $\lambda_{non-sus}$ and $Re_{non-sus}$, the CORREL function of Microsoft Excel 2003 was used. It was found that the value of correlation coefficient (R) was quite low (0.3). This is perhaps because $Re_{non-sus}$ includes the sensitive $D_{h\ (non-sus)}$ term, which can unexpectedly influence the estimation of $Re_{non-sus}$. However, it was observed the strength of relationship between $\lambda_{non-sus}$ and $V_{non-sus} = V$ is quite good [R = -0.97]. Therefore, it was decided that $\lambda_{non-sus}$ may best be represented in terms of V. The following model was obtained:

$$\lambda_{non-sus} = V^{-3.76} \qquad\qquad [R^2 = 0.99] \qquad\qquad\qquad (10.13)$$

Using equation (10.13) for the non-suspension layer and equation (10.7) for the suspension layer, total pipeline pressure loss was estimated for various lengths and diameters of pipes (69 mm I.D. × 168 m, 105 mm I.D. × 168 m and 69 mm I.D. × 554 m) for ESP dust. Because the model for the non-suspension layer was active only for a relatively narrow range of Fr (4<Fr<5), the predictions ended up being very similar to that obtained previously in section 10.2.1. Figure 10.15 shows a typical comparison plot between predicted and experimental PCC for the 105 mm I.D. × 168 m pipe. Results of prediction for the 69 mm I.D. × 168 m and 69 mm I.D. × 554 m pipes are shown in Figures A4.3 and A4.4 (Appendix A4.1), respectively. For the 69 mm I.D. × 554 m pipe, predictions were found to become unexpectedly unstable for

$Fr_i < 4.5$. This is perhaps because the method involves delicate calculation steps (such as calculation of $D_{h\,(non\text{-}sus)}$, $D_{h\,(sus)}$ etc).
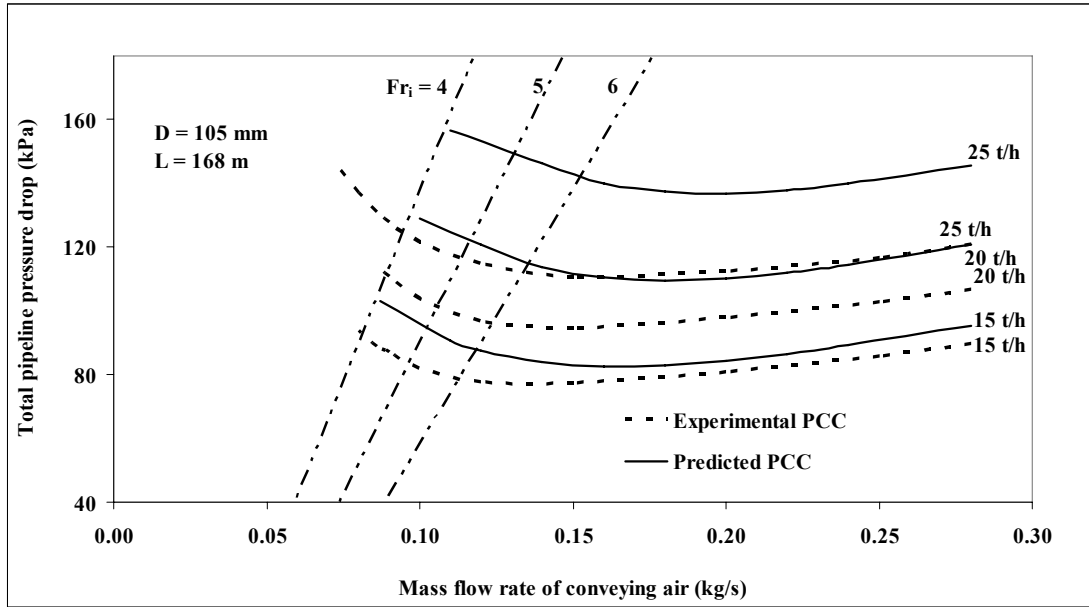
Figure 10.15: Experimental Versus Predicted PCC for ESP Dust and 105 mm I.D. × 168 m Pipe, using "Two-Layer" Model

10.2.3 "Suspension density" and air velocity method

In the final stages of the thesis, another modelling method was attempted using "suspension density" and "air velocity" in the expressions for solids friction factor. Bradley (1990) mentioned that "suspension density" (defined by equation 10.14a) might be a better representative of flow characteristics compared to the popular use of m* (equation 7.1). He found it logical to think that the "controlling influences on the

regime of flow of solids in a pipe should be air velocity and the extent to which the pipe is filled, rather than a simple mass ratio".

$$\rho_{sus\ (Bradley)} = m_s/(AV) \qquad\qquad (10.14a)$$

Equation (7.1) was modified by replacing the m* term with $\rho_{sus\ (Bradley)}$. The Froude number term was replaced by air velocity (V). Using the steady state "straight pipe" pressure drop data obtained from the P9-P10 and P11-P12 tapping points for the 69 mm I.D. × 168 m long pipe for fly ash conveyed over a wide range of flow conditions (dilute- to fluidised dense-phase), models for λ_s were derived by representing straight pipe pressure loss as per Barth (1958). The models are given by equations (10.15) and (10.14).

Based on P9-P10 data:

$$\lambda_s = (\rho_{sus\ (Bradley)})^{-0.26}\ (V)^{-1.58} \qquad [R^2 = 0.99] \qquad (10.14)$$

Based on P11-P12 data:

$$\lambda_s = (\rho_{sus\ (Bradley)})^{-0.28}\ (V)^{-1.55} \qquad [R^2 = 0.99] \qquad (10.15)$$

The high values of R^2 indicated "good fit". It is to be highlighted that the exponents for $\rho_{sus\ (Bradley)}$ and V are similar for equations 10.14 and 10.15. This indicated that

there could be some merit with these parameters selected for modelling. The model

given by equation (10.14) was evaluated for scale-up accuracy and stability by using

it to predict the total pipeline drop for the larger and longer pipelines (viz. 69 mm I.D.

× 168 m, 105 mm I.D. × 168 m and 69 mm I.D. × 554 m) for various solids flow rates

for and comparing the predicted and experimental PCC. Since the two models have

similar values of exponents, thus it was considered adequate to only evaluate equation

(10.14). Chambers and Marcus (1986) model was used to estimate the losses due to

the bends (see Chapter 11 regarding the choice of bend model). The results are shown

in Figures 10.16 to 10.18.
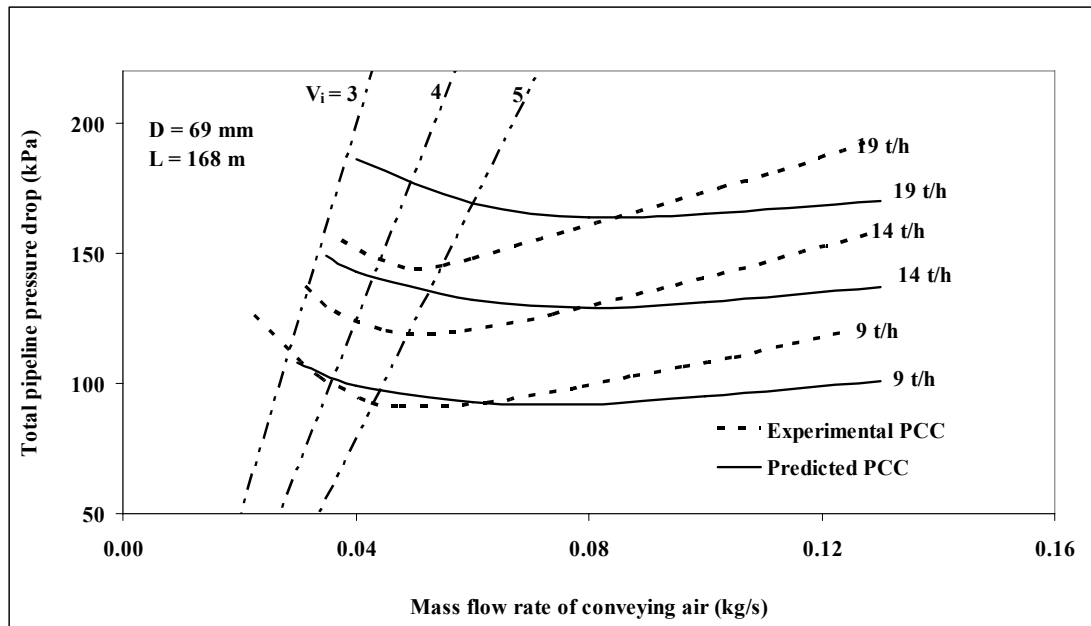
Figure 10.16: Experimental Versus Predicted PCC for Fly Ash and 69 mm I.D. × 168

m Pipe using Equation (10.14)

273
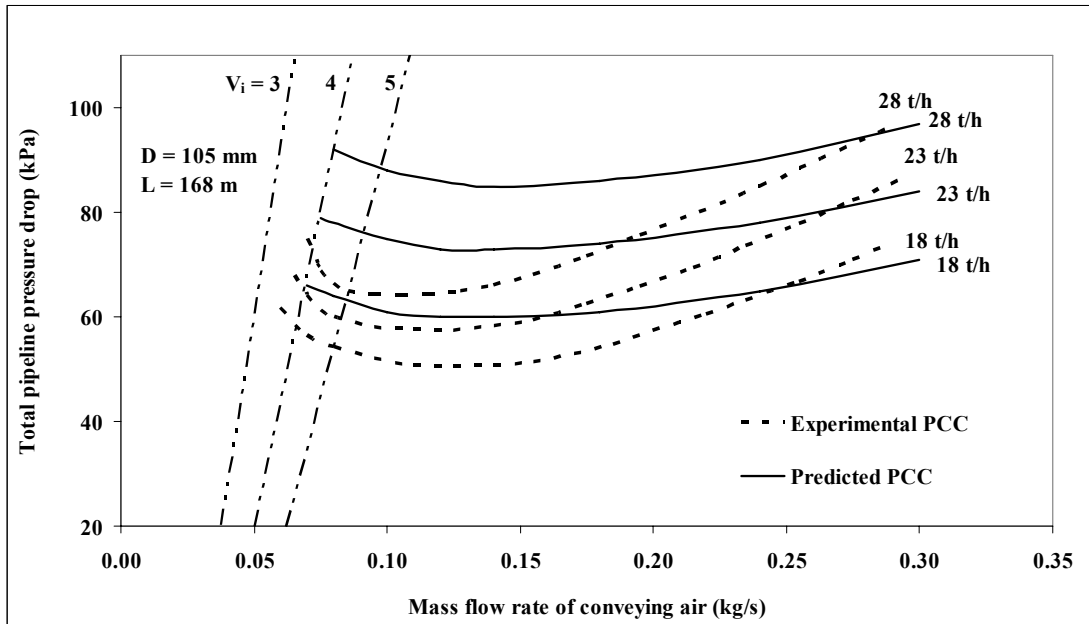
Figure 10.17: Experimental Versus Predicted PCC for Fly Ash and 105 mm I.D. × 168 m Pipe using Equation (10.14)
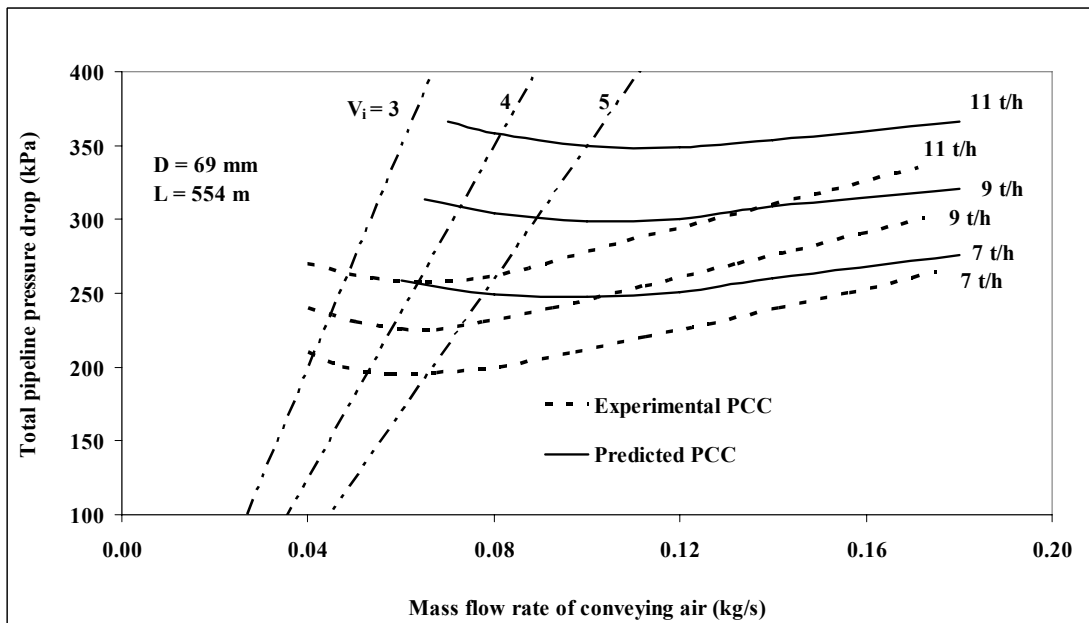
Figure 10.18: Experimental Versus Predicted PCC for Fly Ash and 69 mm I.D. × 554 m Pipe using Equation (10.14)

Figure 10.16 shows that for the 69 mm I.D. × 168 m pipe, the 19 t/h and 14t/h lines provided in some over-predictions in dense-phase. However, good predictions were obtained for m_s = 9 t/h in dense-phase. The dilute-phase results for all the three solids flow rates are somewhat under-predictions. However, the dilute-phase inaccuracies could be also caused by the bend loss model. For diameter scale-up (Figure 10.17), the model results in good predictions (especially in comparison to some of the m*, Fr based models, e.g. as shown in Figure 7.5), though some over-prediction still exist in dense-phase. For the 69 mm I.D. × 554 m long pipeline, Figure 10.18, the model results in considerable over-predictions in dense-phase, but much better predictions are obtained in dilute-phase.

Similar investigations were further carried out for ESP dust. Using the "straight pipe" pressure loss data from P9-P10 tapping points on the 69 mm I.D. × 554 m long pipe the following model was derived:

$$\lambda_s = (\rho_{sus\,(Bradley)})^{-0.12}\,(V)^{-1.62} \qquad [R^2 = 0.99] \qquad\qquad (10.16)$$

The model was evaluated for scale-up accuracy and stability by using it to predict the total pipeline drop for the larger and longer pipelines (viz. 69 mm I.D. × 168 m, 105 mm I.D. × 168 m and 69 mm I.D. × 554 m) for various solids flow rates for and comparing the predicted and experimental PCC. The Chambers and Marcus (1986)

model was used to estimate the losses due to the bends. The results are shown in Figures 10.19 to 10.21.
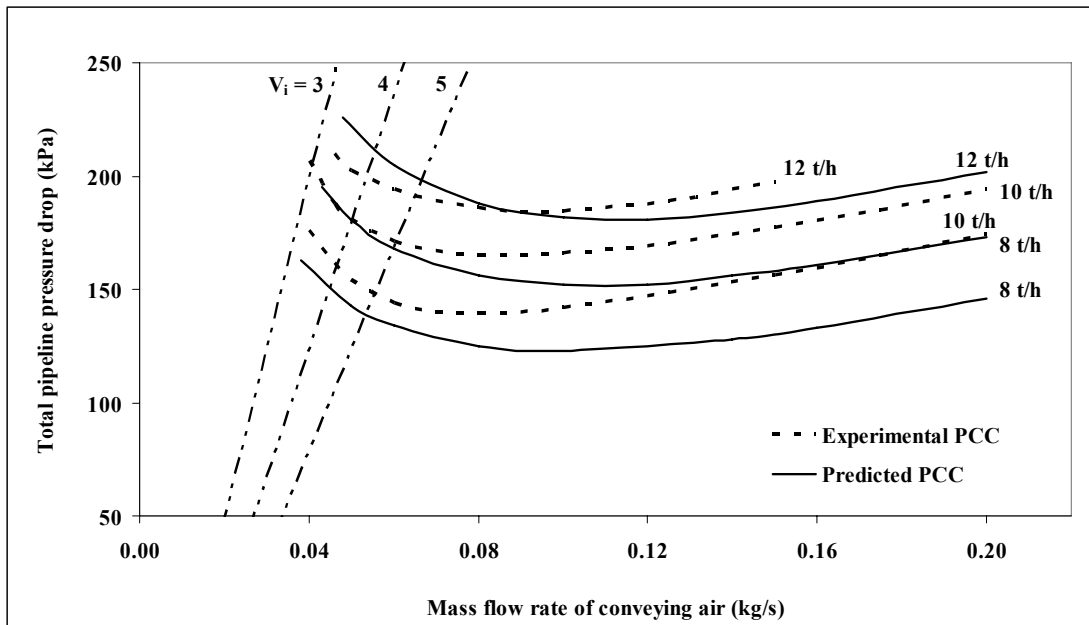
Figure 10.19: Experimental Versus Predicted PCC for ESP Dust and 69 mm I.D. × 168 m Pipe using Equation (10.16)
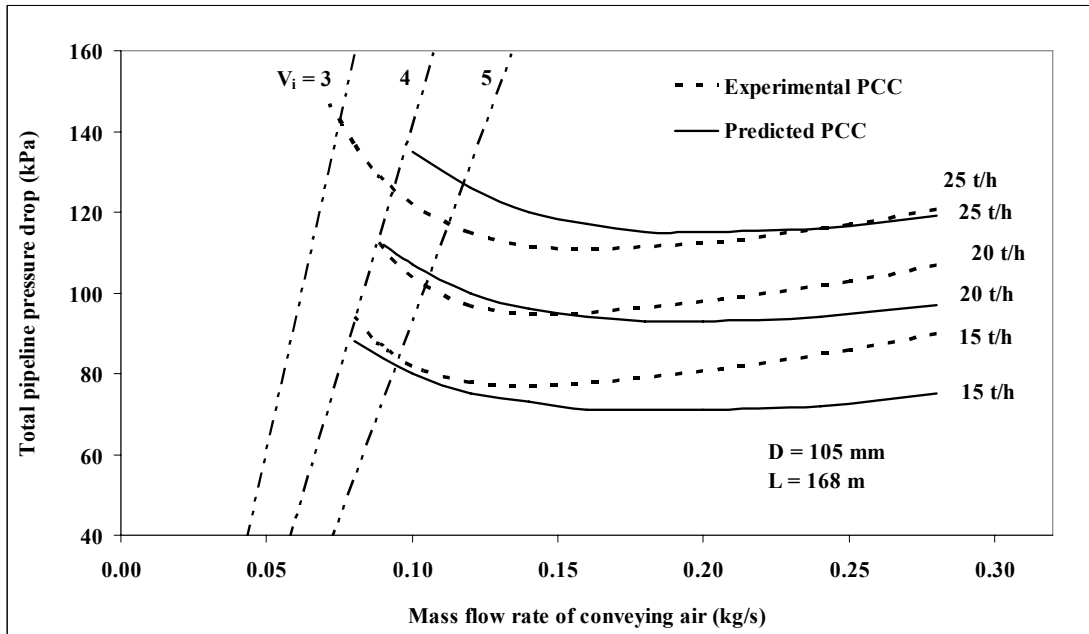
Figure 10.20: Experimental Versus Predicted PCC for ESP Dust and 105 mm I.D. ×

168 m Pipe using Equation (10.16)
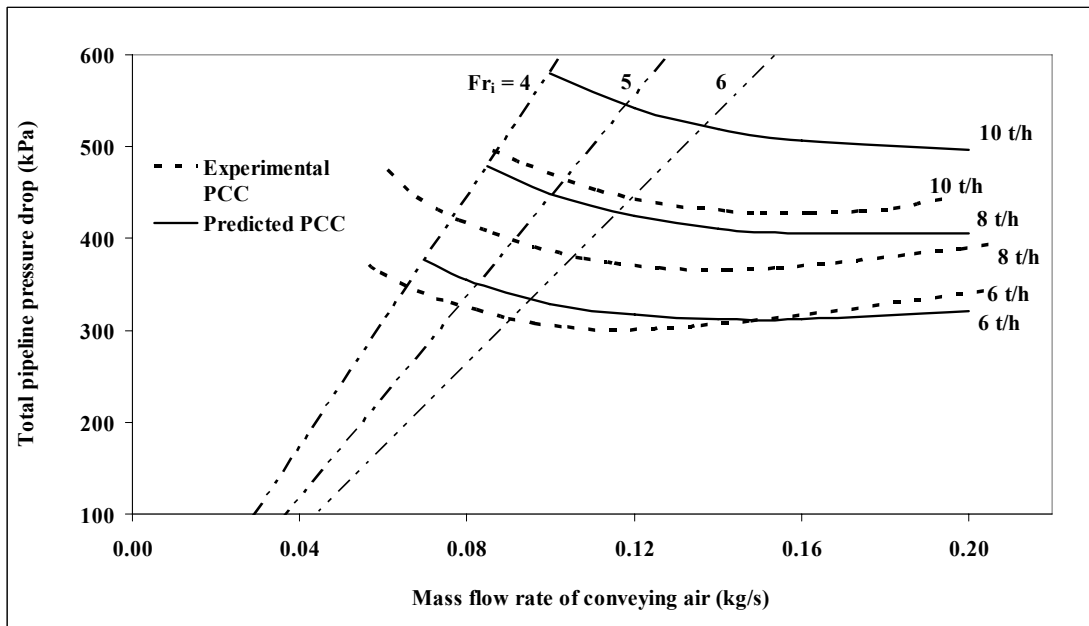
Figure 10.21: Experimental Versus Predicted PCC for ESP Dust and 69 mm I.D. ×

554 m Pipe using Equation (10.16)

The results show that for the 69 mm I.D. × 168 m and 105 mm I.D. × 168 m pipes (Figures 10.19 and 10.20, respectively), equation (10.16) provides very good predictions (especially in dense-phase). There are some over-predictions for the length scale-up.

From the results shown in Figures 10.16 to 10.21, it can be said that the parameters mentioned by Bradley (1990) have provided reasonably reliable and consistent predictions (though there exists a considerable over-prediction for the longer pipelines with fly ash). Encouraged by these results, this model format was further tested for the following cases:

a) Evaluation for diameter scale-up for cement and fly ash mixture (Wypych, 1989) by scaling up experimental PCC of 60 mm I.D. × 168 long pipe to 105 mm I.D. × 168 long pipe and comparing the predicted and experimental PCC (i.e. diameter scale-up from 60 to 105 mm I.D.).

b) Evaluation for length scale-up for pulverised brown coal (Pan, 1992) by scaling up experimental PCC of 69 mm I.D. × 168 long pipe to 69 mm I.D. × 554 long pipe and comparing the predicted and experimental PCC (i.e. length scale-up from 168 to 554 m).

c) Evaluation for diameter and length scale-up for pulverised brown coal (Pan, 1992) by scaling up experimental PCC of 69 mm I.D. × 168 long pipe to 69/81/105 mm I.D. × 1208 m long stepped-diameter pipe and comparing the predicted and experimental PCC (i.e. diameter scale-up from 69 to 81 to 105 mm and length scale-up from 168 to 1208 m).

The derived models are provided in equations 10.17 to 10.19. In absence of any "straight pipe" pressure tapping data, the models were derived using estimated straight pipe loss, obtained by subtracting calculated bend (Chambers and Marcus, 1986), vertical (Marcus et al., 1990) and acceleration (Marcus et al., 1990) loss from total pipeline pressure drop values.

For fly ash (Pan, 1992),

$$\lambda_s = (\rho_{sus \, (Bradley)})^{-0.32} \, (V)^{-1.14} \qquad [R^2 = 0.99] \qquad\qquad (10.17)$$

For fly ash and cement mixture (Wypych, 1989),

$$\lambda_s = (\rho_{sus \, (Bradley)})^{-0.33} \, (V)^{-1.47} \qquad [R^2 = 0.99] \qquad\qquad (10.18)$$

For pulverised coal (Pan, 1992),

$$\lambda_s = (\rho_{sus \, (Bradley)})^{-0.34} \, (V)^{-1.29} \qquad [R^2 = 0.99] \qquad\qquad (10.19)$$

The results of evaluation of the above models are displayed in the following figures (Figures 10.22 to 10.24).

'Please see print copy for image'

Figure 10.22: Experimental Versus Predicted PCC for Fly Ash (Pan, 1992) and 69 mm I.D. $\times$ 554 m Pipe using Equation (10.17)

'Please see print copy for image'

Figure 10.23: Experimental Versus Predicted PCC for Fly Ash and Cement Mixture (Wypych, 1989) and 105 mm I.D. $\times$ 168 m Pipe using Equation (10.18)

'Please see print copy for image'

Figure 10.24: Experimental Versus Predicted PCC for Pulverised Brown Coal (Pan, 1992) and 69 mm I.D. × 554 m Pipe using Equation (10.19)

'Please see print copy for image'

Figure 10.25: Experimental Versus Predicted PCC for Pulverised Brown Coal (Pan, 1992) and 69/81/105 mm I.D. × 1208 m Pipe using Equation (10.19)

Figure 10.22 shows that the fly ash model (equation 10.17) has predicted very well for length scale-up. The results are very similar (in fact slightly better) to that obtained using "modified Weber A4" model. Figure 10.23 shows that for cement and fly ash mixture, the model (equation 10.18) has provided reasonably good predictions for dense-phase (with some over-predictions), but significant over-prediction in dilute-phase. Again, the results are similar to that obtained using "modified Weber A4" model, except the suspension density approach has resulted in some additional over-prediction. Figure 10.24 shows that for pulverised coal, the model (equation 10.19) has provided considerable over-prediction for dense-phase for the 2.5 kg/s solids flow rate line. Comparatively better predictions were obtained for the 1.5 and 0.5 kg/s lines (though there exists still some over-prediction). Significant over-predictions were obtained for the 1.2 Km long stepped pipeline. Comparatively better predictions were obtained with the "modified Weber-A4" approach for pulverised coal.

10.3   Conclusions

Two new approaches and another approach based on the parameters used by other researcher were employed in this study to improve the modelling and scale-up procedures for the dense-phase pneumatic conveying of powders. The "Modified Weber-A4" model, derived by modifying an existing reliable dilute-phase model (to make it suitable for dense-phase), has resulted in stable predictions for diameter and length scale-up conditions for two types of fly ash, ESP dust, fly ash and cement

282

mixture and pulverised brown coal. Although some over-predictions still generally remain for diameter scale-up, there seems to be a substantial relative improvement in the overall accuracy of predictions. The merit of the model is in the fact that the model predicted with some consistent reliability for different products, whereas Chapter 6 and 7 have shown that some model formats which are good for ESP dust, have failed for fly ash (such as the m*, Fr based models, even with K = 1). The second method was derived using the concept of "two-layer" slurry flow modelling (suspension flow occurring on top of a non-suspension layer) and has also resulted in similar improvements (for ESP dust). The "two-layer" technique is believed to be more representative of the actual flow conditions under dense-phase conveying. However, because the two methods seem to provide similar results, it may be more prudent to use the simpler "modified Weber-A4" method for practical design purposes. The third method that was tried uses suspension density and air velocity term in a power function model format. The method was evaluated for various products and pipelines (similar to the evaluation of "modified Weber-A4" model). The method has generally resulted in reliable predictions for two fly ash samples. The predictions were comparable to that obtained using "modified Weber A4" approach. Further verification of the above methods is needed for various products and scale-up pipelines.

CHAPTER 11: Evaluation of Bend Pressure Drop Models

11.1   Introduction

Bends are frequently encountered in most industrial and even laboratory pneumatic conveying systems. Bends are easy to install and provide flexibility to the layout of a pneumatic conveying plant. However, bends introduce additional pressure losses to the system. On exit from a bend, the velocity of solids can get reduced significantly, sometimes resulting in drop out of the solids from the conveying gas stream (Marcus et al., 1990). The solids would then try to extract kinetic energy from the gas-stream to be again in suspension. This re-acceleration of particles causes pressure drop of the conveying gas-stream. Also, there would be losses due to the change in direction of the solids-gas stream going through the bend. A review of the various previous studies conducted on solids-gas flow through a bend and the associated pressure losses have been already provided in Chapter 2 (literature review) of this thesis.

In the initial stages of the thesis, it was not anticipated that due attention would need to be provided on the aspect of pressure loss due to the bends. As modelling solids friction through horizontal straight pipe sections was the broad aim of this thesis, most of the initial studies were focussed on the aspects of pressure drops through straight pipes. The necessity to be able to accurately (or at least reasonably) estimate the losses due to the bends was first realised when Dr. Farid Rizk provided his λ_s model (equation 7.12) for fly ash for horizontal straight pipe lengths. It was decided that his model would be investigated for its scale-up accuracy and stability by predicting the total pipeline pressure drops for various larger and/or longer pipes (69 mm I.D. × 168 m; 105 mm I.D. × 168 m and 69 mm I.D. × 554 m long pipes) and

comparing with experimentally obtained PCC. Using the "component" approach, losses due to bends, verticals and initial acceleration were to be separately estimated using appropriate models and added to the predicted pressure drop for horizontal straight pipe (only), to obtain the total pipeline pressure drop. Accurate estimations of the losses due to lifting product through a vertical section were not considered to be a major concern, as a 7 m vertical height in a 168 and 554 m long total pipe length was only a small proportion and hence should not cause any significant variation to the overall prediction of total pipeline pressure drop. It was also believed that losses due to initial acceleration would be trivial in pipes of such lengths. However, the bend losses can be significant (Mills, 2004) and hence, due attention was needed for its accurate prediction.

11.2   Bend models

Although in recent years some efforts have been made to model the solids friction factor for fine powder and hence the pressure drop for straight horizontal pipe lengths (Wypych and Hastie, 2006; Jones and Williams, 2003; Williams and Jones, 2004; Williams and Jones, 2006), but the issue of investigating the impact of selection of a bend model on the prediction of total pipeline pressure loss has not been given similar attention. As a result, the number of bend models available in literature for evaluation/use for the cases of fine powder systems is somewhat limited. It must be admitted though that since the main aim of the thesis was to investigate straight pipe losses, hence limited efforts could only be dedicated on the subject of bend pressure

drop. Nonetheless, the following are the three bend models found in literature and were selected in the present study for evaluation (i.e. to compare the effect of selecting different bend models on the total system pressure drop). These models have been discussed in Chapter 2, but it was considered appropriate to provide a brief statement on the models in this portion of the study.

11.2.1 *Pan and Wypych (1998)*

Pan and Wypych (1998) derived a bend loss model based on the experimental data obtained from four different fly ash samples with median particle size ranging from 3.5-58 μm, particle density and loose poured bulk density ranging from 2180-2540 kg/m^3 and 634-955 kg/m^3, respectively. The model was derived for a wide range of flow conditions (estimated air velocity range at pipe inlet: 3 to 25 m/s). The bend loss due to solids only is expressed as:

$$\Delta p_{bs} = 0.5 \ m^* \ \lambda_{bs} \ \rho_{bo} \ V_{bo}^{\ 2} \qquad\qquad (11.1)$$

Where: $\lambda_{bs} = 0.0097 \ (m^*)^{0.5676} \ (Fr_{bo})^{0.9647} \ (\rho_{bo})^{-0.6232}$ (11.2)

Although equation (11.1) is a semi-empirical one, it was found (Pan and Wypych, 1998) accurate for a wide range of fly ash of varying size range. This range covers the median size of the tested fly ash sample (viz. 30 μm). Hence, this model was considered relevant for the evaluations in the present study. This model was given preference over the models derived by Pan (1992), who used data of only one fly ash

sample, whereas Pan and Wypych (1998) used data from four fly ash samples (wide size range).

11.2.2 Chambers and Marcus (1986)

The total pressure loss in bends (Δp_b) due to the flow of air and solids, as presented by Chambers and Marcus (1986):

$$\Delta p_b = N \, B \, (1 + m^*) \, \rho \, V^2/2 \tag{11.3}$$

This bend model was used by other researchers (Jones and Williams, 2003; Williams and Jones, 2006) in the "back calculation" method of deriving an expression for the solids friction factor. The model was selected for evaluation in the present study due to its apparent popularity. Chambers and Marcus (1986) did not provide any derivation details of the model.

11.2.3 Schuchart (1968)

Schuchart's work (Schuchart, 1968) was based on a number of different bends using glass and plastic granules as the test materials. The particles were of rather larger size, 1-2 mm in diameter for volumetric concentrations up to only 5% (dilute-phase). In spite of this, the model was tested for fine powders (in dense-phase) as the model seemed to be popular (Klinzing, 1980; Marcus et al., 1984) for dilute-phase flow; it was considered interesting to examine its potential under dense-phase conveying

conditions. The solids contribution of the pressure drop due to solids-gas flow through the bends was given by the following formula:

$$(\Delta p_{\text{bend}} / \Delta p_z)_{\text{solids}} = 210 \ (2R_B / D)^{-1.15} \tag{11.4}$$

Here, $(\Delta p_{\text{bend}})_{\text{solids}}$ is the contribution to pressure drop by the solids flowing through the bend; $(\Delta p_z)_{\text{solids}}$ is the solids contribution to the pressure drop through a straight pipe of straight length equivalent to the bend. Finally, the total bend loss is obtained by calculating the pressure drop due to $(\Delta p_{\text{bend}})_{\text{gas}}$ (gas-only friction) using Ito's expression (Ito, 1959) as mentioned in Marcus et al. (1990) and Wypych and Pan (1991), and then adding it to $\Delta p_{\text{bend solids}}$.

11.3   Evaluation of bend models

The effect of selecting a particular bend model on the prediction of total system pressure loss was evaluated by estimating the total pipeline conveying characteristics for fly ash for different solids throughput ranges for the 69 mm I.D. × 168 m test rig by using each of the three different bend models separately and comparing the predicted PCC thus obtained (with themselves and with the experimental PCC). Initially the λ_s model (equation 7.12) derived by Dr. Rizk was used to calculate the pressure drop in straight pipe lengths. Losses due to verticals and initial acceleration were estimated as per Marcus et al. (1990). Since the same set of models were used

to estimate losses occurring in horizontal pipe lengths, verticals and for initial acceleration, therefore any variation in magnitude (and trend) of the predicted total pipe PCC should occur only because of the choice of different bend models. Results are shown in Figures 11.1 to 11.3. The "dashed" lines shown in the figures are the predicted PCC for a hypothetical pipe having only straight pipe portions equal to the length of the straight pipe (i.e. no bends, verticals etc). Therefore the difference between total pipe PCC (solid lines) and dashed lines indicate contribution of pressure drops due to the bends. Of course, this "difference" also includes losses due to the vertical and initial acceleration, but this representation was considered acceptable for the purpose of a comparative study on the bend effects. To improve the accuracy of prediction using Chambers and Marcus (1986) model, instead of applying the model by grouping all the bends in the pipe together, it was considered prudent to apply the model separately for each bend along the pipe. Using this approach, the "V" term in the equation (11.3) was replaced by "V_{bo}", as the pressure losses for bends are reported to depend on the prevailing flow condition at the outlet of bend (Pan, 1992).

'Please see print copy for image'

Figure 11.1: Predicted versus experimental PCC using Pan and Wypych (1998) bend model for 69 mm I.D. × 168 m long pipe

'Please see print copy for image'

Figure 11.2: Predicted versus experimental PCC using Chambers and Marcus (1986) bend model for 69 mm I.D. × 168 m long pipe

Figure 11.3: Predicted versus experimental PCC using Schuchart (1968) bend model for 69 mm I.D. × 168 m long pipe

The above results/comparison plots show that the selection of different bend models can generate significantly different predicted conveying characteristics (even though they all use the same solids friction factor model to calculate pressure drop in straight horizontal runs). Schuchart (1968) bend model predicts dramatically higher bend pressure drop values in the dense-phase regime and low values at high-velocity (dilute-phase) conditions. This trend appears to be in contrast to the experimental data of Pan (1992). This indicates that models which were derived for the conveying of coarse particles in dilute-phase (such as Schuchart's model), may not be suitable for application in dense-phase flow with fine powders. On the other hand, the bend pressure drop calculated using the other two models (i.e. Pan and Wypych, 1998 and Chambers and Marcus, 1986) seems to follow the experimental trends much better.

However, the model presented by Chambers and Marcus (1986) is shown to under-predict somewhat in the dilute-phase regime. The Pan and Wypych (1998) bend model appears to be the best choice for this fly ash sample.

Based on the above findings, the Pan and Wypych (1998) bend model was selected to estimate the contribution of losses due to bends to the total pipeline pressure drop for evaluating various solids friction models for fly ash (as described in Chapters 6 and 7). However, in spite of its apparent suitability, questing arose on whether the comparisons shown in Figures 11.1 to 11.3 can actually describe the true "story" regarding the accuracy of a bend model. The inferences, which were drawn from the results shown in Figures 11.1 to 11.3, are actually based on the differences in the estimated pressure drop values between the "total pipe" and "straight pipe" PCC. The predicted values of "straight pipe" loss were based on existing/derived models for solids friction (e.g. λ_s). Therefore, to reach to a correct conclusion, one first needs to ensure that the model representing solids friction for the horizontal straight sections of pipe are correct. With the progress of evaluation work regarding scale-up accuracy of various solids friction models (Chapters 6 and 7), it was realised that the existing models/modelling techniques for solids friction are generally incorrect (especially under significant scale-up conditions of diameter and/length). Scale-up prediction using a derived λ_s model (equation 7.7), whose values of power function "constant" and exponents are very similar to that of model Dr. Rizk (equation 7.12), had resulted in gross inaccuracies under scale-up conditions (Chapter 7) of length and diameter. This, in turn, raised doubt over the earlier inference that the Pan and Wypych (1998) model is more accurate than Chambers and Marcus (1986) model for

fly ash. However, it was decided that in spite of this uncertainty, for the time being (until a reliable λ_s model became available) it would still make sense to go ahead with the prediction work for the total pipe PCC by using the Pan and Wypych (1998) model for fly ash. It was believed that as the model was derived using the data of four different fly ash samples, so some extent of reliability may be expected in predictions for fly ash cases. Due to this reason, most of the prediction work carried out for fly ash (Chapters 6 and 7) were based on the Pan and Wypych (1998) bend model. However, for the cases of ESP dust, there were no other option but to use Chambers and Marcus (1986) model, as this was considered to be a "general purpose" model; also, no bend model could be found in the literature, which was derived exclusively for ESP dust data.

Fortunately, in the final stages of the thesis, an improved modelling procedure for solids friction in straight horizontal pipes was derived, which has been referred to as the "modified Weber-A4" modelling (Chapter 10). Using this new modelling approach, predicted total pipe PCC for fly ash were obtained for the 69 mm I.D. × 168 m long pipe by employing both Pan and Wypych (1998) and Chambers and Marcus (1986) bend models. Since the same set of models were used to estimate losses occurring in horizontal pipe lengths, verticals and for initial acceleration, therefore any variation in magnitude (and trend) of the predicted total pipe PCC should occur because of the choice of different bend models. The comparison plots are shown in Figure 11.4.

'Please see print copy for image'

Figure 11.4: Predicted versus experimental PCC using Pan and Wypych (1998) and Chambers and Marcus (1986) bend models for 69 mm I.D. × 168 m long pipe

In Figure 11.4, the top group of ms lines corresponds to 19 t/h, middle ones for 14 t/h, bottom ones for 9 t/h. Surprisingly, the results show that the dependence of prediction of bend pressure drop on the choice of bend model is significantly different from that previously obtained (Figures 11.1 and 11.2). Both the bend models provide very similar trends (and magnitudes) of total pipeline pressure drop (i.e. in effect, both the models predicted similar bend loss characteristics). Because of this sharp contradiction in findings, a thorough investigation was undertaken to discover the possible causes for the above. While minutely examining the calculation steps in the EXCEL program (for total pipeline pressure drop), it was found that equation (7.12) seemed to under-predict the straight pipe pressure losses compared to the "modified Weber-A4" model for the "straight" pipe sections towards the end of the pipe. As a result, the estimated values of air density and superficial air velocity at the bend outlet

(i.e. at the entry point to the previous pipe section, when approached starting from the pipe exit) are different depending upon the choice of "straight pipe"pressure drop model. Although this difference does not appear very significant, it was sufficient to dramatically over predict an estimation for the Pan and Wypych (1998) bend model. The reason for this could be that as the estimated bend loss by Pan and Wypych (1998) model varies in direct proportion to $V_{bo}^{2.96} \approx V_{bo}^{3}$, whereas that for Chambers and Marcus (1986) is V_{bo}^{2}, therefore Pan and Wypych (1998) model is relatively far more sensitive to the changes in estimation of superficial air velocity at bend outlet. Thus, it is apparent that Chambers and Marcus (1986) model is more stable. Similar exercises were carried out for the diameter and length scale-up pipes (105 mm I.D. × 168 m and 69 mm I.D. × 554 m long pipes). The results are provided in Figures 11.5 and 11.6. The results again show that when used in conjunction the "modified Weber-A4" model (for straight losses), both the Pan and Wypych (1998) and Chambers and Marcus (1986) bend models result in similar predictions for fly ash. In fact, for the 69 mm I.D. × 554 m pipe, both the models result in almost identical predictions. As a result, the Chambers and Marcus (1986) model was used in Chapter 10 for estimation of bend losses for fly ash (and for ESP dust).

'Please see print copy for image'

Figure 11.5: Predicted versus experimental PCC using Pan and Wypych (1998) and

Chambers and Marcus (1986) bend models for 105 mm I.D. × 168 m long pipe

'Please see print copy for image'

Figure 11.6: Predicted versus experimental PCC using Pan and Wypych (1998) and

Chambers and Marcus (1986) bend models for 69 mm I.D. × 554 m long pipe

11.5 Conclusions

The predicted PCC for fly ash and 69 mm I.D. × 168 m long pipe, obtained using three different bend models in combination with equation (7.12) for straight pipe losses, were found to be significantly different depending on the selection of bend model, in terms of both predicted values and overall trends. Results indicated that Schuchart (1968) model is unsuitable in the dense-phase region; whereas the Pan and Wypych (1998) model appears to be more valid for the dense-phase conveying of fly ash (as could be expected because it was derived using various fly ash data). However, when used in conjunction with a more accurate model for straight pipe loss ("modified Weber-A4" approach), both the Pan and Wypych (1998) and Chambers and Marcus (1986) models provided similar predictions (even for larger and longer pipes). Thus, it was found that estimation of bend loss depends to a great extent on the choice of an accurate solids friction model (for straight pipes). The Chambers and Marcus (1986) bend model was found slightly more stable than power function based models used by Pan and Wypych (1998).

CHAPTER 12: Conclusions and Suggested Further Work

12.1   Conclusions

Based on the "straight pipe" PCC obtained using steady state pressure drop data of static pressure measuring points along the pipeline, it can be concluded that each "straight pipe" section has its own PCC, having different shapes (even for the same powder and pipeline) indicating potential change in the local flow conditions. Also, different "straight pipe" PCC are obtained from different pipes (indicating the effect of change of pipe diameter and air density). The nature of the "U"-shape and the location of PMC for total pipeline PCC are significantly influenced by the pipe layout (e.g. location and number of bends) and not entirely by the dense- to dilute-phase transition of flow mechanisms.

Several existing/popular models for solids friction were evaluated for scale-up accuracy and stability by predicting the total pipeline pressure drop for different diameters and lengths of pipes and comparing with experimental PCC. None of the models were found to be consistent for accurately predicting the pressure drop under scale-up situations for different powders. Models derived using steady state "straight pipe" pressure drop data using different power function formats and parameter groupings are also found to be generally inaccurate under scale-up evaluation. Models derived using "back calculation" method, generally result in dramatic over-predictions. Power function type models in $K = 1$ format generally provide relatively better predictions than $K \neq 1$ format. It is concluded that the parameter groupings, which are frequently used in modelling solids friction (such as m*, Fr), are

inappropriate and/or insufficient to adequately represent the turbulent (and complex) flow phenomenon of dense-phase pneumatic conveying of powders.

Scale-up procedures using "system" approach do not seem to be valid for the dense-phase conveying. Original "scale-up laws" resulted in significant over-predictions under diameter scale-up conditions, whereas evaluation of an improved diameter scale-up criterion provided somewhat better results. Comparisons between experimental and predicted PCC have shown considerable under-prediction for significant length scale-up conditions in dense-phase. However, the "system" approach predicts quite well for dilute-phase. The accuracy of the method seems to be largely dependent on the system layout. It appears that the issue of pressure drop in bends has not been properly addressed. Scaling-up when the pipe length to bend number ratio of the test rig and proposed plant are quite different results in significant inaccuracy. This should serve a warning to the engineers and researchers involved in designing industrial plants using the "system" approach.

Based on the experimental data of various powders conveyed over a wide range of pipe lengths and diameters, it is found that with increase in pipe diameter, the requirement of minimum conveying air velocity increases. To capture the pipe diameter effect, a Froude number based approach has been introduced to reliably represent the minimum transport boundary. This has shown some promise in that increase in pipe diameter for a particular powder has not changed the requirement of minimum Froude number values for three products and minor change for another

product. The minimum air velocity and Froude number requirement both vary quite considerably depending on the powder.

Two new approaches were employed to improve the modelling and scale-up procedures for the dense-phase pneumatic conveying of powders. The "Modified Weber-A4" model, derived by modifying an existing reliable dilute-phase model (to make it suitable for dense-phase), results in stable predictions for diameter and length scale-up conditions for two types of fly ash, ESP dust, fly ash and cement mixture and pulverised brown coal. Although some over-predictions still generally remain for diameter scale-up (approximately 10-30%, depending m_s values, over-prediction on experimental values in dense-phase for both fly ash and ESP dust), there seems to be a substantial relative improvement in the overall accuracy of predictions. The method provides reasonably good predictions even for scale-up to a pipe of length 1.2 km, having three diameters of pipe and for the pulverised brown coal. Another method was derived using the concept of "two-layer" slurry flow modelling (suspension flow occurring on top of a non-suspension layer). This new method also results in similar improvements (for ESP dust). The "two-layer" technique is believed to be more representative of the actual flow conditions under dense-phase conveying. However, because the two methods seem to provide similar results, it may be more prudent to use the simpler "modified Weber-A4" method for practical design purposes. Another method was tried using suspension density and air velocity term (these parameters were also used previously by another researcher) in a power function model format. The method was evaluated for various products and pipelines (similar to the evaluation of "modified Weber-A4" model). The method has generally resulted in

reliable predictions for two fly ash samples. The predictions were comparable to that obtained using "modified Weber A4" approach. Further verification of these methods is needed for various products and scale-up pipelines.

The estimation of bend pressure drop can have a considerable impact on correctly predicting the total pressure loss in a pneumatic conveying system (especially in dilute-phase). Based on estimated bend losses are per Pan and Wypych (1998) (Table 6.1), bend losses can be 10-15% in dense-phase, but 35-45% in dilute-phase for 69 mm I.D. × 168 m pipe (having 5 bends) for fly ash. The estimation of bend loss depends to a great extent on the choice of bend model, as well as, quite surprisingly, on the accuracy of the solids friction models (for straight pipes).

The thesis also examined the suitability of using direct different pressure ("DP") measurement for fine powder conveying in dense-phase. A DP meter arrangement was built. Values of Standard Deviations (SD) of DP, as well as the static pressure signals are presented for one test material. Plots of SD values versus pipe length (location of static pressure tapping) showed that the general trend is: the SD values continually increases with increase in pipe length (from pipe inlet side to exit side), except a drop in SD values after a set of 90 degree bends. The results may instigate further study.

It needs to be stated that the present work does not claim to offer a complete and proven theory of modelling and scale-up, rather it aims to assist the engineers

303

involved in designing industrial systems by providing some guidance on modelling/scale-up supported by an improved understanding on the knowledge of the accuracies/inaccuracies of existing design procedures and with the presentation of some new validated modelling techniques (which are to be further tested). It took researchers almost one hundred years to establish friction factor relationships for the turbulent flow of even for the single fluids and was purely based on empirical methods using dimensionless parameter groupings such as Reynolds number. Therefore, it may still take some time and effort before "dense" turbulent solids-gas flows can be modelled accurately. However, with ongoing research, it is hoped that the overall understanding of the flow phenomenon will improve over time and the design procedures will continue to improve. It is also hoped that the new modeling methods and knowledge gained in this thesis will help others to achieve this goal.

12.2 Suggested further work

Although the results obtained in this thesis have contributed significantly to predicting and understanding the pneumatic transportation of fine powders, the following areas of investigation still require further attention:

a) Despite the rigorous validation of the scale-up accuracy and stability of the developed "modified Weber A4" modelling procedure conducted in this thesis for various powders and lengths/diameters of pipes, it is preferable that the method be further evaluated for other powders and pipe layouts. Also, due

thought should be given to why the model results in somewhat over-prediction for diameter scale-up. Perhaps, boundary layer effect is contributing to this or perhaps a suspension density term needs to be introduced in the model. This requires proper study. The "suspension density, air velocity" approach of modelling also needs further scale-up validations.

b) Flow visualisation (e.g. using a "sight glass") is believed to be important for accurate modelling of the flow mechanisms. Preferably, the "sight glasses" are to be installed in different locations of a pipe; at least, one "sight glass" in the beginning and another, towards the end of pipe. This would reveal the changes in flow mechanisms from non-suspension to suspension mode of conveying (and whether this transition at all happens). Also, sight glasses should be installed on at least two different diameters and lengths of pipes, e.g. in the range from 50 and 150 mm pipe diameters; from 100 to 500 m pipe lengths (i.e. with significant changes in pipe dimensions), to properly examine the changes in flow mechanisms due to the changes in pipe diameters and air density. Specifically, flow of the non suspension wavy/dune type layer would need to be thoroughly supervised for accurate understanding of the rheological properties of the non-suspension layer. However, arranging such a test facility could be a challenge. Also, for proper visualisation, the wall of the "sight glass" should ideally be made of materials on which fine powders do not coat readily. It has been observed that in many occasions, after first few seconds of initial conveying, the entire wall of the "sight glass" became coated with powder and it became difficult to see through the glass. Also,

tomography (ECT) could be tried in addition to sight glass, and of course in cases where sight glasses do not work (glass getting coated with powder).

c) Adequate range of dense-phase conveying data are to be generated for properly evaluating the accuracy of the "2-layer" modelling method. With sufficient data sets, studies should be conducted to establish parameter groupings which could accurately represent the turbulent flow mechanism of the non-suspension layer. In this thesis, the friction factor for the non suspension layer has been expressed with a power function type model using velocity of the non-suspension layer. However, this requires further validation. A thorough study on the rheology of the non-suspension layer should be carried out, e.g. investigation of the apparent density of the non-suspension layer.

d) Actual conveying velocity of the powders (particle velocity) is to be measured experimentally. This value of conveying velocity (experimentally obtained) can be directly fed in to the "modified Weber- A4" model for use.

e) Further studies are to be conducted to investigate the aspect of the pressure drops in bends, such as evaluation of the existing use of parameters in the different expressions of bend models (i.e. whether these parameters adequately describe the physical phenomenon of reacceleration of powders after the bend outlet), the dependence of bend model on product properties etc.

f) Further studies and testing are required towards adequately representing the minimum transport conditions using wide range of conveying data, for various powders and pipelines (different diameters and lengths of pipes).

g) There seems to be much scope of research in studying the fluctuating signals (both static and DP) with different products, pipelines (different diameter and lengths of pipes) and tapping points installed at different locations of pipeline.

h) Suitable quantified/statistical method(s) of reporting of results are to be studied.

REFERENCES

Ahmed, A.M. and Elghobashi, S. 2000. On the mechanisms of modifying the structure of turbulent homogeneous shear flows by dispersed particles. Physics of Fluids. 12: 2906-2920.

Anjaneyulu, P. and Khakhar, D.V. 1995. Rheology of a gas-fluidized bed. Powder Technology. 83: 29-34.

Arnold, P.C., Wypych, P.W. and Reed, A.R. 1994. Advances in the design of pneumatic transport systems. Powder Handling and Processing. 6 (1): 9-19.

Barth, W. 1958. Strömungsvorgänge beim transport von festteilchen und flüssigkeitsteilchen in gasen. Chemie – Ing. – Techn. 30 (3): 171-180.

Blasius, H. 1913. Das ahnlichkeitsgesetz bei reibungsvorg angen in flussigkeiten. forsch. Arb. Ing.

Bi, H.T., and Grace, J.R. 1995. Flow regime diagram for gas-solid fluidization and upward transport. International Journal of Multiphase Flow. 21 (6): 1229-1236.

Bohnet, M. 1985. Advances in the design of pneumatic conveyors. International Chemical Engineering. 25 (3): 387-405.

Bosse, T., Kleiser, L. and Meiburg, E. 2006. Small particles in homogeneous turbulence. Physics of Fluids. 18: 027102 1 – 17.

Bradley, M. S. A. and Mills, D. 1988. Approaches to dealing with the problem of energy loss due to bends. In the proceedings of 13th Powder and Bulk Solids Conference: 705-715.

Bradley, M. S. A. 1989. An improved method of predicting pressure drop along pneumatic conveying pipelines. In the proceedings of 3rd International

Conference on Bulk Materials Storage and Transportation, Newcastle, Australia, 27-29 June: 282-288.

Bradley, M.S.A. 1990. PhD Dissertation: Prediction of pressure losses in pneumatic conveying pipelines, Thames Polytechnic.

Bradley, M. S. A. 1990a. Pressure losses caused by bends in pneumatic conveying pipelines Effects of bend geometry and fittings. Powder Handling and Processing. 2 (4): 315-321.

Breaultt, R.W. and Mathur, V.K. 1989. High-velocity fluidized bed hydrodynamic modeling. Ind. Eng. Chem. Res. 28: 684-688.

Bricout, V. and Lounge, M.Y. 2004. A verification of Glicksman's reduced scaling under conditions analogous to pressurized circulating fluidization. Chemical Engineering Science. 59: 2633-2638.

Chambers, A. J., and Marcus, R. D. 1986. Pneumatic conveying calculations. In the proceedings of 2nd International Conference on Bulk Materials Storage and Transportation, Wollongong, Australia, 7–9 July: 49-52.

Cheng, H. and Lounge, M. 1992. Fluid dynamic similarity of circulating fluidized beds. Powder Technology. 92: 259-270.

Colebrook, C.F. 1939. Turbulent flow in pipes with particular reference to the transition region between the smooth and rough pipe laws. J. Inst. Civ. Eng. Lond. 11: 133-156.

Colafigli, A., Mazzei, L., Lettieri, P. and Gibilaro, L.G. Apparent viscosity measurements in a homogeneous gas-fluidized bed. Chemical Engineering Science (in press).

Crowe, C.T. 2000. On models for turbulence modulation in fluid-particle flows. International Journal of Multiphase Flow. 26: 719-727.

Darcy, H. 1857. Recherches experimentales relatives au mouvement de l'eau dans les tuyaux, 2 volumes, Mallet-Bachelier, Paris. 268 pages and atlas. ("Experimental Research Relating to the Movement of Water in Pipes").

Datta, B.K. and Ratnayaka, C. 2003. A simple technique for scaling up pneumatic conveying systems. Particulate Science and Technology. 21: 227-236.

Datta, B.K. and Ratnayaka, C. 2005. A possible scaling-up technique for dense phase pneumatic conveying. Particulate Science and Technology. 23: 201-204.

Daugherty, R.L., Franzini, J.B. and Finnermore, E.J. 1989. Fluid mechanics with engineering applications. Publ. McGraw-Hill.

Detamore, M.S., Swanson, M.A., Frender, K.R. and Hrenya, C.M. 2001. A kinetic-theory analysis of the scale-up of circulating fluidized beds. Powder Technology. 116: 190-203.

Dick, R.H. Measurement Uncertainty: Methods and Applications. 4th Ed., ISA Publ.

Duckworth, R.A. 1977. Course notes of two day intensive course on pneumatic conveying, ed. Leung, L.S., Organised by Dept. of Cjhemical Engineering – University of Queensland, The Institution of Chemical Engineering, Queensland Group and the Queensland Branch of the College of Chemical Engineers, 27 – 28th June, Surfers Paradise, Queensland, Australia.

Elgobashi, S. and Truesdell, G.C. 1993. On the two-way interaction between homogenous turbulence and dispersed solid particles. I: turbulence modification. Physics of Fluids. 5: 1790-1801.

Elgobashi, S. 1994. On predicting particle laden turbulent flows. Applied Scientific Research. 52: 309-329.

Giacinto, M.D., Sabetta, F. and Piva., R. 1982. Two-way coupling effects in dilute gas-particle flows. Journal of Fluids Engineering. 104: 304-312.

Gibilaroa, L.G., Gallucci, K., Di Felice, R. and Pagliai, P. 2001. On the apparent viscosity of a fluidized bed. Chemical Engineering Science. 27: 415-435.

Giles, R.G., Shook, C.A. and Wilson, K.C. 1991. An improved two layer model for horizontal slurry pipeline flow. Canadian Journal for Chemical Engineering. 69 (1): 173-178.

Giles, R.G. and Shook, C.A. 2000. Modelling high concentration settling slurry flows. Canadian Journal for Chemical Engineering. 78 (4): 706-716.

Glicksman, L.R. 1984. Scaling relationships for fluidized beds. Chemical Engineering Science: 39 (9): 1373-1379.

Glicksman, L.R, Hyre, M.R. and Woloshun, K. 1993. Simplified scaling relationships for fluidized beds. Powder Technology. 77: 177-199.

Glicksman, L.R. and Farrell, P. 1995. Verification of simplified hydrodynamic scaling laws for pressurized fluidized bed combustors: Part 1 – bubbling fluidized beds. In the proceedings of 13th International Conference for fluidized bed combustion.

Goossens, W.R.A. 1998. Classification of fluidized particles by Archimedes number. Powder Technology. 98: 48-53.

Gore, R.A. and Crowe, C.T. 1989. Effect of particle size on modulating turbulent intensity. International Journal for Multiphase Flow. 15 (2): 279-285.

Hadinoto, K., Jones, E.N., Yurteri, C. and Curtis, J.S. 2005. Reynolds number dependence of gas-phase turbulence in gas–particle flows. International Journal of Multiphase Flow. 31: 416-434.

Huang, Y., Turton, R., Park, J., Parviz, F. and Boyle, E.J. 2006. Dynamic model of the riser in circulating fluidized bed. Powder Technology. 163: 23-31.

Huber, N. and Sommerfeld, M. 1998. Modelling and numerical calculation of dilute-phase pneumatic conveying in pipe systems. Powder Technology. 99: 90-101.

Ito, H. 1959. Pressure losses in smooth pipe bends. Trans. ASME, Paper 59- Hyd-4.

Jones, M.G. and Williams, K.C. 2003. Solids friction factors for fluidized dense phase conveying. Particulate Science and Technology. 21: 45-56.

Jones, M.G. Williams, K.C. and Busteed, S.S. 2008: Analysis of transient behaviour in the dense phase conveying of powders. In the Proceedings of 4th International Symposium Reliable Flow of Particulate Solids, Norway.

Keys, S. and Chambers, A.J. 1993. Scaling pneumatic conveying characteristics for pipeline pressure drop. In the proceedings of National Conference on Bulk Materials Handling, Preprints, Capricorn International Resort, Yeppoon, Queensland, 22-25 September: 205-213.

Kehlenbeck, R., Yates, J., Felice, R.D., Hofbauer, H. and Reinhard Rauch. 2001. Novel scaling parameter for circulating fluidized beds. AIChE Journal. 47 (3): 582-589.

Kenning, V.M. and Crowe, C.T. 1997. On the effect of particles on carrier phase turbulence in gas-particle flows. International Journal of Multiphase Flow. 23: 403-408.

Keys, S. and Chambers, A.J. 1995. Scaling pneumatic conveying characteristics for Pipeline Pressure. Powder Handling and Processing. 7 (1): 59-62.

King, D.F., Mitchell, F.R.G. and Harrison, D. 1981. Dense phase viscosities of fluidised beds at elevated pressures. Powder Technology. 28: 55-58.

Klinzing, G.E. 1980. A comparison in pressure losses in bends between recent data and models for gas-solid flow. The Canadian Journal of Chemical Engineering. 58: 670-672

Knowlton, T.M. Karri, S.B.R. and Issangya. A. 2005. Scale-up of fluidized-bed hydrodynamics. Powder Technology. 150: 72-77.

Lightstone, M. F. and Hodgson, S.M. 2004. Turbulence modulation in gas-particle flows. Canadian Journal of Chemical Engineering. 82: 209-219.

Ljus, C., Johanson, B. and Almstedt, A.E. 2002. Turbulence modification by particles in a horizontal pipe flow. International Journal of Multiphase Flow. 28: 1075-1090.

Louge, M.Y, Vincent, B. and Martin-Letellier, S. 1999. On the dynamics of pressurized and atmospheric circulating fluidized bed risers. Chemical Engineering Science. 54: 1811-1824.

Marcus, R. D., Hilbert Jr, J.D. and Klinzing, G.E. 1984. The flow through bends in pneumatic conveying systems. Journal of Pipelines. (4): 103-112

Marcus, R.D., Hilbert, J.D. and Klinzing, G.E. 1985. Flow through bends and acceleration zones in pneumatic conveying systems. Bulk Solids Handling. 5 (4): 769-774.

Marcus, R.D., Leung, L.S, Klinzing, G.E. and Rizk, F. 1990. Pneumatic conveying of solids - A theoretical and practical approach. Publ. Chapman and Hall.

314

Marjanovic, P. 1982. A comparative study of performance characteristics for horizontal and vertical pneumatic conveying in pipelines, In the proceedings of the Pneumatech 1. PAC Conference Stratford-upon-Avon, UK

Martinussen, S.E., Woodhead, S.R., deSilva, S.R., Reed, A.R 1995, Reliable conveying conditions and transitions between flow regimes in pneumatic conveyors, In the proceedings of 5th International Conference on Bulk Materials Storage and Transportation, Newcastle.

Mason, J.S. and Boothroyd, R.D. 1971. Comparisons of friction factors in pneumatically conveyed suspensions using different sized particles in pipes of varying size, In the proceedings of Pneumotransport 1, 1st International Conference on the Pneumatic Transport of Solids in Pipes, Guildford, England, 6-8 September, organised by BHRA fluid engineering, Cranfield, Bedford, England: C1 (1-16).

Mason, J.S. and Smith, B.U. 1973. Pressure drop and flow behaviour for the pneumatic transport of fine particles around 90 degree bends. In the proceedings of Pneumotransport 2, 2nd International Conference on the Pneumatic Transport of Solids in Pipes, Guildford, England, 5-7 September, organised by BHRA fluid engineering, Cranfield, Bedford, England: A2 (17-32)

Mason, D. J., Levy, A.; Marjanovic, P. 1998. Influence of bends on the performance of pneumatic conveying systems. Advanced Powder Technology. 9: 197-206.

Mason, D.J. and Levy, A. 2001. A model for non-suspension gas-solids flow of fine powders in pipes. International Journal of Multiphase Flow. 27: 415-435.

315

Mi, B. and Wypych, P.W. 1994. Pressure drop prediction in low-velocity pneumatic conveying. Powder Technology. 81 (2): 125-137.

Mi, B. and Wypych, P.W. 1995. Investigations into wall pressure during slug-flow pneumatic conveying, Powder Technology 84 (1): 91-98.

Michaelidies, E.E. 1987. Motion of particles in gases: Average velocity and pressure loss. Journal of Fluids Engineering. 109: 172-178.

Mills, D., Mason, J.S. and Stacey, R.B. 1982. A design study for pneumatic conveying of fine particular material. In the proceedings of Solidex 82: The solids handling conference, Harrogate, England, pp. C1-C75.

Mills, D. and Mason, J.S. 1985. The influence of bend geometry on pressure drop in pneumatic conveying system pipelines. In the proceedings of 10th International Conference Powder and Bulk Solids Handling, Chicago, IL, USA. Cahners Exhibition Group, Des Plaines, IL: 203-214.

Mills, D. 2004. Pneumatic conveying design guide. Elsevier/Butterworth-Heinemann, 2nd edition.

Mills, D. 2004a. An investigation of the unstable region for dense phase conveying in sliding bed flow. Grannular Matter. 6: 173-177.

Mills, D. 2005. A review of the research work of Professor Predrag Marjanoví´c. Chemical Engineering and Processing. 44: 141-155.

Moody, L.F. and Princeton, N.J. 1944. Friction factor for pipe flows. Trans ASME. 66 (8): 671-684.

Motte, J. and Molodtsof, Y. 2001. Predicting transport velocities. Powder Technology. 120: 120-126.

Namkung, W., Sung W. K. and Sang D. K. 1999. Flow regimes and axial pressure profiles in a circulating fluidized bed. Chemical Engineering Journal. 72 (6): 245-252.

Nikuradse, J. 1932. Gestzmässigkeiten derturbulenten Strömung in glatten Rofren, ver. Dtsch. Ing. Forscheungsh. 356

Pan, R. 1992. PhD Dissertation: Improving scale-up procedures for the design of pneumatic conveying systems, University of Wollongong.

Pan, R. and Wypych, P.W. 1992. Scale up procedures for pneumatic conveying design. Powder Handling and Processing. 4 (2): 167-172.

Pan, R., Mi, B. and Wypych, P.W. 1994. Pneumatic conveying characteristics of fine and granular bulk solids. KONA (Powder and Particle). 12: 77-85.

Pan, R. and Wypych, P.W. 1997. Pressure Drop and Slug Velocity in Low-Velocity Pneumatic Conveying of Bulk Solids. Powder Technology. 94: 123-132.

Pan, R. and Wypych, P.W. 1998. Dilute and dense phase pneumatic conveying of fly ash. In the proceedings of 6th International Conference on Bulk Materials Storage and Transportation, Wollongong, NSW, Australia: 183-189.

Pan, Y. and Banerjee, S. 1996. Numerical simulation of particle interactions with wall turbulence. Physics of Fluids. 8 (10): 2733-2755.

Pugsley, T.S., Berruti, F., 1996. A predictive hydrodynamic model for circulating fluidized bed risers. Powder Technology. 89: 57-69.

Rashidi, M., Hetsroni, G. and Banerjee, S. 1990. Particle-turbulence interaction in a boundary layer. International Journal of Multiphase Flow. 16 (6): 935-949.

Ratnayake, C. and Datta, B.K. 2007. A Unified scaling-up technique for pneumatic conveying systems. Particulate Science and Technology. 25: 289-302

Rees, A.C., Davidson, J.F., Dennis, J.S. and Hayhurst, A.N. 2005. The rise of a buoyant sphere in a gas-fluidized bed. Chemical Engineering Science. 60: 1143-1153.

Rizk, F. 1976. Pneumatic conveying at optimal operating conditions and a solution of Barth's equation $\lambda_z = \Phi$ (λ_z^*, β). In the proceedings of 3rd International Conference on the Pneumatic Transport of Solids in Pipes, 7-9th April: D4 (43-58).

Rizk, F. 1982. Pneumatic transport in dilute and dense phase. Bulk Solids Handling. 2 (2): 235-241.

Roski, H.-J. 1987. The influence of stepped-pipelines in pneumatic long-distance transport of building materials. In the proceedings of Pneumatech 3: 3rd International conference on pneumatic conveying technology, U.K.

Schi, D and D'Agastino, R. 1995. Practical Engineering Statistics. John Wiley & Sons, Inc.

Schuchart, P. 1968. Widerstansgesetze beim pneumatischen Transport in Rohrkrummern, Symposium series no. 27 (The Institution of Chemical Engineers): 65 – 72.

Shook, C.A. and Roco, M.C. 1991. Slurry flow - principles and practice, Publ. Butterworth – Heinemann.

Streeter, V. L. and Benjamin, W.E. 1979. Fluid mechanics. Publ. McGraw-Hill.

Stegmaier, W. 1978. Zur berechnung der horinentalen pneumatischen forderung feinkorniger feststoffe - for the calculation of horizontal pneumatic conveying of fine grained solids. Fordern and Heben. 28: 363-366.

Swamee, P.K. and Jain, A.K. 1976. Explicit equations for pipe-flow problems, Journal of the Hydraulics Division, ASCE. 102 (5): 657–664.

Teplitskiy, Y. S. 1999. Similarity of transport processes in fluidized beds. International Journal of Heat and Mass Transfer. 42: 3887-3899.

Teplitskiy, Y.S. and Ryabov, G.A. 1999. Scaling in a circulating fluidized bed: particle concentration and heat transfer coefficient in a transport zone. International Journal of Heat and Mass Transfer. 42: 4065-4075.

Wang, W. and Li, Y. 2001. Hydrodynamic simulation of fluidization by using a modified kinetic theory. Ind. Eng. Chem. Res. 40: 5066-5073.

Wang B., Zhang, H.Q. and Wang X. L. 2006. Large eddy simulation of particle response to turbulence along its trajectory in a backward-facing step turbulent flow. International Journal of Heat and Mass Transfer. 49: 415-420.

Weber, M. 1981. Principles of hydraulic and pneumatic conveying on pipes. Bulk Solids Handling. 1 (1): 57-63.

Weber, M. 1982. Correlation analysis in the design of pneumatic transport plant. Bulk Solids Handling. 2 (2): 231-233.

Weber, M. 1991. Friction of the air and the air/solid mixture in pneumatic conveying. Bulk Solids Handling. 11 (1): 99-102.

Williams, K.C. and Jones, M.G. 2004. Numerical model velocity profile of fluidised dense phase pneumatic conveying. In the proceedings of 8th International Conference on Bulk Materials Storage and Transportation, Wollongong, NSW, Australia, 5-8 July: 354-358.

Williams, K.C. and Jones, M.G. 2006. Solid friction power law variations and their influence on pressure losses in fluidised dense phase pneumatic conveying. In

the proceedings of The Fifth World Congress on Particle Technology. April 23-26, Florida, USA.

Williams, K., Olszewski, T., Jones, M. and Singh, B. 2008. Electrical capacitance tomography of dense-phase pneumatic conveying of fly ash powder. In the proceedings of Bulk Europe 2008, Czech Republic.

Wirth, K.E. and Molerus, O. 1983. Prediction of pressure drop with pneumatic conveying of solids in horizontal pipes. Journal of Powder and Bulk Solids Technology. 7 (2): 17-20

Wirth, K.E., 1988. Axial pressure profile in circulating fluidized beds. Chem. Eng. Technol. 11: 11-17.

Westman, M.A., Michaelidies, E.E and Thompson, F.M. 1987. Pressure losses due to bends in pneumatic conveying. Journal of Pipelines. 7: 15-20.

Wypych, P.W. and Arnold, P.C. 1984. The use of powder and pipe properties in the prediction of dense phase pneumatic transport behaviour. In the proceedings of Proceedings of the Technical Program, Pneumatech 2, International Conference on Pneumatic Conveying Technology, University of Kent, Canterbury, England, 4-6 September, Organised by the Powder Advisory Centre, London, England.

Wypych, P.W. and Arnold, P.C. 1985. A standardised test procedure for pneumatic conveying design. Bulk Solids Handling. 5 (4): 755-763.

Wypych, P.W. and Arnold, P.C. 1987. On improving scale-up procedures for pneumatic conveying design. Powder Technology. 50: 281-294.

Wypych, P. W. 1989. PhD Dissertation: Pneumatic conveying of bulk solids, University of Wollongong.

Wypych, P.W. and Arnold, P.C. 1989a. Meeting the demands of long distance and large throughput pneumatic transportation. In the proceedings of 3rd International Conference on Bulk Materials Storage and Transportation, Newcastle, Australia, 27-29 June: 78-83.

Wypych, P. W., Arnold, P. C. and Armitage, W.R. 1989b. Demands of long distance and large throughput pneumatic conveying applications in Australia. In the proceedings of 6th International Symposium on Freight Pipelines, Columbia, USA: 81-84.

Wypych, P.W., Kennedy, O.C. and Arnold, P.C. 1990. The future potential of pneumatically conveying coal through pipelines. Bulk Solids Handling. 10 (4): 421-427

Wypych, P.W., Kennedy, O.C. and Arnold, P.C. 1990a. Pneumatic conveying of pulverized and crushed R.O.M. coal. In the proceedings of 4th International Conference on Pneumatic Conveying Technology, Glasgow, Scotland, 26-28 June.

Wypych, P.W. and Pan, R. 1991, Determination of air only pressure drop in pneumatic conveying systems. Powder Handling and Processing. 3 (4): 303-309.

Wypych, P.W. 1993. Optimising and up rating pneumatic transport systems. National Conference on Bulk Materials Handling, Preprints, Capricorn International Resort, Yeppoon, Queensland, 22-25 September: 197-203.

Wypych, P.W and Yi, J. 2003. Minimum transport boundary for horizontal dense-phase pneumatic conveying of granular materials. Powder Technology. 129: 111-121.

Wypych, P.W., Hastie, D. B. and Yi, J. 2005. Prediction of optimal operating conditions for dense-phase pneumatic conveying systems. Final research report for the International Fine Particle Research Institute, Inc, USA.

Wypych, P.W. and Hastie, D.B. 2006. Modelling solids friction factor for dense-phase pneumatic conveying of powders. In the proceedings of the Fifth World Congress on Particle Technology, April 23 – 26, Florida, USA.

Yuan, Z. and Michaelides, E.E. 1992. Turbulence modulation in particulate flows – a theoretical approach. International Journal of Multiphase Flow. 18 (5): 779-785.

Yi, J., Wypych, P.W. and Pan, R. 1998. Minimum conveying velocity in dilute-phase pneumatic conveying. Powder Handling and Processing. 10 (3): 255-261.

Zhang, M.C. and Wang, R.Y.K. 1987. On the scaling laws of bubbling gas fluidized bed dynamics. Powder Technology. 51: 159-165.

APPENDIX: A1

A1.1 Calibration of DP meters (80 and 150 inch)

Calibration of Differential Pressure (DP) Meter

trial1

80 inch DP meter

% Reading (of full range of DP meter)	Differetial Pressure (kPa) & mv*		calibration factor (Pr/mv)
	kpa	mv	
8.2	1.66	4.28	0.387850467
10.6	3.66	8.31	0.440433213
28.8	5.73	13.071	0.438375029
41.3	8.2	18.334	0.447256463
49.6	9.89	22.355	0.44240662
61.5	12.24	26.848	0.455899881
71.1	14.1	30.541	0.46167447
78.8	15.65	34.04	0.459753231
91.8	18.22	39.527	0.460950743
100.0	19.85	42.985	0.461788996
Average calibraion factor			0.85902

trial2

80 inch DP meter

% Reading (of full range of DP meter)	Differetial Pressure (kPa) & mv*		calibration factor (Pr/mv)
	kpa	mv	
10.2	2.1	5.144	0.408242613
21.1	4.23	9.519	0.444374409
29.2	5.89	13.122	0.448864502
39.2	7.83	17.219	0.45473024
49.1	9.8	21.593	0.453850785
58.0	11.58	25.442	0.455152897
68.3	13.65	30.439	0.448437859
79.4	15.87	34.336	0.462197111
88.0	17.53	38.191	0.459008667
99.9	19.91	43.219	0.460677017
Average calibraion factor			0.865243

Average calibration factor of trial-1 and 2   0.46874

trial1

150 inch DP meter

% Reading (of full range of DP meter)	Differetial Pressure (kPa) & mv*		calibration factor (Pr/mv)
	kpa	mv	
9.9	3.66	5.09	0.719056974
19.6	7.33	9.475	0.773614776
30.6	11.43	14.386	0.794522452
41.8	15.68	19.615	0.799388223
51.0	19.13	22.801	0.83899829
63.5	23.82	28.332	0.840745447
69.3	26.01	30.901	0.841720333
79.0	29.61	35.017	0.845589285
90.6	33.96	40.598	0.836494409
99.8	37.37	44.307	0.843433318
Average calibraion factor			0.85902

trial2

150 inch DP meter

% Reading (of full range of DP meter)	Differetial Pressure (kPa) & mv*		calibration factor (Pr/mv)
	kpa	mv	
9.6	3.54	4.931	0.717907118
19.9	7.45	9.341	0.797559148
30.0	11.22	13.658	0.821496559
38.2	14.34	17.272	0.830245484
49.4	18.53	22.146	0.836719949
60.2	22.57	26.988	0.836297614
68.9	25.82	30.657	0.842222005
79.0	29.58	35.489	0.833497704
89.6	33.55	39.169	0.856544716
99.6	37.27	44.017	0.846718313
Average calibraion factor			0.865243

Average calibration factor of trial-1 and 2   0.862

* the mv readings were read from the "raw data" sheet of data taker/processing program

A1.2 Results: Preliminary air only tests with 80 inch DP meter installed on 69 mm I.D. × 148 m long pipeline

START TIME sec	FINISH TIME sec	AIR MASS FLOWRATE kg/s	LOAD CELL KBI SILO kg/s	PRESSURE CH9 = P8 kPa g	PRESSURE CH13=P11* kPa g	PRESSURE CH14=P12 kPa g	80 inch DP CH15=DP kPa g	DP as per Static Diff	DP(static diff)- DP(meter)	% variation w.r.t DP
50	100	0.039938	0.050694	2.756227	1.0147356	0.3736129	0.318879	0.641123	0.322244	101.06
51	74	0.058852	0.445761	4.683651	1.8081211	0.5173445	0.568571	1.290777	0.722206	127.02
60	90	0.082835	0.402048	9.715406	2.991295	1.532609	1.077203	1.458686	0.381483	35.41
55	75	0.108473	0.530668	15.05207	4.6499711	2.9245185	1.758849	1.725453	-0.0334	-1.90
60	85	0.128867	0.191334	20.3602	5.8478732	3.7201067	2.389827	2.127767	-0.26206	-10.97
50	90	0.15766	0.047185	29.69071	9.218621	5.697446	3.555807	3.521175	-0.03463	-0.97
80	120	0.179822	0.085673	36.82603	11.802716	7.0541312	4.455582	4.748585	0.293003	6.58
70	100	0.204526	0.058668	45.64075	15.032602	8.785803	5.699532	6.246799	0.547267	9.60

A1.3   Results: Preliminary air only tests with water manometer and 80 inch DP meter installed on 69 mm I.D. × 148 m long pipeline

START TIME sec	FINISH TIME sec	AIR MASS FLOWRATE kg/s	LOAD CELL KBI SILO kg/s	PRESSURE CH13=P11* kPa g	PRESSURE CH14=P12 kPa g	80 inch DP CH15=DP kPa	DP as per Static Diff CH13-CH14 kPa	DP as per Manometer kPa	(Static-DP)/ DP %	(Static-Mano)/ Mano %	(DP-Mano)/ Mano %
160	200	0.056	0.040	1.485	0.956	0.535	0.530	0.551	-0.992	-3.843	-2.880
80	110	0.080	0.045	2.776	1.675	1.010	1.101	1.062	9.063	3.695	-4.922
60	90	0.109	0.046	4.821	2.978	1.832	1.843	1.938	0.547	-4.927	-5.445
60	95	0.127	0.071	6.305	3.923	2.408	2.382	2.480	-1.073	-3.961	-2.920
70	110	0.154	0.041	9.135	5.586	3.442	3.549	3.641	3.133	-2.514	-5.475
60	100	0.179	0.054	11.794	7.248	4.526	4.546	4.743	0.445	-4.161	-4.586
125	150	0.205	0.103	14.923	9.133	5.753	5.791	6.000	0.650	-3.486	-4.109
110	130	0.238	0.774	19.200	11.823	7.299	7.377	7.665	1.066	-3.759	-4.775

A1.4 Specification of data-logger DT800

Analog Channels

Channel Number
Two wire: 24, or 42 with one shared terminal
Three wire: 12, or 18 with one shared terminal, 36 with two shared terminals
Four wire: 12, or 18 with two shared terminals
Six wire bridges: 6, or 18 with two shared terminals
Sensor configurations may be mixed in any combination.

Fundamental Input Ranges
The fundamental inputs that the *DT800* can measure are voltage, resistance and frequency. All other measurements are derived from these.

Full Scale	Resolution	Full Scale	Resolution
±10 mVdc / mVac	1 µV	20 Ω	100 µΩ
±20 mVdc / mVac	2 µV	50 Ω	25 µΩ
±50 mVdc / mVac	5 µV	100 Ω	500 µΩ
±100 mVdc / mVac	10 µV	200 Ω	1 mΩ
±200 mVdc / mVac	20 µV	500 Ω	3 mΩ
±500 mVdc / mVac	50 µV	1,000 Ω	5 mΩ
±1 Vdc / Vac	100 µV	2,000 Ω	100 mΩ
±2 Vdc / Vac	200 µV	5,000 Ω	25 mΩ
±5 Vdc / Vac	500 µV	10,000 Ω	50 mΩ
±10 Vdc / Vac	1 mV	10 kHz	0.01 Hz
±13 Vdc / Vac	2 mV		

Accuracy

Measurement at ...	25°C	−45°C to 70°C
DC Voltage	0.02%	0.10%
AC Voltage (50Hz - 1kHz)	1.0%	1.5%
DC Resistance	0.04%	0.20%
Frequency	0.02%	0.04%

Accuracy table above is % of reading ±0.01% of full scale.

Sensor Excitation
Programmable with 12 bit resolution, available on any analog channel as a balanced output:
DC Voltage mode: 0 to 20V
DC Current mode: 0 to 15mA
DC Power mode: 0 to 200mW

Multiplexer
Type: solid-state
Common mode range: ±13V or −2V to 22V selectable
Over voltage protection: ±40V
Lightning protection: secondary, via ±30V varistors

Sampling Modes
Normal Mode
Sampling for accuracy and noise rejection by interleaved sampling over one or more line cycle periods.
Effective resolution: 16 bits
Common mode rejection 20mV range: 130dB
Fast Mode
Fast continuous sampling with reduced noise rejection
Effective resolution: 15 bits
Burst Mode
Provides sampling of fast events with triggering capability
Sampling speed: 1kHz to 100kHz
Effective resolution: 13bits
Trigger: pre, mid and post triggering
Trigger sources: analog level or digital input
Buffer size: 100 to 65,000 raw samples
Minimum time between bursts: 100ms - 30ms

The table following indicates the speed in samples per second per channel attainable for various channel types and in different sampling modes with default settings. Higher speeds are possible by fine tuning the *dataTaker* data logger settings.

Sampling Speed

Input Type	Mode	No. Channels			
		1	5	10	20
Voltage (no corrections)	Normal	37	27	14	9
	Fast	98	50	36	20
	Burst	50k	6k	3k	1.5k
Voltage, Current Strain (voltage excite)	Normal	29	8	4	2
	Fast	72	27	15	8
	Burst	25k	3k	1.5k	750
Thermocouple	Normal	25	6	3	1.7
	Fast	59	20	10	5
	Burst	12k	3k	1.5k	750
Resistance, RTDs Strain (current excite)	Normal	23	4	2	1
	Fast	48	15	8	4
	Burst	12k	1.5k	750	350
AC (rms) Voltage	Normal	1	0.2	0.1	0.05
Frequency	Normal	32	8	4	2
		Samples / Second / Channel			

Sensor Support
Supports a wide range of sensors including, but not limited to, those listed below. A wide range of sensor scaling and linearising facilities is provided including polynomials, expressions and functions.

Thermocouples
Types: B, C, D, E, G, J, K, N, R, S, T
Calibration standard: ITS-90
Accuracy (case at 25°C): per NIST Monograph 125
Reference junction compensation accuracy:

Case Temperature	25°C	−20°C to +60°C
Accuracy	±0.2°C	±0.5°C

Thermocouple integrity testing by resistance measurement.

RTD's
Materials supported: Pt, Ni, Cu
Resistance range: 10 to 10KΩ
Resistance measurement accuracy:
4 wire: 0.05 %, 3 wire: 0.15 %

Thermistors
Types: YSI 400xx Series
Resistance range: <10kΩ,
<20kΩ with parallel resistor

Monolithic Temperature Sensors
Types supported: LM34 - 60, AD590, 592

Bridge Sensors
Configurations: 4-wire and 6-wire
Excitation: voltage or current
Bridge completion: external

4-20mA Current Loop
Shunt: External 20Ω - 200Ω resistor

Analog Output
Number of channels: 1 (share with burst mode trigger)
Voltage range: −10V to +10V (10mV resolution)
Maximum current: 20mA

Digital Channels
Bi-directional channels: 8, 2 of which have 10mV sensitive inputs for magnetic pick-ups
Input only channels (logic level): 8

Counter Channels
Number: 16, shared with digital I/O channels
Size: 32 bit (>4,000,000,000 counts)
Speed: Channels 1-6 100Hz (3Hz in Sleep Mode)
Channels 7-8 10kHz (1kHz in Sleep Mode)
Channels 9-16 100Hz (3Hz in Sleep Mode)

Digital Output
Number: 8 shared with bi-directional channels
Output type: open-drain FET, +30V, 100mA

Serial Sensor Channel
Modes: RS232, RS422, RS485, SDI-12
Handshake lines: RTS, CTS
Baud rate: 300 to 56k baud
Power for sensors: derived from system supply (9-26 at 300mA)
Programmable prompt string
Data parsing allows multiple assignments to variables

Calculation Channels
Any expression involving variables and functions
Functions: sin(), cos(), tan(), asin(), acos(), atan(), abs(), sqrt(), average, maximum, minimum, time of max, time of min, variance, integral, histogram, rainflow (fatigue analysis)

Alarms
Condition: high, low, within range and outside range
Delay: optional time period for alarm response
Actions: set digital outputs, execute any *dataTaker* command, transmit message

Scheduling of Data Acquisition
Number of schedules: 11
Schedule rates: 10ms to days
Maximum number of channels: 500

Data Storage
Internal RAM
Capacity: >130k data points, dual battery backed SRAM
PC Card
Types: ATA FLASH and hard-disks, all sizes, 3V or 5V
Compact Flash, Smart Media, Sony Stick with adaptor
Capacity: >65,000 data points per megabyte,
5 channels/schedule, Windows file format

Communication Interfaces
Ethernet
Interface: 10BaseT
Protocols: TCP/IP (UDP, FTP)
RS232
Speed: 300 to 115k baud (57,600 default)
Handshake lines: DCD, RI, DSR, DTR, RTS, CTS
Modem support: auto-answer and dial out
Protocols: PPP, TCP/IP (UDP, FTP)

System
Firmware Upgrade
Via: RS232, Ethernet or FLASH PC Card
Real Time Clock
Normal resolution: 200µs
Accuracy: 10s per month at 25°C
PC Card (PCMCIA) Support
Number of slots: 1 x Type I, II or III (PCMCIA 2.1)
Card types: ATA FLASH
Socket voltage: 3V or 5V (400mA) and 12V (60mA)
Power Supply
External voltage range: 11 to 28V$_{dc}$
Power Consumption
In normal mode: 5W
Sleep mode: 5mW (400µA from internal 12V battery)
Internal Main Battery
Voltage (Capacity): 12V (2.2AHr) lead acid gel cell
Temperature compensated charging: −10°C to +70°C
Operating time: continuous sampling: 5 hours
10 minute sampling: 1 months
1 hour sampling: 4 months
Memory and Real Time Clock Battery
Voltage (Capacity): 3.6V (400mAHr) lithium, 1/2 AA

Physical and Environment
Construction: Powder coated fabricated steel
Dimensions: 260 x 110 x 90mm
Weight: 3.1kg (5.5kg shipping)
Temperature range: −45°C to 70°C
Humidity: 85% RH, non-condensing

Accessories Included
Resource CD: includes software, video training and user manual
Line adaptor: 110/240Vac to 15Vdc, 800mA
Comms cable: for PC RS232 and USB adaptor
Tools: single and dual cage clamp tools

dataTaker®

'Please see print copy for image'
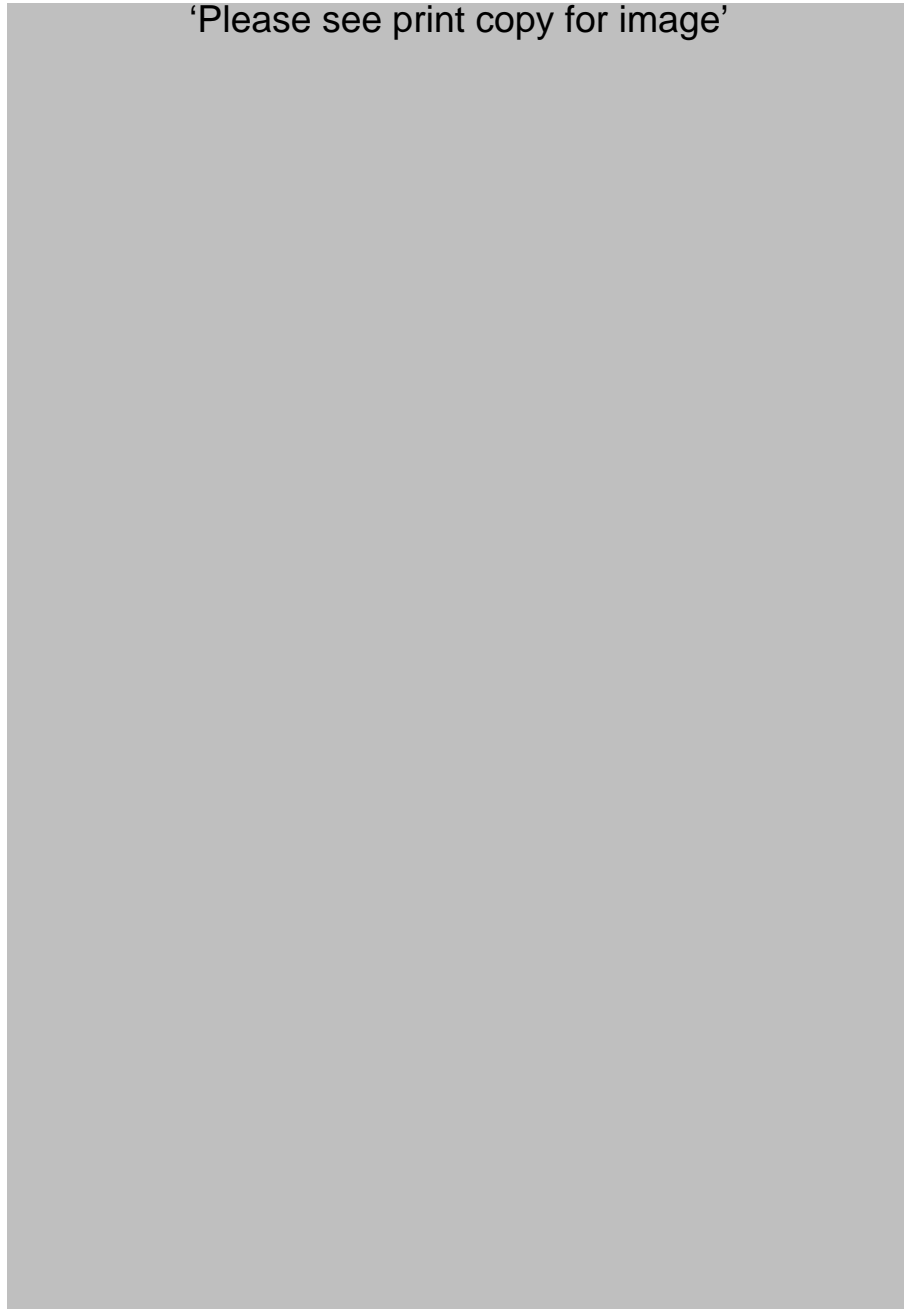
Figure A1.1: Exploded View of a Typical Static Pressure Tapping (Pan 1992)

APPENDIX: A2

'Please see print copy for image'

Figure A2.1: Experimental Versus Predicted PCC for Fly Ash (Pan, 1992) and 69 mm I.D. × 168 m Pipe using Stegmaier (1978) Model

'Please see print copy for image'

Figure A2.2: Experimental Versus Predicted PCC for Fly Ash (Pan, 1992) and 69 mm I.D. × 554 m Pipe using Stegmaier (1978) Model

'Please see print copy for image'

Figure A2.3: Experimental Versus Predicted PCC for "White Powder" and 69 mm I.D. × 148 m Pipe using Stegmaier (1978) Model

'Please see print copy for image'

Figure A2.4: Experimental Versus Predicted PCC for Fly Ash (Pan, 1992) and 69 mm I.D. × 168 m Pipe using Weber (1981) Model

'Please see print copy for image'

Figure A2.5: Experimental Versus Predicted PCC for "White Powder" and 69 mm I.D. × 148 m Pipe using Weber (1981) Model

'Please see print copy for image'

Figure A2.6: Experimental Versus Predicted PCC for ESP Dust and 105 mm I.D. × 168 m Pipe using Jones and Williams (2003) Model

'Please see print copy for image'

Figure A2.7: Experimental Versus Predicted PCC for Fly Ash (Pan, 1992) and 69 mm I.D. × 168 m Pipe using Jones and Williams (2003) Model

APPENDIX: A3

A3.1 Results of scale-up evaluation
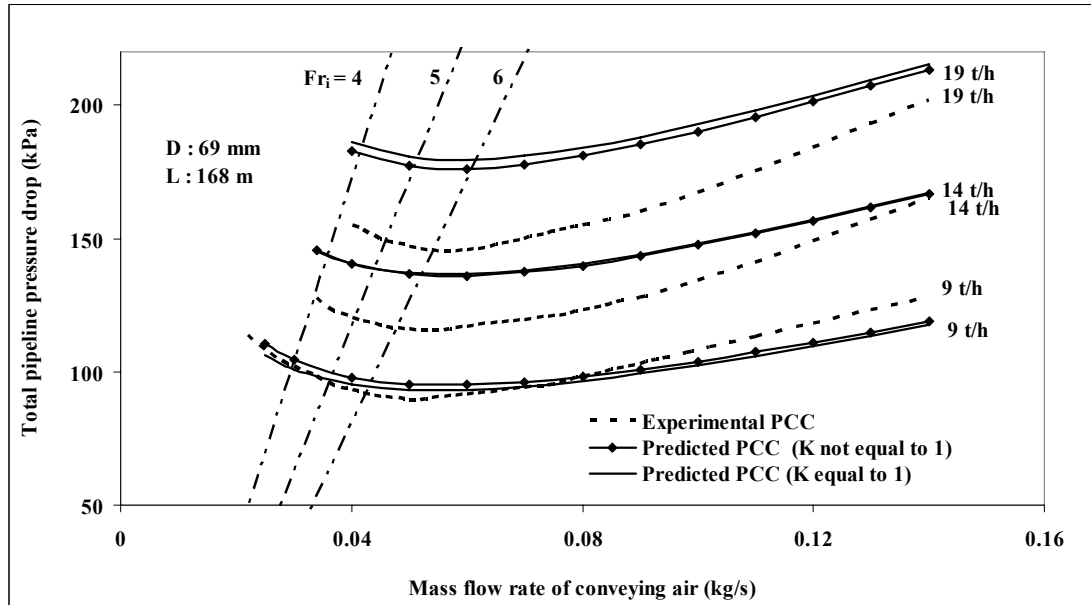
Figure A3.1: Experimental Versus Predicted PCC for Fly Ash and 69 mm I.D. × 168 m Pipe using Equations (7.10) and (7.11)
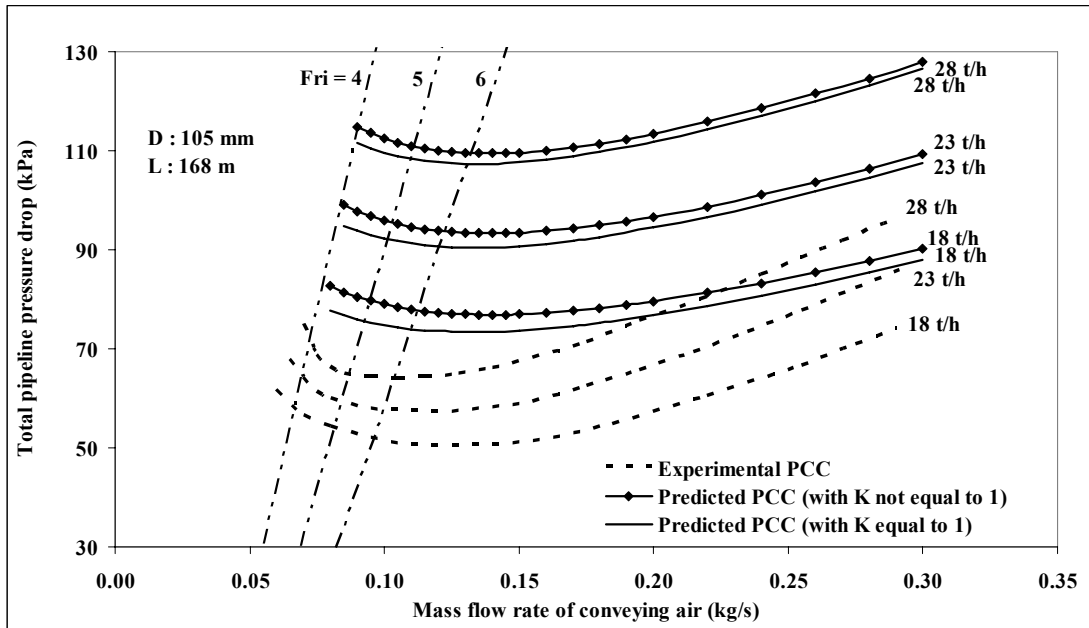
Figure A3.2: Experimental Versus Predicted PCC for Fly Ash and 105 mm I.D. ×

168 m Pipe using Equations (7.10) and (7.11)
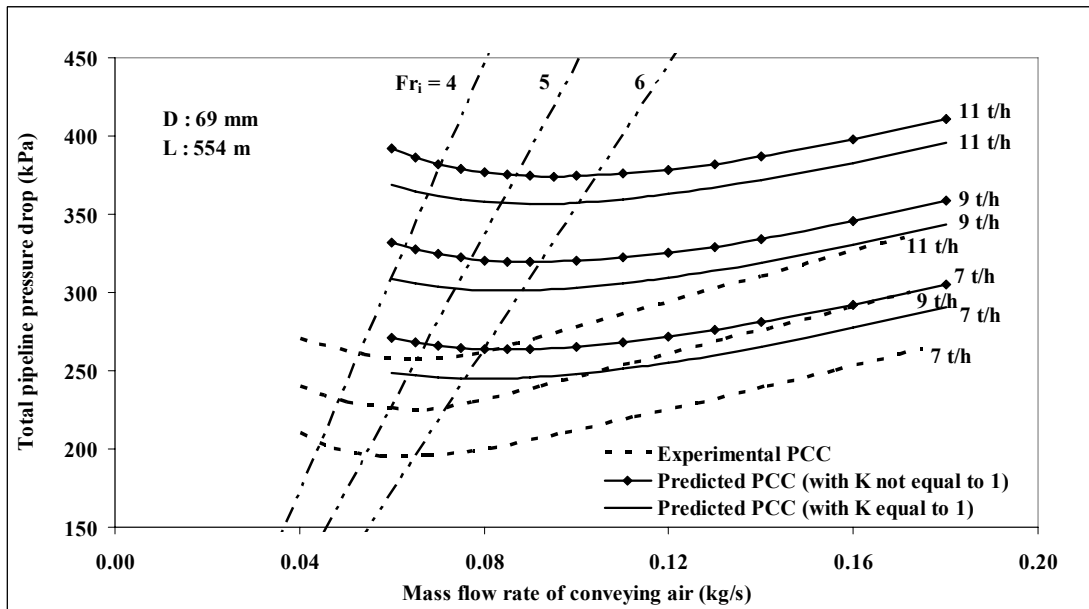
Figure A3.3: Experimental Versus Predicted PCC for Fly Ash and 69 mm I.D. × 554

m Pipe using Equations (7.10) and (7.11)
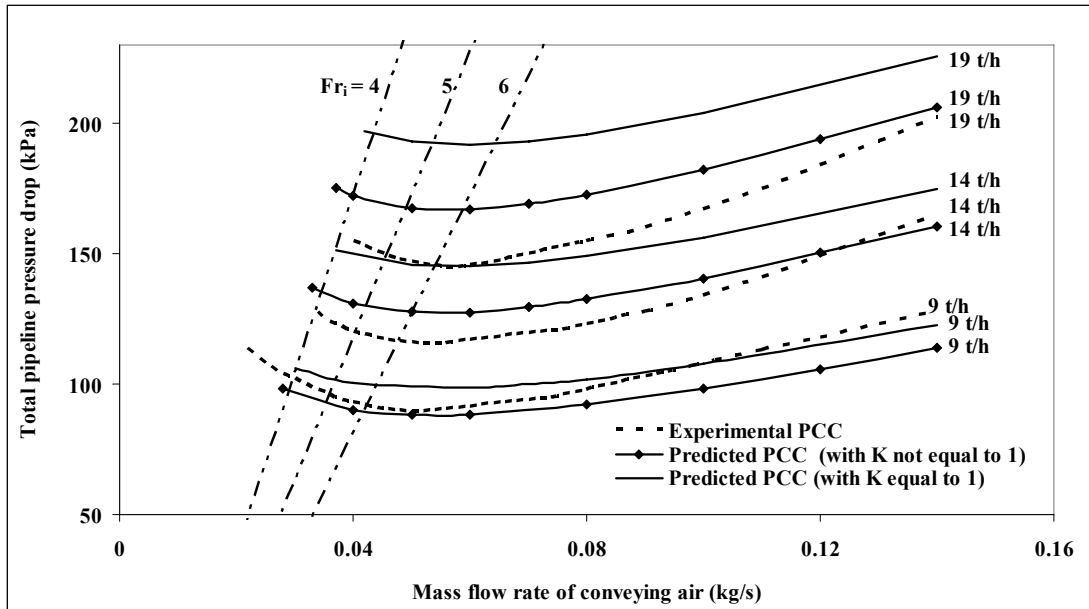
Figure A3.4: Experimental Versus Predicted PCC for Fly Ash and 69 mm I.D. × 168 m Pipe using Equations (7.27) and (7.28)
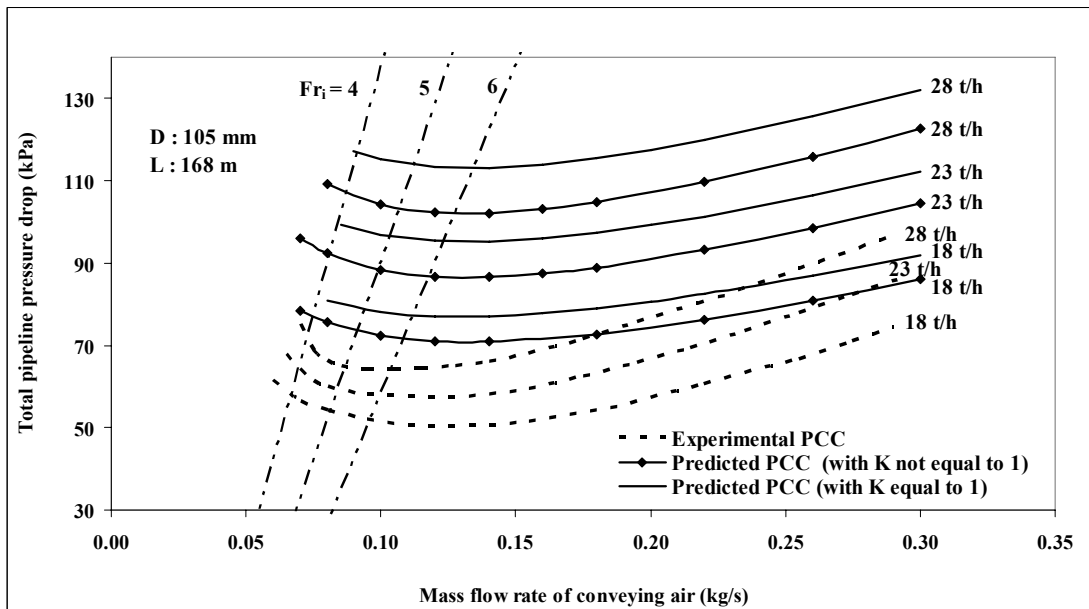
Figure A3.5: Experimental Versus Predicted PCC for Fly Ash and 105 mm I.D. × 168 m Pipe using Equations (7.27) and (7.28)

337
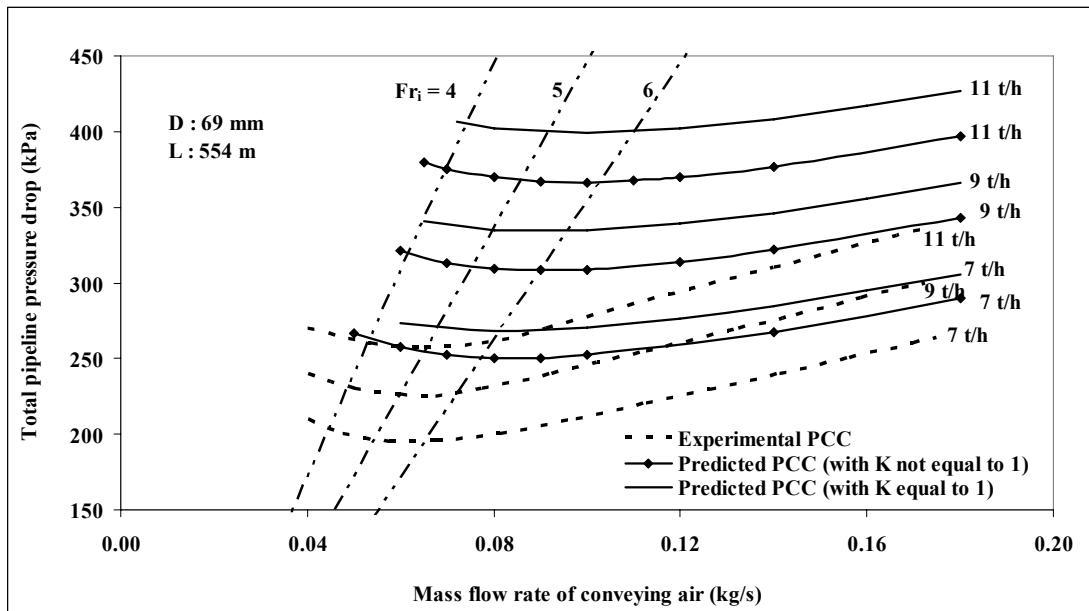
Figure A3.6: Experimental Versus Predicted PCC for Fly Ash and 69 mm I.D. × 554

m Pipe using Equations (7.27) and (7.28)
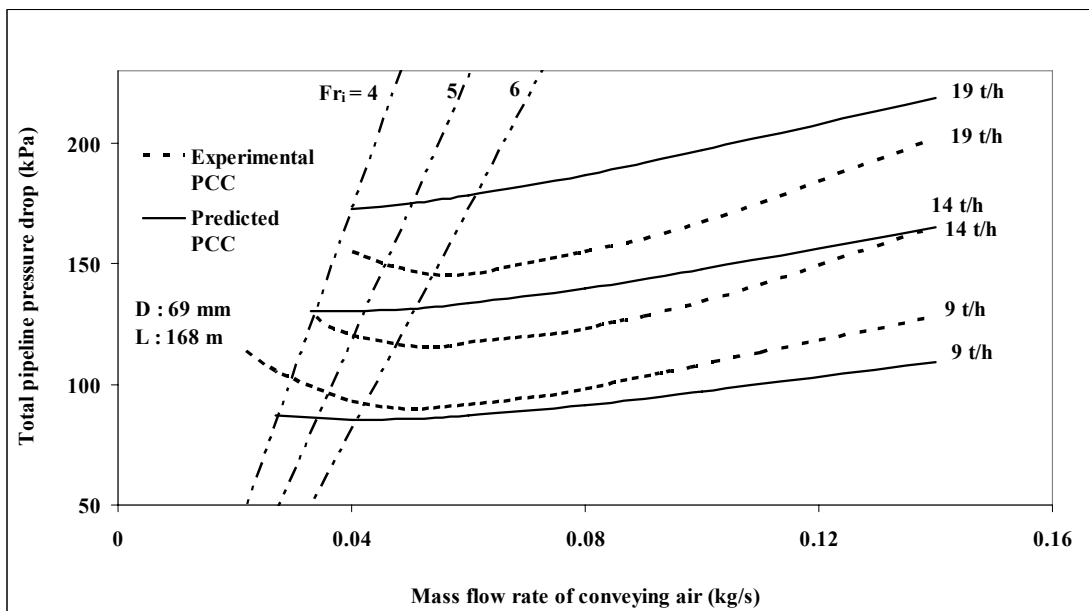
Figure A3.7: Experimental Versus Predicted PCC for Fly Ash and 69 mm I.D. × 168

m Pipe using Equation (7.44)
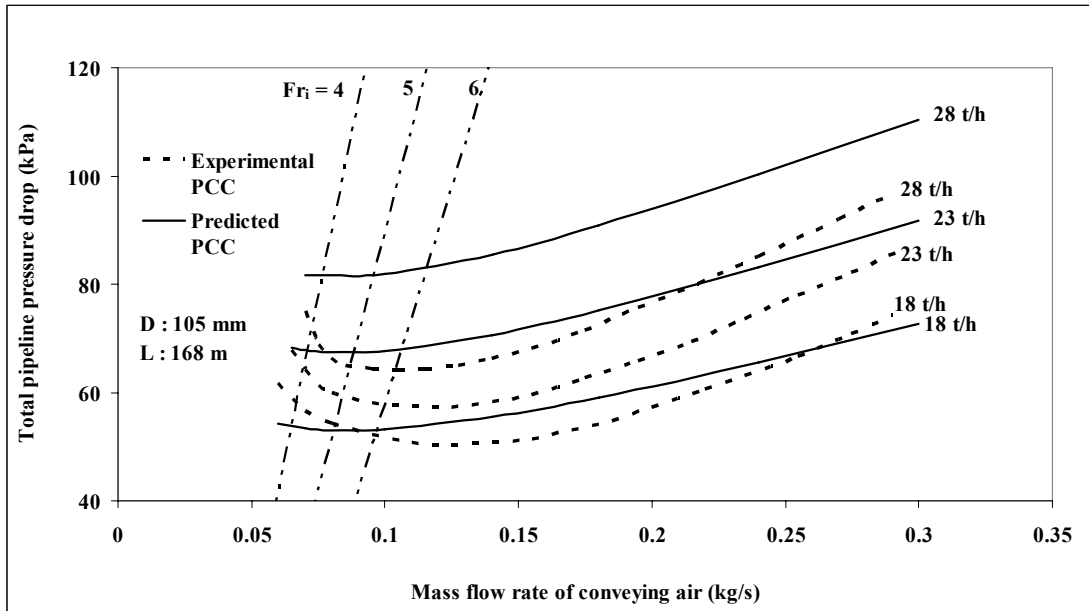
Figure A3.8: Experimental Versus Predicted PCC for Fly Ash and 105 mm I.D. × 168 m Pipe using Equation (7.44)
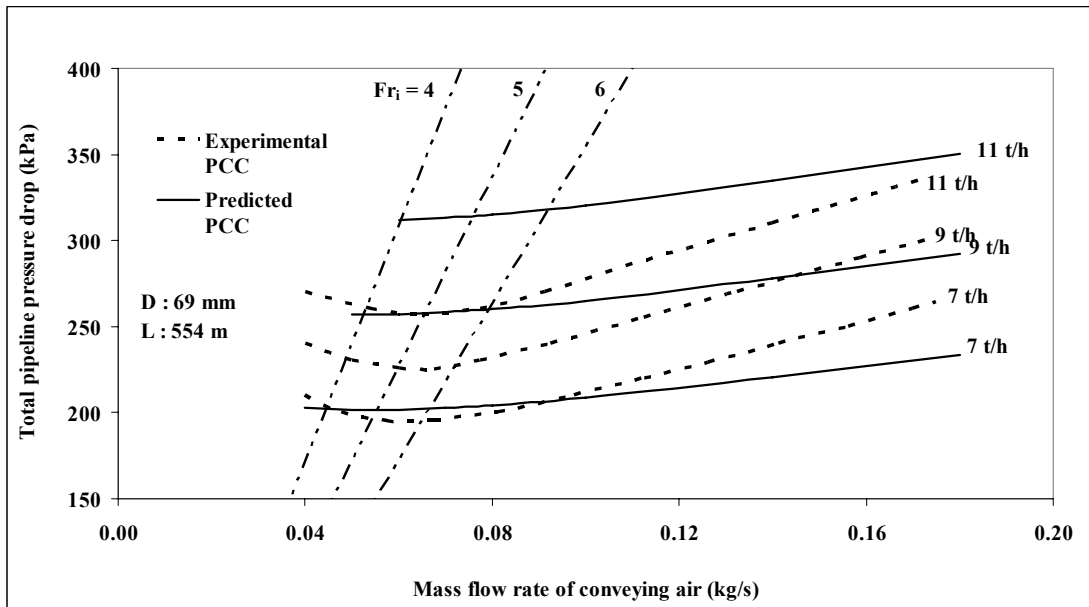
Figure A3.9: Experimental Versus Predicted PCC for Fly Ash and 69 mm I.D. × 554 m Pipe using Equation (7.44)
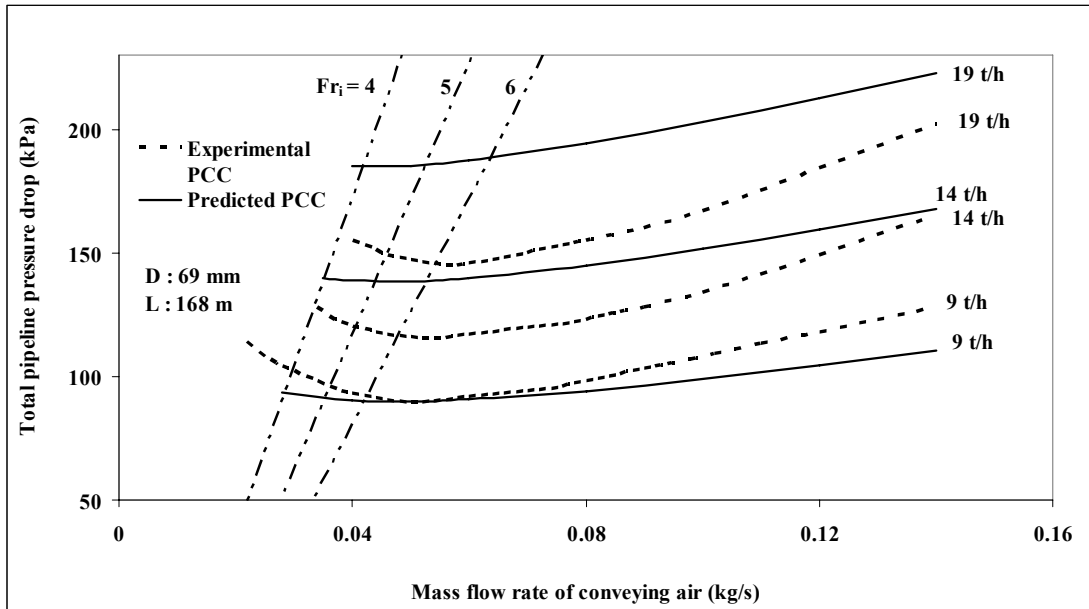
Figure A3.10: Experimental Versus Predicted PCC for Fly Ash and 69 mm I.D. ×

168 m Pipe using Equation (7.45)
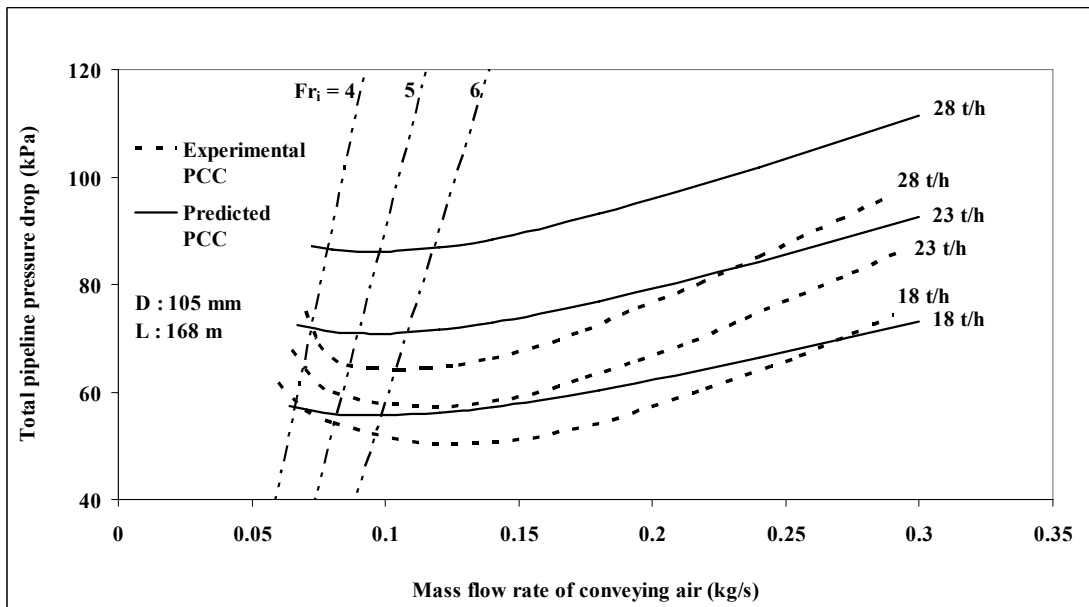
Figure A3.11: Experimental Versus Predicted PCC for Fly Ash and 105 mm I.D. ×

168 m Pipe using Equation (7.45)
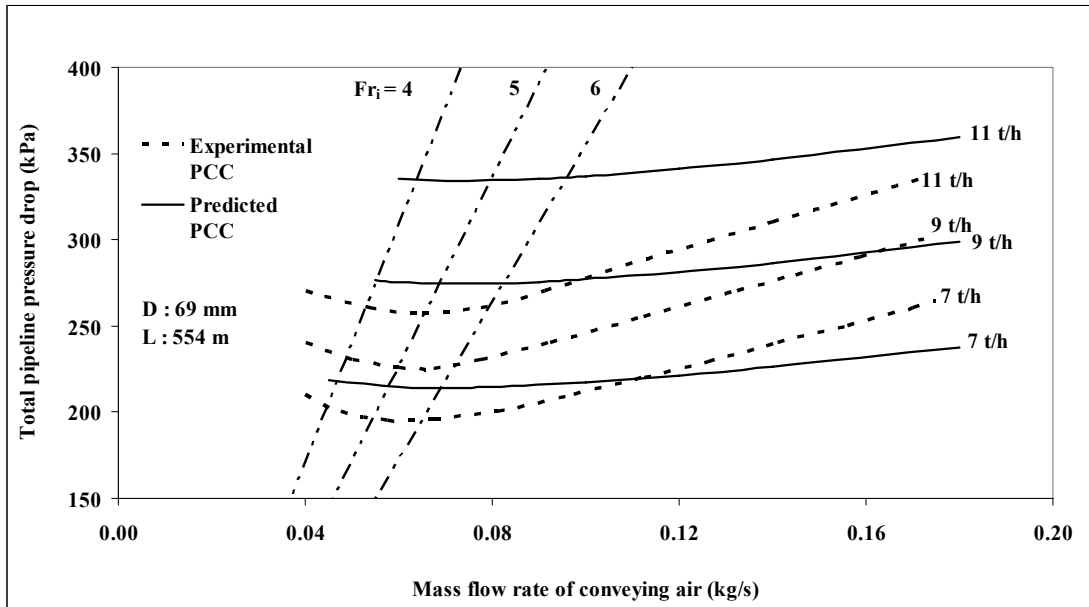
Figure A3.12: Experimental Versus Predicted PCC for Fly Ash and 69 mm I.D. × 554 m Pipe using Equation (7.45)
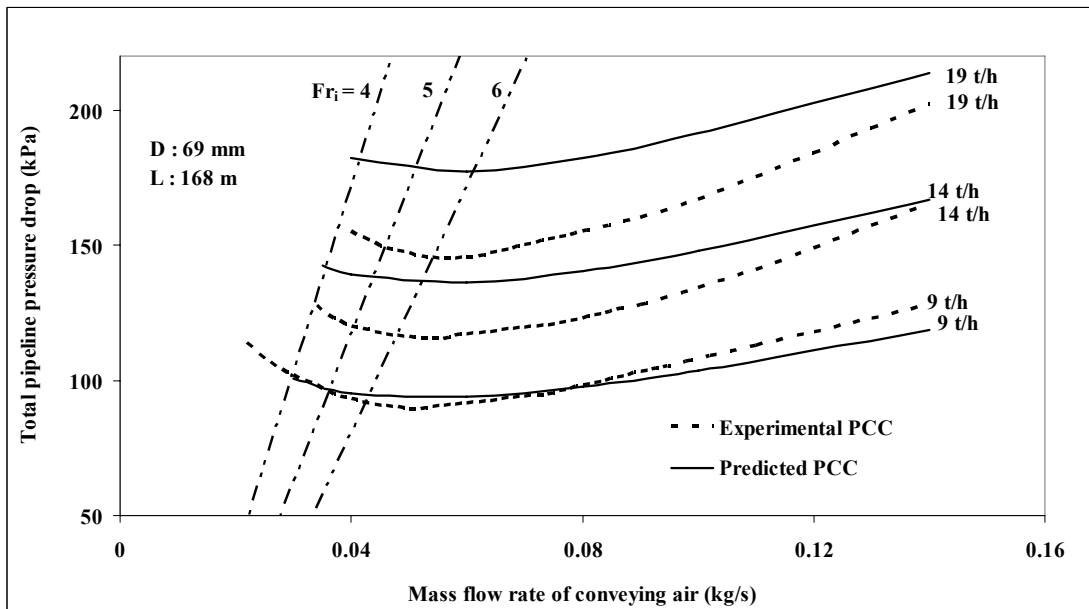
Figure A3.13: Experimental Versus Predicted PCC for Fly Ash and 69 mm I.D. × 168 m Pipe using Equation (7.49)
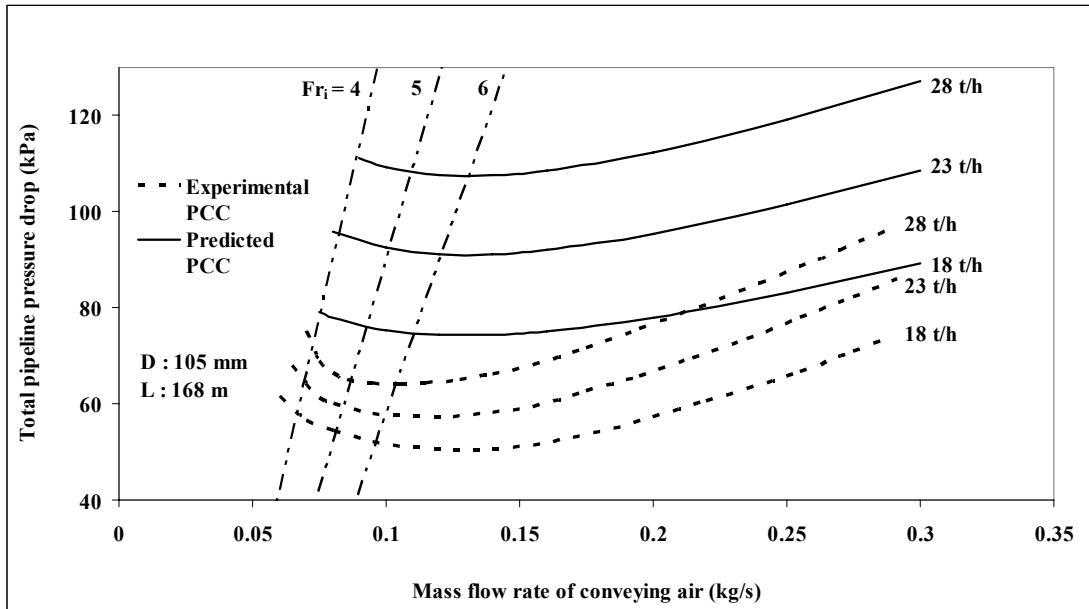
Figure A3.14: Experimental Versus Predicted PCC for Fly Ash and 105 mm I.D. ×

168 m Pipe using Equation (7.49)
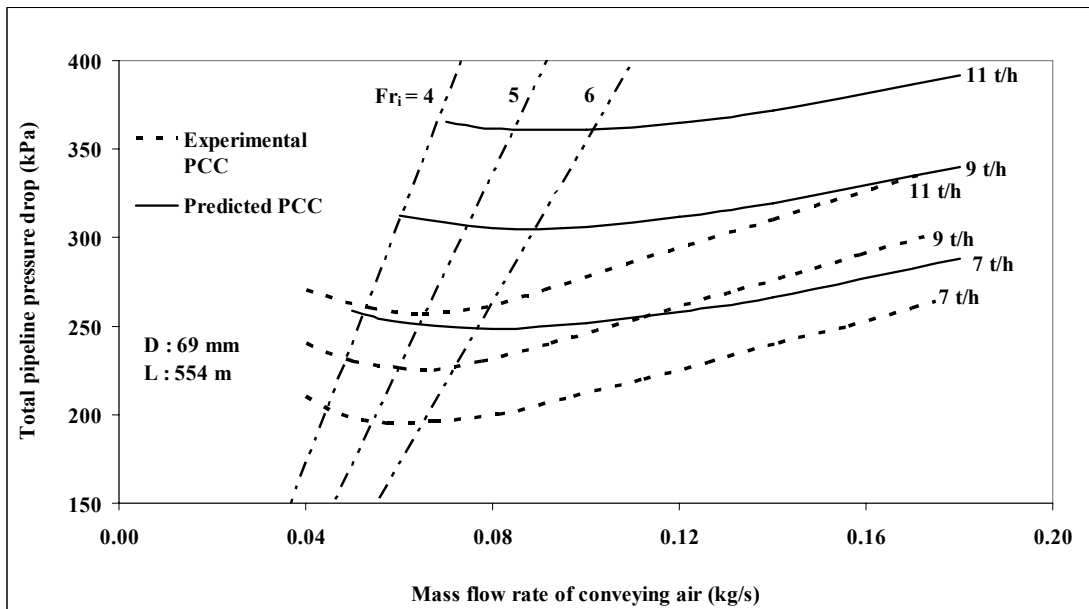
Figure A3.15: Experimental Versus Predicted PCC for Fly Ash and 69 mm I.D. ×

554 m Pipe using Equation (7.49)

A3.2   Use of dimensionless parameters in modelling fluidised beds

An extensive literature survey was carried out covering the various studies, which have been conducted over the last two decades towards identifying dimensionless parameters governing the dynamics of fluidised beds, some of which are mentioned in the following.

In an effort to determine the scaling relationships for bubbling type fluidised beds, Glicksman (1984) proposed different sets of non-dimensional parameters for different flow regimes, as given in the following:

$\{gd_s/V^2, \rho_s^2 d_s^3 g/\mu^2, L/d_s, D/d_s, \varphi$, particle size distribution, bed geometry$\}$, within viscous limit ($Re_p < 4$);

$\{\rho_s \rho d_s^3 g/\mu^2, gd_s/V^2, \rho/\rho_s, L/d_s, D/d_s, \varphi$, particle size distribution, bed geometry$\}$, for intermediate region ($4 < Re_p < 400$);

$\{gd_s/V^2, \rho/\rho_s, L/d_s, D/d_s, \varphi$, particle size distribution, bed geometry$\}$, within inertial limit ($Re_p > 400$),

where, L had been referred to as the bed height or bed dimension.

Zhang and Yang (1987) conducted experimental studies on bubbling fluidised beds and reduced the number of dimensionless parameters proposed by Glicksman (1984). The dimensionless groupings suggested by them are as given in the following:

$\{gd_s/V^2, \rho_s^2 (\varphi d_s^4)g/D\mu^2\}$; within viscous limit ($Re_p < 4$)

$\{gd_s/V^2, \rho_s^2 (\varphi d_s^4)g/D\mu^2, \rho D/\rho_s \varphi d_s\}$; for intermediate region ($4 < Re_p < 400$)

$\{gd_s/V^2, \rho D/\rho_s \varphi d_s\}$; within inertial limit ($Re_p > 400$)

Cheng and Lounge (1992) studied the fluid dynamics similarity of circulating fluidised beds and introduced Fr_p and Ar as parameter groupings. The complete set of dimensionless parameters proposed by them is mentioned below:

$\{Fr_p = V/(gd_s)^{0.5}, Ar = \rho_s \, \rho d_s^3 g/\mu^2, \rho_s / \rho, D/d_s\}$

Ar was further used to characterise transition between different flow regimes in fluidised bed (such as packed bed to fast fluidisation) by Bi and Grace (1995) and Namkung et al. (1999). In an attempt to predict the transport velocities in fast fluidization, Motte and Molodtof (2001) suggested the use of Re_p and Ar.

In an effort to study the scaling relationships for fluidised beds, Glicksman et al. (1993) introduced Re and Re_p and proposed the following set:

$\{\rho_s/\rho, V^2/(gD), \rho VD/\mu, \rho Vd/\mu, \varphi, m_s/(\rho_s V)\}$

The use of these parameters was later validated by Bricout and Lounge (2004). Similar set was also proposed by Glicksman and Farell (1995) to study the scaling parameters for commercial pressurised fluidised bed combustors.

The importance of inclusion of Fr_p and Ar was further emphasisd by Lounge et al. (1999) in studying dynamics of pressurised and atmospheric circulating fluidized bed risers. They proposed the following dimensionless parameter groupings:

$\{Fr_p, m^*, Ar, \rho_s/\rho_f, D/d_s\}$

It was mentioned that Ar combines the gas and solids properties. It arises naturally in the analysis capturing the terminal velocity of an individual particle.

In their study of scaling in circulating fluidised beds, Teplitskiy and Ryabov (1999) had mentioned different parameter groupings for different flow conditions, where they have included Re_p to balance between viscous and inertia force. In the same year, Teplitskiy (1999) conducted studies on the heat and mass transfer of bubbling fluidised beds. He considered the fluidised bed as an emulsion phase at minimum fluidisation state and proposed a set dimensionless groups, out of which the parameters of interest from a fluid dynamics point of view are given below:

$\{Fr, Ar, Re, \rho_s/\rho\}$

The above parameters were also included in the work of Detamore et al. (2001) on scale-up analysis of circulating fluidised beds. Further use of the above parameters was found in the work of Kehlenback et al. (2001). Their full set of dimensionless parameters is given below:

$\{Fr, Ar, Re, \rho_s/\rho, \varphi, m_s/\rho_s V, \text{ bed geometry, particle size distribution}\}$

In addition to the above, further studies were conducted with an aim to achieve a better understanding on the aspects of hydrodynamic modelling in the work of Wirth (1988), Breaultt and Mathur (1989), Pugsley and Berruti (1996), Goossens (1998), Wang and Li (2001) Knowlton et al. (2005) and Huang et al. (2006). It appears that more research efforts have been conducted over the years to model fluidised beds compared to the fluidised dense-phase pneumatic conveying, but there still remain inconsistencies amongst the findings of various researchers regarding the use and on the relative importance of the different dimensionless parameter groupings. It was realised that comprehensive understanding of the hydrodynamics of fluidised beds is still a subject of ongoing research. Therefore, it would perhaps be too ambitious to

expect that the literature on the hydrodynamics of fluidised beds could be able of providing any direct information regarding modelling of dense-phase pneumatic conveying of powders. However, it was noted that certain dimensionless groupings were repeatedly mentioned in various literature of fluidised beds, such as Fr , Re (both based on pipe and particle diameter) and Ar. Fr based models for solids friction in power function formats have been already examined for their scale-up accuracy (Chapter 6 and 7). The models failed to provide consistently accurate predictions for different powders and pipelines. Hence, it was decided that instead of Fr, the applicability of Ar and Reynolds number (gas and particle) could be be investigated. To evaluate the strength of the relationship between λ_s and Ar, the correlation coefficient (R) between the two parameters was estimated (while representing Ar as per Kehlenbeck et al., 2001). It was found that the strength of association was rather low (R = -0.31 for P9-P10 data and R= - 0.45 for P11-P12 data for fly ash conveyed in the 69 mm I.D. × 168 m long pipe). Comparatively, the correlations between λ_s and Re (were found to be much higher (R = -0.76 for P9-P10 and R= -0.79 for P11-P12 data for fly ash). Hence, it was considered that attempts with modelling using Re may be worth pursuing.

A3.2.1   Modelling using Reynolds number (Re and Re$_p$)

Using the steady state "straight pipe" pressure drop data obtained from both P9-P10 and P11-P12 tapping locations for fly ash (69 mm I.D. × 168 m long pipe) for a range of flow conditions (dilute- to fluidised dense-phase), power function based models for

346

λ_s were derived using Re and Re_p (where, $Re_p = \rho V d / \mu$). The models are given by equations (A3.1) to (A3.4).

Based on P9-P10 data:

$$\lambda_s = 0.016 \, (m^*)^{-0.23} \, (Re/10^5)^{-1.487} \qquad [R^2 = 0.982] \qquad\qquad (A3.1)$$

$$\lambda_s = 2.8 \, (m^*)^{-0.17} \, (Re_p)^{-1.43} \qquad\qquad [R^2 = 0.977] \qquad\qquad (A3.2)$$

Based on P11-P12 data:

$$\lambda_s = 0.00725 \, (m^*)^{-0.08} \, (Re/10^5)^{-1.19} \quad [R^2 = 0.973] \qquad\qquad (A3.3)$$

$$\lambda_s = 0.037 \, (m^*)^{-0.001} \, (Re_p)^{-1.16} \qquad [R^2 = 0.971] \qquad\qquad (A3.4)$$

The following conclusions can be drawn based on the above derived models:

a) The derived models were found to be different depending on the location of the pressure tapping points (i.e. P9-10 and P11-12). This seems to fundamentally wrong, as a model for a particular powder should be expected to have a unique solution.

b) According to the Reynolds number based formats, for a set of m_f and m_s, the values of m^* and Re (both gas and particle Reynolds numbers) are the same throughout the length of pipe (from pipe inlet to exit). Hence, the predicted values of λ_s remain unchanged throughout the pipe length. This

is incorrect, as the experimental data suggests that even for the same set of values of m_f and m_s, the values of λ_s are different for P9-P10 and P11-P12 pressure tapping locations (i.e. λ_s varies along the length of pipe).

Due to the above limitations, the Reynolds number based models were not further pursued for scale-up evaluation.

A3.3   Turbulence of solids-gas flow

Due to the highly concentrated nature of the fluidised dense-phase type flow (verified from the "sight glass" observation), it was considered that the powders may actually alter the turbulence of the gas phase. This could in turn influence the energy dissipation (and pressure drop) of the gas. In fact, it was found that Duckworth (1977) had a similar suspicion, where he stated that for the fine particles "the value of solids friction factor depends to a large extent on the modification of the turbulence pattern of the flow vis a vis that of a fluid flow". However, he did not propose any validated model that can properly represent turbulent interaction between the solids and gas. For a better understanding of the phenomenon of effect of solids (suspended in air/gas) in modifying the turbulence of gas and vice-versa, an extensive literature survey was conducted, a summary of which is presented in the following:

Giacinto et al. (1982) defined the terms "one-way" and "two-way" coupling as: if the gas turbulence is unaffected by the presence of solids, then it is known as "one-way"

coupling. Whereas, if the presence of solids (suspended) causes turbulence modulation of the carrier gas phase, then the phenomenon is called "two-way" coupling. They proposed that m* and Stokes number (St) are the basic parameters governing the solids-gas flows. The Stokes number was expressed as:

$$St = \tau_p/\tau_f = \rho_s d_s^2 V / 18\mu D \tag{A3.5}$$

where, τ_p: particle relaxation time = $\rho_p d_s^2 / 18\mu$; τ_f: characteristic time for the supporting flow field = D/V. Their studies further suggested that for larger values of m*, the effect of the particles on the fluid flow field can not be neglected anymore. This is more relevant at low Stokes number. However, for higher values of Stokes number (where the particles have larger inertia), the fluid is slightly affected by the particles.

Gore and Crowe (1989) conducted studies on the effect of particle size on modulating turbulent intensity, where they mentioned that the small particles will follow the eddy for at least part of its lifetime. In this process, the turbulent energy of the eddy will be transformed into the kinetic energy of the particle, resulting in reduction of the turbulent intensity of the eddy. On the contrary, the larger particles will create turbulence in its wake, thus increasing the turbulent intensity of the gas. Similar conclusions were also found in Crowe (2000).

Rashidi et al. (1990) studied the particle turbulent interaction in wall turbulent flow. A series of experiments was conducted with varying particle size, particle density, m*

and flow Reynolds number. The results showed that larger polystyrene particles (1100 μm) caused an increase in the measured value of turbulent intensities and Reynolds stress, whereas, smaller polystyrene particles (120 μm) decreased the turbulence intensity. The effect was found to be increasing with an increase in m*. It was also observed that heavier glass particles (88 μm) did not cause any significant modulation of gas turbulence. It was proposed that particles with Re_p greater than 100 would increase turbulence, whereas, particles with Re_p below 100 would suppress turbulence.

In a theoretical approach to examine the turbulence modulation in solids-gas flows, Yuan and Michaelides (1992) mentioned various mechanisms for turbulence modification in dispersed two phase systems, which are given in the following:

a) Dissipation of turbulent kinetic energy by the particles, which was indicated as the cause responsible for reducing the turbulence intensities;

b) Increase of the apparent viscosity due to the presence of particles;

c) Shedding of vortices or the presence of wakes behind the particles, which increases the intensity of turbulence;

d) Fluid moving with the particles as added fluid mass to the particles;

e) Enhancement of the velocity gradients between two rigid particles;

f) Deformation of the dispersed phase.

Elgobashi and Truesdell (1993) carried out direct numerical simulations (in the range of volumetric loading ratio below 5×10^{-5}) to investigate the "two-way" interaction between the dispersed solids and the carrying media. The effects of several

350

parameters on the phenomenon of "two-way coupling" were investigated, such as the effect of particle inertia (consisting of particle response time, particle diameter, volume fraction of solids) and the effect of gravity. The results showed that in the absence of gravity, the turbulence energy of particle laden flow decays at a faster rate than in the particle free turbulence. It was also indicated that increase in particle surface area increases the "two-way coupling". Thus smaller particles would introduce more "two-way coupling" effect than larger particles (for the same solids flow rate).

Further analysis of turbulence of particle laden flow using direct numerical simulation was carried out by Elgobashi (1994), where he proposed that "one-way coupling" would exist when ε_p is in the range of 10^{-7}. However, the effect of "two-way coupling" will become prominent with increase in ε_p (to about 10^{-5}). Further increase in φ_p will result in "4-way coupling", which Elgobashi (1994) had mentioned as the regime where particle-particle collision will also be present. It was further mentioned that as the distance between the particles decreases ($< 10d_s$), the presence of their rigid body boundaries would alter the flow field around them, thus modifying the relative velocity distribution around each particle. This modification would change all the forces imparted on each particle. Similar way of differentiating between different flow conditions were found in the work of Bosse et al. (2006), where they proposed that "one-way coupling" is applicable for dilute-phase suspensions, whereas, dense-phase flow is characterised by "two-way coupling".

Pan and Banerjee (1996) carried out studies on "two-way coupling" using numerical simulation. It was reported that generally the larger particles would increase turbulence, whereas, the smaller particles will suppress it. The smaller particles reduce energy production and increase energy dissipation, whereas, the larger particles would increase both energy production and dissipation, with larger change in production, than dissipation. It was mentioned that the phenomenon of turbulent modification depends on the value of m*. Similar conclusions were also drawn in the work of Ahmed and Elgobashi (2000), where they proposed that the change in turbulence energy production rate of the carrier fluid occurs due to the modification of vorticity dynamics. It was stated that regions of larger turbulence production rate become "sandwiched between counter rotating longitudinal vortex tubes".

Kenning and Crowe (1996) had attempted to model the effect of particles on carrier phase turbulence. They stated that a source of energy loss in the carrier phase is the rate of work done by the carrier phase to oscillate the dispersed phase. This indicates that for the finer particles, at least one of the causes for the energy loss of gas (carrier fluid) could be the energy spent in keeping the particles in turbulent/oscillating condition.

Huber and Sommerfield (1998) carried out numerical analysis to study "two-way coupling" in dilute-phase pneumatic conveying. They proposed that at higher particle mass loading (which may also be interpreted as with increase in the value of m*), turbulence of the gas-phase will be considerably altered by the presence of particles (i.e. either enhanced or reduced, depending on the particle size). They stated that

higher particle mass flux near the bottom section of pipe would result in a stronger coupling with the gas-phase. Furthermore, it was suggested that small particles would get caught in the eddies and hence, they would have the similar velocities (i.e. not much relative velocities amongst the particles within an eddy). This would reduce the inter-particle collision effect.

Ljus et al. (2002) conducted experimental studies on turbulence modification using special particles under very dilute-phase conditions (m* = 0.1-0.3). It was observed that the alteration of turbulence structure of the carrier fluid was occurring even at such low values of m*. They were able to suggest an explanation for the turbulence modulation. They proposed that for the larger particles (which do not respond to turbulence), wake is formed at the back-end of the particles. These eddies increase the overall turbulence. However, the smaller particles are able to follow turbulence. As a result the gas can transmit its turbulence to the smaller particles. Thus the turbulence of the gas gets dampened. It was also found that the particles were affected by gravity and the distribution of particles over the pipe cross-section was not uniform. When the turbulence level was not sufficiently high, the particles would accumulate at the bottom of the pipe. Turbulence modulation was found to be more pronounced at the bottom part of the pipe, where the particle concentration was more than the upper section of pipe.

Lightstone and Hodgson (2004) reviewed the various available models for turbulence modulation in gas particle flow systems by comparing with experimental data. The results suggested that larger particles increase gas turbulence, whereas, the smaller

particles decreases the same. They also stated that generally the effect of m* is to amplify the degree of modulation that occurs because of the particles.

Hadinoto et al. (2005) investigated the dependence of gas-phase Reynolds number on gas particle flows. Experimental studies were conducted to analyze the downward flow of glass beds (d_s = 70 and 200 μm) through vertical pipe under wide range of Reynolds number conditions. They explained the importance of Stokes number in understanding the particle interaction with the gas phase. A value of St>1 denoted "unresponsive" particles, which do not follow fluctuations due to their own higher inertia, whereas, St <1 would signify "responsive" particles which would follow fluid fluctuations. This indicates that the "responsive" particles could exhibit a turbulent type motion. It was further elaborated that the "unresponsive" particles get involved in particle-particle collisions and these collisions influence their fluctuating motion. However, for the "responsive" particles, velocity fluctuations were governed by fluid fluctuations.

More recently, Wang et al. (2006) conducted numerical studies by varying the particle diameter (2, 20 and 200 μm). The conclusions of their work were found to be very similar to that of Hadinoto et al. (2005). They also employed Stokes number as a means to predict the fluctuation of particles with respect to the gas phase. They observed that 200 μm sized particles did not respond to fluid fluctuations due to their larger inertia, whereas, the smaller particles (2 and 20 μm) were found to be more affected by the turbulence of fluid, thus having a higher fluctuating velocity component.

These studies seem to suggest the following key points:

a) For the range of m* typically encountered in dense-phase pneumatic conveying systems for powders, it is likely that there will be significant alteration of gas-phase turbulence ("two-way coupling"). This would cause the representation of Barth (1958) to separately deal with the solids and gas phases (as given by equation 2.1) to be invalid. However, since no relationship was found, which can be conveniently used to modify Barth (1958) equation to take account of the effect of "two-way coupling", it was decided that Barth's (1958) representation may be persisted with for subsequent modelling work in this thesis.

b) The interaction of particles with air/gas for the entire flow range (dense- to dilute-phase) may not be the same. For St>1, the particles are "unresponsive" to turbulence of the carrier fluid (gas) due to higher particle inertia (i.e. for higher particle/gas velocity and/or for larger sized and/or heavier particles) and will be conveyed in a rather straight-line path (in the direction of mean flow velocity). For St<1, the particles will be "responsive" to turbulence/oscillation of the carrier fluid (i.e. for fine powders at low conveying velocity). However, it is to be noted that the above Stokes number based criteria was established from systems apparently having isolated particles in gas streams or for very low values of m*. It is not certain whether the above criteria will remain valid for high m* or for powder conveying as a "bulk"

APPENDIX: A4

A4.1 Modelling and results of scale-up evaluation
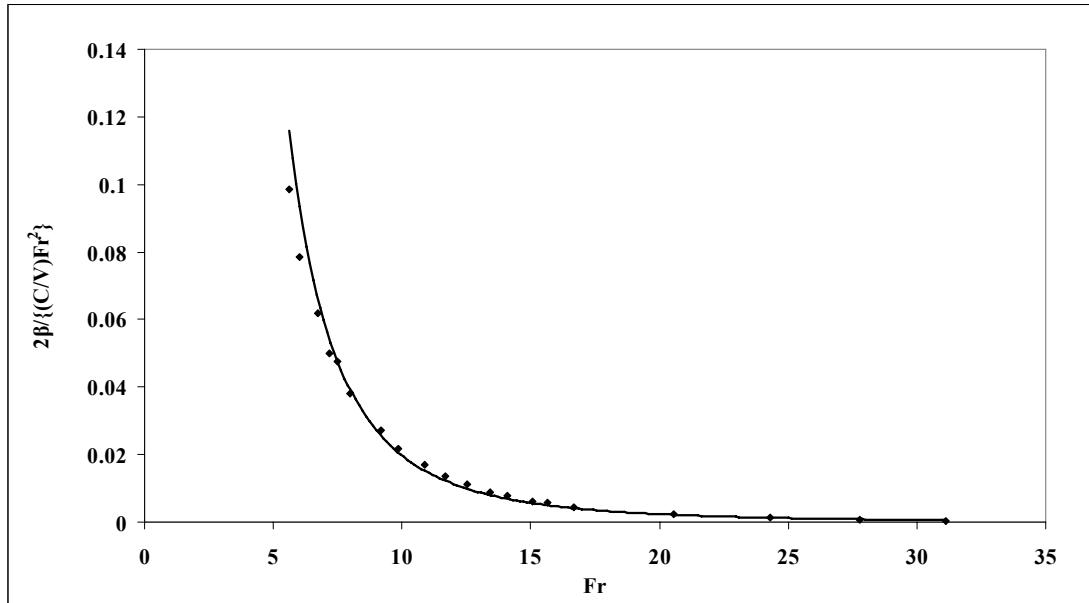
Figure A4.1: $2\beta/[(C/V)\ Fr^2]$ Versus Fr for ESP Dust for 69 mm I.D. $\times$ 168 m Pipe
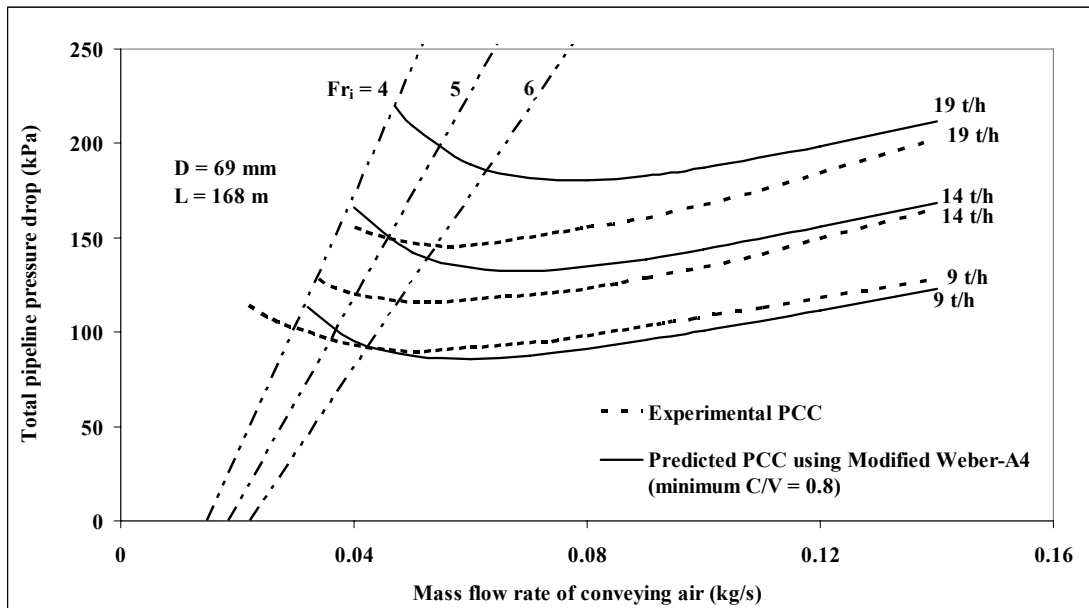
Figure A4.2: Experimental Versus Predicted PCC for Fly Ash and 69 mm I.D. $\times$ 168 m Pipe Using "Modified Weber-A4" Model ($\alpha = 0.8$)

357
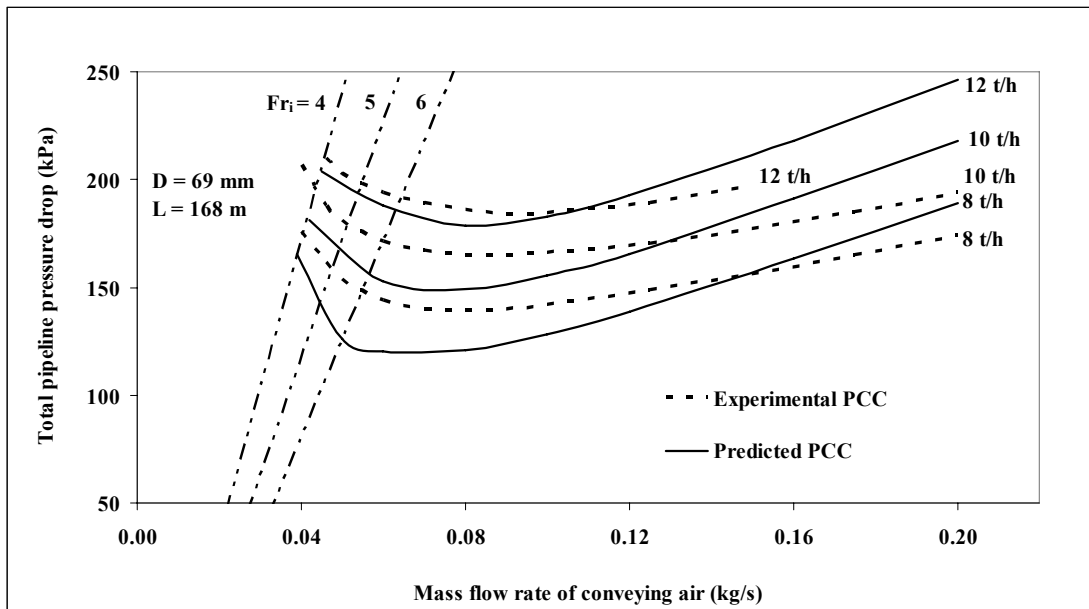
Figure A4.3: Experimental Versus Predicted PCC for ESP Dust and 69 mm I.D. ×

168 m Pipe Using "Two-Layer" Model
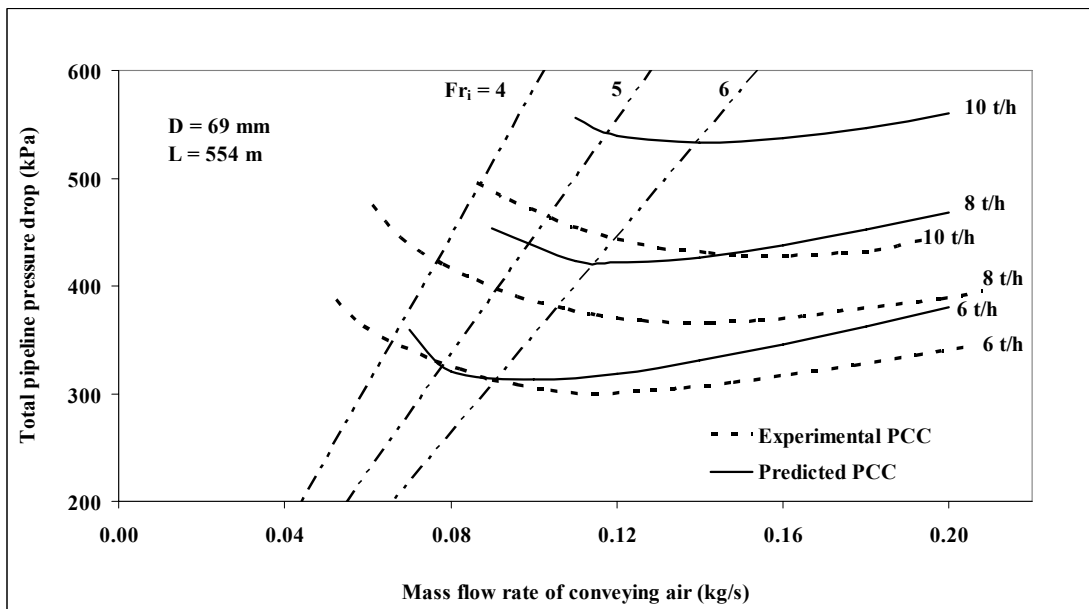
Figure A4.4: Experimental Versus Predicted PCC for ESP Dust and 69 mm I.D. ×

554 m Pipe Using "Two-Layer" Model

358

A4.2 Modelling: EXCEL calculation for "modified Weber-A4" for fly ash

Product   **Fly Ash**   **Pipe diameter**   69 mm
                                         Pipe length   168 m

Exp No.	m_f	m_s	P initial	P exit kPa	Temp	Pipe	Length of secction (L_h) m	Pipe I.D.
	kg/s	kg/s	kPa (g)	(g)	deg C	roughness		m
2	0.1080	2.214	93.76	71.33	20.00	0.000	52.680	0.069
8	0.1076	2.371	95.33	72.47	20.00	0.000	52.680	0.069
11	0.1257	2.485	109.54	84.89	20.00	0.000	52.680	0.069
12	0.0885	2.621	95.07	68.55	20.00	0.000	52.680	0.069
13	0.0816	2.490	92.90	65.30	20.00	0.000	52.680	0.069
14	0.0696	2.735	89.52	61.55	20.00	0.000	52.680	0.069
15	0.0585	2.852	87.80	59.81	20.00	0.000	52.680	0.069
16	0.0404	2.787	86.16	56.60	20.00	0.000	52.680	0.069
17	0.0265	2.411	99.30	62.52	20.00	0.000	52.680	0.069
18	0.0231	2.380	104.57	65.56	20.00	0.000	52.680	0.069
20	0.1264	3.445	135.84	106.64	20.00	0.000	52.680	0.069
21	0.1037	3.762	127.36	96.40	20.00	0.000	52.680	0.069
22	0.0885	3.979	122.46	90.46	20.00	0.000	52.680	0.069
23	0.0818	3.958	120.03	86.67	20.00	0.000	52.680	0.069
24	0.0701	4.169	117.31	83.22	20.00	0.000	52.680	0.069
25	0.0652	4.186	115.72	81.46	20.00	0.000	52.680	0.069
26	0.0504	4.283	114.16	77.51	20.00	0.000	52.680	0.069
27	0.0379	3.901	115.03	74.50	20.00	0.000	52.680	0.069
29	0.1294	5.012	166.41	131.22	20.00	0.000	52.680	0.069
31	0.0924	5.105	150.78	112.42	20.00	0.000	52.680	0.069
32	0.0815	5.195	144.34	106.10	20.00	0.000	52.680	0.069
35	0.0496	5.294	131.91	88.62	20.00	0.000	52.680	0.069
39	0.1075	2.346	92.40	70.17	20.00	0.000	52.680	0.069

Product   **FLY ASH**   **Pipe diameter**   69 mm
                                               Pipe length   168 m

Exp No.	ΔP kPa	ρ_m kg/m3	V_m m/s	m*	μ	Re	λ_f	λ_s	Fr_m
2	22.42	2.18	13.22	20.50	1.82E-05	109700	0.018	0.0067	16.07
8	22.86	2.20	13.08	22.03	1.82E-05	109335	0.018	0.0064	15.90
11	24.65	2.36	14.25	19.77	1.82E-05	127664	0.017	0.0060	17.32
12	26.52	2.18	10.88	29.62	1.82E-05	89890	0.018	0.0085	13.22
13	27.61	2.14	10.18	30.52	1.82E-05	82884	0.019	0.0101	12.37
14	27.97	2.10	8.86	39.29	1.82E-05	70727	0.019	0.0108	10.77
15	27.99	2.08	7.52	48.77	1.82E-05	59413	0.020	0.0124	9.14
16	29.57	2.05	5.26	69.02	1.82E-05	41015	0.022	0.0194	6.40
17	36.79	2.16	3.27	91.05	1.82E-05	26901	0.024	0.0454	3.98
18	39.01	2.21	2.79	103.18	1.82E-05	23439	0.025	0.0574	3.39
20	29.20	2.64	12.79	27.24	1.82E-05	128459	0.017	0.0059	15.54
21	30.97	2.53	10.95	36.27	1.82E-05	105385	0.018	0.0069	13.31
22	32.00	2.47	9.59	44.97	1.82E-05	89885	0.018	0.0078	11.65
23	33.36	2.43	8.99	48.41	1.82E-05	83054	0.019	0.0088	10.93
24	34.09	2.39	7.82	59.51	1.82E-05	71174	0.019	0.0099	9.51
25	34.26	2.38	7.34	64.17	1.82E-05	66269	0.019	0.0106	8.93
26	36.65	2.34	5.76	84.91	1.82E-05	51251	0.021	0.0143	7.00
27	40.53	2.33	4.35	102.86	1.82E-05	38533	0.022	0.0232	5.29
29	35.19	2.97	11.64	38.74	1.82E-05	131446	0.017	0.0055	14.15
31	38.36	2.77	8.93	55.26	1.82E-05	93840	0.018	0.0079	10.85
32	38.24	2.69	8.10	63.73	1.82E-05	82812	0.019	0.0086	9.84
35	43.29	2.51	5.28	106.71	1.82E-05	50407	0.021	0.0150	6.42
39	22.23	2.17	13.25	21.82	1.82E-05	109239	0.018	0.0062	16.11

Product	**FLY ASH**					**Pipe diameter**	69 mm	
						Pipe length	168 m	

Exp No.	C/V at exp point	C (m/s)	Fr*^{2}	w$_{fo}$ m/s	K$_1$	β	Log(2β /{(C/V) Fr^2})	Log(Fr)
2	0.92	12.15	218.24	0.06	19.989	0.091	-3.117	1.206
8	0.92	12.02	213.49	0.06	20.405	0.094	-3.094	1.201
11	0.92	13.13	254.61	0.06	20.566	0.087	-3.203	1.238
12	0.91	9.95	146.24	0.06	18.735	0.103	-2.888	1.121
13	0.91	9.30	127.72	0.06	17.506	0.103	-2.831	1.092
14	0.91	8.07	96.25	0.06	17.414	0.118	-2.651	1.032
15	0.91	6.83	68.86	0.06	16.779	0.134	-2.452	0.961
16	0.90	4.76	33.42	0.06	14.068	0.160	-2.062	0.806
17	0.90	2.94	12.80	0.06	9.594	0.176	-1.607	0.599
18	0.90	2.50	9.27	0.06	8.623	0.186	-1.443	0.530
20	0.92	11.75	203.86	0.06	21.510	0.101	-3.041	1.192
21	0.91	10.02	148.35	0.06	20.790	0.114	-2.852	1.124
22	0.91	8.74	112.96	0.06	20.144	0.126	-2.691	1.066
23	0.91	8.19	99.14	0.06	19.246	0.128	-2.627	1.039
24	0.91	7.11	74.68	0.06	18.619	0.143	-2.459	0.978
25	0.91	6.67	65.70	0.06	18.192	0.149	-2.386	0.951
26	0.90	5.21	40.13	0.06	16.220	0.169	-2.118	0.845
27	0.90	3.93	22.79	0.06	13.139	0.181	-1.844	0.724
29	0.92	10.67	168.16	0.06	22.919	0.118	-2.890	1.151
31	0.91	8.13	97.70	0.06	20.318	0.137	-2.594	1.035
32	0.91	7.37	80.15	0.06	19.857	0.147	-2.476	0.993
35	0.90	4.77	33.63	0.06	16.018	0.182	-2.009	0.807
39	0.92	12.19	219.43	0.06	20.687	0.094	-3.105	1.207

A4.3 EXCEL calculation for total pipeline pressure drop using "modified Weber-A4" model for fly ash

INPUT DATA

| Product | Fly ash | | | Pipe diameter | 69 mm |
| | | | | Pipe length | 168 m |

PIPELINE DETAILS

HORIZONTAL SECTION

Pipe section length	L1	m	11.915	Pipe section diameter	D1	m	0.069
Pipe section length	L2	m	30.215	Pipe section diameter	D2	m	0.069
Pipe section length	L3	m	30.215	Pipe section diameter	D3	m	0.069
Pipe section length	L4	m	4.729	Pipe section diameter	D4	m	0.069
Pipe section length	L5	m	36.215	Pipe section diameter	D5	m	0.069
Pipe section length	L6	m	36.215	Pipe section diameter	D6	m	0.069
Pipe section length	L7	m	6.515	Pipe section diameter	D8	m	0.069

VERTICAL LIFT

| Vertical lift | h | m | 7 | Pipe section diameter | | m | 0.069 |
| Effective elevation | H | m | 8.571 | Pipe section diameter | | m | 0.069 |

BENDS   comment: Bend details not needed for Chambers and Marcus (1986) model

B1	Radius of curvature	m	1	Pipe diameter at Bend		m	0.069
B2	Radius of curvature	m	1	Pipe diameter at Bend		m	0.069
B3	Radius of curvature	m	1	Pipe diameter at Bend		m	0.069
B4	Radius of curvature	m	1	Pipe diameter at Bend		m	0.069
B5	Radius of curvature	m	1	Pipe diameter at Bend		m	0.069

| Absolute roughness of pipe | m | 0 |

| Atmospheric Pressure (abs) | kPa | 101.33 |
| Ambient temperature | deg C | 20 |

| λs^* | | 0.0054 |
| Exponent of Froude no. (power function exponent) | | -2.55 |

| Mass flow rate of solids | t/h | 19 |
| Mass flow rate of air | kg/s | 0.039 |

| Pipe exit pressure (g) | kPa | 0 |

| For | Fr | 4 | C/V | 0.9 |
| For | Fr | 60 | C/V | 0.99 |

Pressure loss		SOLUTION	
Horizontal straight section L1: 1st section from exit			
Pipe cross sectional area	m²		0.0037
solid loading ratio (m*)			135.328
Exit Condition			
density of air at exit	kg/m³		1.204
superficial air velocity at exit	m/s		8.660
Froude number at exit			10.526
Assumed Pressure loss	**kPa**		**7.924**
Entry Condition			
density of air at inlet	kg/m³		1.299
superficial air velocity at inlet	m/s		8.032
Froude number at inlet			9.763
Average Condition			
Average air density	kg/m³		1.251
Air velocity at average condition	m/s		8.334
Air viscosity at average condition	Pa.S		0.000018
Reylonds Number for average condition			39621.720
Froude Number for average condition			10.130
C/V			0.9099
C (particle velocity)	m/s		7.5831
Solid friction factor (λ_s) for average condition			0.0076
Air only friction factor (λ_f) for average condition			0.022
Pressure drop for average condition	**kPa**		<u>**7.924**</u>
Pressure difference	kPa		**0.000**
Pressure at entry to the section	kPa (g)		7.924
Pressure at entry to the section	kPa (a)		109.249

Bend B1			
Air density at bend outlet	kg/m³		1.299
Air velocity at bend outlet	m/s		8.032
Pressure drop due to solid + air through bend	kPa		2.855
Total pressure drop due to bend	**kPa**		<u>**2.855**</u>
Pressure at the entry of bend	kPa (g)		**10.779**
Pressure at the entry of bend	kPa (a)		112.104

Vertical lift loss due to elevation H		
Pipe cross sectional area	m^2	0.0037
solid loading ratio (m*)		135.328
Exit Condition		
density of air at exit	kg/m^3	1.332
superficial air velocity at exit	m/s	7.828
Froude number at exit		9.514
Assumed Pressure loss	**kPa**	**21.254**
Entry Condition		
density of air at inlet	kg/m^3	1.585
superficial air velocity at inlet	m/s	6.580
Froude number at inlet		7.998
Average Condition		
Average air density	kg/m3	1.459
Air velocity at average condition	m/s	7.150
Air viscosity at average condition	Pa.S	0.000018
Reylonds Number for average condition		39621.720
Froude Number for average condition		8.690
C/V		0.9075
C (particle velocity)	m/s	6.4887
Solid friction factor (λ_s) for average condition		0.0089
Air only friction factor (λ_f) for average condition		0.022
Pressure drop due to friction for average condition through lift of 'h'	**kPa**	**4.655**
Pressure drop due to Elevation of materials through evelation of 'H'	**kPa**	**16.599**
Total pressure loss through the elevation	**kPa**	**21.254**
Pressure difference	kPa	**0.000**
Pressure at entry to the section	kPa (g)	**32.033**
Pressure at entry to the section	kPa (a)	**133.358**

Bend B2		
Air density at bend outlet	kg/m^3	1.585
Air velocity at bend outlet	m/s	6.580
Pressure drop due to solid + air through bend	kPa	2.339
Total pressure drop due to bend	**kPa**	**2.339**
Pressure at the entry of bend	kPa (g)	**34.372**
Pressure at the entry of bend	kPa (a)	**135.697**

Horizontal straight section L2		
Pipe cross sectional area	m²	0.0037
solid loading ratio (m*)		135.328
Exit Condition		
density of air at exit	kg/m³	1.613
superficial air velocity at exit	m/s	6.467
Froude number at exit		7.860
Assumed Pressure loss	**kPa**	**21.052**
Entry Condition		
density of air at inlet	kg/m³	1.863
superficial air velocity at inlet	m/s	5.598
Froude number at inlet		6.804
Average Condition		
Average air density	kg/m³	1.738
Air velocity at average condition	m/s	6.001
Air viscosity at average condition	Pa.S	0.000018
Reylonds Number for average condition		39621.720
Froude Number for average condition		7.294
C/V		0.9053
C (particle velocity)	m/s	5.4328
Solid friction factor (λ_s) for average condition		0.0112
Air only friction factor (λ_f) for average condition		0.022
Pressure drop for average condition	**kPa**	<u>21.052</u>
Pressure difference	kPa	**0.000**
Pressure at entry to the section	kPa (g)	**55.424**
Pressure at entry to the section	kPa (a)	156.749

Horizontal straight section L3		
Pipe cross sectional area	m^2	0.0037
solid loading ratio (m*)		135.328
Exit Condition		
density of air at exit	kg/m^3	1.863
superficial air velocity at exit	m/s	5.598
Froude number at exit		6.804
Assumed Pressure loss	kPa	22.636
Entry Condition		
density of air at inlet	kg/m^3	2.132
superficial air velocity at inlet	m/s	4.892
Froude number at inlet		5.946
Average Condition		
Average air density	kg/m^3	1.998
Air velocity at average condition	m/s	5.221
Air viscosity at average condition	Pa.S	0.000018
Reylonds Number for average condition		39621.720
Froude Number for average condition		6.346
C/V		0.9038
C (particle velocity)	m/s	4.7187
Solid friction factor (λ_s) for average condition		0.0139
Air only friction factor (λ_f) for average condition		0.022
Pressure drop for average condition	kPa	22.636
Pressure difference	kPa	0.000
Pressure at entry to the section	kPa (g)	78.060
Pressure at entry to the section	kPa (a)	179.385

Bend B3		
Air density at bend outlet	kg/m^3	2.132
Air velocity at bend outlet	m/s	4.892
Pressure drop due to solid + air through bend	kPa	1.739
Total pressure drop due to bend	kPa	1.739
Pressure at the entry of bend	kPa (g)	79.798
Pressure at the entry of bend	kPa (a)	181.123

366

Horizontal straight section L4		
Pipe cross sectional area	m^2	0.0037
solid loading ratio (m*)		135.328
Exit Condition		
density of air at exit	kg/m^3	2.153
superficial air velocity at exit	m/s	4.845
Froude number at exit		5.889
Assumed Pressure loss	**kPa**	**3.758**
Entry Condition		
density of air at inlet	kg/m^3	2.197
superficial air velocity at inlet	m/s	4.746
Froude number at inlet		5.769
Average Condition		
Average air density	kg/m^3	2.175
Air velocity at average condition	m/s	4.795
Air viscosity at average condition	Pa.S	0.000018
Reylonds Number for average condition		39621.720
Froude Number for average condition		5.828
C/V		0.9029
C (particle velocity)	m/s	4.3296
Solid friction factor (λ_s) for average condition		0.0160
Air only friction factor (λ_f) for average condition		0.022
Pressure drop for average condition	**kPa**	**3.758**
Pressure difference	kPa	0.000
Pressure at entry to the section	kPa (g)	83.556
Pressure at entry to the section	kPa (a)	184.881

Bend B4		
Air density at bend outlet	kg/m^3	2.197
Air velocity at bend outlet	m/s	4.746
Pressure drop due to solid + air through bend	kPa	1.687
Total pressure drop due to bend	**kPa**	**1.687**
Pressure at the entry of bend	kPa (g)	85.243
Pressure at the entry of bend	kPa (a)	186.568

Horizontal straight section L5		
Pipe cross sectional area	m²	0.0037
solid loading ratio (m*)		135.328
Exit Condition		
density of air at exit	kg/m³	2.218
superficial air velocity at exit	m/s	4.703
Froude number at exit		5.717
Assumed Pressure loss	**kPa**	31.236
Entry Condition		
density of air at inlet	kg/m³	2.589
superficial air velocity at inlet	m/s	4.029
Froude number at inlet		4.897
Average Condition		
Average air density	kg/m³	2.403
Air velocity at average condition	m/s	4.340
Air viscosity at average condition	Pa.S	0.000018
Reylonds Number for average condition		39621.720
Froude Number for average condition		5.275
C/V		0.9020
C (particle velocity)	m/s	3.9150
Solid friction factor (λ_s) for average condition		0.0193
Air only friction factor (λ_f) for average condition		0.022
Pressure drop for average condition	**kPa**	<u>31.236</u>
Pressure difference	kPa	**0.000**
Pressure at entry to the section	kPa (g)	**116.479**
Pressure at entry to the section	kPa (a)	217.804

Horizontal straight section L6

Pipe cross sectional area	m²	0.0037
solid loading ratio (m*)		135.328

Exit Condition

density of air at exit	kg/m³	2.589
superficial air velocity at exit	m/s	4.029
Froude number at exit		4.897

Assumed Pressure loss   kPa   36.332

Entry Condition

density of air at inlet	kg/m³	3.021
superficial air velocity at inlet	m/s	3.453
Froude number at inlet		4.197

Average Condition

Average air density	kg/m³	2.805
Air velocity at average condition	m/s	3.719
Air viscosity at average condition	Pa.S	0.000018
Reylonds Number for average condition		39621.720
Froude Number for average condition		4.520
C/V		0.9008
C (particle velocity)	m/s	3.3499
Solid friction factor (λ_s) for average condition		0.0262
Air only friction factor (λ_f) for average condition		0.022

Pressure drop for average condition   kPa   <u>36.332</u>

Pressure difference   kPa   **0.000**

Pressure at entry to the section	kPa (g)	152.811
Pressure at entry to the section	kPa (a)	254.136

Bend B5

Air density at bend outlet	kg/m³	3.021
Air velocity at bend outlet	m/s	3.453
Pressure drop due to solid + air through bend	kPa	1.227

Total pressure drop due to bend   kPa   <u>1.227</u>

Pressure at the entry of bend	kPa (g)	154.039
Pressure at the entry of bend	kPa (a)	255.364

Horizontal straight section L7

Pipe cross sectional area	m²	0.0037
solid loading ratio (m*)		135.328

Exit Condition

density of air at exit	kg/m³	3.035
superficial air velocity at exit	m/s	3.436
Froude number at exit		4.177

Assumed Pressure loss kPa 7.246

Entry Condition

density of air at inlet	kg/m³	3.121
superficial air velocity at inlet	m/s	3.341
Froude number at inlet		4.061

Average Condition

Average air density	kg/m³	3.078
Air velocity at average condition	m/s	3.388
Air viscosity at average condition	Pa.S	0.000018
Reylonds Number for average condition		39621.720
Froude Number for average condition		4.118
C/V		0.9002
C (particle velocity)	m/s	3.0500
Solid friction factor (λ_s) for average condition		0.0319
Air only friction factor (λ_f) for average condition		0.022

Pressure drop for average condition kPa 7.246

Pressure difference	kPa	0.000

Pressure at entry to the section	kPa (g)	161.284
Pressure at entry to the section	kPa (a)	262.609

Acceleartion Pressure Loss at Feed Point

Pipe cross sectional area	m2	0.0037
density of air at feed point	kg/m³	3.121
superficial air velocity at exit	m/s	3.341
solid loading ratio (m*)		135.328

Accelation pressure loss kPa 4.716

Pressure at Feed point	kPa (g)	166.001
Pressure at Feed point	kPa (a)	267.326

Pressure drop contributed by Horizontal straight pipes	kPa	130.183
Pressure drop contributed by Vertical pipes + Bends + Entry losses	kPa	35.817
Total Pressure drop for the entire pipe	kPa	166.001
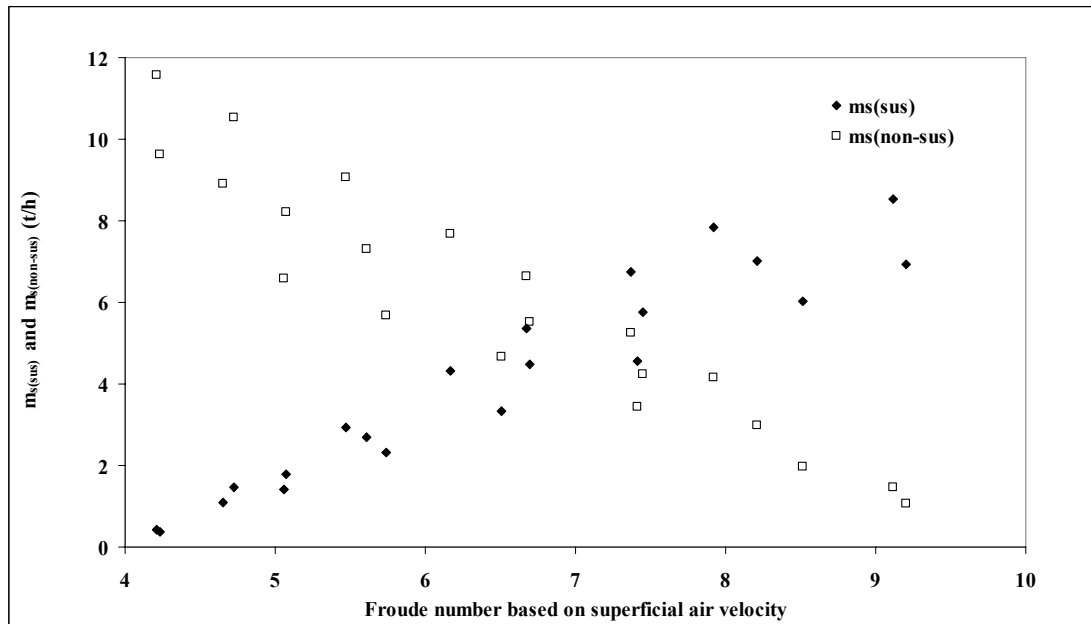
Figure A4.5: Plot of $m_{s(sus)}$ and $m_{s(non\text{-}sus)}$ with increase in Froude number

APPENDIX: A5

Table A5.1: Ratio of amount of over/under-prediction to the experimental PCC of the various scale-up evaluation results of Chapter 6, 7, 8 and 10.

Figure No.	Percentage
6.1	+170
6.2	-30
6.3	+17
6.4	-5
6.5	-38
6.6	-16
6.7	-34
6.8	-78
6.9	+5
6.10	+45
6.11	+34
6.12	-4
6.13	-5
6.14	+250
6.15	+50
7.4	+1 (for K not equal to 1) +12 (for K equal to 1)
7.5	+67 (for K not equal to 1) +55 (for K equal to 1)

7.6	+63 (for K not equal to 1) +33 (for K equal to 1)
7.7	-23 (for K not equal to 1) -17 (for K equal to 1)
7.8	+11 (for K not equal to 1) +11(for K equal to 1)
7.9	+10 (for K not equal to 1) -1 (for K equal to 1)
7.10	-20 (for K not equal to 1) -1 (for K equal to 1)
7.11	+10 (for K not equal to 1) +24 (for K equal to 1)
7.12	+14 (for K not equal to 1) +26 (for K equal to 1)
7.13	- 0 (for K not equal to 1) -15 (for K equal to 1)
7.14	-14 (for K not equal to 1) +25 (for K equal to 1)
7.15	-10 (for K not equal to 1) +12 (for K equal to 1)
7.16	+8 (for K not equal to 1) +20 (for K equal to 1)
7.17	+80 (for K not equal to 1)

	+85 (for K equal to 1)
7.18	+75 (for K not equal to 1)
	+22 (for K equal to 1)
7.19	-70 (for K not equal to 1)
	-10 (for K equal to 1)
7.20	-52 (for K not equal to 1)
	+24 (for K equal to 1)
7.21	-63 (for K not equal to 1)
	+8 (for K equal to 1)
7.22	+60 (for K not equal to 1)
	+42 (for K equal to 1)
7.23	+150 (for K not equal to 1)
	+50 (for K equal to 1)
7.24	+44 (for K not equal to 1)
	+24 (for K equal to 1)
7.25	+90 (for K not equal to 1)
	+40 (for K equal to 1)
7.26	+18
7.27	+45
7.28	+40
7.29	+25
7.30	+24
7.31	+35

7.32	+2
7.33	+2
7.34	+8
7.35	+20
7.36	+80
7.37	+55
7.38	-2
7.39	+40
7.40	+18
8.1	+60 (Mills, 2004) +30 (Wypych and Arnold, 1987)
8.2	+50 (Mills, 2004) +20 (Wypych and Arnold, 1987)
8.3	-13
8.4	-13
8.5	+5
8.6	-60 (based on pipe I) -40 (based on pipe II)
10.6	+20
10.7	+1
10.8	+25
10.9	+9
10.10	-2

10.11	+7
10.12	-3
10.13	+6
10.15	+25
10.16	+12
10.17	+24
10.18	+35
10.19	+2
10.20	+5
10.21	+17
10.22	+4
10.23	+12
10.24	+35
10.25	+45

Note:

a) Refer to the note provided in page 111 for the basis of calculation for this table.

b) (+) stands for over-prediction; (-) stands for under-prediction

c) Percentages are provided only for dense-phase region

d) Percentages for different solids flow rates are calculated and averaged. The averaged percentage values are provided in the above table.

Table A5.2: Uncertainty (SD/√N) values of m_f, m_s and various pressure measurement values for "white powder" tests

TEST NAME	START TIME sec	FINISH TIME sec	SD/√N OF P8 kPa	SD/√N OF P9 kPa	SD/√N OF P10 kPa	SD/√N OF P11 kPa	SD/√N OF P11⁺ kPa	SD/√N OF P12 kPa	SD/√N OF Direct DP kPa	SD/√N OF m_f kg/s	SD/√N OF m_s kg/s
exp2	125	155	0.040	0.066	0.260	0.191	0.245	0.400	0.244	0.00002	0.096
exp3	165	190	0.039	0.071	0.239	0.193	0.247	0.294	0.164	0.00002	0.128
exp4	155	180	0.053	0.063	0.175	0.157	0.191	0.309	0.175	0.00002	0.121
exp5	170	195	0.024	0.059	0.248	0.262	0.279	0.336	0.223	0.00002	0.112
exp6	165	195	0.037	0.085	0.255	0.181	0.309	0.368	0.175	0.00002	0.084
exp8	165	185	0.058	0.120	0.199	0.173	0.220	0.285	0.155	0.00003	0.074
exp9	125	155	0.066	0.089	0.145	0.129	0.153	0.133	0.097	0.00003	0.059
exp11	220	255	0.030	0.056	0.208	0.138	0.193	0.250	0.155	0.00001	0.094
exp14	195	225	0.002	0.026	0.114	0.127	0.188	0.260	0.000	0.00001	0.078
exp15	205	240	0.029	0.060	0.204	0.175	0.243	0.272	0.000	0.00002	0.071
exp16	115	135	0.049	0.071	0.191	0.212	0.307	0.474	0.000	0.00002	0.145
exp17	105	125	0.050	0.083	0.124	0.198	0.318	0.424	0.000	0.00002	0.163
exp19	95	125	0.061	0.087	0.206	0.156	0.213	0.311	0.000	0.00002	0.072
exp20	120	165	0.021	0.033	0.163	0.184	0.229	0.232	0.134	0.00002	0.068
exp21	135	170	0.024	0.104	0.153	0.134	0.170	0.182	0.127	0.00000	0.092
exp23	130	190	0.010	0.023	0.144	0.149	0.184	0.184	0.107	0.00000	0.053
exp24	137	180	0.017	0.034	0.086	0.071	0.107	0.168	0.117	0.00000	0.067
exp25	140	190	0.029	0.029	0.097	0.084	0.093	0.118	0.084	0.00001	0.058
exp26	135	180	0.028	0.070	0.066	0.063	0.128	0.169	0.107	0.00002	0.046
exp52	140	160	0.077	0.094	0.305	0.148	0.256	0.365	0.195	0.00003	0.098
exp53	130	160	0.061	0.048	0.146	0.069	0.143	0.200	0.102	0.00002	0.091
exp54	124	155	0.042	0.042	0.119	0.067	0.118	0.128	0.061	0.00002	0.052
exp55	115	145	0.067	0.051	0.251	0.203	0.299	0.357	0.206	0.00002	0.064
exp56	175	210	0.045	0.029	0.074	0.058	0.064	0.092	0.054	0.00002	0.025
exp57	175	200	0.048	0.041	0.084	0.063	0.085	0.173	0.101	0.00003	0.072
exp58	175	205	0.039	0.039	0.090	0.088	0.117	0.148	0.076	0.00002	0.080
exp59	155	190	0.054	0.068	0.141	0.145	0.161	0.189	0.097	0.00003	0.046
exp60	155	190	0.063	0.078	0.194	0.213	0.210	0.210	0.123	0.00002	0.087
exp61	100	130	0.045	0.051	0.094	0.086	0.118	0.131	0.092	0.00002	0.118
exp62	95	125	0.020	0.026	0.050	0.000	0.077	0.076	0.053	0.00001	0.020
exp63	110	130	0.080	0.069	0.340	0.201	0.376	0.609	0.328	0.00003	0.124
exp64	100	120	0.081	0.076	0.258	0.191	0.325	0.414	0.219	0.00003	0.225

Coefficient of variation

Coefficient of variation is expressed as the ratio of Standard Deviation to the Mean of a set of data (Schi and D'Agastino, 1995). Values of coefficient of variations for the "white powder" tests, expressed as percentage of mean, are provided in Table A5.3. The plots of coefficient of variation values of static pressure signals of P8 to P12 are shown in Figures A5.1 to A5.5. A, B, C, D, E, F corresponds to tapping locations P8, P9, P10, P11, P11[+] and P12, respectively. P8 is at the beginning of pipeline for the 69 mm, 148 m long test rig; approximate distance between A and B: 16 m, B and C: 53 m, C and D: 11 m, D and E: 23 m, E and F: 20 m. There was 1 no. 90 degree bend between A and B and 2 no. 90 bends between C and D. The plots show that the general trend of coefficient of variation values is to increase from P8 to P12 tapping location.

Table A5.3: Coefficient of Variation (CV) of Static and DP Pressure Signals

Test name	Air flow (kg/s)	Solids flow (kg/s)	CV of P8 (kPa)	CV of P9 (kPa)	CV of P10 (kPa)	CV of P11 (kPa)	CV of P11+ (kPa)	CV of P12 (kPa)	CV DP meter (kPa)	CV of P8 (kPa)	CV of P9 (kPa)	CV of P10 (kPa)	CV of P11 (kPa)	CV of P11+ (kPa)	CV of P12 (kPa)	CV DP meter (kPa)
	Steady state values															
exp23	0.040	1.97	0.64	1.40	8.81	9.11	11.23	11.24	6.55	0.32	0.78	8.10	11.61	22.46	47.33	29.11
exp25	0.040	2.06	1.49	1.48	4.95	4.28	4.73	6.01	4.28	0.75	0.82	4.46	5.52	8.41	28.28	19.02
exp24	0.040	2.14	0.76	1.50	3.78	3.13	4.69	7.38	5.16	0.77	0.83	3.52	4.06	9.38	32.09	24.81
exp21	0.044	2.38	0.86	3.73	5.52	4.81	6.11	6.55	4.58	0.38	1.87	4.60	5.98	10.37	28.35	18.89
exp20	0.044	2.24	0.98	1.54	7.49	8.45	10.52	10.66	6.16	0.45	0.77	6.14	9.26	16.83	31.59	25.04
exp4	0.049	1.90	1.37	1.65	4.54	4.08	4.97	8.03	4.55	0.77	1.03	4.79	5.92	10.90	36.46	21.86
exp26	0.050	2.34	1.27	3.24	3.03	2.91	5.89	7.77	4.92	0.66	1.89	2.96	4.01	11.22	32.72	22.16
exp17	0.056	2.69	1.06	1.75	2.61	4.16	6.67	8.90		0.51	0.93	2.31	4.97	12.21	31.95	
exp3	0.064	2.10	1.02	1.85	6.22	5.03	6.42	7.65	4.26	0.60	1.20	6.52	7.24	13.38	29.64	21.39
exp11	0.070	1.81	1.08	2.03	7.50	4.98	6.93	8.99	5.58	0.80	1.69	10.05	9.02	18.65	47.67	38.10
exp16	0.077	2.68	1.03	1.50	4.02	4.45	6.45	9.95		0.52	0.82	3.56	5.31	11.39	31.43	
exp2	0.085	2.40	1.23	2.04	8.05	5.91	7.58	12.39	7.57	0.71	1.29	8.16	8.31	15.25	45.48	40.79
exp15	0.088	1.59	1.05	2.17	7.35	6.29	8.74	9.78		0.79	1.79	9.45	11.19	23.21	44.13	
exp65	0.094	3.03	1.44	1.42	3.81	3.81	5.86	7.03	3.07	0.74	0.87	3.36	4.80	10.03	20.19	25.25
exp55	0.103	2.17	2.09	1.59	7.79	6.28	9.26	11.07	6.39	1.4	1.05	7.69	8.86	18.72	36.02	36.67
exp60	0.107	1.75	2.27	2.82	6.99	7.67	7.55	7.57	4.44	1.74	2.61	8.95	14.25	18.97	29.07	39.06
exp19	0.108	2.99	1.89	2.69	6.38	4.84	6.61	9.63		1.00	1.50	5.42	5.57	10.46	24.45	
exp6	0.112	2.33	1.14	2.65	7.90	5.61	9.57	11.42	5.42	0.71	1.75	7.85	7.93	18.35	32.58	35.81
exp64	0.112	3.30	1.70	1.60	5.41	4.02	6.82	8.70	4.59	0.87	0.98	4.59	4.78	10.71	21.73	26.20
exp59	0.127	1.85	1.95	2.46	5.06	5.21	5.78	6.81	3.49	1.50	2.26	6.32	9.54	13.77	23.34	30.63
exp63	0.144	3.02	1.68	1.44	7.14	4.22	7.90	12.78	6.89	0.88	0.91	5.91	4.95	11.85	27.54	47.80
exp14	0.146	1.27	0.06	0.82	3.54	3.94	5.83	8.05		0.04	0.56	4.18	6.33	15.64	43.12	
exp8	0.153	2.37	1.21	2.51	4.17	3.63	4.62	5.98	3.25	0.80	1.77	3.96	5.04	7.76	13.95	23.89
exp54	0.154	2.61	1.34	1.33	3.81	2.15	3.77	4.09	1.95	0.82	0.97	3.56	2.91	6.15	8.82	13.70
exp5	0.164	1.69	0.62	1.53	6.44	6.82	7.26	8.74	5.81	0.32	0.90	6.76	10.02	16.80	39.76	29.76
exp62	0.167	3.06	2.57	3.26	6.35	9.05	9.72	9.63	6.71	1.35	2.01	5.08	10.43	13.48	18.63	45.50
exp58	0.176	2.08	1.22	1.22	2.79	2.74	3.64	4.58	2.36	0.91	1.10	3.17	4.59	7.17	11.86	20.20
exp57	0.176	1.93	1.26	1.07	2.19	1.65	2.31	4.49	2.63	0.94	0.96	2.49	2.76	4.36	11.56	23.49
exp9	0.177	2.28	2.060	2.760	4.500	4.010	4.750	4.120	3.020	1.22	1.98	4.22	5.52	7.38	8.91	22.41
exp61	0.194	2.93	1.38	1.57	2.92	2.66	3.66	4.07	2.86	0.72	0.97	2.22	2.97	4.52	6.70	15.86
exp53	0.200	2.52	1.89	1.49	4.52	2.14	4.44	6.20	3.17	1.11	1.04	3.86	2.68	6.28	11.10	21.15
exp52	0.201	2.27	1.62	1.97	6.40	3.10	5.37	7.66	4.10	0.94	1.33	5.54	4.00	7.95	14.28	28.53
exp56	0.201	1.80	1.63	1.06	2.07	2.07	2.31	3.31	1.94	1.19	0.94	2.85	3.19	4.22	7.56	18.42

DP meter did not record pressure signals for experiments 4, 15, 17, 19

Figure A5.1: Coefficient of variation of static signals versus distance of tapping locations; "white powder"; m_f = 0.04 to 0.05 kg/s
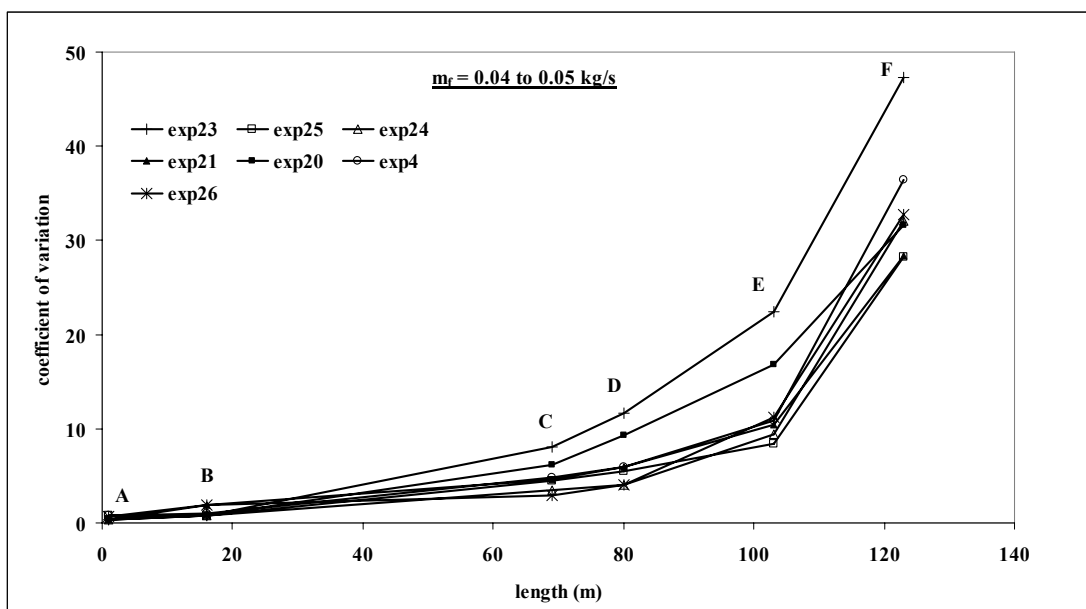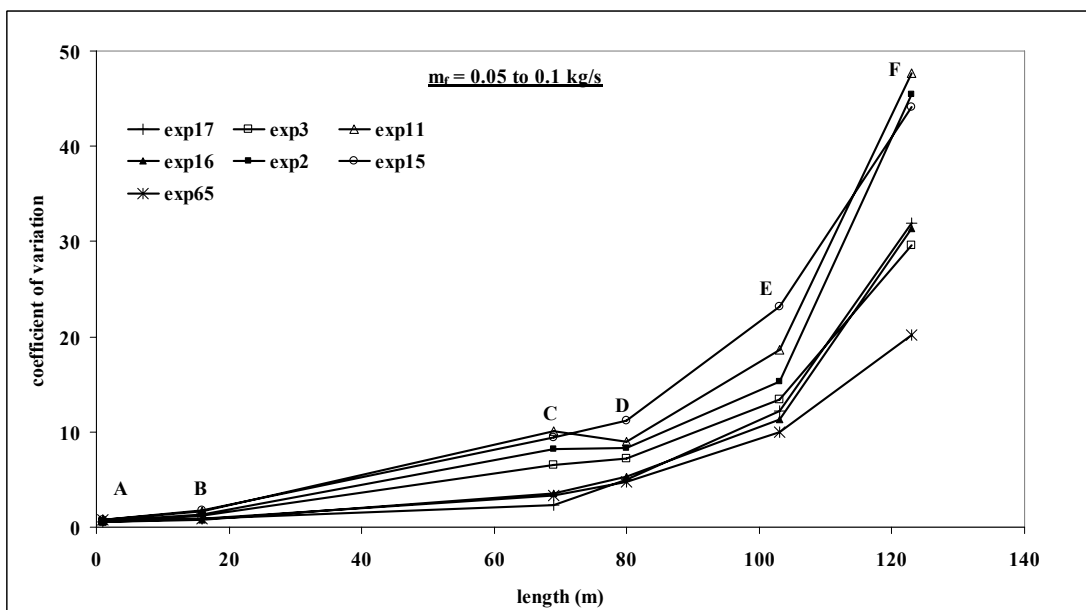
Figure A5.2: Coefficient of variation of static signals versus distance of tapping locations; "white powder"; m_f = 0.05 to 0.1 kg/s
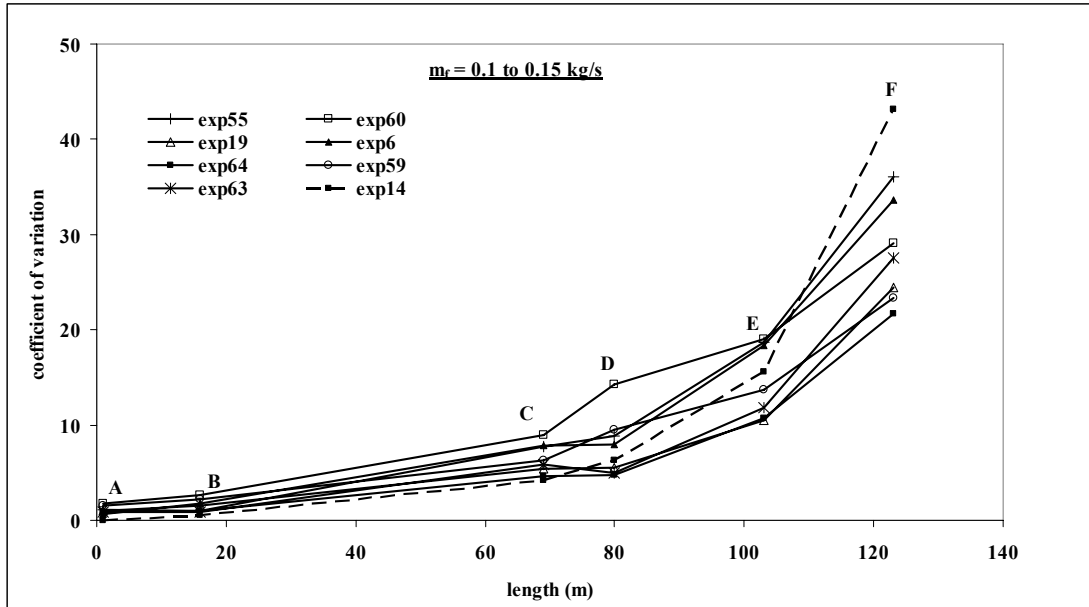

Figure A5.3: Coefficient of variation of static signals versus distance of tapping locations; "white powder"; m_f = 0.1 to 0.15 kg/s
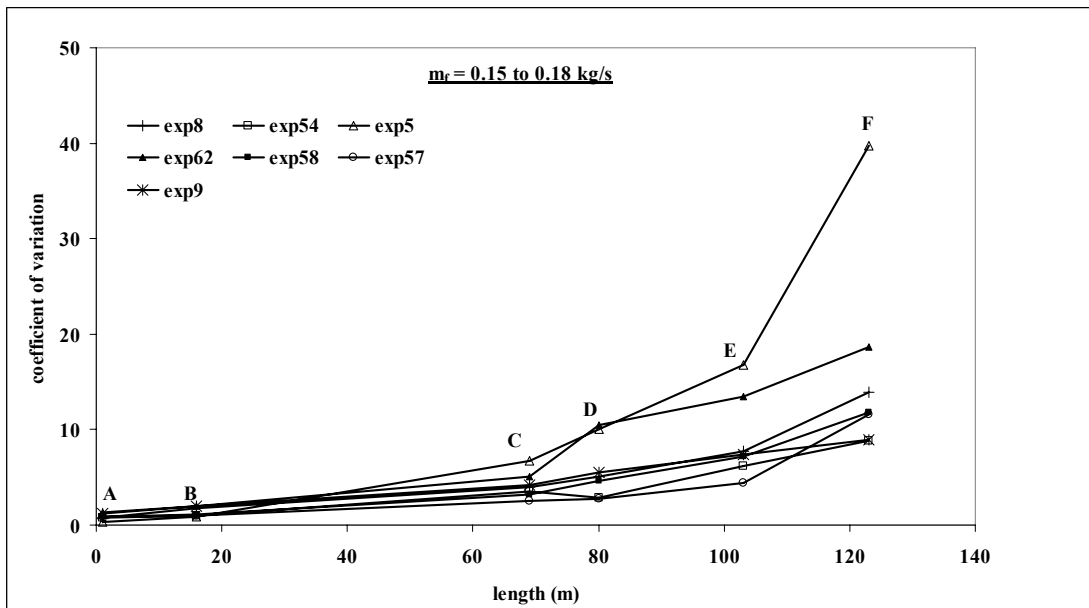
Figure A5.4: Coefficient of variation of static signals versus distance of tapping locations; "white powder"; m_f= 0.15 to 0.18 kg/s
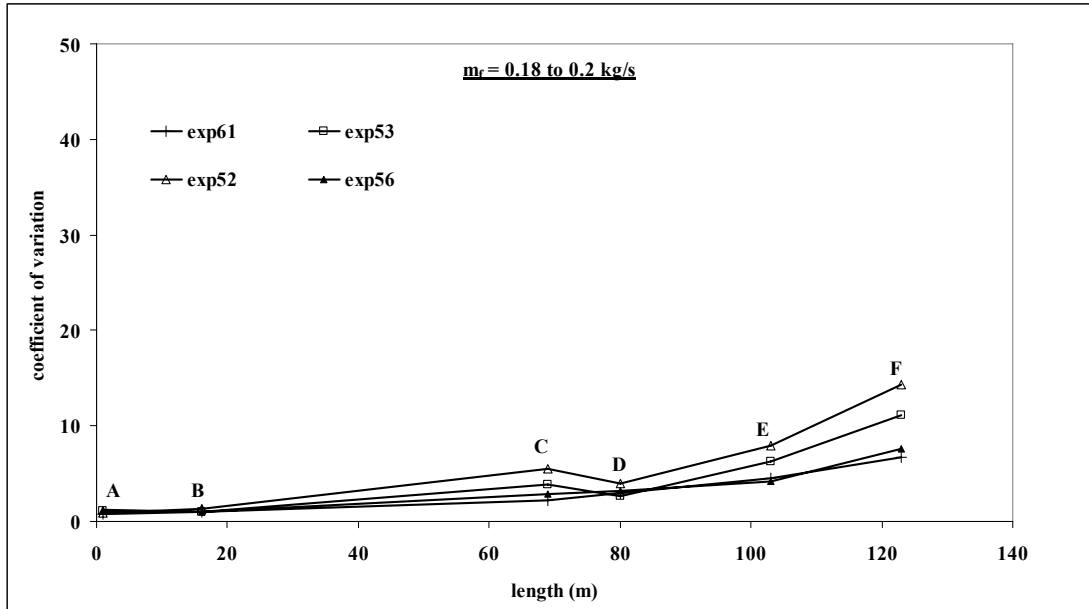

Figure A5.5: Coefficient of variation of static signals versus distance of tapping locations; "white powder"; m_f= 0.18 to 0.2 kg/s

LIST OF PUBLICATIONS DURING COURSE OF PhD

Referred Journals (Published/Accepted) – 6 Nos.

Mallick, S.S. and Wypych, P.W. 2009. Minimum transport boundaries for pneumatic conveying of powders. **Powder Technology**. 194: 181-186

Mallick, S.S. and Wypych, P.W. 2010. Evaluation of scale-up procedures using "system" approach for pneumatic conveying of powders. **Particulate Science and Technology**. 28: 40-50

Mallick, S.S. and Wypych, P.W. An investigation into modelling of solids friction for dense-phase pneumatic conveying of powders. **Particulate Science and Technology**. 28: 51-66

Mallick, S.S. and Wypych, P.W. 2009. Modelling solids friction for dense-phase pneumatic conveying of powders. **Particulate Science and Technology**. 27: 444-455.

Mallick, S.S. and Wypych, P.W. 2009. Improved modelling and scale-up procedure for dense-phase pneumatic conveying of powders. **Bulk Solids and Powder - Science and Technology**. 4 (3)

Mallick, S.S. and Wypych, P.W. 2008. Investigation into modelling solids friction for dense-phase pneumatic conveying of powders. **Bulk Solids and Powder - Science and Technology**. 3 (1): 1-14.

Referred Journals (Under Review) – 1 No.

Mallick, S.S. and Wypych, P.W. On improving scale-up procedures for dense-phase pneumatic conveying of powders. **Particulate Science and Technology**

Book Chapter – 1 No.

Mallick, S.S. and Wypych, P.W. Investigation into modelling solids friction for dense-phase pneumatic conveying of powders, Current Developments in Bulk Solids Handling, Ed. G. Lodewijks, Vogel 2010.

Referred Conferences (Published) – 6 Nos.

Mallick, S.S. and Wypych, P.W. 2010. Improved modelling and scale-up procedure for fluidised dense-phase pneumatic conveying systems. **The International Conference: Bulk Solids India 2010,** Mumbai 2010. (only abstract was reviewed)

Mallick, S.S. and Wypych, P.W. 2009. Improved scale-up procedure for dense-phase pneumatic conveying of powders. **The 6th International Conference for Conveying and Handling of Particulate Solids,** Brisbane, Australia.

Mallick, S.S. and Wypych, P.W. 2008. On the modelling of pressure drop for the dense-phase pneumatic conveying of powders. In the proceedings of **Bulk Europe 2008**, Czech Republic.

Mallick, S.S. and Wypych, P.W. 2008. Evaluation of scale-up procedures for fluidised dense-phase pneumatic conveying design. In the proceedings of **4th International Symposium Reliable Flow of Particulate Solids**, Norway.

Mallick, S.S. and Wypych, P.W. 2007. Evaluation of solids friction factor models for fluidised dense-phase pneumatic conveying. In the proceedings of **9th International Conference on Bulk Materials Storage and Transportation**, Newcastle, NSW, Australia.

Mallick, S.S., Wypych, P.W and Rizk, F. 2007. Effect of bend model on prediction of pressure drop for pneumatic conveying systems. In the proceedings of **9th International Conference on Bulk Materials Storage and Transportation**, Newcastle, NSW, Australia.

Other Publications – 2 Nos.

Mallick, S.S. and Wypych, P.W. 2007. Solids friction in fluidised dense-phase flow. **Bulk Solids Handling**, 27 (6): 398-404.

Mallick, S.S. and Wypych, P.W. 2007. Pressure drop prediction for fluidised dense-phase pneumatic conveying of powders. **The Australian Bulk Handling Review**. 12 (3): 100-102.

Poster Presentation – 2 Nos.

Mallick, S.S. and Wypych, P.W. **The 6th International Conference for Conveying and Handling of Particulate Solids,** Brisbane, Australia, 3rd – 7th August 2009 (Presented by Prof. Peter Wypych)

Mallick, S.S. and Wypych, P.W. **International Fine Particle Research Institute, Inc, USA**, Perth, Australia, 8-12th July 2007.